Interpretation of Geochemical Evolution in the Dakota Aquifer in Kansas Based on Coupled Hydrogeochemical Models

by

Tyan-ming Chu

B.S., National Taiwan College of Marine Science and Technology, 1982
M.S., University of Nebraska-Lincoln, 1988

Submitted to the Department of
Geology and the Faculty of the
Graduate School of The University
of Kansas in partial fulfillment
of the requirements of the degree
of Doctor of Philosophy

Donald O. Whittemore
Professor in Charge

Ernest E. Angino
Co-Chairman

+ Bruce M. McEnroe

Committee Members

for the Department

Date Defended: 26 July 95

Kansas Geological Survey
Open-file Report 95-47

Kansas Geological Survey
Open-file Report

Disclaimer

The Kansas Geological Survey does not guarantee this document to be free from errors or inaccuracies and disclaims any responsibility or liability for interpretations based on data used in the production of this document or decisions based thereon. This report is intended to make results of research available at the earliest possible date, but is not intended to constitute final or formal publication.

ABSTRACT

Tyan-ming Chu, Ph.D.
Department of Geology, 1995
University of Kansas

Distinct water types occur in different regions of the Dakota aquifer system in north-central and central Kansas. Mixing of these waters has caused cation exchange and concomitant chemical reactions. Mixing of regional Dakota water from the west, saltwater intruding from the underlying Cedar Hills sandstone, and surface recharge occurs in the Dakota aquifer east of the Cedar Hills subcrop. Geochemical simulation indicates that the major water-rock interactions in the ground-water system include cation exchange, calcite dissolution/precipitation, gypsum dissolution, and anhydrite and magnesite dissolution (in the underlying Cedar Hills Sandstone).

A one-dimensional (1-D) HYDROGEOCHEM coupled model was developed to simulate the hydrogeochemical processes involving cation exchange and calcite precipitation/dissolution in the aquifer. Ion chromatography occurs along the flow path due to different selectivity coefficients for cation exchange. A plateau zone of temporary stable conditions forms between the conservative mixing front and the retardation front. Mg and Ca first replace Na on clays in the mixing front and plateau zone. Ca then replaces Mg on the exchange sites before the aquifer materials equilibrate with the incoming freshwater. Calcite dissolution mainly occurs near the retardation front.

Sensitivity analyses indicate that selectivity coefficients and cation exchange capacity (CEC) are not important controls on the dissolved concentrations of Ca and Mg in the plateau zone. CEC is important in determining the velocity of the retardation front. The intensity of

cation exchange is mainly dependent on the salinity contrast of the incoming and initial waters. The concentrations of Ca and Mg in the plateau zone are mainly controlled by the salinity of the incoming water.

The TDS content of the previous saltwater in the upper Dakota aquifer west of the Cedar Hills subcrop is estimated to have been about 5,000 to 10,000 mg/L based on comparison of water chemistry data with the 1-D model results. Surface recharge from southeastern Colorado and western Kansas has reached and substantially affected the Dakota water chemistry in central Kansas.

A transient, semi-empirical 2-D model of a hydrogeochemical profile for the Dakota aquifer in central Kansas suggests that the aquifer system is sensitive to vertical geohydrological components. Cation exchange and calcite dissolution occur at the top of the Dakota aquifer where the Dakota water mixes with recharge from the overlying confining layer. Dispersion of Dakota water into the Cedar Hills Sandstone appears to cause cation exchange within the upper part of the Permian aquifer.

DEDICATION

獻給

不斷支持鼓勵我的

父母

妻子

弟弟們

和在這期間出生的兩個淘氣的

兒子

ACKNOWLEDGMENTS

First of all, I would like to thank Dr. Donald O. Whittemore for giving me the opportunity to conduct the research in the Geohydrology Section of the Kansas Geological Survey. He led me to the field of ground-water chemistry and gave me the best guidance throughout the period. He also contributed many useful suggestions for conducting the research and presenting of the final report. I particularly appreciate the financial and equipment support of the Dakota project and the KGS, and the chance to participate all the events related to the project.

I also thank my academic advisor, Dr. Ernest E. Angino for encouraging me with my research through all these years. My great appreciation also extends to Dr. Gwendolyn Macpherson, Dr. Wakefield Dort Jr., Dr. Donald Steeples, Dr. David Parr, and Dr. Bruce McEnroe who were willing to serve as my doctoral committee and provide guidance, organizational suggestions and editorial comments.

I am indebted to Dr. Vijay Tripathi, the second author of HYDROGEOCHEM for giving me free advice about running the program and comments on some of the chemical modeling strategies. I also appreciate the help of Dr. Carl McElwee and Dr. Jim Butler, Jr. for giving advisement in transport modeling.

Finally, I would like to express my gratitude to my parents, my wife, my brothers, and my friends for their moral support.

TABLE OF CONTENTS

LIST OF FIGURES

LIST OF TABLES

CHAPTER 1
INTRODUCTION

Ground-water studies of the Dakota aquifer in Kansas have been conducted for more than a half century. However, the early investigations of the Dakota aquifer were piecemeal and have produced overly generalized results. Recently, the over-development of the High Plains aquifer in western Kansas and stream-aquifer systems in central Kansas has caused critical water shortages in some areas. A long-term multi-disciplinary program to assess the water-resources potential of the Dakota aquifer in Kansas has been conducted at the Kansas Geological Survey (KGS) to help the state to plan the use of this valuable water resource. In the last several years, the Dakota aquifer project and other projects at the KGS have performed detailed studies to characterize the hydrogeological properties of the Dakota aquifer at both regional and local scales (Macfarlane et al., 1988, 1990, 1991a, 1991b, 1994; Hamilton, 1989; Wade, 1992; Whittemore et al., 1993). The study methods include test-hole drilling, geophysical well log analyses, geologic stratigraphy correlation, geostatistic analyses, aquifer tests, and ground-water flow modeling.

For the ground-water geochemistry study, the KGS collected all the available historical Dakota water chemistry data and created a Dakota water chemistry database named KWATCHEM (Macfarlane et al., 1990). The quality of the database was verified by manually checking data with the original published sources and by charge balance calculation. A water type study, conservative mixing curve techniques, statistical analyses, geochemical simulation, and geophysical well log analyses have been applied in investigations on regional and local scales (Macfarlane et al., 1988, 1990, 1991a, 1992; Whittemore, et al., 1993;

Boeken, 1995). State-wide regional studies of Dakota water chemistry indicate that distinct water types occur in different regions in Kansas. Some of the major chemical reactions have been identified, including calcite dissolution/precipitation, cation exchange, oxidation of pyrite, dissolution of anhydrite (gypsum) and halite (in the underlying Permian Cedar Hills Sandstone).

In spite of the increased understanding of the hydrogeological characteristics of the Dakota aquifer and the geochemical reactions occurring in the system, there are still many questions about how and where the chemical reactions occur. How do the chemical reactions affect the water quality along the flow path? How do the water-rock interactions affect the aquifer properties? To understand those problems requires more than correlation of chemistry, geology, and hydrology. The development of coupled hydrogeochemical models allows investigation of the interactions between the physical and chemical processes occurring in the aquifer system.

The use of coupled hydrogeochemical models for the transport of active solutes can greatly aid the study of ground-water evolution. There is currently much international interest in modeling the subsurface transport of reacting solutes. A variety of mathematical models have appeared in the literature which include the effect of single and multiphase flow, one and many components, advective and dispersive mass transport, equilibrium and kinetic chemistry. The ability to describe the movement of conservative species has reached a high state of development. Modeling of nonconservative chemical species is not as advanced, but the level of interest has greatly increased. Hydrogeochemical evolution in ground-water systems is one of the most challenging problems to simulate. Realistic descriptions of subsurface geology involve understanding complex ground-water flow patterns. In addition, because solutes are

usually chemically active, there is always the potential for extensive water-rock interactions. These two related mass transport and chemical reaction problems are often attacked with coupled hydrogeochemical models. Yeh and Tripathi (1989) discussed the numerical strategies of hydrogeochemical models and their advantages and disadvantages. They concluded that models with iteration between coupled mass transport and chemical reaction modules have the most potential for practical purposes.

1.1. STUDY AREA

Because of the complex pattern of water types, flow systems, and uneven distribution of data in the Dakota aquifer across the state of Kansas, a subregion including 10 counties in central and north-central Kansas was selected for detailed study of the factors controlling Dakota water chemistry (Figure 1.1). The study area was selected because more hydrogeological data is available from the area than in much of the Dakota aquifer in Kansas and there are substantial chemical changes in Dakota ground waters across the study area. The eastern boundary of the study area is at the east edge of the Dakota Formation. The Dakota aquifer crops out in the eastern and southeastern parts of the study area (Figure 1.2). The outcrop belt of the Dakota aquifer in north-central Kansas ranges from about 24 km (15 miles) wide at the Kansas-Nebraska border to about 64 km (40 miles) near the southern boundary of the study area. To the west of the outcrop zone, the Dakota aquifer is covered by Upper Cretaceous strata. The western portion of the study area includes the Cedar Hills subcrop and the area west of the Cedar Hills subcrop zone. The Cedar Hills subcrop zone extends from just south of the study area northward into Nebraska.

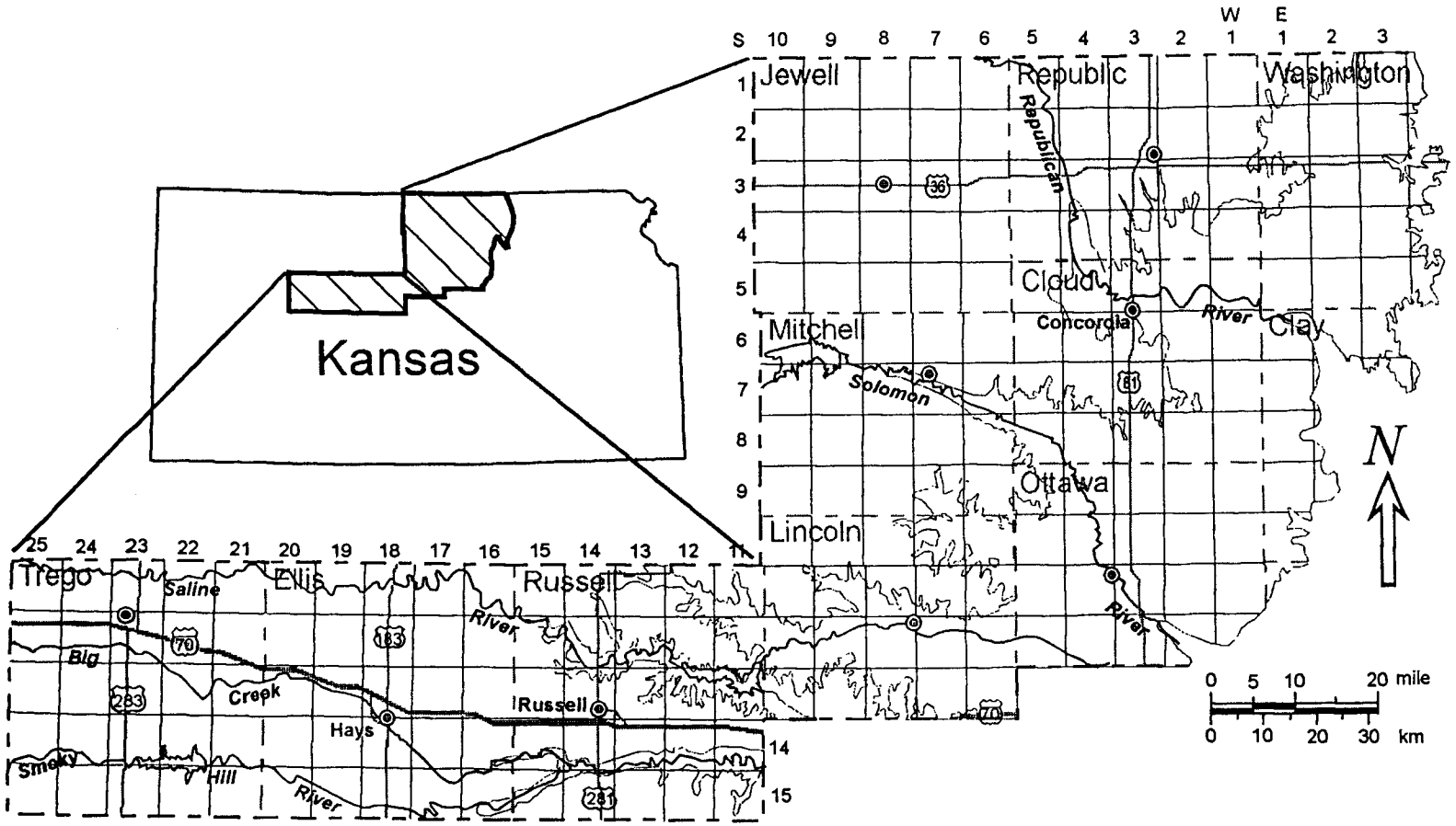

Figure 1.1. The study area in central and north-central Kansas.

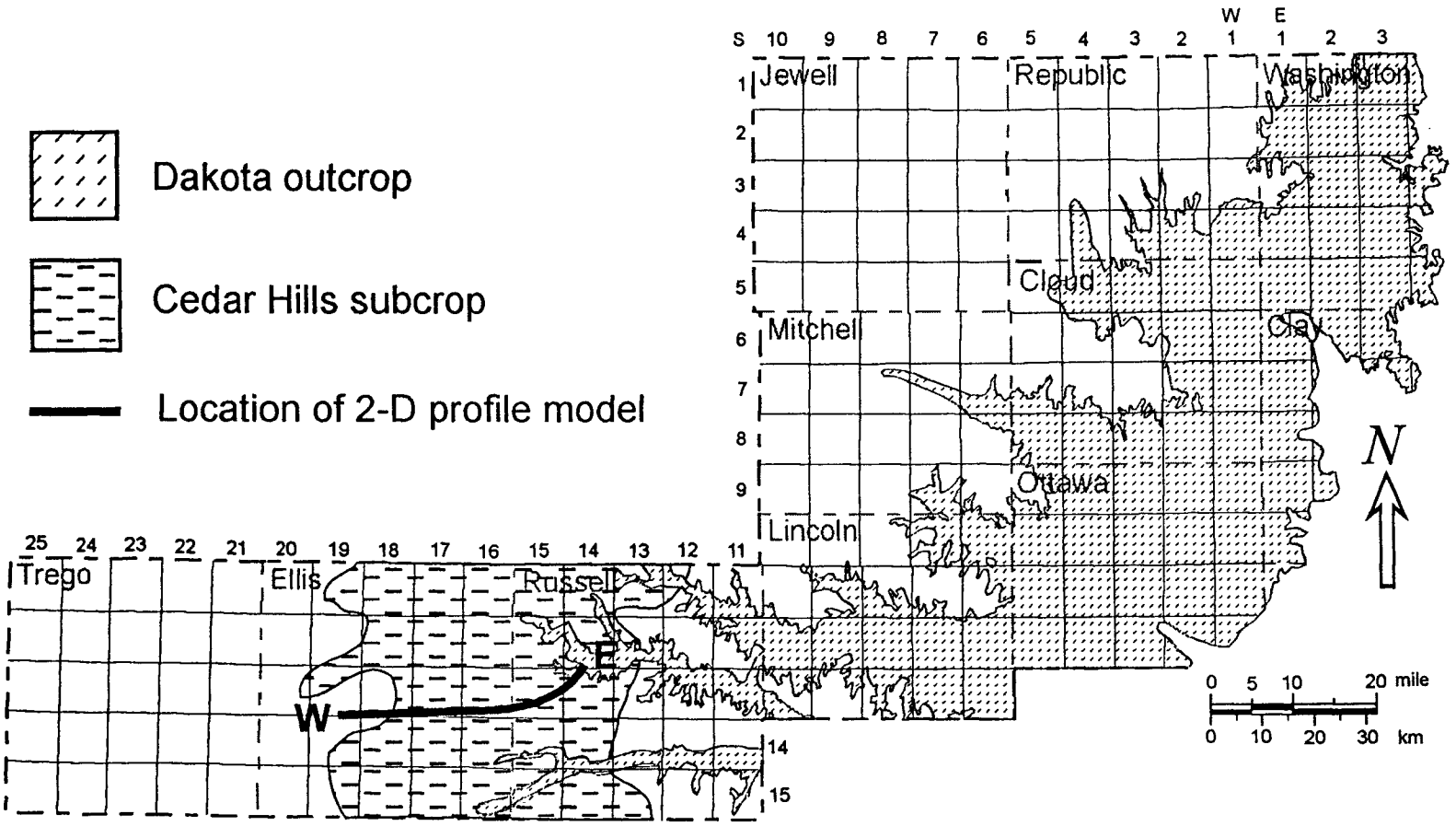

Figure 1.2. The major geological zones in the study area. The W-E line is the location of the 2-D coupled semi-empirical profile model.

The study area is dissected by four major east-flowing streams. From north to south, they are the Republican, Solomon, Saline, and Smoky Hill rivers. In the outcrop zone, the surface of the divides between these and other smaller streams are generally covered by deposits of loess and the major valleys contain thick Pleistocene alluvium deposits. These river systems normally serve as discharge zones for the regional Dakota ground-water flow. In some areas near the outcrop zone, the river valleys have cut into the Dakota Formation and cause the local ground-water flow systems to intersect the regional Dakota ground-water flow.

Ground water from the Dakota aquifer in the study area is one of the most important water sources in this area except in the northwestern part where the Dakota water is too salty to use. The Dakota aquifer generally yields small to moderate amounts of water for stock and domestic use. However, some high-permeability channel sandstones are able to produce large quantities of water for irrigation in Washington and Cloud counties (Macfarlane et al., 1991a; Wade, 1992).

The regional Dakota ground-water flow in the study area is from the west and northwest to the east and discharges to the river systems in the Dakota outcrop zone (Figure 1.3). Intrusion of Cedar Hills saltwater in central Kansas has affected the Dakota water quality to the east of the Cedar Hills subcrop zone. In the Dakota outcrop zone, local surface recharge is the major source of fresh ground water in the local flow systems. The Dakota aquifer to the west of the Cedar Hills subcrop zone is a partially closed system and contains water that is less affected by outside water sources than the Dakota aquifer to the east. This complex system allows investigation of the geochemical evolution in the Dakota aquifer along the regional flow path from west of the Cedar Hills subcrop to the Dakota outcrop.

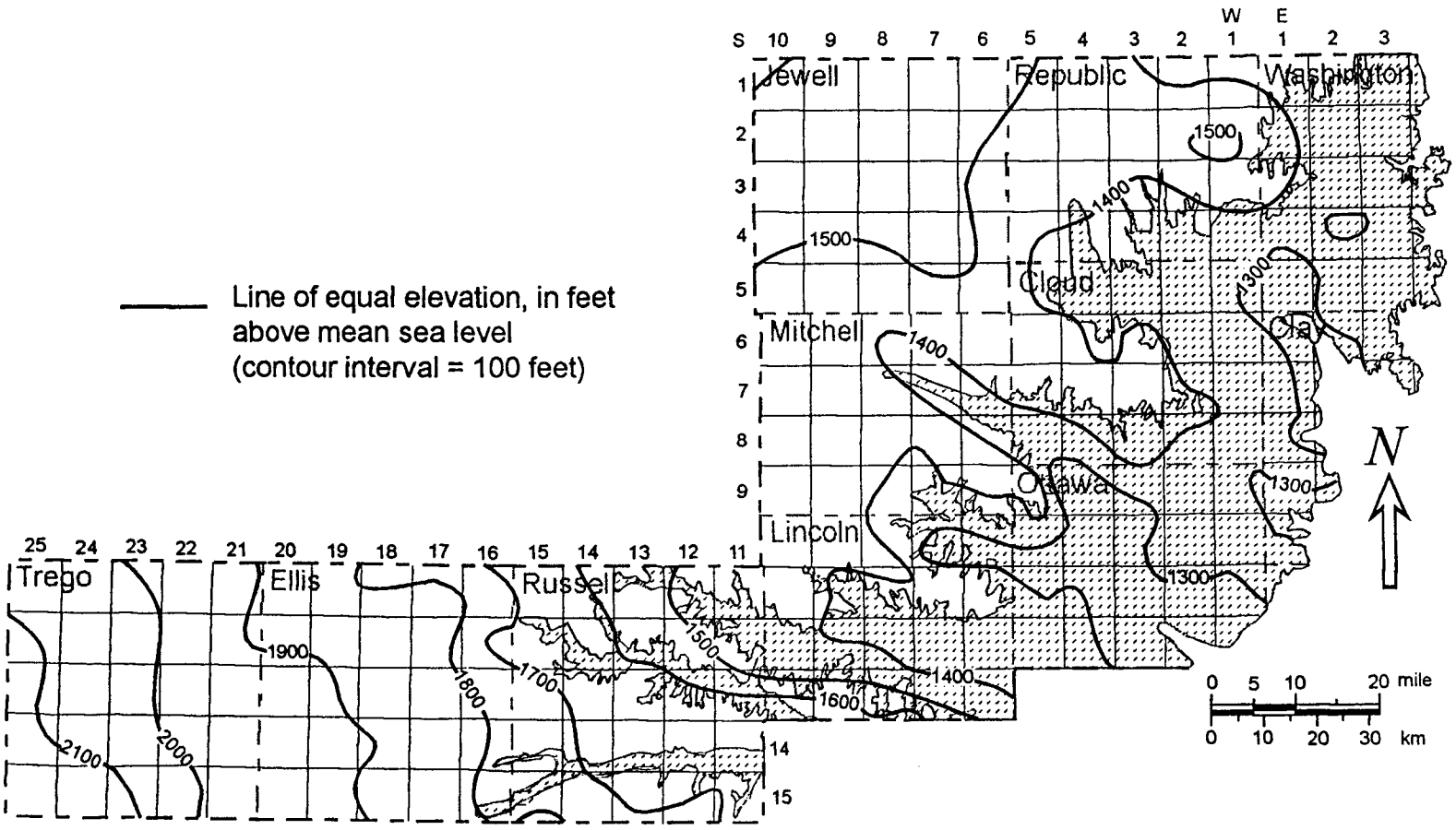

Figure 1.3. Predevelopment potentiometric surface for the Dakota aquifer (adapted from Macfarlane et al., 1995a)

1.2. PURPOSE

The purpose of the study is to understand the mechanisms of flow and major chemical reactions, particularly cation exchange and concomitant reactions, that control the ground-water evolution in the Dakota aquifer. The approach involved systematic study of a subregional set of ground-water chemistry data and use of a coupled flow and chemical reaction model to simulate the patterns of hydrogeochemical evolution. Due to the limited functions of the numerical model, computer resources, and inadequate amount of data for both physical and chemical properties of the Dakota aquifer system, a one-dimensional (1-D) conceptual model and a two-dimensional (2-D) semi-hypothetical profile model were applied to describe the conceptual hydrogeochemical evolution. A predictive model is far from being applicable due to the lack of data and technology. However, the resultant improvement in understanding of the chemical evolution processes is helpful in evaluating the present patterns of and predicting general changes in ground-water quality on a regional scale.

This dissertation first reviews previous studies of geology, hydrogeology, and water quality of the Dakota aquifer. A discussion of studies of aquifer geochemical evolution and principles of hydrogeochemical processes, especially cation exchange, follows. Ground-water chemistry data obtained in the study area is then classified into different groups and analyzed. Presentation of methodology and discussion of results from the 1-D and 2-D simulations of the coupled flow and chemical reactions in the Dakota aquifer system comprise the main part of the dissertation. Evaluation of the numerical results includes comparison with field data.

CHAPTER 2

HYDROGEOLOGY OF THE DAKOTA AQUIFER SYSTEM IN NORTH-CENTRAL AND CENTRAL KANSAS

The Dakota aquifer consists of the Cheyenne Sandstone, Kiowa Formation and Dakota Formation of the Lower and Upper Cretaceous series. In the study area the Dakota aquifer overlies the Wellington Formation and Ninnescah Shale of the Sumner Group of the Permian System, Salt Plain Formation, Cedar Hills Sandstone, Flower-pot Shale, and Blaine Formation of the Nippewalla Group of the Permian System, and the Jurassic Morrison Formation in western Trego County. The Harper Sandstone, normally lying between the Ninnescah Shale and Cedar Hills Sandstone in the stratigraphic column of Kansas, does not exist in the study area. The Graneros Shale and Greenhorn Limestone of the Upper Cretaceous Series, and Pleistocene-Recent alluvium overlies the Dakota Formation. The contact between the Lower Cretaceous and Permian and Jurassic rocks is an uncomformity. The contact between the Dakota Formation and the Graneros Shale is considered a continuous depositional series. This chapter presents a literature review describing the geological and hydrogeological characteristics of each related geological formation. Figure 2.1 shows the relationships of the geological formations.

2.1. PERMIAN SYSTEM

Permian rocks underlie the Dakota aquifer in most of the study area except in western Trego County. All the Permian rocks belong to the Leonardian Series and consist almost entirely of clastics and evaporites. The sediments represent cyclic marginal marine to continental deposits that reflect the regression and withdrawal of marine water from the

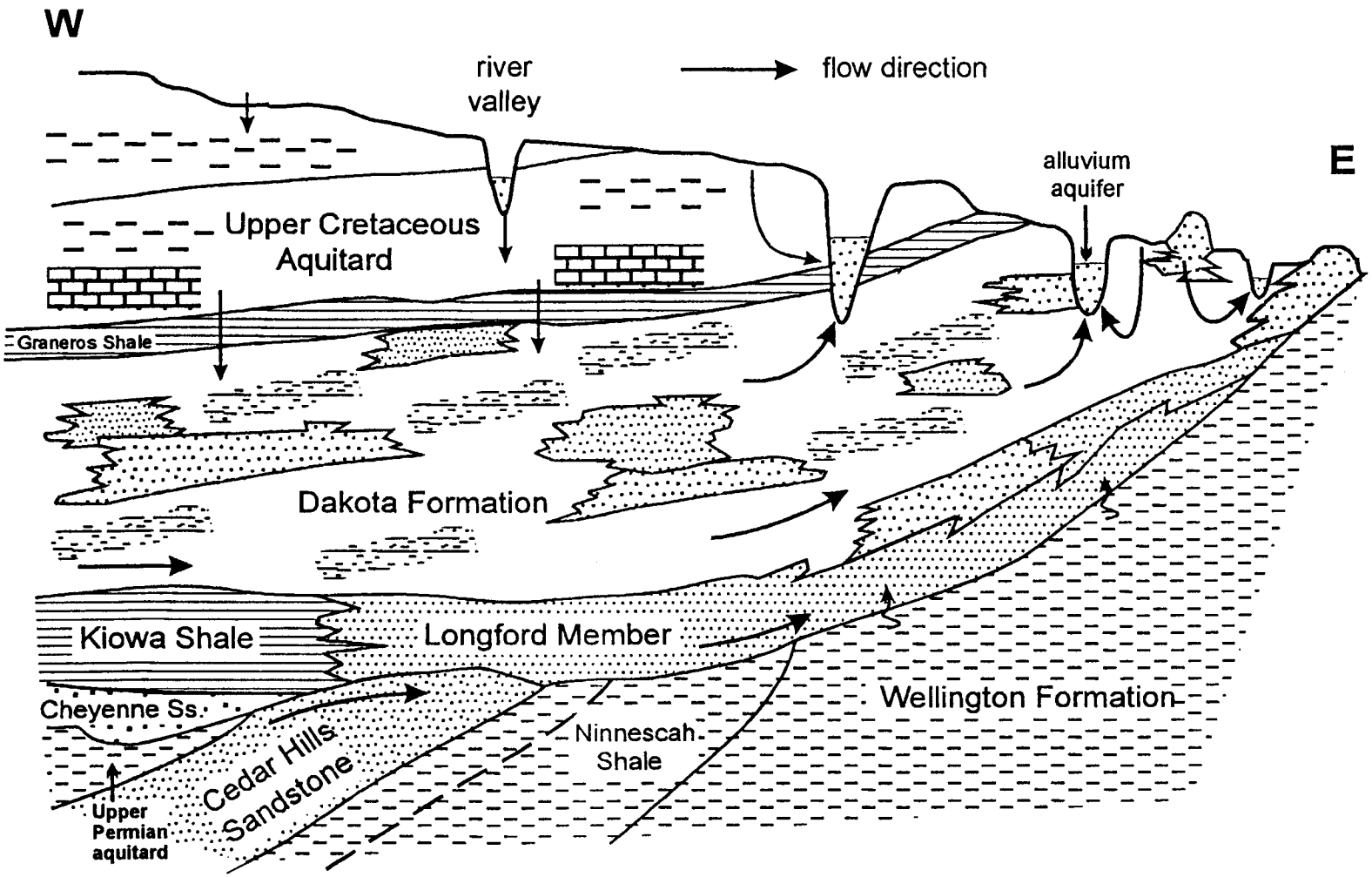

Figure 2.1. The geological setting of the study area in relation to the Dakota aquifer. The objects are not drawn to scale.

western Mid-Continent during Permian time (Rascoe, 1968). The Sumner Group includes the Wellington and Ninnescah formations underlying the Dakota aquifer in the eastern part of the study area. The Nippewalla Group includes the Salt Plain, Cedar Hills, Flower-pot, and Blaine formations underlying the Dakota aquifer in the western part of the study area.

Because the Dakota aquifer and underlying units dip toward the west and northwest, the Nippewalla Group is at a depth greater than the Sumner Group. Moreover, because of the poor quality of ground water in the lower portions of the Dakota aquifer in the western part of the study area, the Permian bedrock is not explored for potable water supplies. Thus little information is available about the Nippewalla Group. The Cedar Hills Sandstone is hydraulically interconnected to the Dakota aquifer in the study area and discharges saltwater to the Cretaceous aquifer. Therefore, study of the Cedar Hills Sandstone has drawn more attention in the past several decades. The rest of the Nippewalla Group are of low permeability and are considered as aquitards. Because there is not much information available in the western part of the study area for the Permian low permeability layers, only the geology of the Cedar Hills Sandstone will be further discussed.

2.1.1. Wellington Formation

The pre-Cretaceous erosional surface of the Wellington Formation underlies the Dakota aquifer in the eastern most part of the study area and outcrops to the east (Bayne and Walters, 1959; Walters and Bayne, 1959; Mack, 1962). The Wellington Formation represents a transitional zone from normal marine limestone and shale to red beds deposited under restricted marine conditions (Swineford, 1955). It is about 215 m (700 ft) thick in south-central Kansas and thins toward the northwest. In north-central Kansas, the

approximate thickness of the formation ranges between 120 and 180 m (400 - 600 ft). The formation is divided into three lithological members: a lower anhydrite member, the Hutchinson Salt Member, and an upper shale member (Norton, 1939). The lower anhydrite member is composed of gray shale and anhydrite ($CaSO_4$) interbedded with gray to brownish-gray dolomite ($CaMg(CO_3)_2$). Both the anhydrite and shale are dolomitic and contain a little halite (NaCl) and a very small amount of pyrite (FeS_2) and bituminous matter (Jones, 1965). Massive beds of gypsum ($CaSO_4 \cdot 2H_2O$) are exposed in Saline, Dickinson, and Clay counties to the south and east of the study area. The gypsum beds are also found in the subsurface of the study area.

The Hutchinson Salt Member consists of an irregular alternation of relatively thick salt beds and thinner beds of clayey and silty shale, anhydrite, dolomite, and magnesite ($MgCO_3$). In the subsurface, halite is the most abundant mineral, followed in abundance by clay and associated allogenic minerals, anhydrite, and carbonate minerals. The major clay minerals are illite, montmorillonite, and chlorite. Carbonate minerals, predominantly magnesite and dolomite, form only several percent of the sequence. Only a minor amount of calcite ($CaCO_3$) is scattered rather sporadically through the rock. The magnesite and dolomite are believed to be a product of diagenesis. The carbonate minerals were originally deposited as calcite. The calcite reacted with Mg-rich fluid and Mg replaced Ca to form magnesite and dolomite. The replaced Ca then reacted with SO_4 to form anhydrite (Jones, 1965). A core study by Jones (1965) at south-central Kansas indicates that halite and anhydrite are distributed throughout the entire section of Wellington Formation. Magnesite, pyrite, quartz (SiO_2), and hematite (Fe_2O_3) are the next most widespread minerals. Dolomite only occurs in the lower part of the Hutchinson Salt Member. Marcasite (FeS_2), polyhalite

($2CaSO_4 \cdot K_2SO_4 \cdot MgSO_4 \cdot 2H_2O$), celestite ($SrSO_4$), and chalcedony ($SiO_2$) are present in very minute quantities.

The Hutchinson salt bed extends from the Oklahoma-Texas panhandle up to central Kansas. The north limit of the Hutchinson Salt Member occurs in southwestern Ottawa, and southern Mitchell counties, and extends to the northwest of the study area (Rascoe, 1968; Gogel, 1981). The salt bed is buried more than 250 m (850 ft) below the surface and its maximum thickness is about 90 m (300 ft) in the study area (Angino et al., 1972; Bayne and Brinkley, 1972; Gogel, 1981)

The upper shale member is a monotonous succession of gray shale beds resembling those in the Hutchinson Salt Member and the lower anhydrite member. It includes some anhydrite near the base and a few thin beds of dolomite scattered in the section. The thickness of this upper shale member is approximately 75 m (250 ft).

There is no obvious evidence of discomformity at the contact between the Wellington Formation and the above Ninnescah Shale. However, the boundary can be recognized by the color change from gray to purplish-red shale or reddish-brown shale (Norton, 1939; Zeller, 1968).

In Clay County, east of the study area, the Wellington Formation yields only very small amounts of water of poor quality to wells (Walters and Bayne, 1959). A large quantity of halite brine was produced from the collapsed zone in the dissolution edge of Hutchinson Salt Member to the south of the study area (Gogel, 1981). No water is produced from the Wellington Formation in the study area.

2.1.2. Ninnescah Shale

The Ninnescah Shale underlies the Dakota aquifer in the middle part of the study area. In the outcrop zone south of the study area, the Ninnescah Shale consists primarily of brownish-red, calcareous and dolomitic silty clay shale. A minor amount of gray shale and thin, impure, limestone beds, and beds of calcareous sandstone and sands are also found in this formation (Norton, 1939; Swineford, 1955; Bayne et al., 1971). In central and northern Kansas, a sandstone bed is well developed at the top of the formation. This sandstone contains grayish-green, copper-bearing, sandy siltstone about 2.5 m (8 ft) thick.

The thickness of the formation decreases north and west toward the margins of the depositional basin. It is 130 m (425 ft) at the outcrop near the Oklahoma state line and thins to about 15 m (50 ft) in the subsurface in northern Osborne County (Norton, 1939; Swineford, 1955; Zeller, 1968). Based on the cross-sections of Norton (1939), the estimated thickness of Ninnescah Shale in the study area ranges from less than 15 m (50 ft) in the north to about 45 m (150 ft) in the south.

No reports of wells yielding water from the Ninnescah Shale were found for the study area. Both the Wellington and Ninnescah formations form a lower confining aquitard for the Dakota aquifer in north-central Kansas. However, some water chemistry of the Dakota aquifer near the eastern edge and the bottom of the Dakota outcrop zone indicates that a small amount of saltwater may have diffused from the Wellington and Ninnescah formations up to the Dakota aquifer.

2.1.3. Cedar Hills Sandstone

The Cedar Hills Sandstone extends from eastern Colorado to central Kansas and was truncated by pre-Cretaceous erosion in eastern Russell County. The formation consists of red sandstone and interbedded sandy siltstone and shale in the study area (Swineford, 1955; Macfarlane et al., 1988). The Cedar Hills Sandstone is probably eolian sediment deposited under desert conditions in an oxidizing, continental deflation-flat basin. A central "core" of evaporites of the Cedar Hills Sandstone is located in western Kansas and eastern Colorado and grades into red shale and sandstone to the northwest, east and southeast (Rascoe, 1968). The sedimentary basin in which the "evaporite core" is located is named the "Syracuse Basin". A study of a core from Wichita County, Kansas by Holdoway (1978) indicates that the Cedar Hills Sandstone consists of silt- to sand size sediments cemented by halite. The sandstone is usually a quartz arenite. Quartz is the dominant mineral of the sandstone grains; feldspar comprises about 5 to 10% of the clastic grains. Very little clay is present. The red color is caused by a hematite coating on most of the clastic grains. Hematite also forms patches in the matrix.

Halite is the major matrix material for the evaporite deposits of the Cedar Hills Sandstone in western Kansas. Anhydrite nodules occur at several horizons within the formation. Miner amounts of dolomite and magnesite also occur in the evaporites of the Nippewalla Group. James (1972) indicates that magnesite is a major component in the water-insoluble residue of several strata in the Cedar Hills Sandstone portion of the core taken from AEC Test Hole 5 located at 19S-37W-22ACCC (the legal location used in this dissertation conforms to the procedure of the U. S. Geological Survey), in Wichita County.

No K or other Mg salts have been found in the evaporite sequence (Holdoway, 1978). The salt cement in the formation toward the margin of the depositional basin was removed due to subaerial exposure in pre-Cretaceous time and by ground water that flowed through the formation (Macfarlane et al., 1990).

The Cedar Hills Sandstone aquifer is hydraulically connected to the Dakota aquifer where the Upper Permian confining layer occurring between the two aquifers pinches out at the west of its subcrop zone in western Russell and eastern Ellis counties (Figures 1.2. and 2.1) (Frye and Brazil, 1943; Swineford and Williams, 1945; Macfarlane et al., 1988, 1990). Chemical data indicates that there is mixing between waters from the Cedar Hills Sandstone and from the Dakota aquifer (Macfarlane et al., 1990). In the Cedar Hills subcrop area, the potentiometric maps show that the hydraulic head in the Cedar Hills aquifer is generally subparallel or higher than that of the lower portion of the Dakota aquifer. However, the maps also show that a reverse flow direction occurs in many local areas due to local flow systems (Macfarlane et al., 1988).

No quantitative determination of hydraulic properties for the Cedar Hills Sandstone near the study area has been done. Regional numerical flow models indicate that the Cedar Hills aquifer is slightly less permeable than the Dakota aquifer at the discharge zone (Whittemore et al., 1993).

The Jurassic Morrison Formation only exists in western Trego County in the study area. Due to its great depth, no investigation of the geologic unit has been conducted in central Kansas. The Morrison Formation will not be discussed due to lack of data in the study area.

2.2. CRETACEOUS SYSTEM

Paleozoic deposition was brought to a close by uplifting of the entire area by the end of Permian time. The study area was subjected to erosion throughout all the Triassic and Jurassic periods except the area of western Trego County. Erosion continued through early Cretaceous time until the deposition of the Cheyenne Sandstone during a short invasion by the "Kiowa" sea. According to Lee et al. (1948), a dip of about 1.9 m/km (10 ft/mile) in a southwest direction was imparted to Permian rocks in north-central Kansas prior to deposition of the Lower Cretaceous sediments. Post-Dakota deformation tilted the Permian rocks in the Salina Basin to a dip of 1.1 to 1.9 m/km (6 - 10 ft/mile) toward the northwest in the northern part of the study area (Figure 2.2).

The Cheyenne Sandstone, Kiowa, and Dakota formations are separated from underlying Permian and Jurassic rocks by a transgressive disconformity along which they show progressive northeastward overlap of older strata. The three formations record an initial transgressive-regressive cycle of Cretaceous sedimentation along the Kansas portions of the early to mid-Cretaceous Western Interior Sea (Franks, 1966, 1975, 1979).

2.2.1. Cheyenne Sandstone

Frye and Brazil (1943), and Swineford and Williams (1945) indicate that the eastern boundary of the Cheyenne Sandstone is located in eastern Russell County. A recent test-hole study in north-central Kansas (Hamilton, 1989; Macfarlane et al., 1991b) shows that the Cheyenne Sandstone pinches out at places nearly coincident with the underlying Permian Cedar Hills Sandstone subcrop (R18W) in western Ellis County. East of this line the

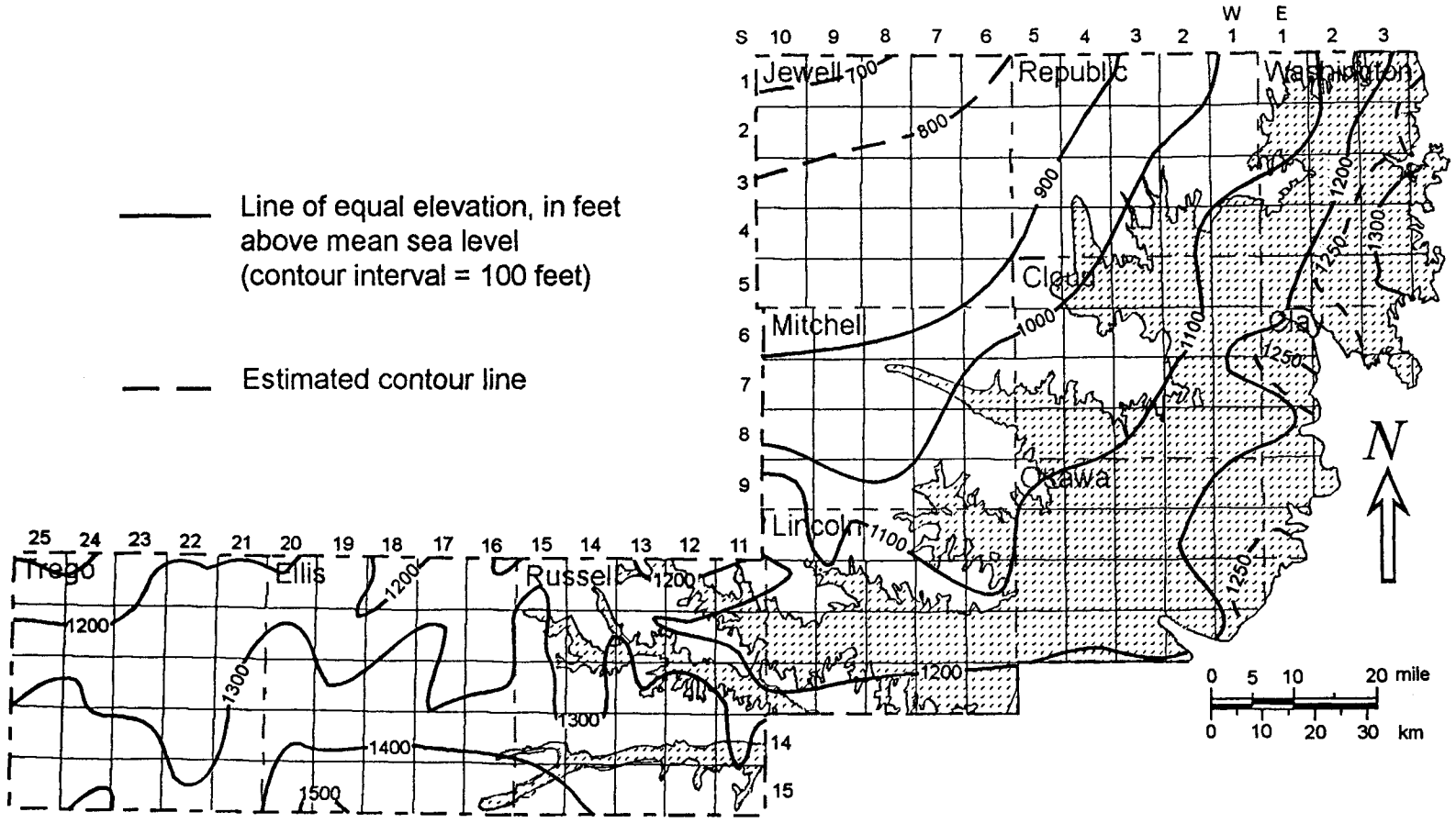

Figure 2.2. Bottom configuration of the Dakota aquifer in the study area. Data for Russell, Ellis, and Trego counties are adapted from Macfarlane et al. (1995b).

Cheyenne Sandstone is present as only a thin, locally mappable unit. The thickness of the Cheyenne Sandstone ranges from 0 to 19 m (0 - 62 ft) in Russell County (Swineford and Williams, 1945), and exceeds 61 m (200 ft) in north-eastern Ellis County (Frye and Brazil, 1943).

In the subsurface the Cheyenne Sandstone is predominantly a buff to light-gray fine- to medium-grained sandstone containing a small amount of shale and siltstone. The sandstone contains predominantly quartz and less than 5% feldspar. The clays are composed chiefly of kaolinite and montmorillonite. The grain size of Cheyenne sediments decreases upward from primarily medium-grained sandstone at the bottom to fine-grained sandstone near the top. Calcite, anhydrite, pyrite, siderite ($FeCO_3$), hematite, and glauconite are common in the formation (Swineford and Williams, 1945; Franks, 1975).

The Cheyenne Sandstone is interpreted as nonmarine fluvial and estuarine sediments consisting of horizontally stratified sandstones, channel sandstones, and associated overbank deposits as part of the transgressive sequence of the invasion of the Kiowa sea (Franks, 1975; Macfarlane et al., 1991b). The variable thickness of the Cheyenne Sandstone implies that the unit accumulated in some locally topographic lows on the Permian bedrock.

Water in the Cheyenne Sandstone is highly mineralized (Frye and Brazil, 1943; Macfarlane et al., 1988). The source of saltwater is mainly diffusion and upward-flowing water from the underlying Permian rocks. Oil brine injection in disposal wells may contribute saltwater locally.

2.2.2. Kiowa Formation

The Kiowa Formation rests directly on Permian bedrock where the Cheyenne Sandstone does not exist and is marked by a major unconformity indicated by a cobble zone at the base. Where the Cheyenne Sandstone is present, the Cheyenne-Kiowa contact occurs as a transgressive disconformity (Scott, 1970; Franks, 1975, 1979; Macfarlane et al., 1991b). The Kiowa Formation in north-central Kansas is not the relatively monotonous shale sequence as seen in the type area in Kiowa County. Rather, the Kiowa lithology changes considerably in lateral and vertical dimensions (Bayne et al., 1971; Franks, 1966, 1975, 1979; Hamilton, 1989; Macfarlane et al., 1991b; Wade, 1992). The formation contains an unnamed upper marine shale unit and the Longford Member at the base. East of R19W in the study area, the Kiowa marine shale was eroded away and the Dakota Formation rests directly on the Longford Member (Hamilton, 1989). The Kiowa Formation pinches out beneath the Dakota Formation near the eastern margin of the Dakota outcrop zone where the Dakota Formation rests directly on the Permian Wellington Formation (Plummer and Romary, 1942; Walters and Bayne, 1959; Franks, 1966; Wade, 1992).

The upper Kiowa shale generally is predominantly a medium- and dark-gray to black fissile marine shale with minor sandstone lenses, siltstone beds, and fossiliferous limestones. In general, sandstone increases in abundance upward in the Kiowa Formation and is more abundant in north-central Kansas than in southwestern Kansas (Franks, 1975).

The predominant clay minerals in the shale are illite and smectite. Kaolinite is also present in minor amounts and is more abundant higher in the formation, whereas smectite is more abundant near the base (Franks, 1966, 1975, 1979). Although a core study in northwest

Kansas indicated that the Kiowa Formation contains appreciable chlorite and vermiculite, these clay minerals were rarely found in north-central Kansas. Concretions and lenticular layers of calcareous cone-in-cone structure and siderite are intercalated in the shale. Assemblages of fish scales, bone fragments, and glauconite pellets with other organic materials are abundant in the shale. The euhedral crystals of gypsum found on weathered exposures is a secondary product derived mainly from the weathering of disseminated marcasite in the shale (Berry, 1952; Mack, 1962; Bayne et al., 1971; Franks, 1966, 1979). Franks (1966) indicates that, in north-central Kansas, most sandstone in the Kiowa Formation is fine grained. Most of the medium- to coarse-grained sandstone occurs along the eastern fringes of the outcrop belt. Most of the sandstones are well sorted and contain 95% or more quartz. Rounded pellets of glauconite exist mainly in fine-grained sandstone that is intercalated with thick sequences of shale (Franks, 1966). Normally, glauconite only comprises less than 1% of the sandstone. Calcite cement is a common feature in Kiowa sandstone at various stratigraphic levels in the formation (Swineford, 1947). Marcasite and pyrite with organic matter commonly are associated with calcite cement in the sandstone.

The Longford Member of the Kiowa Formation represents the easternmost record of continental and paralic sediments deposited during the transgressive phase of the Cheyenne-Kiowa-Dakota cycle (Franks, 1979). The Longford contains a heterogeneous assemblage of siltstone, mudstone, claystone, and carboneous beds of variable thickness. The argillaceous rocks in the Longford Member contain a greater variety of clay minerals than similar rocks in the Dakota Formation. Locally, kaolinite, illite and montmorillonite with chlorite or vermiculite can comprise a large portion of the argillaceous rocks (Table 2.1). From the test holes drilled in north-central Kansas, Macfarlane et al. (1991b) interpreted the Kiowa sequence

Table 2.1. Mineral weight percentages of sediment samples from the KGS #1 Jones core (10S-08W-02AAAC). All the Kiowa samples were taken from the Longford Member (Holt and Devoton, 1994, unpublished data).

Sampling depth, ft	Geological formation	Quartz	K-feldspar	Anatase	Siderite	Kaolinite	Chlorite	Illite/ muscovite	I-M ml.	Others
78.6	Dakota	31	1	1	-	21	-	-	46	-
143.2	Dakota	2	-	-	-	80	-	-	18	-
169	Dakota	50	1	-	3	5	2	40	?	-
295.9	Kiowa	62	1	1	-	8	-	28	trace	-
297.5	Kiowa	25	-	1	-	23	2	49	trace	-
306.5	Kiowa	50	-	-	-	7	-	40	?	3% pyrite
309	Kiowa	40	-	1	-	12	-	47	trace	-
326.2	Kiowa	25	-	-	1	10	-	40	trace	6% hematite 18% amorphous
329.8	Kiowa	35	-	-	2	9	-	39	trace	3% goethite 2% dolomite 10% amorphous
335.2	Kiowa	45	1	-	-	8	1	45	trace	-
356.1	Kiowa	40	1	-	3	10	1	45	trace	-
371.1	Kiowa	45	1	-	3	6	2	43	trace	-

Illite/Muscovite : mostly illite but with parts of muscovite or slightly degraded muscovite
I-M ml. : illite-montmorillonite mixed layer

(Longford Member) as deposits in tidally influenced deltaic environments. The member outcrops in a north-south-trending band along the eastern edge of the outcrop belt and extends subsurface to the west to reach the subcrop area of the Cedar Hills Sandstone. The lithology of the Longford Member changes laterally and interfingers with the Kiowa marine shale facies in central Kansas (Franks, 1975, 1979).

The maximum thickness of the Longford Member found at outcrops in north-central Kansas is 30 m (100 ft) (Franks, 1975, 1979). The total thickness of the Longford ranges from 13 to 60 m (43 - 200 ft) as encountered in the subsurface (Macfarlane et al. 1991b). The formation thins irregularly northward to near the Kansas-Nebraska line (Franks, 1966, 1975, 1979; Macfarlane et al., 1991b). Franks stated that the Kiowa Formation pinches out at about 50 km (30 miles) south of the Kansas-Nebraska line along the outcrop belt. However, recent test-hole drilling in Washington County shows that the northeast limit of the Kiowa has been extended to near the Kansas-Nebraska line (Macfarlane et al., 1991b). Much of the thickness variation is due to the pre-Dakota erosion and paleotopography on the Permian bedrock.

The Cheyenne-Kiowa sequence is considered as a hydrostratigraphic unit in a regional scale (Hamilton, 1989; Macfarlane et al., 1994). In the study area, the Longford Member is considered as an aquifer unit. The thickness of the upper Kiowa marine shale and Cheyenne Sandstone increase in western Ellis and Trego counties. The Cheyenne-Kiowa sequence in the two-county area is considered as a single hydrostratigraphic unit with an high horizontal/vertical hydraulic conductivity ratio due to the low permeability of the Kiowa marine shale.

2.2.3. Dakota Formation

The Dakota Formation in north-central Kansas is composed dominantly of varicolored clay and siltstone, including thin beds of fine-grained sandstone and numerous channel sandstones. It contains abundant siderite, hematite, limonite, lignite, and charcoal. Crystals and hard beds of pyrite are often found in the formation. Glauconite was observed in the lower part of the formation (Swineford and Williams, 1945). Calcite- and dolomite- cemented sandstone occurs mainly in the lower half of the Dakota Formation. The rock type most characteristic of the bulk of the Dakota Formation in outcrops is light-gray to light greenish-gray lenticular kaolinitic mudstone and claystone (Franks, 1966). The claystone, mudstone, and siltstone are estimated to comprise 60 to 70% of the Dakota Formation.

Plummer and Romary (1942) divided the Dakota Formation into the Terra Cotta and Janssen Clay members. The Janssen Clay Member contains beds of gray and dark-gray mudstone and claystone as well as lignite in the upper one-third of the formation. The Terra Cotta Clay Member contains red-mottled mudstone and claystone and is found in the lower two-thirds of the formation. However, the boundary between these two members is not well defined.

In contrast to the dominantly illitic shale of the Kiowa Formation, most argillaceous rocks in the Dakota probably contain less than 15% illite (Table 2.1). Similar results were also presented in some early studies (Plummer et al., 1954, 1963; Plummer and Romary, 1947). However, clay near the base and top of the Dakota contains appreciable amounts of illite (Franks, 1966). Pellets of spherulitic siderite are a common component of Dakota mudstone, claystone, and fine sandstone and indicate a mildly reducing depositional

environment. The common occurrence of gypsum in outcrops indicates that pyrite or marcasite may have been an original component that altered by weathering.

Sandstone in the Dakota Formation occurs in lenticular deposits of various sizes and shapes. The sandstone ranges from medium or coarse grained to very fine grained but mainly is fine grained. Quartz comprises 95% or more of the detrital components in most of the well-sorted nonconglomeratic sandstone (Franks, 1966).

The Dakota Formation in north-central and central Kansas is believed to have been deposited mainly in a low-lying nonmarine coastal or deltaic plain bordering the Cretaceous Interior Sea. The dominantly kaolinitic character of the Dakota Formation can be interpreted as evidence of terrestrial or nearshore sedimentation. Deltaic and offshore bar deposits may have also formed part of the Dakota. Franks (1966) believed that the Janssen Clay Member and lower part of the Terra Cotta Clay Member were deposited in near shore environments, perhaps in lagoonal or estuarine environments as well as in freshwater swamps. The abundance of carbonaceous matter, pyrite, siderite spherules and concretionary beds in some shaly sequences indicates that the environment was chemically reducing.

Recently, Hamilton (1989) correlated the Cretaceous sequence in Kansas with that in the Denver Basin and divided the Dakota Formation into J and D sequences. He indicated that the Dakota Formation consists of a series of landward-stepping progradational events. The J sequence is defined from the base of Dakota Formation to an unconformity within the Dakota Formation. The sequence consists of a succession of upward-fining sediments that were deposited aggradationally during relative sea-level rise. In central Kansas, the J sequence is composed entirely of fluvial facies. The D sequence starts from the unconformity on the top of

the J sequence to the top of the Dakota Formation. The upper progradational units consist of deposits of fluvial to shoreface facies.

In central and north-central Kansas, because all but the upper part of the Dakota Formation consists of fluvial deposits, evidence of scour and subarial erosion are numerous, and the criteria alone is insufficient to define the position of an interregional unconformity. Instead, a seaward shift in depositional environments is the best evidence for recognizing a relative sea-level fall and sequence-bounding unconformity. In central Kansas, the unconformity between the J and D sequences within the Dakota Formation is interpreted where the facies indicate an abrupt change from a meandering stream system to a braided stream system. This shift is represented by an upward change from variegated mudstone and fine- to medium-grained trough cross-bedded sandstone, to medium- to coarse-grained planar tabular cross-bedded sandstone. Based on the interpretation of the unconformity between the J and D sequences, the J sequence contains the lower part of the Terra Cotta Clay Member, and the D sequence contains the upper part of the Terra Cotta Clay Member and all of the Janssen Clay Member (Hamilton, 1989).

The thickness of the Dakota Formation is variable because of the basal unconformity. Bayne and Walters (1959) report a thickness range of from less than 1 m to about 120 m (400 ft) in Cloud County. Test holes in northwestern Ottawa County show that the Dakota is as much as 107 m (350 ft) thick (Mack, 1962). In Russell County, the thickness ranges from 61 to 91 m (200 - 300 ft) (Frye and Brazil, 1943; Swineford and Williams, 1945). A range of thickness between 47 and 91 m (155 - 300 ft) in Ellis County was reported by Frye and Brazil (1943) and Leonard and Berry (1961). A thickness of 46 to 76 m (150 - 250 ft) for the Dakota Formation was reported in Trego County (Hodson, 1965). Macfarlane et al. (1991b) shows

that the total thickness of the Dakota Formation ranges from 98 m (320 ft) in Washington and Republic counties to 85 m (280 ft) in Russell County and 67 m (220 ft) in northern Lincoln County. The total thickness of the Dakota Formation in the study area ranges from about 61 m to over 91 m (200 - 300 ft) (Macfarlane et al, 1990, Plate 4).

The regional subsurface dip on top of the Dakota Formation in north-central Kansas is approximately 1.3 m/km (7 ft/mile) to the north and northwest (Figure 2.3) (Lee et al., 1948; Merriam, 1957). West of the outcrop area, the depth to the top of the Dakota Formation is 305 m (1,000 ft) in northwestern Trego and 91 m (300 ft) in southeastern Trego County (Hodson, 1965), 183 m (600 ft) in northwestern Jewell County (Fishel and Leonard, 1955), and about 30 m (100 ft) in the Solomon River valley near Downs, just west of the Mitchell-Osborne County line (Hodson, 1959).

Only a few published field- and core-scale hydraulic conductivity tests of the Dakota aquifer in Kansas are available (Berry, 1952; Merriam et al., 1959; Wade, 1992; Macfarlane et al., 1994). The results show that the core-scale hydraulic conductivities of sandstones range from greater than 33 m/day (100 ft/day) to less than 0.3 m/day (1 ft/day), regardless of the depositional environment for the tested sandstones. Hydraulic conductivities obtained from field pumping and slug tests vary from place to place. Values range from 3.7×10^{-4} m/day (0.0012 ft/day) for a poorly-sorted fine-grained sandstone to 23.2 m/day (76 ft/day) for a thick fluvial channel sandstone in Washington County. Normally, the hydraulic conductivity of Dakota sandstone ranges in between 0.3 to 3.3 m/day (1 to 10 ft/day) (Butler, 1994, personal communication). No field and laboratory data is available for the vertical hydraulic conductivity of the Dakota aquifer. However, previous numerical studies indicate that the vertical hydraulic conductivity of the Dakota aquifer is generally very low, probably less than

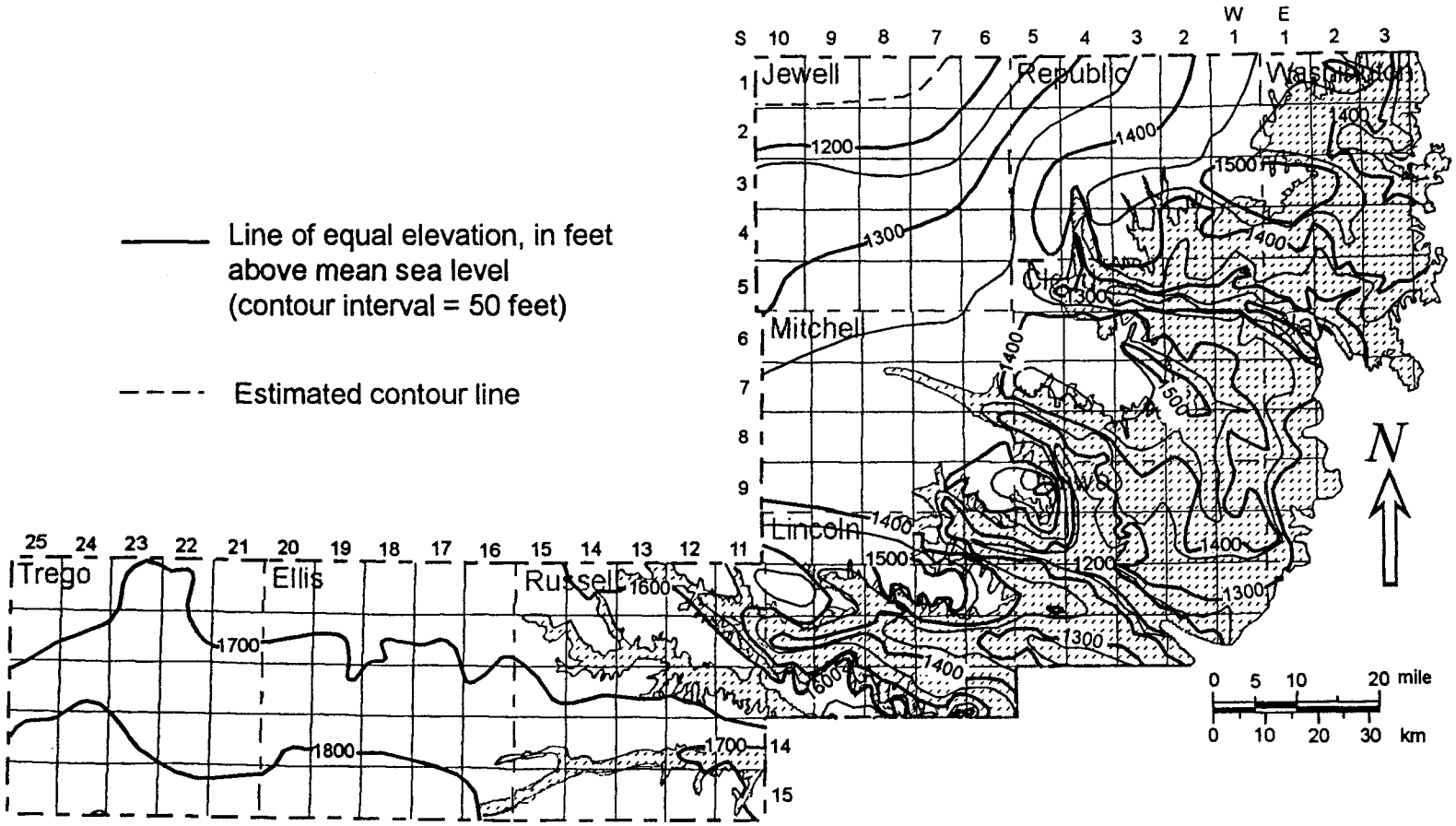

Figure 2.3. Top configuration of the Dakota Formation in the study area. Data for Russell, Ellis, and Trego counties are adapted from Macfarlane et al. (1995c).

1×10^{-3} m/day (3.3×10^{-3} ft/day) (Wade, 1992; Whittemore et al., 1993). The results seem reasonable for the geological characteristics of the Dakota aquifer.

2.2.4. Graneros Shale

The Graneros Shale in the study area consists mainly of dark-gray to brownish black noncalcareous silty and sandy shale that is locally interbedded with numerous thin beds of dirty fine-grained sandstone and sandy limestone. The chief clay minerals in the shale are kaolinite, illite, and montmorillonite. Kaolinite is more abundant in the lower part of the formation and montmorillonite is more abundant toward the top of the Graneros, whereas the amount of illite remains nearly uniform throughout (Hattin, 1965). Several bentonite beds occur in the middle and upper part of the formation (Berry, 1952; Fishel and Leonard, 1955; Mack, 1962; Zeller, 1968; Bayne et al., 1971). Glauconite was observed in sandstone beds in the lower part of the formation (Swineford and Williams, 1945). Organic debris is found throughout the formation. Pyrite and marcasite occur largely in clayey sediments in the lower part of the Graneros Shale (Hattin, 1965).

The Graneros sediments were deposited near the eastern margin of the vast, shallow Western Interior Sea. In north-central and central Kansas, the deposition of Graneros sediments was largely influenced by discharge of major stream systems along the eastern sea margin. Stratigraphic, lithologic, and faunal evidence indicates that the lower part of the Graneros Shale was deposited in shallow nearshore marine water of less than normal salinity. Later deposition occurred in progressively deeper offshore water of normal salinity (Hattin, 1965; Hattin and Siemers, 1987).

The thickness of the Graneros Shale ranges from 6 to 12 m (20 - 40 ft) and averages 9 m (30 ft) in the study area (Swineford and Williams, 1945; Berry, 1952; Fishel and Leonard, 1955; Bayne and Walters, 1959; Hodson, 1959; Mack, 1962; Hattin, 1965; Bayne et al., 1971). The shale is usually weathered to a heavy clay and forms a gentle slope from the base of the Greenhorn Limestone to the top of the Dakota Formation.

The Dakota Formation grades laterally in an east-west direction into and intertongues with the Graneros Shale. The Dakota-Graneros contact is transitional through alternating beds of sandy shale, shale, and thin sandstone beds (Hattin, 1965; Franks, 1966, 1975). Macfarlane et al. (1991b) indicates that, in north-central Kansas, the Dakota-Graneros contact is commonly found as an abrupt transgressive disconformity both in outcrops and the subsurface. However, they also concluded that overall, the Dakota-Graneros contact is a transitional boundary.

No wells in the study area are known to yield water from the Graneros Shale. The shale is nearly impermeable. Only a small amount of water leaks downward from the formation through fissures and joints into the Dakota Formation (Mack, 1962; Macfarlane et al., 1990).

2.2.5. Greenhorn Limestone

The Greenhorn Limestone crops out and extends in the subsurface to the west of the Dakota outcrop zone. The Greenhorn Limestone consists of alternating beds of thin limestone and chalky shale with some thin beds of bentonite (Swineford and Williams, 1945; Bayne and Walters, 1959). This formation is divided into four members. They are, from bottom to top,

the Lincoln Limestone, Hartland, Jetmore, and Pfeifer Shale members (Bayne and Walters, 1959; Hattin, 1975; Hattin and Siemers, 1987).

The Greenhorn Limestone consists of three major kinds of carbonate rock including skeletal limestones, laminated impure shaly chalk, and chalky limestone. Skeletal limestones are most abundant in the Lincoln Member and are also common in the upper half of the Jetmore Member and lower part of the Pfeifer Member. Arenaceous terrigenous detritus, consisting of silt and very fine to fine-grained quartz sand, is also common at the base of the Lincoln Member. Shaly chalk is the most common lithology of the Greenhorn Limestone in Kansas. Coccoliths are the principle component of the shaly chalk matrix. Fecal pellets and tests of foraminifera are the next abundant materials characterizing the shaly chalk. Pyrite, a secondary mineral, is common in unweathered shaly chalks, whereas limonite and gypsum are common weathering products in outcrops (Hattin, 1975).

The Greenhorn Limestone represents accumulation of carbonate-dominated sediments on a broad, flat, gently subsiding cratonic shelf lying along the eastern side of the Western Interior Sea. Hattin (1975) indicates that the major sources of terrigenous detritus from the west had little influence on the Greenhorn sediments in central Kansas.

The Graneros-Greenhorn contact is an unconformity and appears to be diachronous south of Lincoln County. The boundary is readily defined as the level where the noncalcareous Graneros Shale underlies, with abrupt lithological change and sharp stratigraphic contact, basal skeletal and /or chalky limestones of the Lincoln Member. However, north of Lincoln County, the Graneros-Greenhorn contact commonly lies within a strata sequence that is transitional between noncalcareous silty shale below and skeletal or chalky limestone-bearing shaly chalk above (Hattin, 1975).

The Greenhorn Limestone in this area ranges in thickness from a featheredge near the Dakota outcrop area to 50 m (150 ft) in the subsurface. The average total thickness is 29 m (95 ft) (Hattin, 1975).

Most of the water in the Greenhorn Limestone occurs in cracks above impervious layers and the water is usually very hard (Bayne and Walters, 1959). In the subsurface, the water leaking through the Graneros Shale into the Dakota Formation resembles the Greenhorn water sampled in the study area.

CHAPTER 3

GEOCHEMICAL CONTROLS ON THE EVOLUTION OF DAKOTA GROUND WATER

Macfarlane et al. (1990, Chapter 6) gave an overview of the hydrogeochemistry of the Dakota aquifer in Kansas. The concentrations of the major constituents in the ground water are affected by different major hydrogeochemical processes in different parts of the aquifer. Those processes include mixing of waters with different chemical characteristics, dissolution/precipitation of carbonate minerals, cation exchange, dissolution of gypsum, oxidation of pyrite and organic matter, and reduction of sulfate. Although the chemical properties of the Dakota aquifer water vary spatially depending on the heterogeneity of the aquifer system, especially in the vertical direction, a general pattern of hydrogeochemistry along the flow path can be clearly seen. Additional discussion of hydrogeochemical reactions in the Dakota aquifer are given in Macfarlane et al. (1991a) and Whittemore et al. (1993).

The absolute reaction rates and solubilities of constituents have a greater effect on ground-water chemistry than do their relative abundance in the solid matrix (Rogers, 1987). Weathering of clay minerals as the dominate process controlling ground-water chemistry has been reported mainly for silicate aquifers (Garrels and Mackenzie, 1967; Paces, 1973, 1983; Nesbitt and young, 1984; Kenoyer and Bowser, 1992a and b). However, weathering of clay minerals becomes less important for ground-water chemistry evolution when there are more soluble minerals, e.g. calcite, dolomite, gypsum etc., in the system. Aluminosilicate mineral weathering will not be discussed because such reactions have minor effects on the chemical evolution of the Dakota water in geologically recent time. Alteration of phyllosilicates in the

geologic past in the aquifer could have had important affects on the exchange properties of the minerals currently in the aquifer.

Ion complexing is an important factor in the hydrogeochemical processes that affect the fate and mass transport of constituents. Aqueous ion complexes normally increase the mobility of a constituent by increasing the dissolved concentration that is in equilibrium or interacts with the solids present (Miller and Benson, 1983). For the major constituents in ground water, sulfate complexes, e.g., $CaSO_4^\circ$, $MgSO_4^\circ$, and $NaSO_4^-$, are the most important (Freeze and Cherry, 1979; Hem, 1985, Domenico and Schwartz, 1990). Bicarbonate complexes, although not as important as sulfate complexes, can be significant when the bicarbonate concentration approaches 1000 mg/L (Hem, 1985). The importance of adsorbed ion complexes to water chemistry has been mentioned in Griffioen (1992) and Griffioen and Appelo (1993). The higher affinity of the exchange media for some ion complexes than the free ion itself can sometimes have a major impact on the distribution of the particular component.

Recharge to and mixing of waters of different quality in the Dakota aquifer originates the major geochemical evolution. The mixing process is discussed below, followed by a discussion of the concomitant chemical reactions of ion exchange, precipitation/dissolution of minerals, and redox reactions. The overall chemical evolution is then described as an ion chromatography mechanism which is the result of mixing and chemical reactions.

3.1. MIXING OF WATERS

Mazor et al., (1993) pointed out that sources of ground-water samples have to be carefully identified. Data could be misinterpreted when lumped in one diagram without

recognization of sources. They indicated that mixing of waters rather than gradual evolution of water chemistry is the reason for variation of water chemistry in the Paleozoic sandstone aquifers of the southern Laramie Basin, Wyoming.

Mixing of different types of waters in the Dakota aquifer has a major effect on the evolution of water chemistry (Macfarlane et al., 1988, 1990; Macpherson, 1990; Whittemore et al., 1993). The major water sources for the Dakota aquifer include surface recharge in the outcrop zone, leakage from the overlying confining layer, and saltwater intruded from the underlying Paleozoic bedrock, particularly the Cedar Hills Sandstone. Surface recharge in the Dakota outcrop area of southeastern Colorado and southwestern Kansas is a major component of the regional Dakota ground-water flow. Recharge in the outcrop zone in central Kansas forms local ground-water flow systems of much smaller scale. Geochemical simulations of waters in two regional ground-water flow paths in the Dakota aquifer in Kansas suggest that local recharge from the overlying confining layer could be important for the confined Dakota water quality (Macfarlane et al., 1990; Macpherson, 1990). Discharge of saltwater from the Cedar Hills Sandstone causes the abrupt increase in total dissolved solids (TDS) concentration in the Dakota aquifer in central Kansas. Mixing of waters from layers of different permeabilities within the Dakota aquifer complicates the water chemistry and makes the interpretation of regional ground-water evolution more difficult.

Many chemical reactions are triggered by mixing of different waters. Cation exchange and dissolution/precipitation of minerals are the dominant processes controlling water type in the mixing zone. Variation of redox conditions associated with mixing of waters is also an important factor affecting water chemistry. Discussion of the different chemical processes is given later in this chapter.

3.2. ION EXCHANGE

One of the major chemical reactions that occurs during mixing of waters is ion exchange. The direction of ion exchange depends upon whether the aquifer water is undergoing freshening or salinization (Appelo and Postma, 1994). Ion exchange acts as a temporary buffer in non-steady state situations. Cation exchange occurs when the incoming solution differs in compositions from the original pore water in contact with clay, soil, and sandstone. Cation exchange of Ca and Mg for Na on surface sites has been found to have a major impact on ground-water chemistry in many aquifers (Renick, 1924; Riffenburg, 1925; Schwartz and Muehlenbachs, 1979; Chapelle and Knobel, 1983; Knobel and Phillips, 1988; Zack and Roberts, 1988; Plummer et al., 1990; Keller et al., 1991; Boyle, 1992; Andrews et al., 1994). Reverse cation exchange (Na for Ca on surface sites) is also commonly found in the area where saltwater intrusion is taking place (Howard and Lloyd, 1983; Mercado, 1985; Xue et al., 1993).

Ion exchange sites in soils include clay minerals, organic matter, and oxides/hydroxides (White and Zelazny, 1986; Sposito, 1989; Appelo and Postma, 1994). All the materials act to some degree as a source of pH-dependent charge. The pH at which the charge of the particle is zero is called the point of zero charge (PZC), or more precisely the point of zero net proton charge (PZNPC). Solid materials have a capacity for anion exchange when the pH of the solution is below PZC and a cation exchange capacity (CEC) when pH is above the PZC (Freeze and Cherry, 1979; Sparks, 1986; Appelo and Postma, 1994).

All the pH-dependent charge reactions are an attribute of surface reactions (White and Zelazny, 1986). The surface charge on organic matter is due to electrostatic interactions

resulting from reactions of cations with organic functional groups and are directly pH-dependent in their charge characteristics. The PZC of soil organic matter may be well below 3 because of its strong acidic carboxyl groups (Perdue and Lytle, 1983; Gregor and Powell, 1988). The high surface charge density of organic materials makes them very powerful as ion exchangers. Variable charges are also formed by surface dissociation or complexation reactions on oxides and hydroxides such as goethite (FeOOH), gibbsite ($Al(OH)_3$), and pyrolusite (MnO_2). Because their PZCs, 7.0 to 9.0, are within the normal pH range of natural water ($6.0 < pH < 9.0$), oxides and hydroxides can act as cation or anion exchangers depending on the solution pH (Atkinson et al., 1967; Parks, 1967; Schwarz et al., 1984; Sposito, 1989). In many areas, organic matter and oxides/hydroxides are the dominant charge sources in the soil zone near the land surface. Those soils normally show a property of variable charge and their ion-exchange capacity and selectivity coefficient for exchangeable ions will vary with the surrounding chemical environment.

The other source of variable charge is nonbonded broken-edge sites on inorganic minerals. For most clay minerals, edge-site charge comprises only a small portion of the total surface charge. However, for minerals without or with little permanent surface charge, such as kaolinite, quartz, and feldspars, the edge site charge becomes the dominant source of surface charge (Sparks, 1986; Domenico and Schwartz, 1990; Appelo and Postma, 1994). Normally, the surface charge on quartz and feldspar can be ignored. However, the surface charge caused by broken edges on kaolinite can be significant for altering ground-water chemistry due to its large surface area (fine grain size).

Another type of surface charge is the "permanent structure charge" that is not affected by pH. The permanent charge in natural systems occurs almost entirely in clay minerals.

Imperfections within the crystal lattice of clay minerals and isomorphic substitutions of cations are the ultimate origin of the charge. The sources normally cause a net negative charge on clay minerals (Robinson, 1962; Bolt, 1979; Freeze and Cherry, 1979). The isomorphic substitutions produce a significant surface charge in the 2:1 layer silicates such as vermiculite and montmorillonite, and to a lesser extent in the mixed layer silicates, such as illite and chlorite. The contribution of cation substitutions to the permanent charge in hydrous oxides and 1:1 layer silicates (kaolinite) is much less than in the 2:1 layer silicates (White and Zelazny, 1986; Sposito, 1989; Appelo and Postma, 1994). Although the surface charge of kaolinite is mainly created by broken-edge sites, which is pH-dependent, its PZC (between 4 and 5) is much lower than the normal pH range of ground water (Parks, 1967; Ferris and Jepson, 1975; Carroll-Webb and Walther, 1988). Therefore, kaolinite normally acts as a cation exchange medium in ground-water systems. In general, clay minerals are the major sources of adsorption and ion exchange sites in aquifers of sedimentary origin with a relatively old age. The activity of organic matter diminishes with time in sediments as a result of diagenesis. The CEC of soils is generally much greater than for aquifer materials because of the abundant organic matter in the soil zone.

Values of CEC for aquifer materials range from about 0.5 meq/100 g of dry solid for coarse sands to 20 meq/100 g for glauconite in glauconitic sands; examples are listed in Table 3.1. The CEC of sandy aquifer materials is usually less than 10 meq/100 g of dry solid mass. Literature data for cation adsorption and exchange on kaolinite are sparse. Measured CEC's for pure kaolinite range from 0 to 15 meq/100g, but are mostly less than 5 meq/100g (Ferris and Jepson, 1975; Bolland et al., 1976; Komarneni, 1978; Lim et al., 1980; Levy et al., 1988;

Domenico and Schwartz, 1990; Gaston and Selim, 1991). These values and the data in Table 3.1 suggest that the CEC values of Dakota aquifer sediments are probably in a similar range.

Table 3.1. Cation exchange capacity values for some aquifer materials in selected studies.

Reference	CEC meq/100g solid	Remarks
Mercado, 1977	about < 5	sandstone aquifer with clay and calcareous layers
Grove and Wood, 1979	7.7	Ogallala Formation
Valocchi et al., 1981a	10.0	shallow alluvial aquifer, sand and gravel with interbedded clay layers
Chapelle and Knobel, 1983	20	fine- to medium-grained glauconitic sand, CEC value for glauconite only
Reardon et al., 1983	0.51 ± 0.09	near surface glaciofluvial sand deposits
Leuchs, 1985*	0.5 ~8	natural aquifer materials
Dahmke et al., 1986*	2 ~ 4	natural aquifer materials
Knobel and Phillips, 1988	14.3	sand & gravel with interbedded clay layers, montmorillonite is the most probable source
Appelo et al., 1990	0.51 1.3 10.1	very coarse sand with calcite shell debris fine sand from a former tidal sand bar clay from a former brackish inland sea
Keller et al., 1991	7.5 ~ 9.8	glacier deposits, drifts and clayey tills
Bjerg et al., 1993	~ 1.0	glacier outwash sandy aquifer, average of 31 samples
Griffioen, 1993	1.5	nonaggregated, noncalcareous fine sand

* : Data from Bjerg et al. (1993), Table 5.

As described earlier, permanently-charged clay minerals are the major sources of the CEC for most aquifer materials. Despite the fact that the CEC of matrix materials is somewhat affected by ionic strength, pH, temperature, composition of exchangeable ions, etc., many studies indicate that a constant CEC gives satisfactory results for modeling purposes, especially for models with neutral pH (Rubin and James, 1973; Grove and Wood, 1979; Valocchi et al., 1981b; Miller and Benson, 1983; Selim et al., 1987; Gaston and Selim, 1990;

Griffioen, 1993; Bjerg et al., 1993; Appelo, 1994a). On the other hand, some studies reveal that CEC varies with chemical conditions and the variations should be incorporated into the model calculations (Pratte et al., 1962; Chapelle and Knobel, 1983; Appelo et al., 1990; Appelo, 1994a). Systems in which surface charge is mainly due to organic matter and oxides/hydroxides may require this approach. A large amount of data is required for such models. However, this type of data is not normally available.

The CEC is sometimes defined as base exchange capacity, that is, the CEC only includes the part of the negative charge surplus of the exchanger that is compensated by alkaline cations but does not include that part occupied by protons (Pratt et al., 1962). Based on this definition, for aquifer materials with a constant total surface charge, CEC can vary with pH if the surface property is pH-dependent (Anderson and Sposito, 1992). Some recent studies have incorporated proton exchange into numerical models to more realistically simulate such systems (Griffioen, 1992, 1993; Appelo, 1994a). In this case, the amount of surface charge sites occupied by protons varies with pH, and hence the base exchange capacity changes with pH although a constant CEC (surface charge) model is applied. The proton exchange reaction is a strong buffer for pH changes in solution. Transfer of hydroxy- or bicarbonate-complexes can also be responsible for pH-buffering (Griffioen, 1992 and 1993).

Selectivity coefficients have been intensively studied in the last few decades. Bruggenwert and Kamphorst (1979) reviewed the experimental data on cation exchange for freshwater conditions. Their survey showed that the selectivity coefficient for a pair of exchangeable cations varies widely for different soils and solution compositions. The variation is caused partially by the properties of the different natural cation adsorbents involved. Variations are also caused by changes in the adsorbed ion activity with water composition.

Cation exchange selectivity values vary as the equivalent fraction of cation species in the solution phase changes (Deist and Talibudeen, 1967; Sposito, 1981; Levy et al., 1988; Mansell et al., 1988; Rieu et al., 1991). Rieu et al. (1991) analyzed 74 different conditions for Na-Ca exchange equilibria and concluded that a direct fit of experimental values of these selectivity coefficients appears questionable because of large experimental errors. Appelo et al. (1990) also found that ion exchange coefficients are not identical in freshwater and saltwater, and thus the exchange capacity could vary. They indicated that it is difficult to quantify the factors which govern the variation of CEC and selectivity coefficient, so that incorporation of variability in the model may be futile at present. Mansell et al. (1988) tried to duplicate a set of experimental data by applying variable selectivity coefficients and two-region (mobile-immobile) flow in a numerical model. However, they were unable to satisfactorily predict the breakthrough curves for divalent cations. They indicated that the absence of additional functions in the model, e.g., ion pairing and kinetic processes may have been responsible. Bjerg et al. (1993) illustrated that the great variation in selectivity coefficients in their study is mainly due to experimental uncertainty related to the very low CEC.

The main cations involved in exchange are Na, K, Ca, and Mg. The divalent cations generally have higher affinity than the monovalent cations (Freeze and Cherry, 1979; Appelo and Postma, 1994). From the standpoint of chemical thermodynamics, multiple-cation exchange simulations, such as a ternary ion exchange of Ca, Mg and Na, are best represented by ternary-exchange isotherms (Mansell et al., 1988). However, such data is generally not available. Most numerical models have applied binary exchange isotherms and assumed that this approach provides a reasonable estimate of the multiple-cation exchange model.

Studies indicate that the selectivity coefficient for the Ca-Mg ion pair is constant over large range of adsorbed Ca/Mg ratios and ionic strength (Jensen and Babcock, 1973). The typical range for the Vanselow selectivity coefficient of Ca-Mg exchange (same as the Gaines and Thomas equation for homovalent exchange) is 0.6 to 0.9 based on Freeze and Cherry (1979). More recent studies show a similar range of 0.5 to 1.0 for the selectivity coefficient (Selim et al., 1987; Gaston and Selim, 1990, 1991).

Some investigations have shown that a preference of Mg over Ca occurs on vermiculite when the adsorbed Mg occupies a certain fraction of the adsorbed cations (e.g., Levy and Shainberg, 1972). The phenomenon is explained by the fact that at high Mg concentration the interlayer spacing of the clay minerals contracts, so that the larger Ca ion cannot easily penetrate. At low Mg concentration, the interlayer spacing is larger and the small Mg ion is more loosely held.

The most often mentioned anion exchange reaction in aquifers is the exchange between hydroxyl and fluoride (Zack, 1980; Boyle, 1992; Burt, 1993). Boyle showed that the F^- anion exchange capacities of a Pennsylvanian sandstone aquifer are less than 0.037 meq/100g. This anion exchange reaction may be important for buffering the solution pH in near neutral conditions.

3.3. PRECIPITATION/DISSOLUTION OF MINERALS

Cation exchange is usually accompanied by precipitation or dissolution of minerals, particularly carbonate minerals. Na-HCO_3 type water is commonly formed where freshwater flushes saltwater. Cation exchange of Ca and Mg for Na on clays increases Na concentration and depletes Ca and Mg concentrations. Concomitantly, HCO_3 concentration increases from

dissolution of calcite and/or dolomite (Riffenburg, 1925; Schwartz and Muehlenbachs, 1979; Thorstenson et al., 1979; Knobel and Phillips, 1988; Zack and Roberts, 1988; Plummer et al., 1990; Boyle, 1992). Na-SO_4-HCO_3, Na-HCO_3-SO_4, and Na-mix-anion waters also occur in aquifers undergoing cation exchange. In some systems, dissolution of carbonate minerals and gypsum occur simultaneously while Ca is depleted by cation exchange (Riffenburg, 1925).

For an aquifer system with saltwater intrusion, reverse cation exchange can form Ca-Cl type water in the mixing zone. Decreases in HCO_3 concentration result from the precipitation of calcite in such systems (Howard and Lloyd, 1983; Mercado, 1985; Appelo and Postma, 1994).

Precipitation/dissolution of calcite is believed to be a common reaction in the Dakota aquifer system because the mineral is common in the formations. Geochemical simulation of ground waters for this dissertation and by Macfarlane et al. (1990) also indicates that most of the Dakota waters from the confined portion of the aquifer are in equilibrium with respect to calcite.

3.4. REDOX REACTIONS

Redox conditions related to mixing of waters have been studied as causes of "Roll front" type uranium deposits in sandstone (Hostetler and Garrels, 1962; Harshman, 1966; Walsh et al., 1984). The studies reveal that characteristic concentration waves develop involving precipitation/dissolution of iron, selenium, and uranium minerals during redox changes. Transformation of chemical species due to change of redox environments have also been described in ground-water pollution investigations (Roberts et al., 1982, 1986; Ceazan et al., 1989; Smith et al., 1991; Kent et al., 1994). Redox conditions and solution-phase

complexation can substantially affect solute transport if the reactants and products of these reactions are also participants in heterogeneous reactions such as precipitation/dissolution and surface reactions (Means et al., 1978; Kirkner et al., 1984; Cederberg et al., 1985; Lewis et al., 1986; Bahr, 1990). Redox reactions are often important controls on the distribution of SO_4 and dissolved CO_2 and associated species in ground water.

The assumption that CO_2 charging of ground water occurs predominantly in the near-surface soil zones has been accepted for a long time (Freeze and Cherry, 1979). More recent studies show that high CO_2 partial pressures can occur at depths of several meters to tens of meters in the vadose zone (Wood and Petraitis, 1984; Keller, 1991), and deep in regional ground-water flow systems (Chapelle and Knobel, 1985; Knobel and Phillips, 1988; McMahon et al., 1990; Plummer et al., 1990). Other than carbonate mineral dissolution, microbial oxidation of organic matter is often quoted as the source of dissolved carbon dioxide and its redistributed species, e.g., HCO_3^- and CO_3^{2-} deep in the subsurface (Thorstenson et al., 1979; Chapelle and Knobel, 1985; Knobel and Phillips, 1988; McMahon et al., 1990; Plummer et al., 1990).

Pyrite oxidation is considered to be one of the most important acid-producing reactions in geological systems. It is often the major source of acid mine drainage (Mayo et al., 1992). The reaction is described as (Appelo and Postma, 1994)

$$FeS_2 + \tfrac{15}{4}O_2 + \tfrac{7}{2}H_2O \rightarrow Fe(OH)_3 + 2SO_4^{2-} + 4H^+ \qquad (3.1)$$

Oxidation of pyrite and organic sulfide occurs near the surface recharge sources where dissolved oxygen is available (Rogers, 1987; Knobel and Phillips, 1988; Keller et al., 1991).

This reaction is also believed to occur in parts of the Dakota aquifer where dissolved oxygen and abundant pyrite beds and scattered crystals exist (Macfarlane et al., 1990).

When SO_4 is carried deeper into the aquifer where the chemical environment becomes moderately reducing, reduction of sulfate is triggered by organic matter or natural gas (Riffenburg, 1925; Champ et al., 1979; Thorstenson et al., 1979; Jackson and Patterson, 1982; Chapelle and Knobel, 1985; Knobel and Phillips, 1988; Plummer et al., 1990). Sulfate reduction by organic matter is catalyzed by bacteria. The redox equation can be written as

$$2CH_2O + SO_4^{2-} \rightarrow 2HCO_3^- + H_2S \qquad (3.2)$$

where CH_2O denotes organic matter. The irreversible equation indicates that reduction of one unit of SO_4 will generate two units of HCO_3. The reaction can explain the relative concentrations of SO_4 and HCO_3 in somewhat isolated aquifers (Rifferburg, 1925; Schwartz and Muehlenbachs, 1979; Thorstenson et al., 1979; Chapelle and Knobel, 1985). The odor of H_2S in well water is an indication that sulfate reduction is occurring. If dissolved concentrations of iron or other metal ions are high enough, sulfide minerals will form.

3.5. ION CHROMATOGRAPHY IN HYDROGEOCHEMICAL PROCESSES

The different selectivity for different cations leads to varying adsorption of cations, which in turn implies variable retardation. The result is a spatial separation of solute cations that occurs during movement of waters with different compositions through an aquifer. The phenomenon was titled "ion chromatography" by DeVault (1943). Ion chromatography caused by cation exchange has been observed in the field and laboratory investigations of solute transport (Grove and Wood, 1979; Valocchi et al., 1981b; Chapelle and Knobel, 1983; Appelo et al., 1990; Bjerg et al., 1993). A variety of numerical models has been developed to simulate

complex multicomponent chromatographic patterns (Grove and Wood, 1979; Valocchi et al., 1981b; Appelo et al., 1990; Friedly and Rubin, 1992; Bjerg et al., 1993; Appelo, 1994a).

Ion chromatography caused by cation exchange is conspicuous in the aquifer freshening process. Due to the low concentrations of ions in freshwater, a long time is required for the incoming freshwater to compensate the buffering capacity of solid surfaces in the aquifer. In saltwater intrusion, the high ionic concentrations of the intruded saltwater can neutralize the surface sites in a relatively short period and distance. Thus, the features of ion chromatography have rarely been observed for natural salinization (Appelo and Postma, 1994).

Figure 3.1 illustrates the general features of ion chromatography. The concentration distribution of any species along a flow path is composed of successive fronts separated by plateau zones (i.e., constant composition). A front is any variation of dependent variables of fluid- or solid-phase concentrations in the direction of flow. Alternative terms used for front are wave, boundary, and transition. Four types of fronts can be developed during hydrogeochemical evolution: self-broadening, self-sharpening, indifferent, and composite fronts (Helfferich and Klein, 1970; Pope et al., 1978; Charbeneau, 1981; Helfferich, 1989; Schweich et al., 1993a). As shown in the diagram, a self-broadening front has spread in addition to that caused by dispersion, and retains or approaches a proportionate pattern in which its diffuseness increases in proportion to the distance traveled. A self-sharpening front becomes or remains a shock in the absence of dispersion. In reality, a steady-state width is attained in which the sharpening effect of the sorption isotherm and the spreading effect of dispersion balance one another. The composite front is a combination of partly self-broadening and partly self-sharpening fronts. An indifferent front is an unretarded front for the movement of

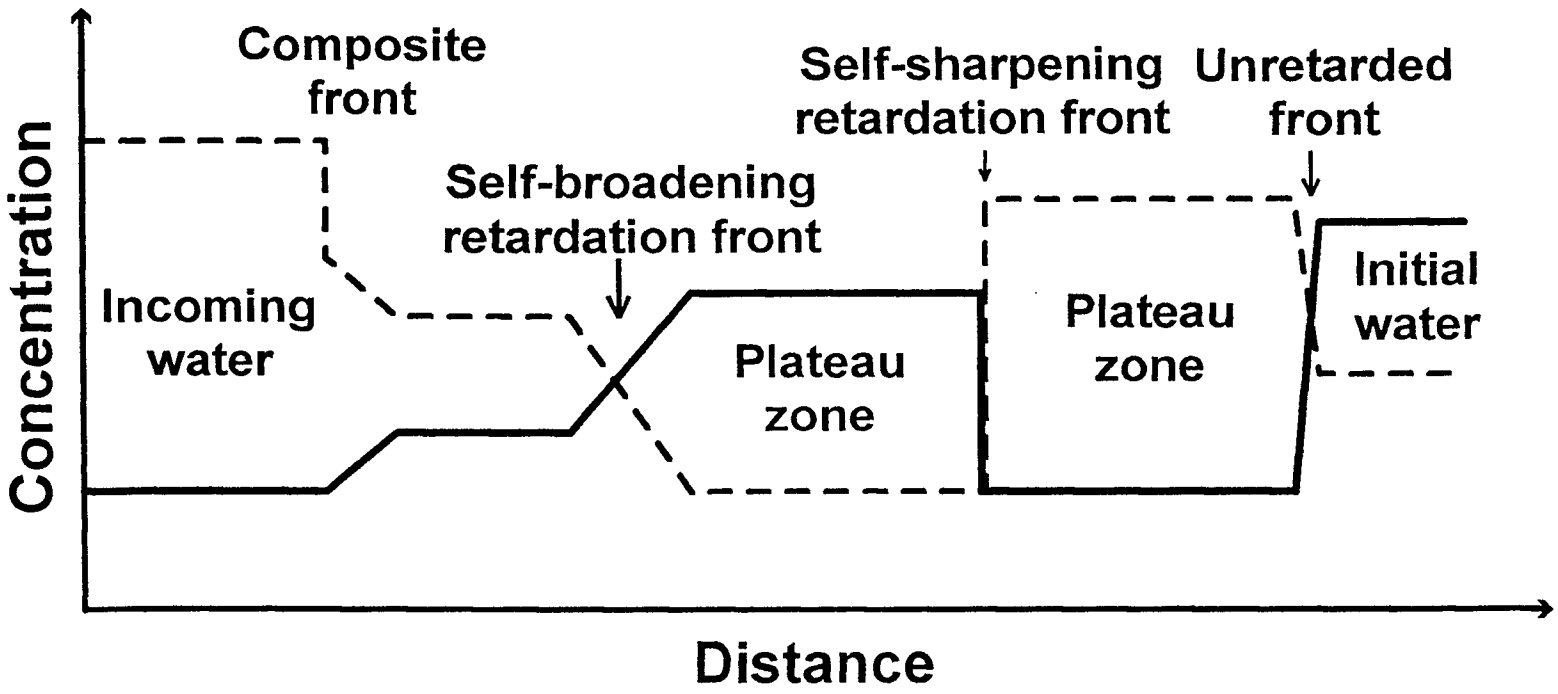

Figure 3.1. Schematic diagram of concentration profiles of species A and B showing the phenomenon of ion chromatography (modified from Schweich et al., 1993a).

conservative species. According to linear dispersion theory, dispersion will cause spreading in proportion to the square root of travel distance. The unretarded indifferent front is also frequently called a "salinity front (wave)" in the literature; it is also referred to as "mixing front" in this report. In Figure 3.1, the simultaneous variation of the concentrations of A and B, and so of all the components present, is a fundamental property of the system which is called "coherence". Following the rule of coherence, the front velocities of each chemical species involved in the reaction are equal at any point in space and time (Novak et al., 1988; Helfferich, 1989; Schweich et al., 1993a).

Ion chromatography can also result from precipitation/dissolution reactions (Walsh et al., 1984; Bryant et al., 1986, 1987; Krebs et al., 1987; Novak et al., 1988; Helfferich, 1989; Schweich et al., 1993b). The importance and applications of precipitation/dissolution reactions to constituent distributions during ground-water flow have only recently been widely recognized. Walsh et al. (1984) studied uranium ore leaching and pointed out the importance of mineral sequences to the wave behavior of constituents. They indicated that the precipitation/dissolution reactions are controlled by redox conditions along a recharge front. Other practical examples are found in leach mining (Gao et al., 1981; Totam et al., 1981) and transport of metals in aquifers (Dria et al., 1987). The development of fundamental theories for such systems has been presented by Bryant et al. (1986 and 1987), Novak et al. (1988), and Helfferich (1989). The features of ion chromatography caused by ion exchange are further discussed for a 1-D conceptual model in Chapter 7.

CHAPTER 4
METHODOLOGY

Water chemistry data used for this research was obtained from the KWATCHEM database and ongoing investigations of the Dakota aquifer project at the KGS (Kansas Geological Survey). Geological information was collected from water-well and oil and gas borehole logs available at the KGS. Sediments sampled from one of the drilling cores were processed and sent to the soil laboratory of Kansas State University for CEC determination.

4.1. CRITERIA FOR THE SELECTION OF WATER CHEMISTRY DATA

Chemical data for more than 450 water samples from different geological formations, mainly the Dakota aquifer, were extracted from the KWATCHEM database. KWATCHEM contains water sample data mainly for the Dakota aquifer, although data are included for the Cedar Hills Sandstone, Greenhorn Limestone, and overlying alluvial aquifers in the Dakota outcrop zone. Data sources include KGS publications, RASA (Regional Aquifer-System Analysis program of the U. S. Geological Survey), the WATSTORE database of USGS, and the Kansas Department of Health and Environment. The sample collection period extends from the late 1940's to the present. Part of the data comprises analyses of water samples collected during the last several years as a part of the Dakota aquifer program of the KGS. Field pH, water temperature, and electrical conductivity were measured during collection of most of the samples. The samples were filtered, acidified, and refrigerated in the field and analyzed by the Analytical Services Section of the KGS.

Two criteria were applied for selecting the water chemistry records used in this dissertation: 1) The record includes analyses for Ca, Mg, Na, HCO_3, SO_4, and Cl, and 2) The charge-balance error is less than 15%. The higher charge-balance errors are for historical records; recent analyses of the KGS usually have errors of less than a few percent. Although most of the records have charge-balance errors less than 10%, a somewhat higher error was accepted for some data because the additional coverage of the data was more important than a low error.

Potassium (K) was not included in this study for three different reasons. First, the amount of K data is less than for the major constituents included in the study because Na and K were not individually determined during early analyses of waters, but calculated based on charge balance. Second, the percentage of K with respect to the total cation concentration is very small in Cedar Hills saltwater in central Kansas (Macfarlane et al., 1988). Therefore, the adsorbed K concentration is expected to be very small on surface sites. The K concentration percentage in freshwater affected by cation exchange is small relative to the Na percentage but can be appreciable relative to the Ca and Mg percentages. However, the overall maximum effect of K on the evolution pattern of cation exchange is negligible (Appelo, 1994a) and is certainly less than other variables that could affect chemical pattern in the system. Third, the inclusion of K in the coupled model would increase the complexity of the simulation, thereby substantially increasing the already lengthy time required for the computations given the computer systems available.

For multi-records at one location, the latest analysis was selected because the reliability of the analytical techniques is generally better. However, none of the time-series records shows a significant variation of water chemistry in the sampling period. Dissolved

constituent activities and mineral saturation indices were then calculated for the sample data selected using the geochemical equilibrium model SOLMINEQ.88 (Kharaka et al., 1988). Temperatures were estimated for records without field measurements by

$$T\ (°C) = 15.0 + (\text{well or sampling depth, ft})/100$$

where 15 °C is the mean annual air temperature in the general region. The second term of the right-hand side of the equation assumes a thermal gradient of 1 °C/100 ft.

A pH value was estimated for samples without field analysis by forcing the solution to be saturated with respect to calcite. This assumption is normally true for waters from the Permian aquifer and confined part of the Dakota aquifer in the study area since carbonate minerals are ubiquitous in the aquifer system (Macfarlane et al., 1990). The assumption was verified for some data by procedures such as comparison of a simulated pH with the field pH of water with similar properties and location, or examination of the saturation indices for minerals known to exist in the sampled interval. Although the assumption of calcite saturation may not be true for some of the water samples in the outcrop zone, the simulated data were still valuable for the data analyses.

4.2. GEOLOGY DATABASE FOR DAKOTA AQUIFER IN NORTH-CENTRAL KANSAS

Maps of the geological configuration of the Dakota aquifer published by Macfarlane et al. (1990) did not cover the area near the Dakota outcrop zone in north-central Kansas. Data were obtained to map the top and bottom surfaces of the Dakota aquifer in the study area. The mapping was needed as basic information for developing models of the geohydrological system. The area includes Jewell, Republic, Washington, Mitchell, Cloud, Clay, Lincoln,

Ottawa counties. Data were also collected from Smith, Osborne, eastern Russell, northern Ellsworth, and northern Saline counties as an outside buffer zone.

More than 500 geological logs in KGS publications, water-well records, and oil and gas files were examined. The well-log record of test holes published in KGS Bulletins are the most detailed and reliable of the data. The most numerous log data were the water-well driller's reports (WWC-5 files of the KGS). The quality of these data is not as good as the KGS publications. Knowledge of the local geology and comparison of several logs to each other within a small area were used as methods to determine geological boundaries from these data. Most of the oil and gas well logs were used to obtain information where no water-well logs are available, such as in the northwestern part of the study area. Since the Dakota Formation was not the target zone for oil exploration, it was often not recorded or only approximately interpreted. Dakota boundaries estimated from the oil and gas well log data are the least reliable.

The Longford Member comprises the major part of the Kiowa Formation in north-central Kansas. Its lithology is very similar to that of the Dakota Formation and it is very difficult to distinguish from the Dakota in the subsurface. Also, the quality of most of the well-log records is not sufficient for determining a reliable Dakota-Kiowa boundary. Therefore, only contour maps for the top and bottom of the Dakota aquifer were constructed (Figures 2.2 and 2.3).

4.3. DETERMINATION OF CATION EXCHANGE CAPACITY IN SEDIMENTS

In September, 1993, sediments were sampled from variable depths of the KGS #1 Jones core through the Dakota aquifer and analyzed for bulk CEC. The KGS #1 Jones test hole was drilled and cored during May, 1990, at 10S-08W-02AAAC in north-central Lincoln County (Macfarlane et al., 1991b). The samples included various lithologies which represent different depositional environments. The samples were ground to their original grain sizes or to pass a sieve of 250 μm. Each sample was split into two separate portions, each consisting of a little more than 100 g, for a duplicate check of laboratory results. The samples were sent to the Soil Test Laboratory of Kansas State University for CEC determination by standard procedures (Hesse, 1972).

CHAPTER 5

RESULTS AND INTERPRETATION OF THE DAKOTA GROUND-WATER CHEMISTRY

5.1. CLASSIFICATION OF WATER SAMPLES

Saltwater from the Cedar Hills Sandstone discharges into the Dakota aquifer in the Cedar Hills subcrop zone. The mixture of Permian saltwater and Dakota water from the west follows the regional flow to the east. The regional flow also mixes with local recharge from the Upper Cretaceous confining layer and the Dakota outcrop zone to the east. The complicated water chemistry due to mixing of waters in the system allow examination of the possible scenario of a relatively recent evolution history of water chemistry in the Dakota aquifer.

Water sample data were categorized into several groups to analyze systematically the water chemistry and possible chemical reactions in the Dakota aquifer. Four major groups of waters were selected based on the geological formations from which the water samples came: Quaternary terrace and alluvial deposits, the Greenhorn Limestone, the Dakota aquifer, and the Permian Cedar Hills Sandstone. The selected Quaternary alluvial waters were used to examine the relationships of the stream-aquifer interactions in the study area. The Dakota waters were further divided into three subgroups based on the geographic location, sampling depth, and salinity of the water. The three subgroups are waters in the unconfined portion of the Dakota aquifer, the confined portion of the Dakota aquifer east of the Cedar Hills subcrop zone, and the confined Dakota aquifer west of the Cedar Hills subcrop. The geographic distribution of the water samples is displayed in Figure 5.1. The water chemistry data for different groups are listed in Appendix A. Data in Table A.4 are not shown in Figure 5.1 and the following

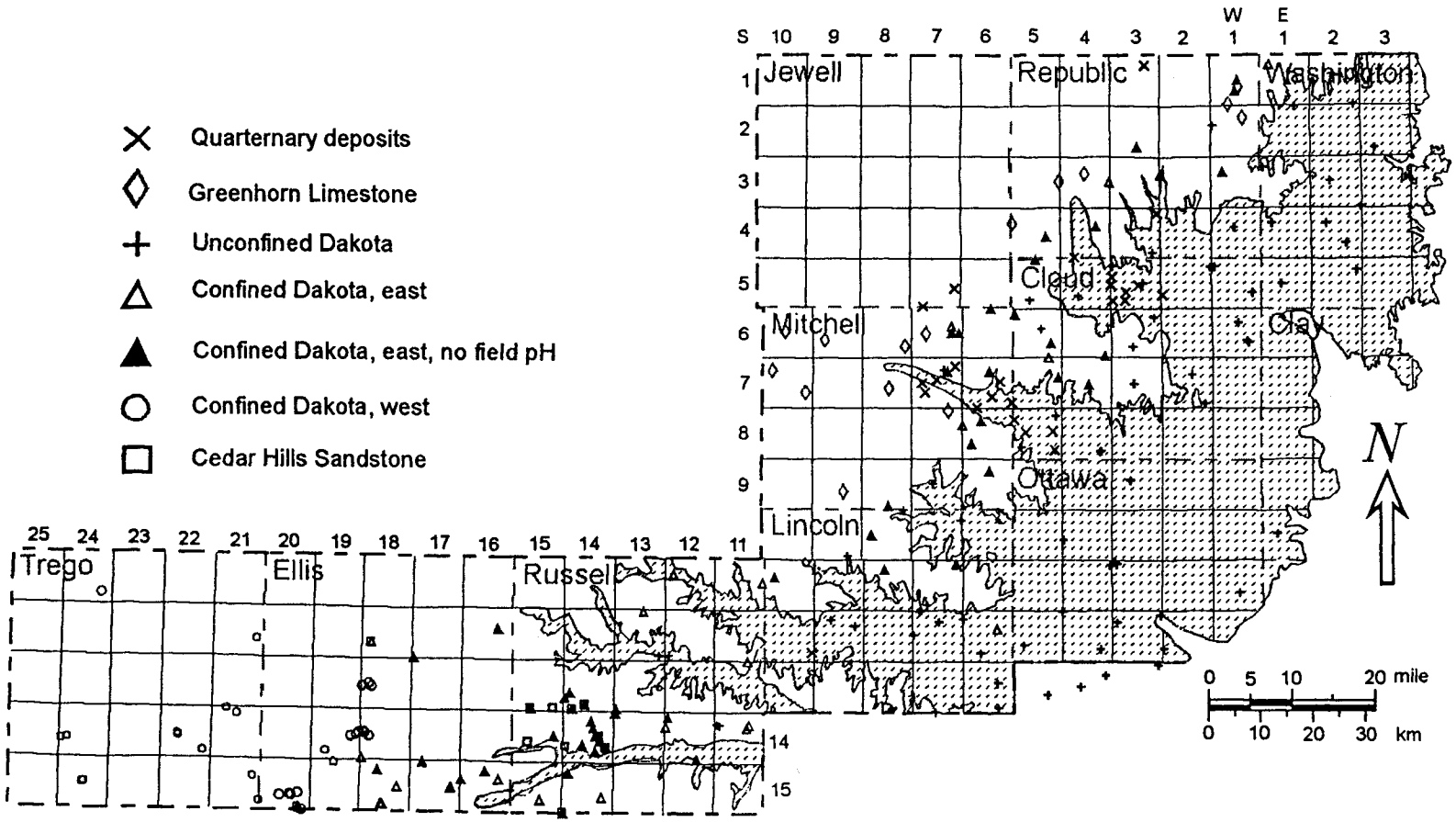

Figure 5.1. The location of ground-water samples.

diagrams because data in Table A.3 alone are enough to represent the unconfined Dakota water group.

A major transition of water chemistry in the study area occurs where saltwater from the Cedar Hills Sandstone intrudes into the confined portion of the Dakota aquifer. The chemical divide in the confined Dakota aquifer is located in the vicinity of R18W in western Ellis County. Dakota water to the west of the Cedar Hills subcrop represents ground water that flows from the recharge area in southeastern Colorado and southwestern Kansas. Leakage through the top and bottom confining units also affects the water chemistry in this region. Confined Dakota water above and to the east of the Cedar Hills subcrop, which has been influenced by the Cedar Hills saltwater, has very different characteristics from the water to the west.

The criteria for determining whether waters are grouped as confined or unconfined Dakota are: 1) The geographic location. When the Dakota water is located geographically far into the confined area, the water is classified as the confined Dakota group. If the sampling location is in the Dakota outcrop zone, the water generally is classified as the unconfined Dakota group. 2) The water salinity. If the sampling location is in the confined area close to the Dakota outcrop zone where the confining layer is thin, the classification is determined by examining its water quality. If the TDS concentration is low, it indicates that the water is largely from recent surface recharge and is classified as the unconfined Dakota group. If the TDS content is high, the water is considered to be less affected by recent surface recharge and is classified as the confined Dakota group. There are some cases where waters with unusually high TDS contents were sampled in the Dakota outcrop zone near the east edge because they were affected by water from the underlying Permian bedrock. 3) The sampling depth. Where

high salinity water was found in the Dakota outcrop zone, the sampling depth was examined to see if the sampling zone is deep enough to be considered as a possible confined zone. The mixing of waters forms a wide transition zone, thus no exact TDS values were used for the grouping criteria. The grouping decisions were based on "best judgment" after weighting the importance of all the criteria.

The number of samples, means and standard deviations of the concentrations of the major constituents and TDS for the six water groups are listed in Table 5.1. In general, water chemistry varies more in the Quaternary deposits and both the confined Dakota water groups than in the other three groups due to mixing of different water sources. The low TDS concentrations of the unconfined Dakota water clearly show the effect of surface recharge on the chemistry in contrast with the high TDS content of water in the Cedar Hills Sandstone which is the major source of saltwater intrusion. Water in the Greenhorn Limestone contains high Ca/cation and SO_4/anion ratios and relatively stable HCO_3 concentration. In comparison to the water in Quaternary deposits, water in the west confined Dakota has a lower Ca/cation ratio and higher Na/cation ratio although their average TDS concentrations are at the same range. The abnormally high Mg concentration of the Cedar Hills water indicates additional sources of Mg in the formation.

As described in Chapter 2, halite is the major matrix cement for the Cedar Hills Sandstone in western Kansas. The adjacent formations above and below the Cedar Hills Sandstone also contain halite. The halite solution from those halite-contained formations is conducted by the Cedar Hills Sandstone to the east and discharges to the Dakota aquifer in central Kansas. Thus Na and Cl are the major components of dissolved constituents in the Cedar Hills water. Figure 5.2 shows that the Na/Cl equivalent ratio is very close to one for

Table 5.1. The means and standard deviations for the major constituents and TDS for the categorized water groups.

Water group	Quaternary deposits		Greenhorn Limestone		Unconfined Dakota		Confined Dakota, east		Confined Dakota, west		Cedar Hills Sandstone	
Number of samples	29		15		206		130		68		10	
	mean	S.D.	mean	S.D.	mean	S.D.	mean	S.D.	mean	S.D.	mean	S.D.
Ca meq/L	9.27	7.50	11.5	6.24	4.88	3.26	7.89	9.48	2.31	3.22	26.9	8.89
Mg meq/L	2.86	2.93	1.98	1.27	1.46	1.33	10.9	19.3	2.10	3.59	81.4	36.2
Na meq/L	19.0	38.8	4.98	3.26	3.05	2.76	133	212	29.1	32.8	763	220
HCO_3 meq/L	7.29	2.15	6.08	0.729	4.61	2.00	9.63	5.51	5.91	2.29	18.4	7.97
SO_4 meq/L	7.27	10.7	7.37	6.92	2.50	2.93	19.4	27.1	6.98	5.02	113	38.6
Cl meq/L	15.7	33.9	3.72	2.91	1.63	1.99	123	209	20.0	30.1	741	230
TDS mg/L	1850	2560	1130	656	570	371	9690	14700	1980	2150	51600	15200

S.D. : standard deviation

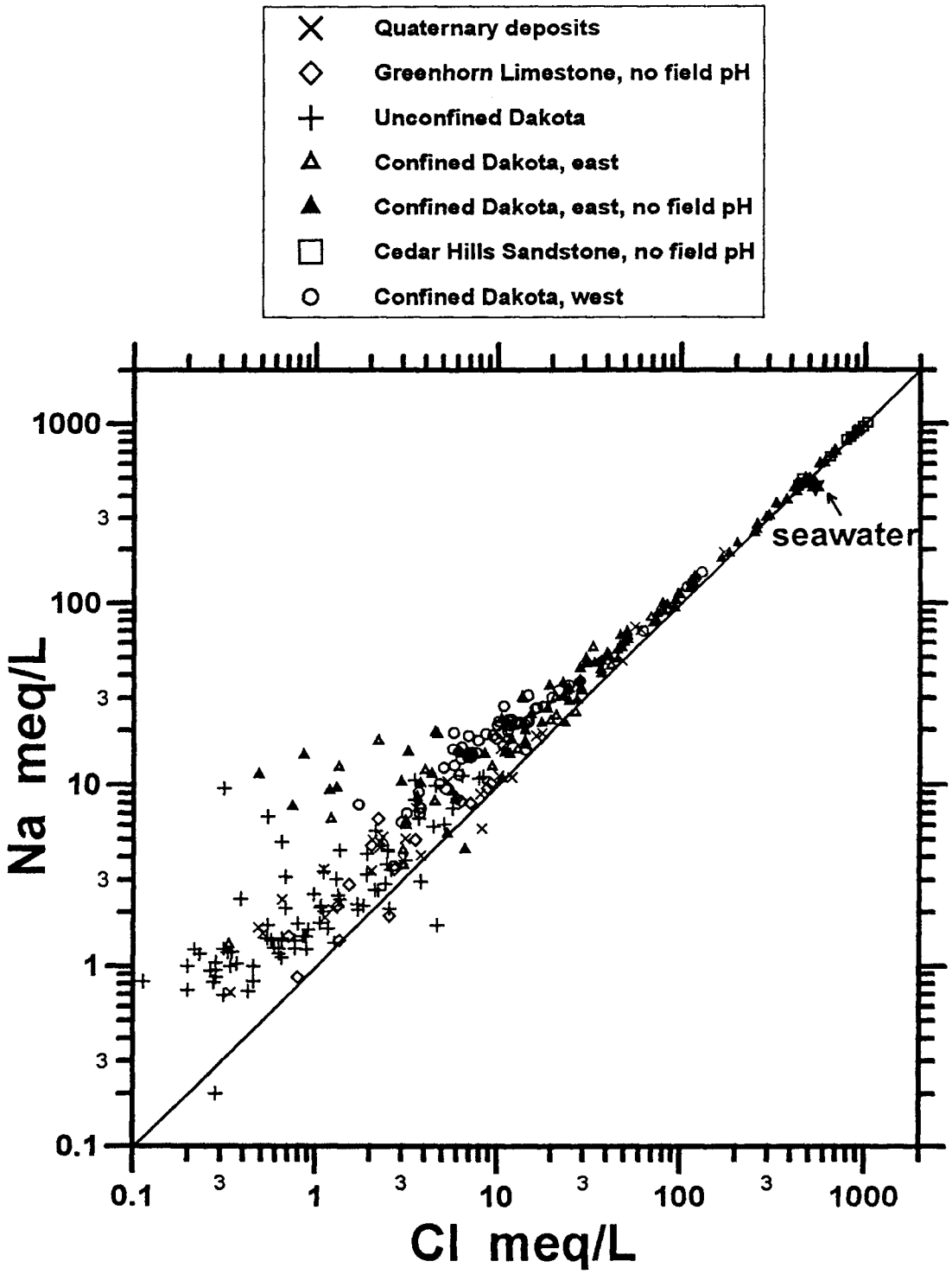

Figure 5.2. Dissolved Na versus Cl. The solid line represents the 1:1 equivalent ratio.

Cedar Hills water (0.999 for the water of highest TDS concentration). Na and Cl are the major dissolved constituents in all the different ground waters with TDS content greater than 4,000 mg/L as the logarithmic linear relationships show in Figures 5.3 and 5.4. The logarithmic linear relationship of Na/TDS extending to even lower salinity indicates that dissolved Na remains as the dominant cation for water in the confined Dakota aquifer, especially to the west of Cedar Hills subcrop. In general, dissolved constituents other than Na and Cl start to increase in percentage in solution for water with lower TDS concentrations. The Ca percentage is generally higher in waters of Quaternary alluvium, Greenhorn Limestone, unconfined Dakota, and part of the confined Dakota aquifers. Most of the west confined Dakota waters and some of the east confined Dakota waters contain very low Ca concentrations (Figure 5.5). Most of the waters from west confined Dakota also contain relatively low Mg concentrations (Figure 5.6). Both Ca and Mg show that part of the waters in the west confined Dakota have been affected by recharge from both above and below.

Figure 5.7 depicts that there are two different relationships of SO_4 with TDS concentration. Waters of unconfined Dakota, Greenhorn Limestone, and Quaternary deposits have a similar SO_4 relationship. Waters of Cedar Hills Sandstone and east confined Dakota aquifer follow another SO_4 relationship. The SO_4/TDS values of waters in the west confined Dakota overlap the transition zone of these two different groups. The HCO_3 concentrations for the ground-water system are in a relatively narrow range compared to the ranges for the other major dissolved constituents (Figure 5.8). It appears that the HCO_3 concentrations for most of the ground-water samples are confined to an upper limit of about 17 meq/L except waters (TDS of 30,000 to 60,000 mg/L) from near the Cedar Hills subcrop. Apparently, dissolution of carbonate minerals has been triggered by the mixing of Cedar Hills and Dakota waters

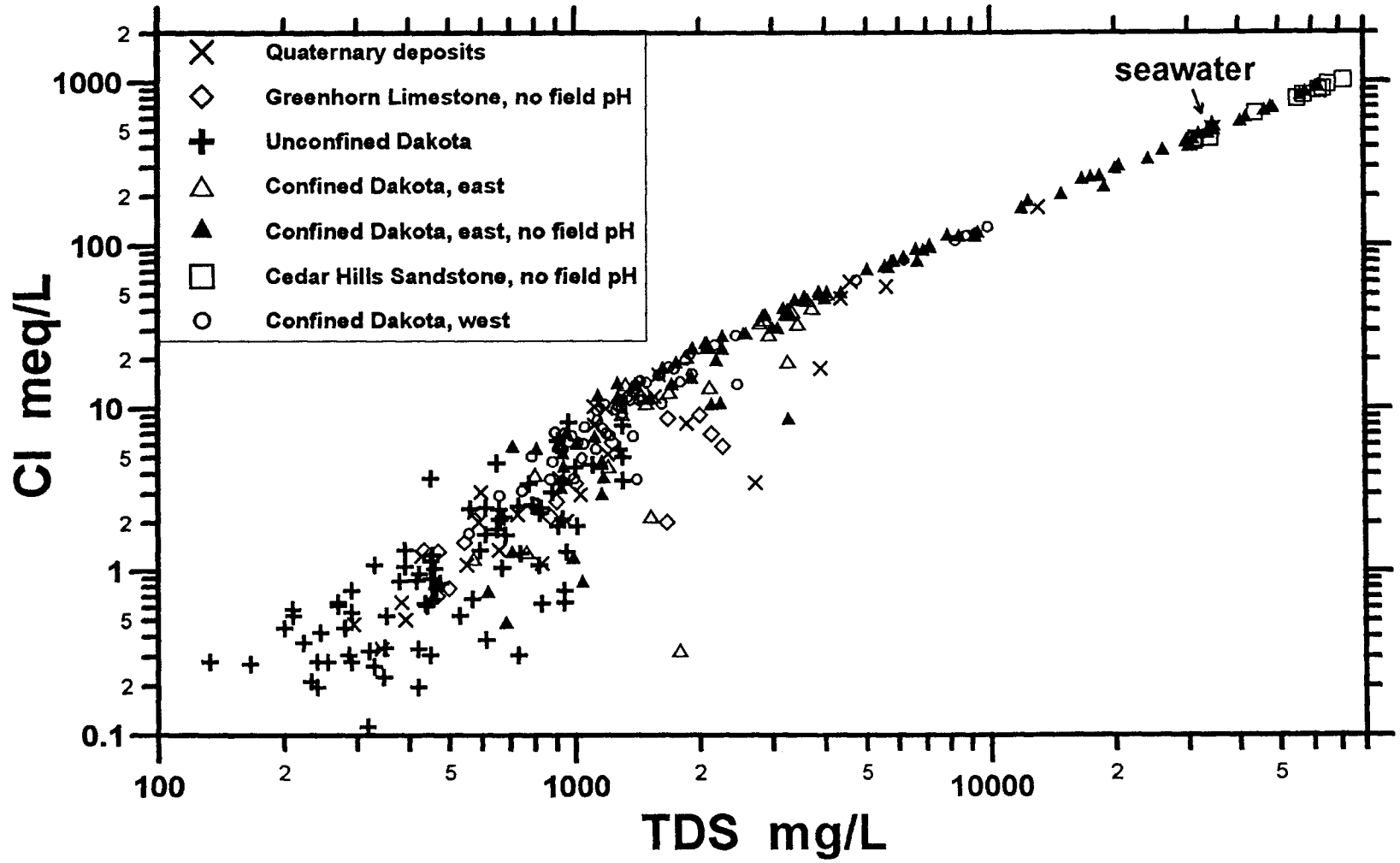

Figure 5.3. Dissolved Cl concentration versus TDS content.

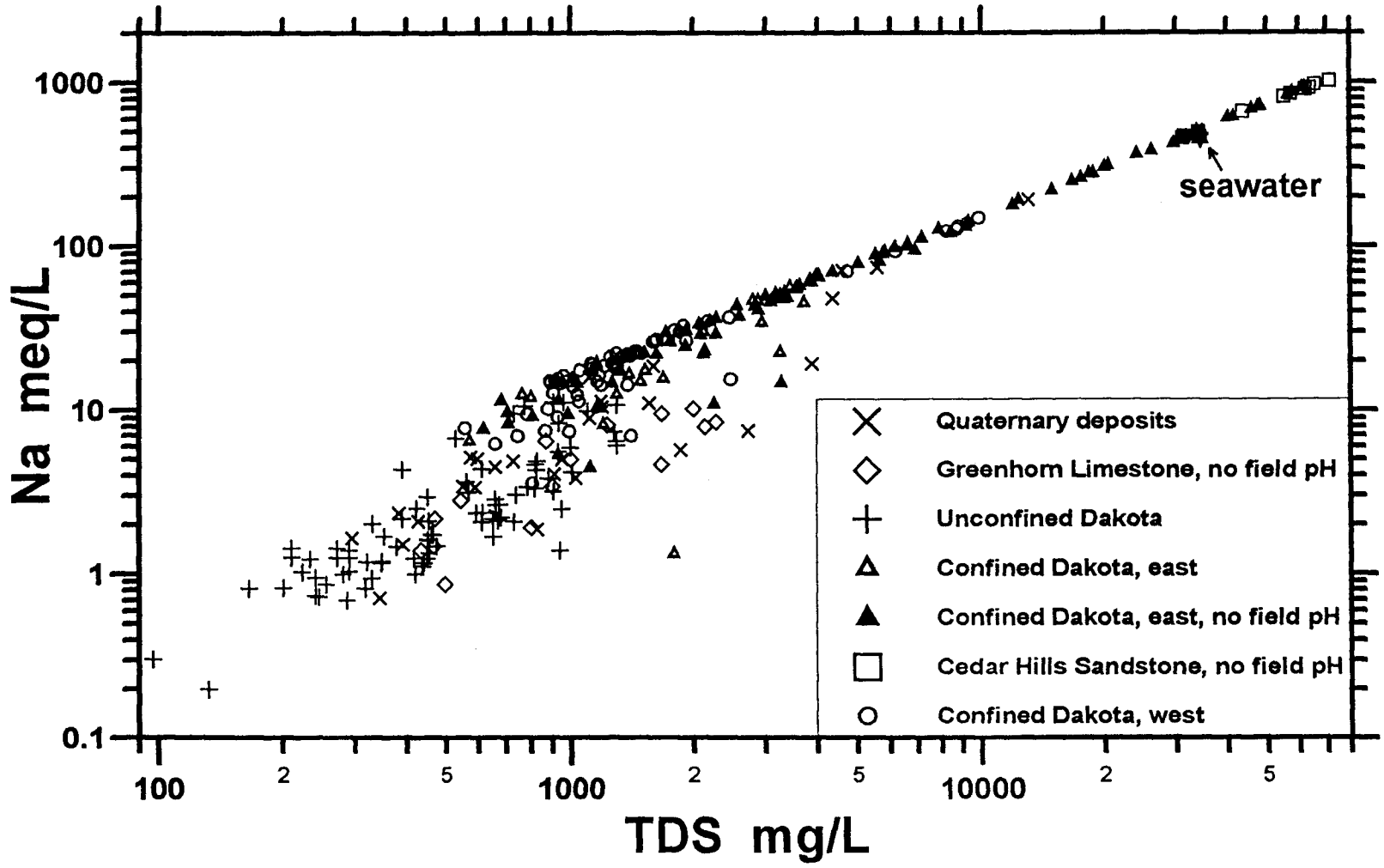

Figure 5.4. Dissolved Na concentration versus TDS content.

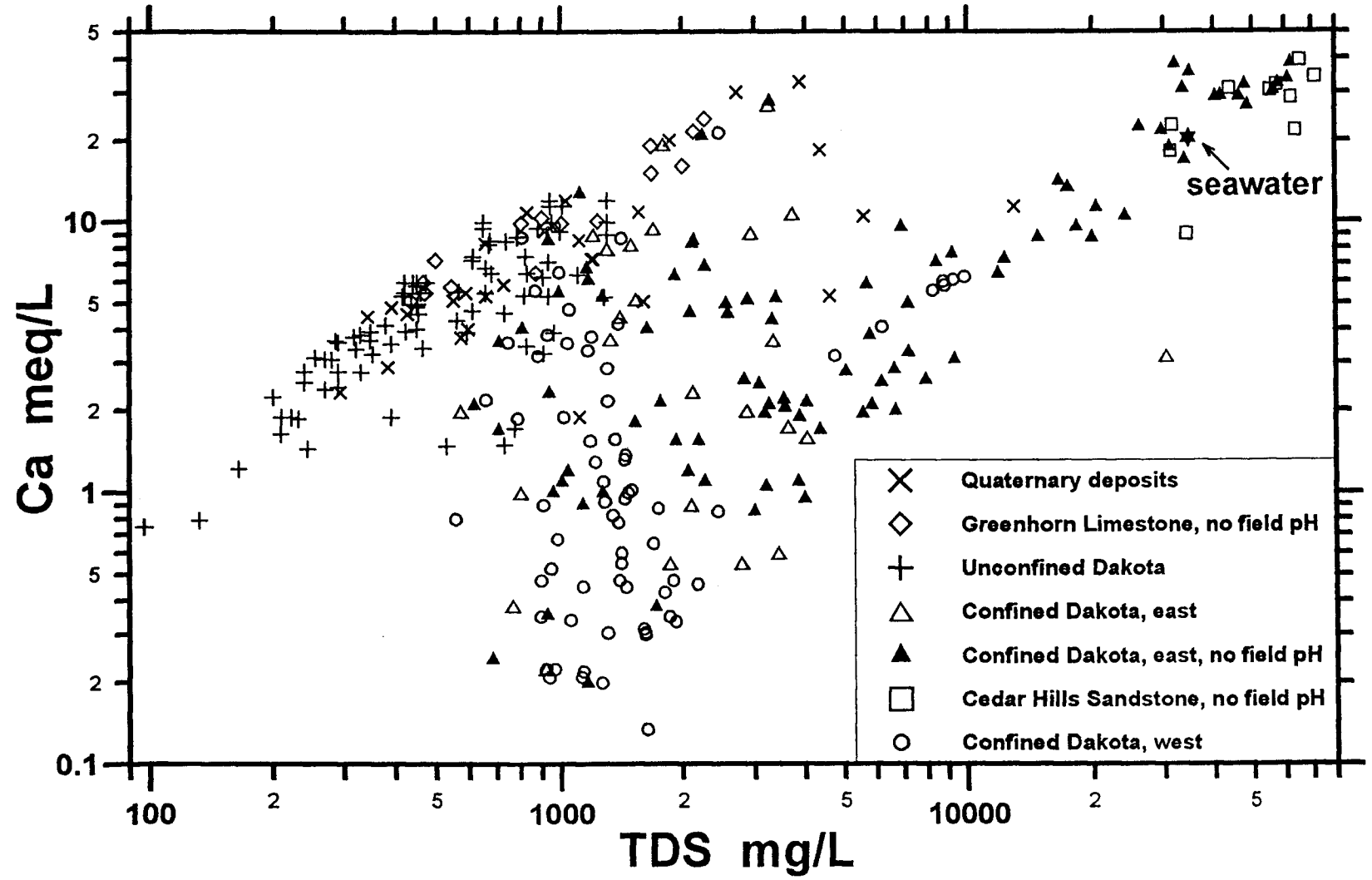

Figure 5.5. Dissolved Ca concentration versus TDS content.

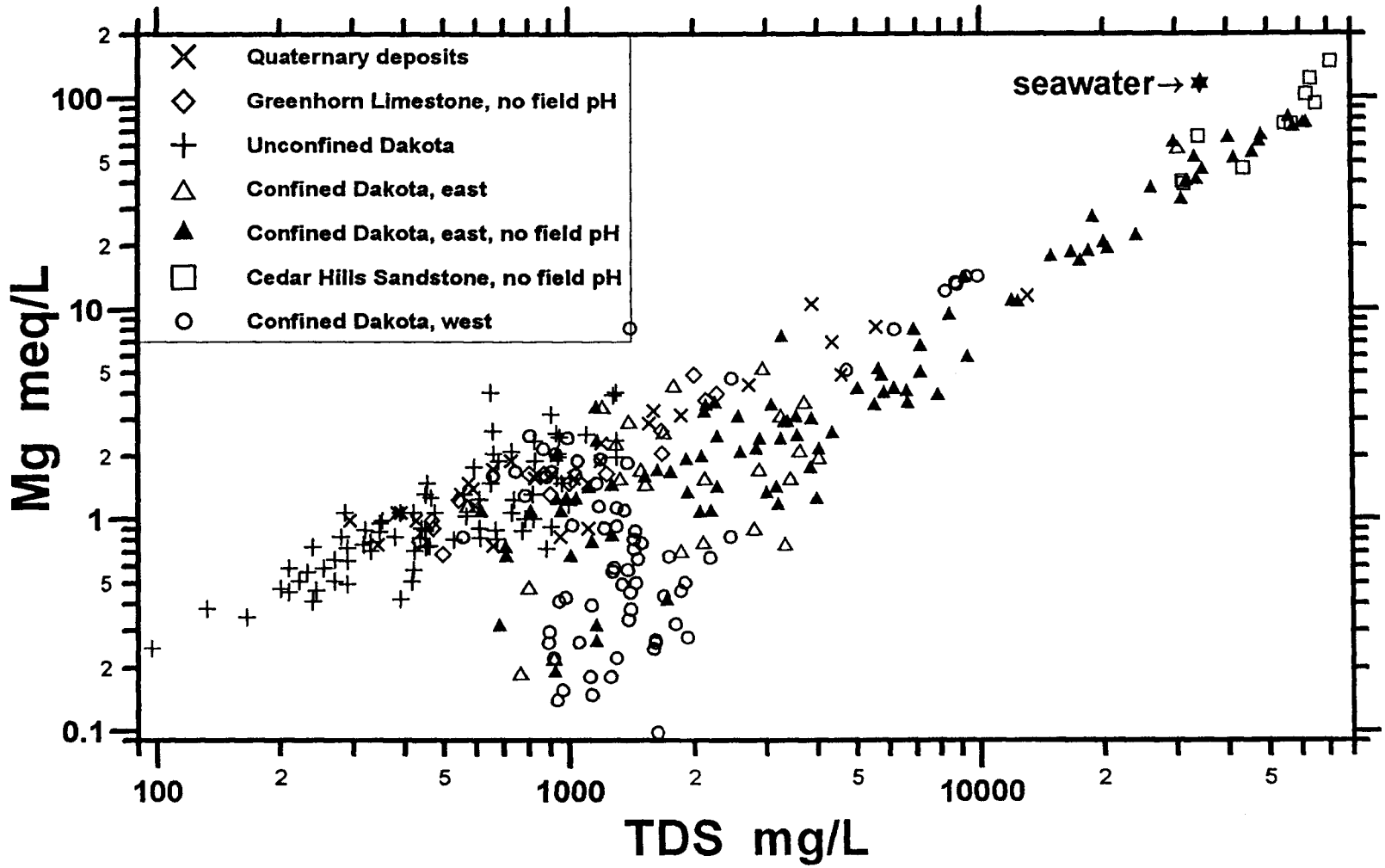

Figure 5.6. Dissolved Mg concentration versus TDS content.

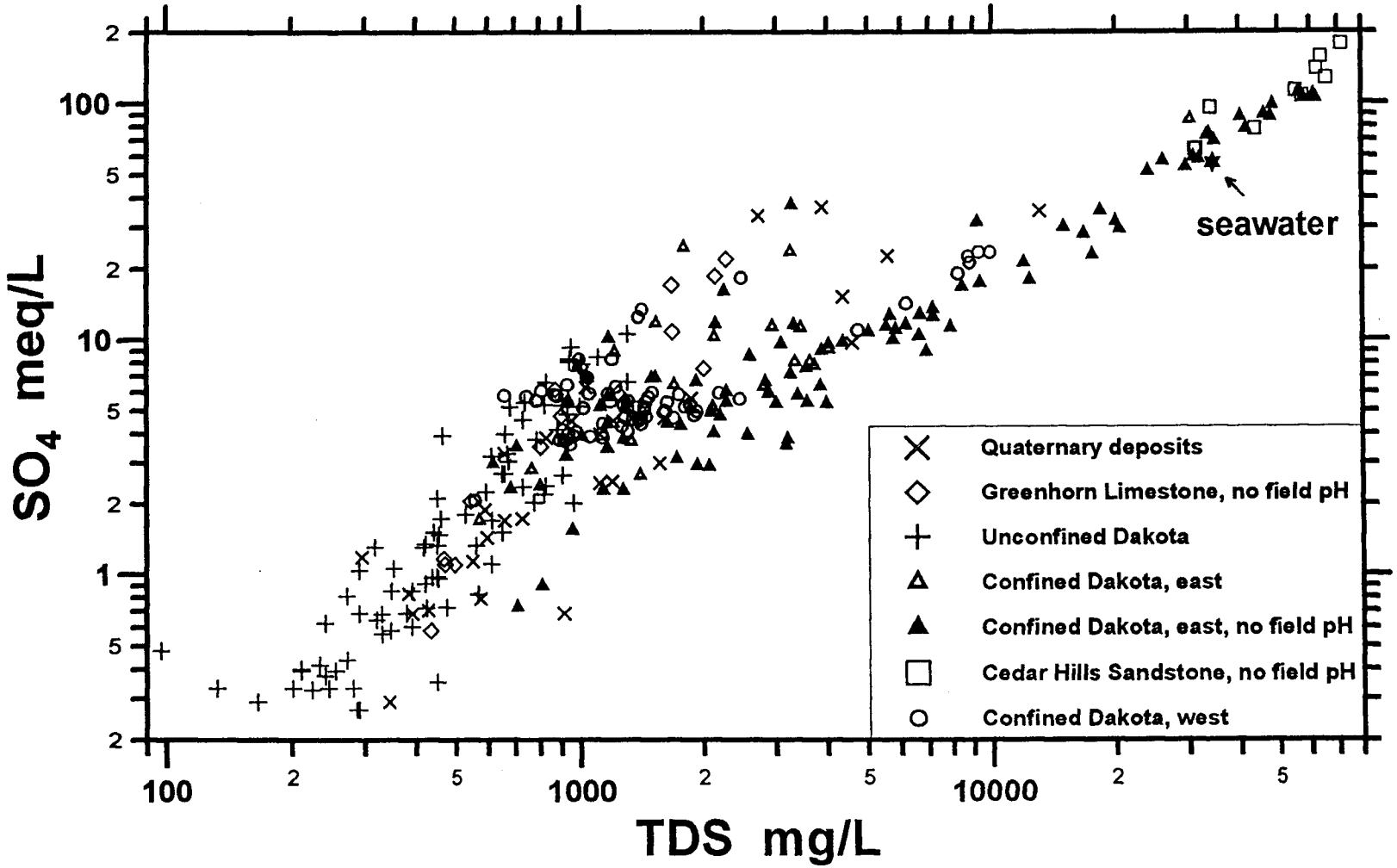

Figure 5.7. Dissolved SO_4 concentration versus TDS content.

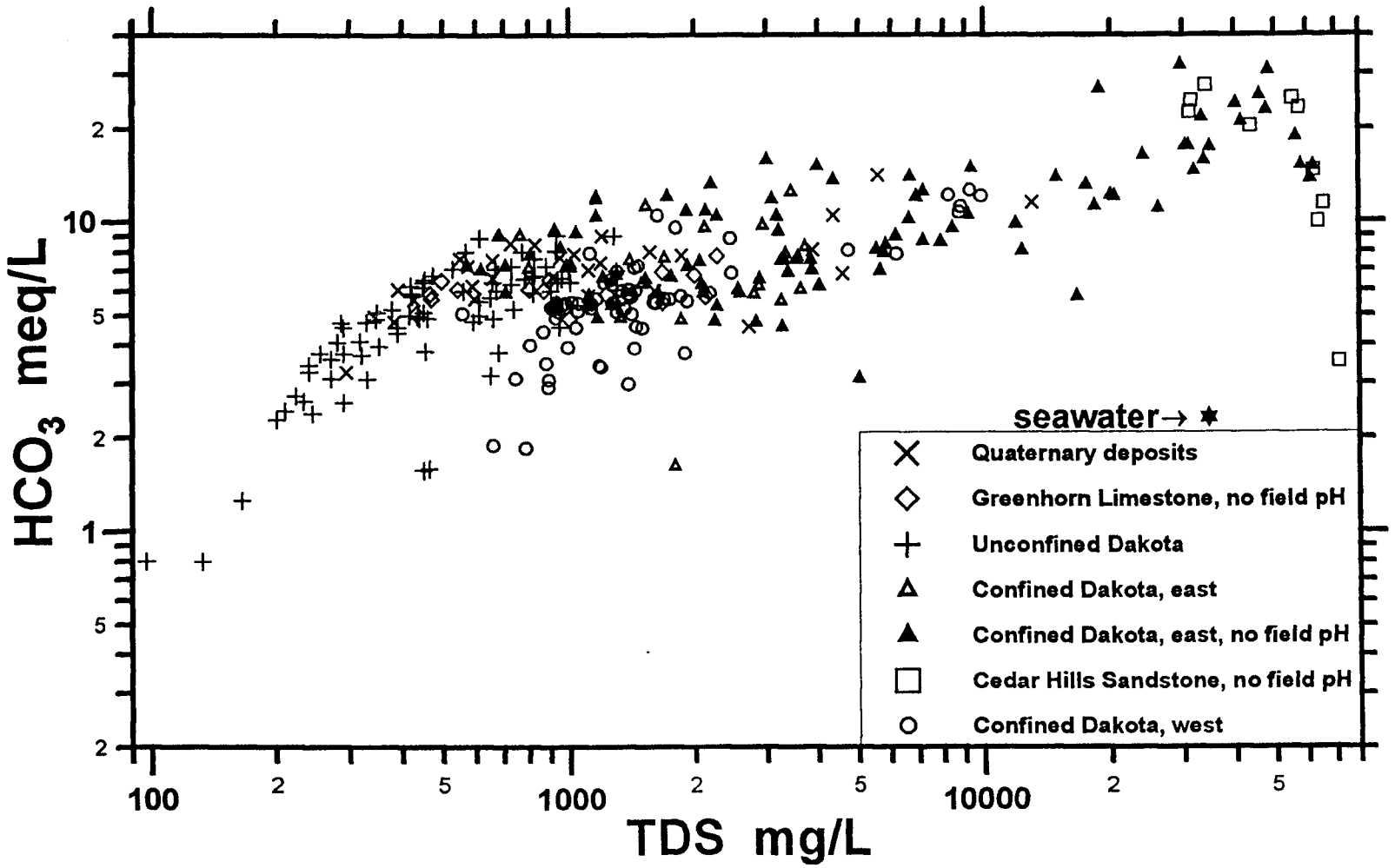

Figure 5.8. Dissolved HCO_3 concentration versus TDS content.

(Macpherson, 1990). In general, Figures 5.2 to 5.8 indicate that there is a systematic change of water chemistry in the Dakota aquifer system. In addition, some major features shown in the diagrams indicate that other kinds of chemical and physical mechanisms are affecting the water chemistry in the system. Detailed discussion of water chemistry and possible chemical reactions for each water group and overall aquifer system will be presented in the following sections.

5.2. INTERPRETATION OF WATER CHEMISTRY DATA

5.2.1. Ground Water in the Quaternary Terrace and Alluvial Deposits

Figure 5.9 shows that the alluvium contains a mixture of Ca-HCO_3 and Na-Cl type waters, but also includes some Ca-SO_4 type water. The TDS concentrations for the Na-Cl type water range from several thousands to more than ten thousand mg/L (Table A.1). Apparently, the alluvial aquifers receive surface recharge and subsurface intrusion of saline water from the Dakota aquifer (Figure 5.3 to 5.8). Studies in central Kansas also depict saltwater discharge as a very common feature in most of the major stream valleys (Bayne and Walters, 1959; Fader, 1968; Whittemore et al., 1993). The Ca-SO_4 type water could result from local dissolution of gypsum (Figure 5.10) or oxidation of pyrite and dissolution of calcite in the formation. In the area west of the Dakota outcrop zone, most of the recharge from alluvium is restricted to local shallow flow systems which form a narrow zone along river valleys (Figure 5.11). Therefore, the regional ground-water quality in the Dakota aquifer, particularly the confined portion, is not affected by the overlying alluvial aquifers. Also, the fresh alluvial water has characteristics similar to that of the unconfined Dakota water since

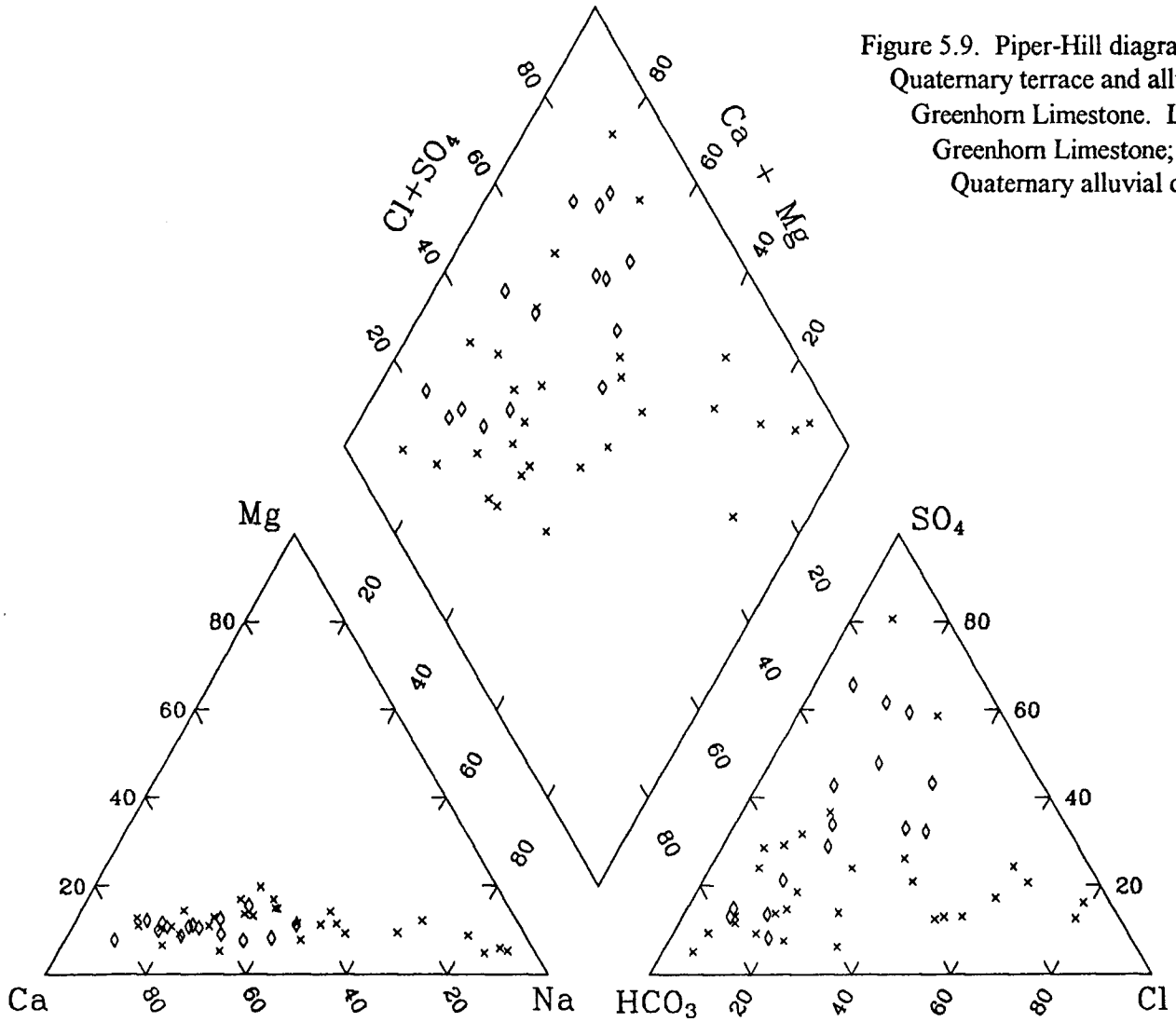

Figure 5.9. Piper-Hill diagram for water groups of the Quaternary terrace and alluvial deposits and the Greenhorn Limestone. Legend: ◊ :water from Greenhorn Limestone; and × : water from the Quaternary alluvial deposits.

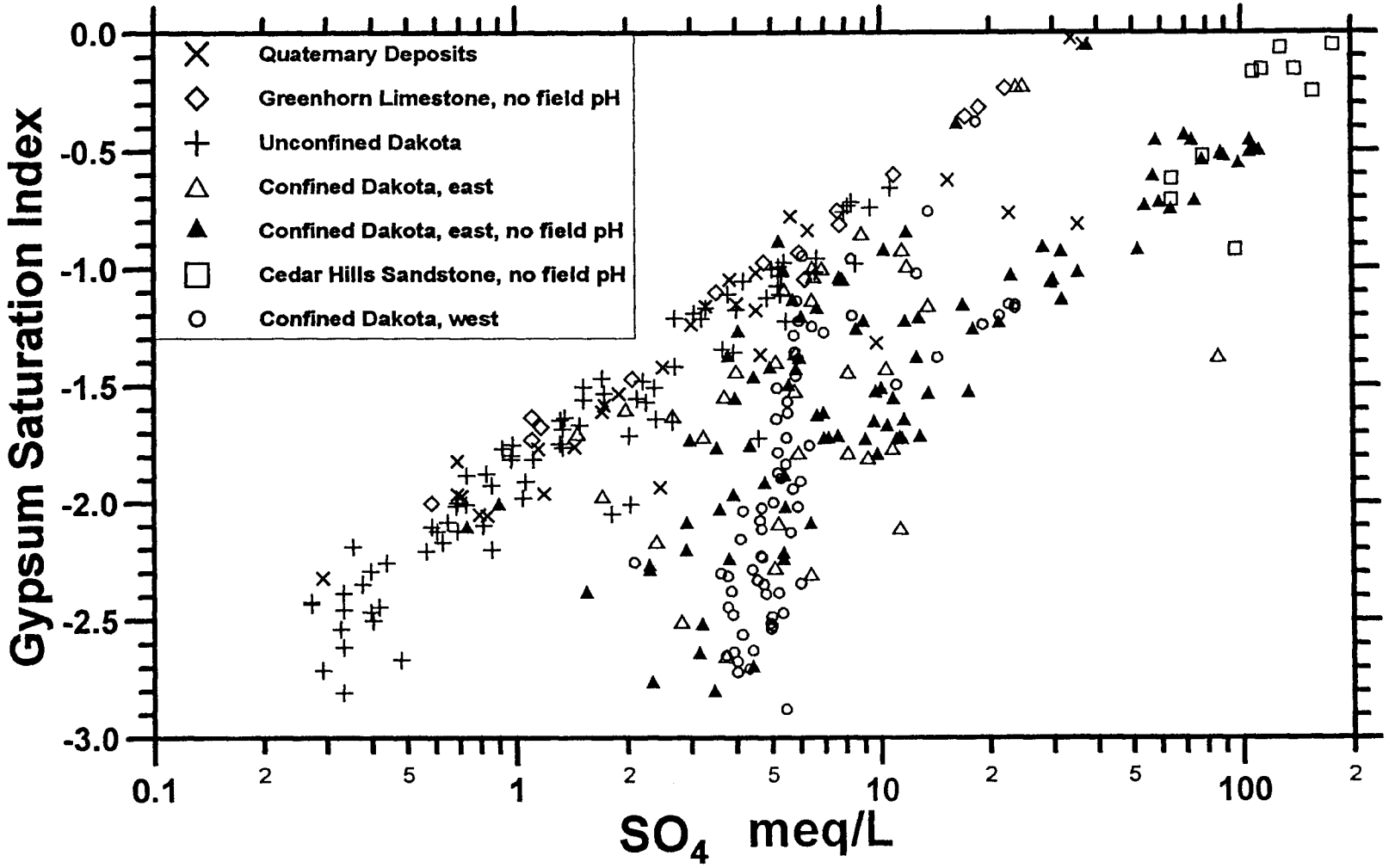

Figure 5.10. Gypsum saturation index versus dissolved SO_4 concentration.

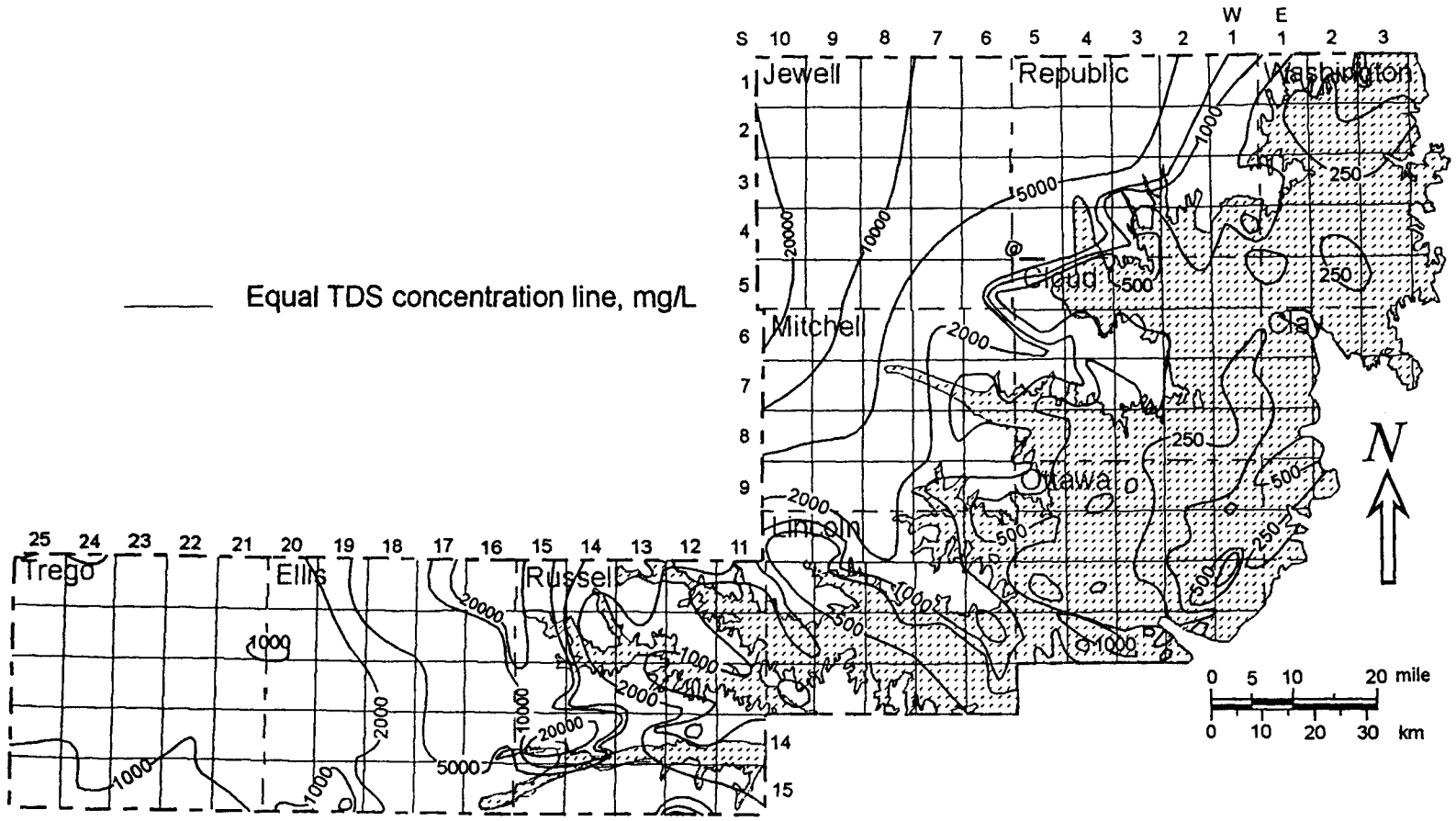

Figure 5.11. TDS contours for the upper part of the Dakota aquifer (adapted from Whittemore et al., 1995)

both of them receive mainly surface precipitation. Due to the above reasons, the alluvial water group will not be discussed in the following pages.

5.2.2. Ground Water in the Greenhorn Limestone

Figure 5.9 shows that ground water in the Greenhorn Limestone ranges from a $Ca\text{-}HCO_3$ type to a $Ca\text{-}SO_4$ type. No field pH data are available for any of the water samples. The pH's of the Greenhorn waters were simulated by forcing the waters to be calcite saturated. The geochemical model results show that the simulated pH range for the Greenhorn waters (6.5 - 7.25) is reasonable. The major chemical type for the low TDS waters which are controlled by the equilibrium of calcite is $Ca\text{-}HCO_3$. The $Ca\text{-}SO_4$ type is dominant in the higher TDS waters for which equilibrium with respect to gypsum is an important control (Figure 5.10). Figure 5.8 shows that the HCO_3 concentrations for all the Greenhorn waters are limited to a small range similar to waters of the same TDS range in Quaternary alluvial deposits. The relatively constant bicarbonate concentrations of the Greenhorn and alluvial waters indicate that both the aquifer systems are fairly open to the atmosphere.

The SO_4 and Ca concentrations of the Greenhorn water increase with TDS content (Figures 5.5 and 5.7). Figure 5.10 shows that the gypsum saturation index of the Greenhorn waters increases linearly with increasing logarithmic SO_4 concentration. Figure 5.12 indicates that Ca concentration is much higher than SO_4 concentration for Greenhorn water with low SO_4 concentrations, but the ratio of these two constituents approaches one for Greenhorn water with higher TDS contents. This suggests that the main control on the water chemistry is mixing of $Ca\text{-}HCO_3$ type water with water dissolving gypsum. Although no gypsum or anhydrite beds occur in the formation in the subsurface, there are abundant gypsum crystals found in the

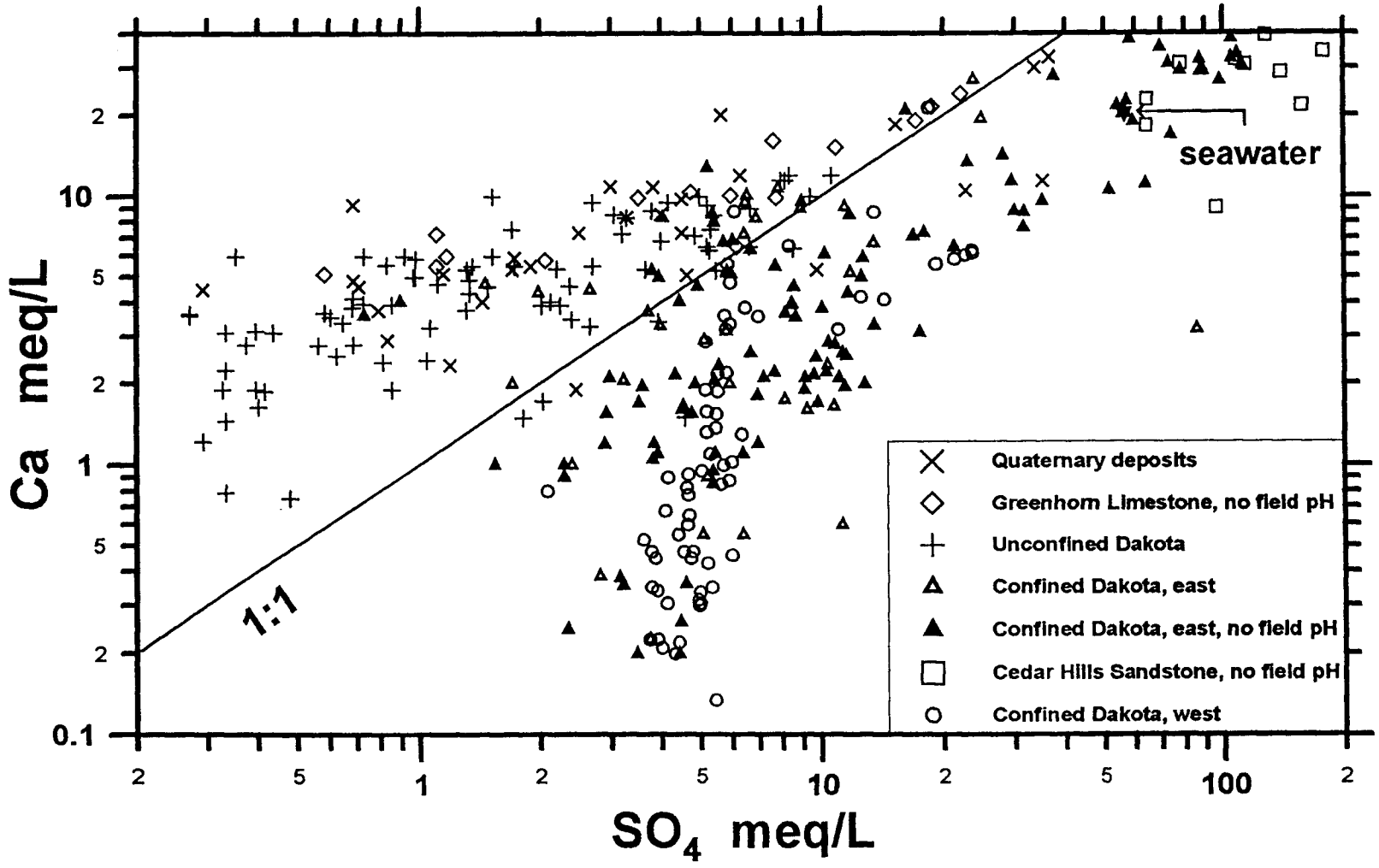

Figure 5.12. Dissolved Ca versus SO_4. The solid line represents the 1:1 equivalent ratio.

outcrop zone. The gypsum crystals form in the shallow subsurface weathering zone by reaction of SO_4 from the oxidation of pyrite with Ca from the dissolution of calcite in the formation.

5.2.3. Ground Water in the Unconfined Portion of the Dakota Aquifer

The dominant water type in the unconfined part of the Dakota aquifer is Ca-HCO_3; water types transitional toward Ca-SO_4 and Na-HCO_3 are also important (Figure 5.13). Surface recharge is the major water source for this part of the Dakota aquifer. However, differing from the alluvial and Greenhorn waters, points for the unconfined Dakota water generally plot near the 1:1 equivalent ratio line for HCO_3 versus Ca (Figure 5.14). This indicates that the system is somewhat isolated from the atmosphere and dissolution of calcite is the major source of Ca and HCO_3. The occurrence of Ca-SO_4 type water, similar to the alluvial water, could be a result of dissolution of calcite and oxidation of pyrite and organic matter.

There are two reasons for the occurrence of Na-HCO_3 and Na-mixed-anion type waters in the unconfined part of the Dakota aquifer. As described in Chapter 3, the Na-HCO_3 water is a result of cation exchange of Ca and Mg for Na on clay surfaces during the time the aquifer is being flushed by local fresh surface recharge. At the same time, the depleted Ca and Mg cause dissolution of calcite, dolomite, and gypsum if those minerals exist in the system. Before the occurrence of the cation exchange reactions, the Dakota aquifer contained much more saline water derived from the intrusion of Permian saltwater. Another source of Na-HCO_3 and Na-mixed-anion waters could also be those waters directly flowing from the confined Dakota aquifer in the west.

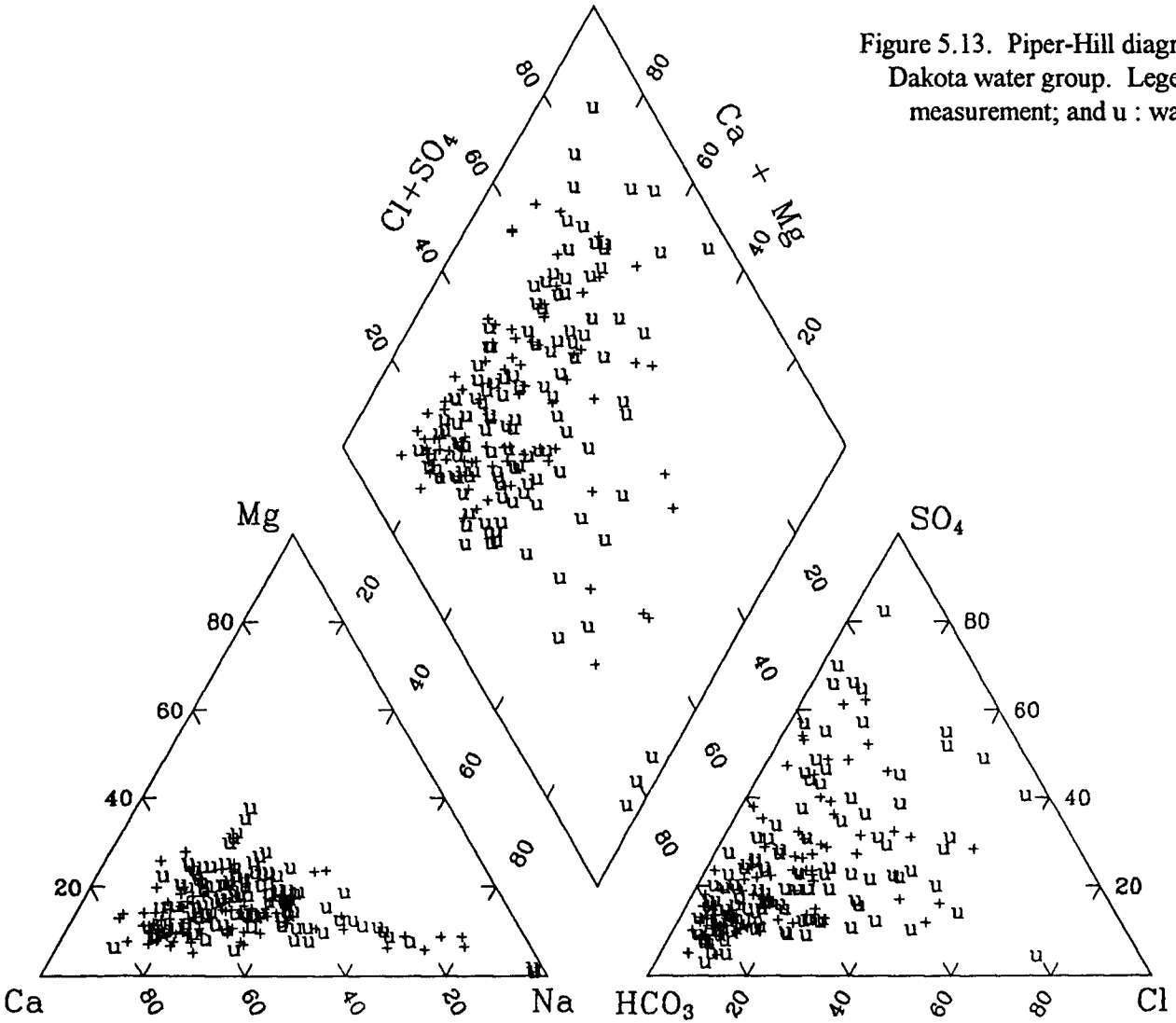

Figure 5.13. Piper-Hill diagram for the unconfined Dakota water group. Legend: + : water with field pH measurement; and u : water sample without field pH.

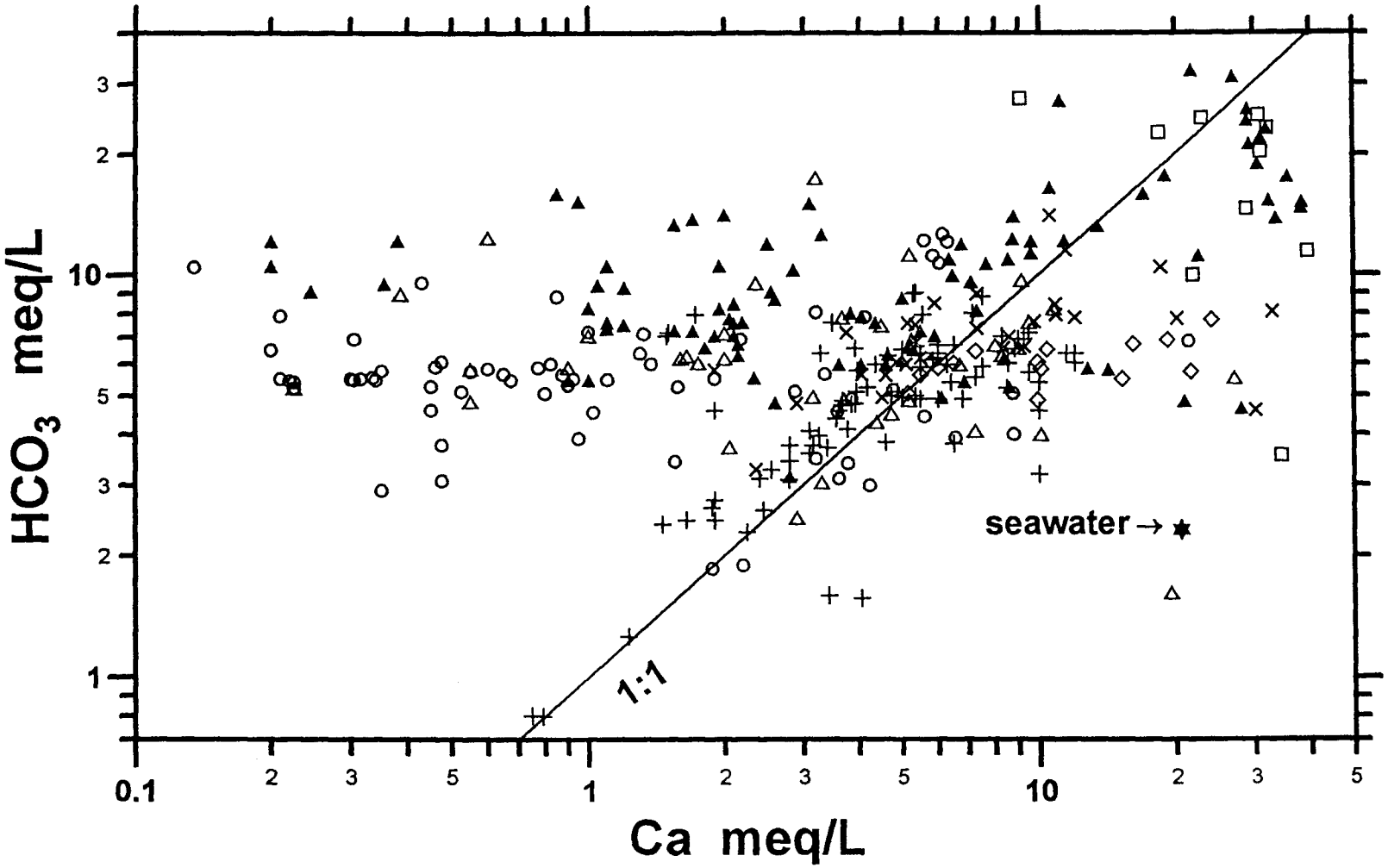

Figure 5.14. Dissolved HCO_3 versus Ca. The solid line represents the 1:1 equivalent ratio for these two constituents. Refer to Figure 5.12 for legend.

The TDS concentration distribution in the upper part of the Dakota aquifer shows that freshwaters (TDS < 1,000 mg/L) are normally found near river valleys and in the outcrop zone (Figure 5.11). Artesian pressure, a thick confining layer, and saltwater intrusion from underlying Permian strata restrict penetration of the fresh surface recharge in the aquifer system. Local surface recharge in the Dakota outcrop only travels in local ground-water flow systems and discharges to the surface in a short distance.

5.2.4. Ground Water in the Cedar Hills Sandstone

Ground water in the Cedar Hills Sandstone is exclusively of Na-Cl type (Figure 5.15). Halite dissolution from the same formation in western Kansas and adjacent halite-bearing formations is the major source of dissolved Na and Cl.

Geochemical modeling indicates that the Cedar Hills water is saturated with respect to magnesite if the water is forced to be saturated with respect to calcite (Figure 5.16), whereas the water is supersaturated with respect to dolomite. This result agrees with the geological evidence found in the formation. Thus, dissolution of magnesite appears to be the major supply for the Mg and HCO_3 concentrations in the Cedar Hills water although incongruent dissolution of dolomite may also contribute to the concentrations. Anhydrite is another common mineral in the Cedar Hills Formation. Although geochemical simulation shows that none of the water samples are close to saturation with respect to anhydrite, the Cedar Hills water is nearly saturated with respect to gypsum (Figure 5.10).

As discussed in Chapter 2, the hydraulic interaction between the Dakota and Cedar Hills aquifers is largely affected by local flow systems. The variation of TDS concentration in the waters from the Cedar Hills Sandstone suggests that some local flow conditions have

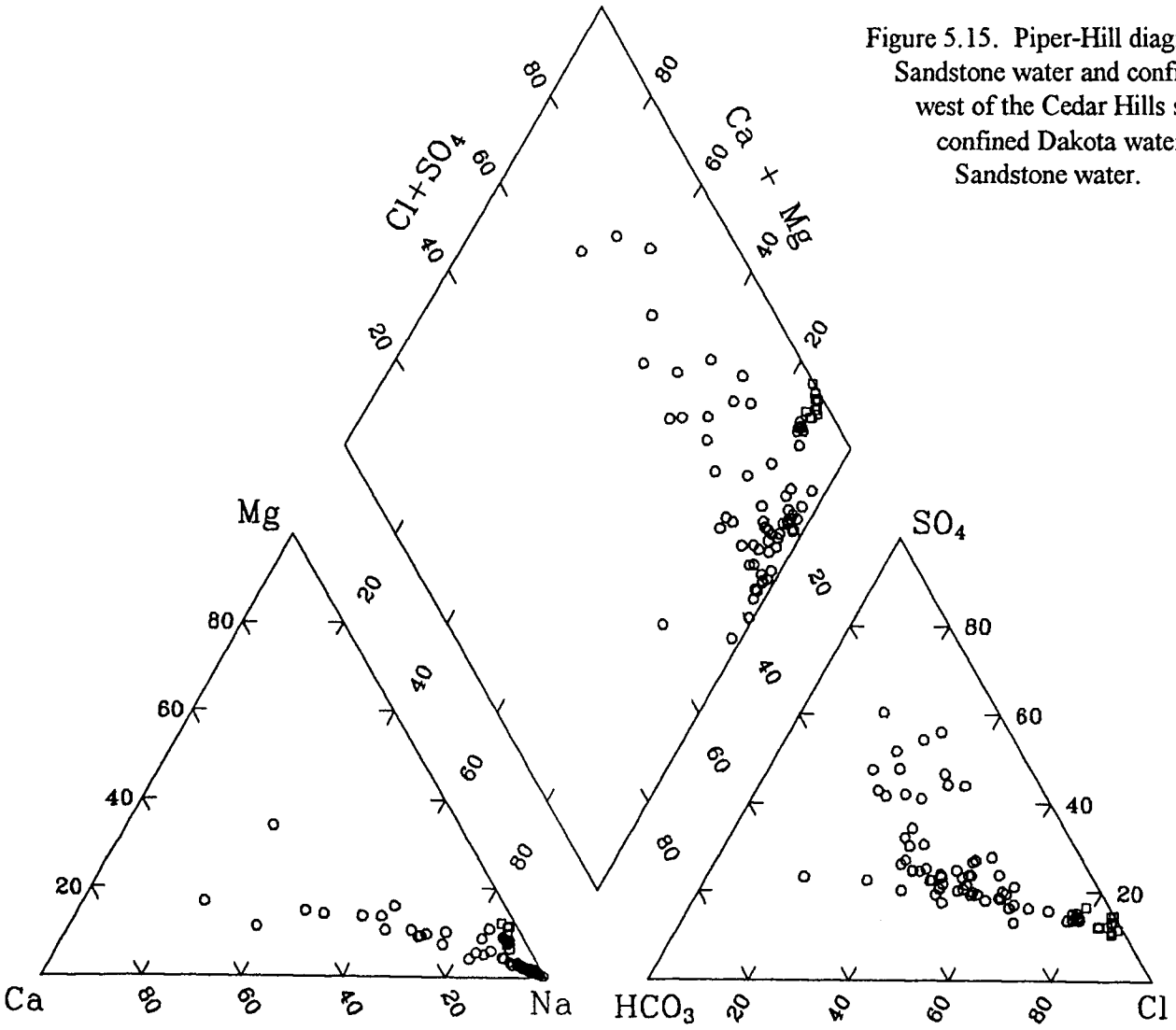

Figure 5.15. Piper-Hill diagram for the Cedar Hills Sandstone water and confined Dakota water to the west of the Cedar Hills subscrop. Legend: o : west confined Dakota water; and □ :Cedar Hills Sandstone water.

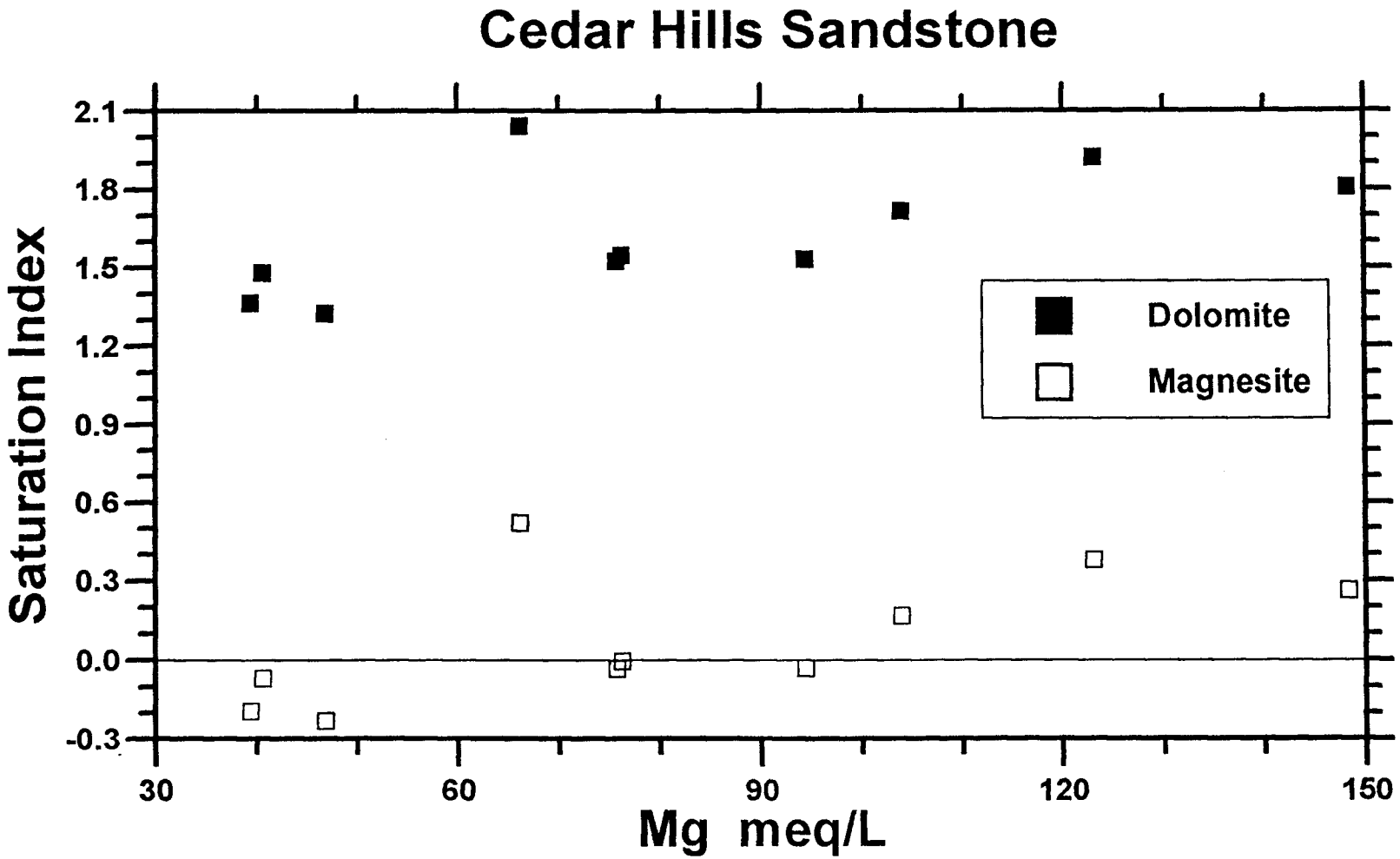

Figure 5.16. Saturation indices of dolomite and magnesite for Cedar Hills water.

allowed Dakota water to reach the top part of the Cedar Hills Sandstone in the Cedar Hills subcrop area and mix with the Permian water. The dilution process causes cation exchange to occur even in the Permian strata. More discussion of the effect of cation exchange will be given later in this chapter.

The dilution and cation-exchange reactions cause anhydrite and magnesite to dissolve in the Cedar Hills Sandstone (Figures 5.10 and 5.16). The reactions increase the pH, HCO_3, and SO_4 concentrations in the diluted Cedar Hills water. However, geochemical modeling suggests that pH's of the diluted Cedar Hills water are lower than those of higher TDS waters if the waters are forced to be saturated with respect to calcite (Figure 5.17). The lower simulated pH's for the diluted waters are a result of the precipitation of calcite. The precipitation of calcite, in turn, will cause further dissolution of magnesite and anhydrite (or gypsum) in the Cedar Hills Sandstone. These reactions will result in elevated Mg and SO_4 concentrations in the Cedar Hills water. The combined results of cation exchange, calcite precipitation, dissolution of magnesite and anhydrite should greatly increase SO_4 concentration. Concentration of HCO_3 and pH will reach an equilibrium condition between calcite precipitation and magnesite dissolution. The effect of the chemical reactions on the water chemistry can not be confirmed because no field pH measurements are available. No increase of SO_4 is shown for the diluted Cedar Hills waters (Figure 5.7), and abnormally high HCO_3 concentrations occur in these waters. Those results do not seem consistent with the predicted results. However, based on the redox reaction of Equation (3.2), reduction of SO_4 by organic matter which generates HCO_3 may explain the field data. Moreover, the intensity of cation exchange causing magnesite dissolution may be stronger than the calcite precipitation which will also cause HCO_3 concentration to increase.

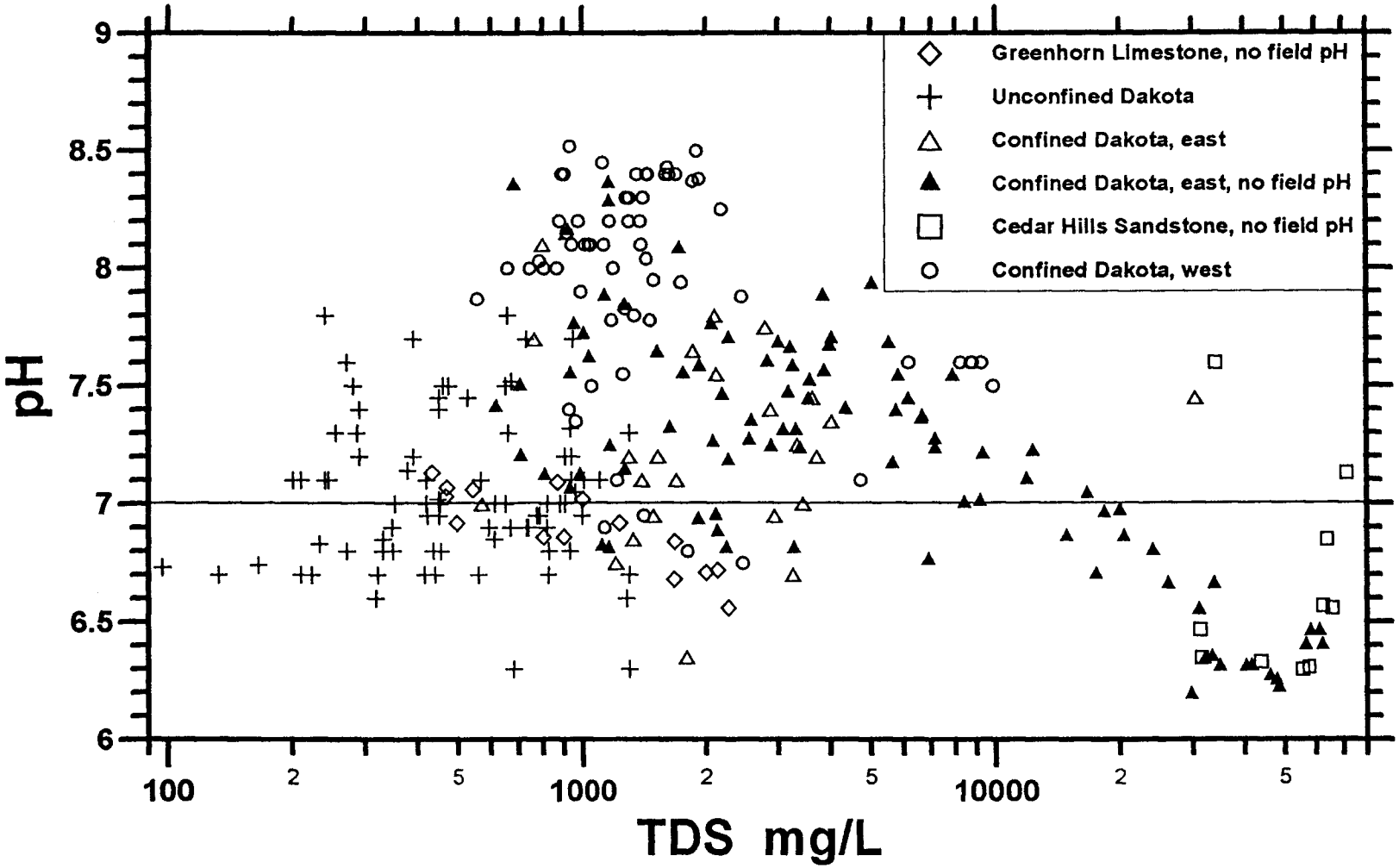

Figure 5.17. pH versus TDS content for different ground-water groups. For samples without field pH measurements, the values of pH were obtained from SOLMINEQ.88 simulation by forcing the waters to be calcite saturated.

5.2.5. Ground Water in the West Confined Portion of the Dakota Aquifer

Dakota waters in the study area to the west of the Cedar Hills subcrop are mostly of Na-Cl and Na-mixed-anion types (Figure 5.15). High pH and low (Ca + Mg)/Na ratios are the major characteristics of this water (Figures 5.17 and 5.18). Figures 5.5 and 5.6 show that Ca and Mg concentrations in the west confined Dakota aquifer are the lowest of all the water groups, especially for waters with TDS content range from 800 to 2,000 mg/L. Cation exchange of Ca and Mg for Na on clays is the reason for the decreased Ca and Mg contents. Figure 5.18 shows that the (Ca + Mg)/Na equivalent ratios of waters in the west confined Dakota aquifer are the lowest and extend from the lower-central part of the diagram toward the water group of the Greenhorn Limestone (or unconfined Dakota) and the Permian water. This is an indication of the influence of water chemistry from the above Upper Cretaceous confining layer and the underlying Permian strata in the area. Waters in the west confined Dakota aquifer, which have the lowest (Ca + Mg)/Na ratios, are the waters least affected by outside sources and represent the regional Dakota ground-water flow from the west where cation exchange is the major control on the cation ratios in solution.

Figure 5.8 shows a relatively low HCO_3 concentration for the west confined Dakota water compared to the other water groups except the unconfined Dakota water. However, the geochemical model suggests that most of the west confined Dakota waters are saturated with respect to calcite despite many samples with low Ca concentrations (Figure 5.19). Figure 5.14 shows that the HCO_3 concentration range for west confined Dakota water does not change appreciably with decreasing Ca concentration. A close inspection reveals that the high pH in the west confined Dakota water allows equilibrium conditions with respect to calcite in water of low Ca concentration in which HCO_3 does not appreciably increase (Figure 5.17). An

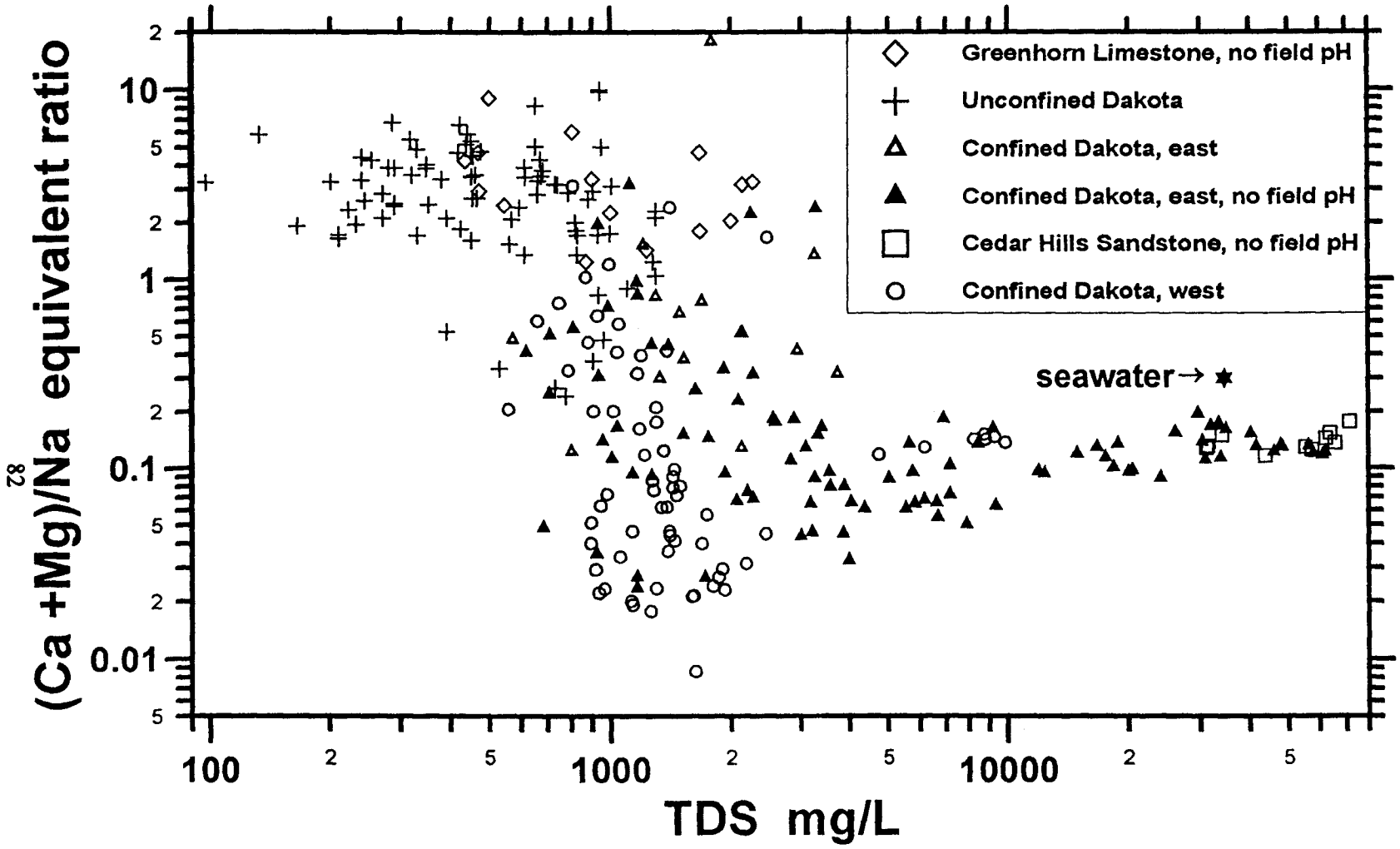

Figure 5.18. (Ca + Mg)/Na equivalent ratio versus TDS concentration for different water groups.

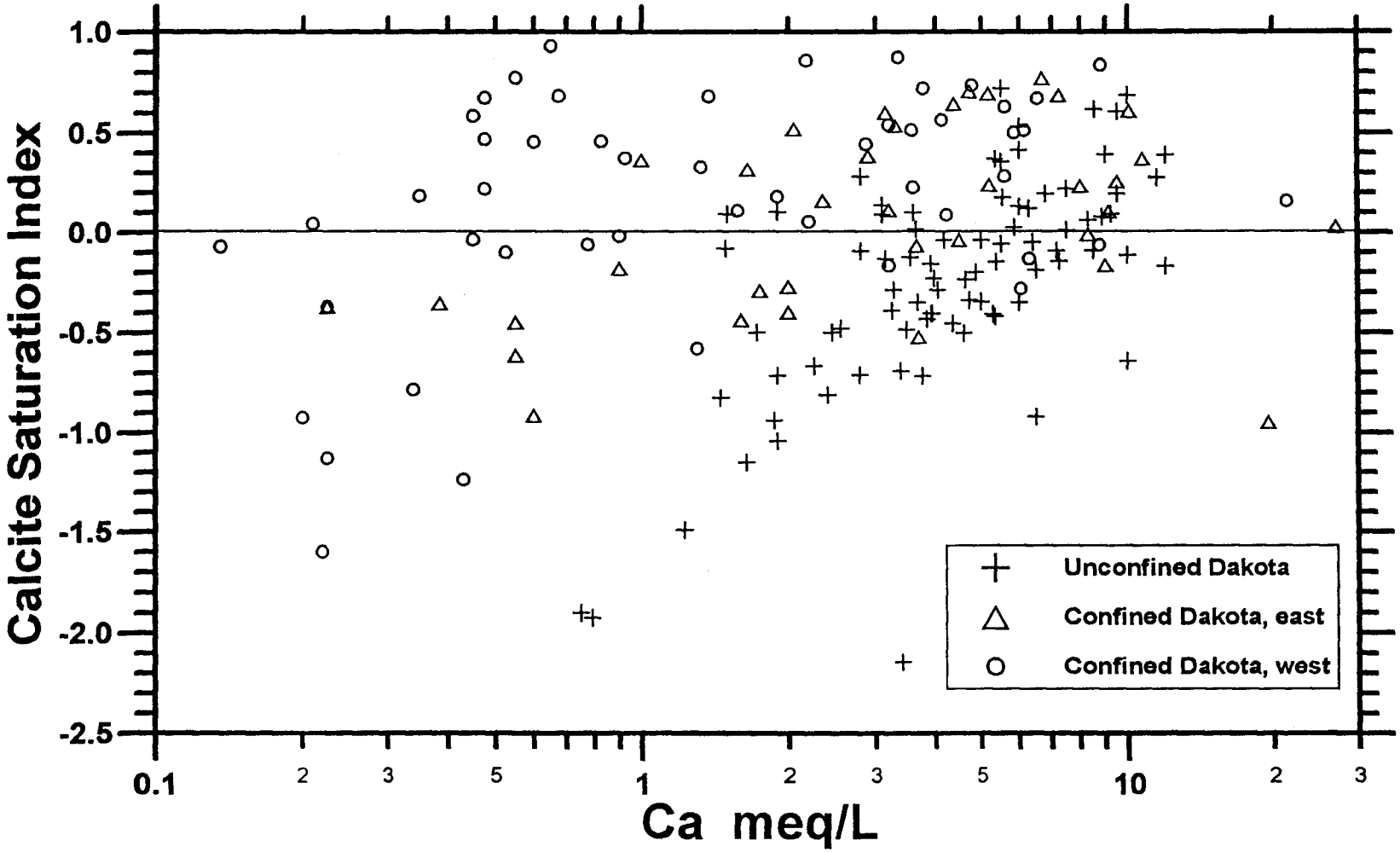

Figure 5.19. Calcite saturation index versus Ca concentration for water samples with field pH measurements.

example illustrating the effect of pH on the solubility of calcite in a closed-system condition is shown in Figure 5.20. The type of chemical evolution in the west confined Dakota aquifer suggests a closed system for the confined Dakota aquifer in Trego and western Ellis counties.

Figure 5.7 displays that, except for the waters affected by recharge from confining layers at the top and bottom, the SO_4 concentrations of the west confined Dakota waters are constrained in a narrow range. Evidently, dissolution of gypsum is not a controlling factor for SO_4 concentration in the confined Dakota aquifer west of Cedar Hills subcrop (Figure 5.10). Sulfate concentration in solution increases early in the flow path of surface recharge from Dakota outcrops in southeastern Colorado and southwestern Kansas to central Kansas in the Dakota aquifer. Oxidation of pyrite is the major source of the dissolved SO_4. However, the redox potential is greatly reduced when the Dakota water reaches central Kansas. Figure 5.12 shows a trend of slightly smaller SO_4 concentration with decreasing Ca concentration in the west confined Dakota water. As discussed earlier, water with the lowest (Ca + Mg)/Na ratios represents regional Dakota water flow from the west and is in a relatively closed system. The relationship of Ca and SO_4 in the west Dakota water suggests that the SO_4 concentration decreases along the flow path in central Kansas. Since mineral precipitation is not a reason for the decrease in SO_4 concentration, chemical reduction could be the reason as suggested by Equation 3.2. However, no pronounced increase of HCO_3 occurs along the same flow path (Figure 5.14). The redox effect on the HCO_3 concentration might be obscured by other factors, such as precipitation/dissolution of calcite and/or siderite and variation of pH. In addition, based on Figure 5.12, only a small amount of HCO_3 may be contributed from reduction of SO_4.

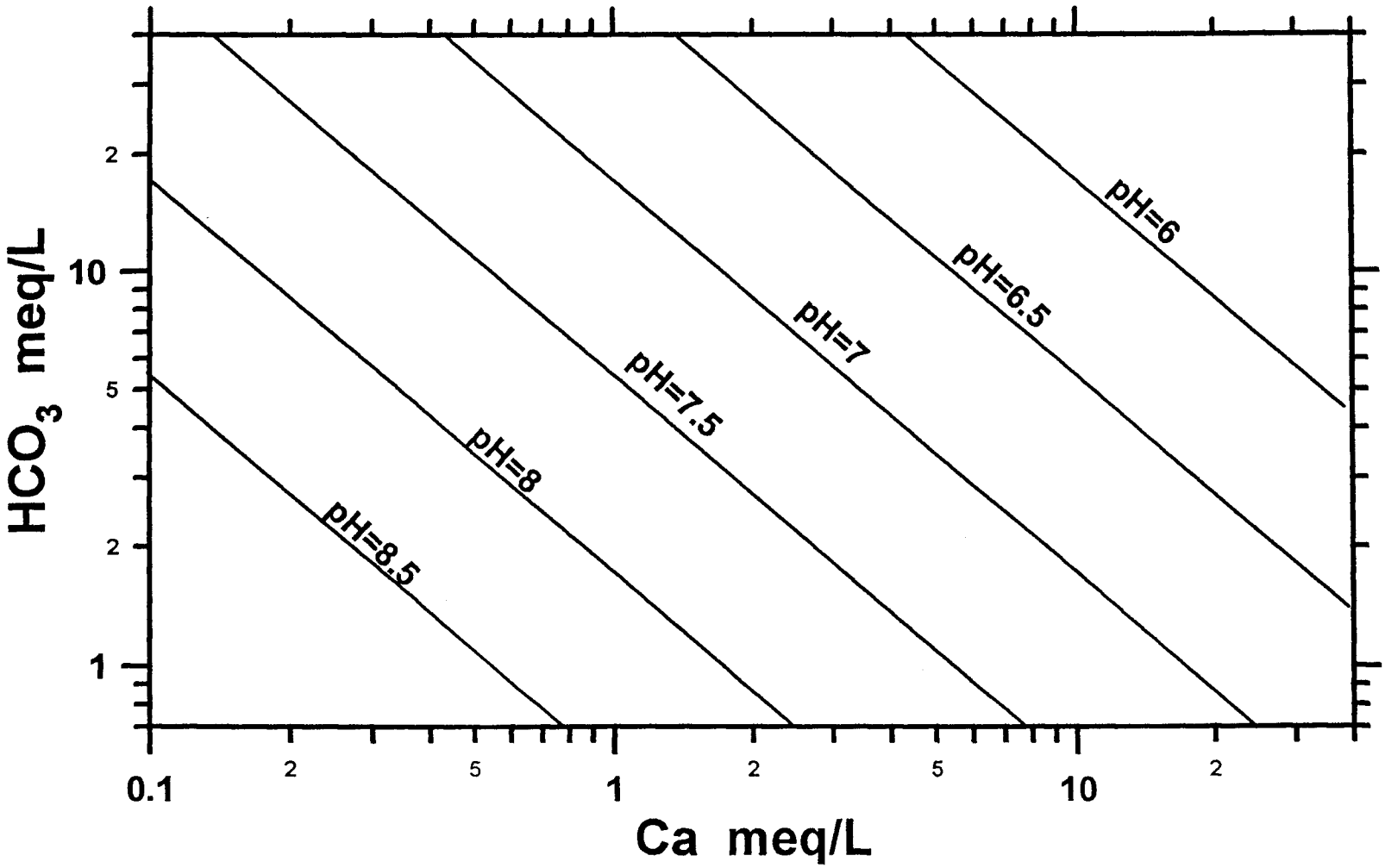

Figure 5.20. Solubility of calcite at 15 °C expressed as a function of pH, Ca^{2+}, and HCO_3^-. Solubility lines computed from the relation $K = (Ca^{2+})(HCO_3^-)/(H^+)$. Refer to Table 7.3 for chemical reaction equations and equilibrium constants.

The water chemistry of the west confined Dakota group is a result of complex coupled mass transport and chemical reaction processes. The proposed mechanism generating this type of water is partially based on the geochemical simulation results. The Dakota aquifer previously contained water much saltier than at present. Changes in the hydrogeological conditions in the aquifer system increased the freshwater recharge to the Dakota aquifer in southeastern Colorado and southwestern Kansas. Freshwater recharge with a (Ca + Mg)/Na ratio appreciably higher than in the pore water enters the Dakota aquifer and flushes out the saline water. The freshening process causes exchange of dissolved Ca and Mg with Na on clays. The replacing water and the aquifer materials soon attain a temporary equilibrium condition due to the great buffering capacity of the exchange sites. The (Ca + Mg)/Na ratio in solution is reduced to adapt to the adsorbed cation ratios on clays which are still in equilibrium with the previous saltwater. Calcite dissolution also occurs when the Ca and Mg are depleted by the cation exchange reactions. The dissolution causes saturation with respect to calcite in the replacing freshwater and elevates pH and HCO_3 concentration (Figures 5.14, 5.17, and 5.19). The water then flows downgradient with only minor chemical reactions occurring. Such a type of water is represented by the water group of the west confined Dakota. At a certain point in the flow path, the temporary stable condition ends when sufficient recharge water has flowed through and replaced all the exchangeable cations (with respect to the recharging freshwater) on surface sites. After that, the part of the aquifer upgradient from the particular point is in equilibrium with the incoming freshwater. Based on the ground-water chemistry data, the Dakota aquifer in western Kansas is in a temporary equilibrium condition with the incoming freshwater. This indicates that ground-water chemistry evolution still occurs in a large part of the Dakota aquifer in western and central Kansas.

Potable water is available mainly in the top 45 meters (150 feet) of the Dakota aquifer in Trego and western Ellis counties. Ground water in the lower half to two-thirds of the Dakota aquifer in this two-county area is too salty for domestic and agricultural uses. There are several possible explanations for the geohydrological conditions in this area. First, the higher hydraulic head in the underlying Permian strata (Macfarlane et al., 1988) and the high salinity of the upward-diffusing saltwater are able to contaminate the ground water half way up into the overlying Dakota aquifer. Secondly, the relatively impermeable Kiowa shale restricts the Permian saltwater intrusion. Thus saltwater from below is prevented from spreading to the upper part of the Dakota aquifer. The third possibility is that leakage through the top confining layer also contributes a significant portion of the potable water.

5.2.6. Ground Water in the East Confined Portion of the Dakota Aquifer

Na-Cl is the major water type in the east confined part of Dakota aquifer. Other water types include transitions from Na-Cl to Ca-SO_4 and to Na-HCO_3 types (Figure 5.21). The water chemistry shows distinctly the influence of the intrusion of Cedar Hills saltwater into the confined Dakota aquifer east of the Cedar Hills subcrop zone. Water of highest TDS concentration in the Dakota aquifer occurs at and above where the Cedar Hills Sandstone hydraulically joins the Dakota aquifer. Regional ground-water flow from the west, fresh surface recharge, heterogeneity of the aquifer properties, and variation of local chemical environments have made the water chemistry even more complicated in this region. As Figures 5.2 to 5.8 show, the water chemistry of the east confined Dakota is a mix of all the different water groups in the aquifer system. Nonetheless, the complexity of water chemistry provides

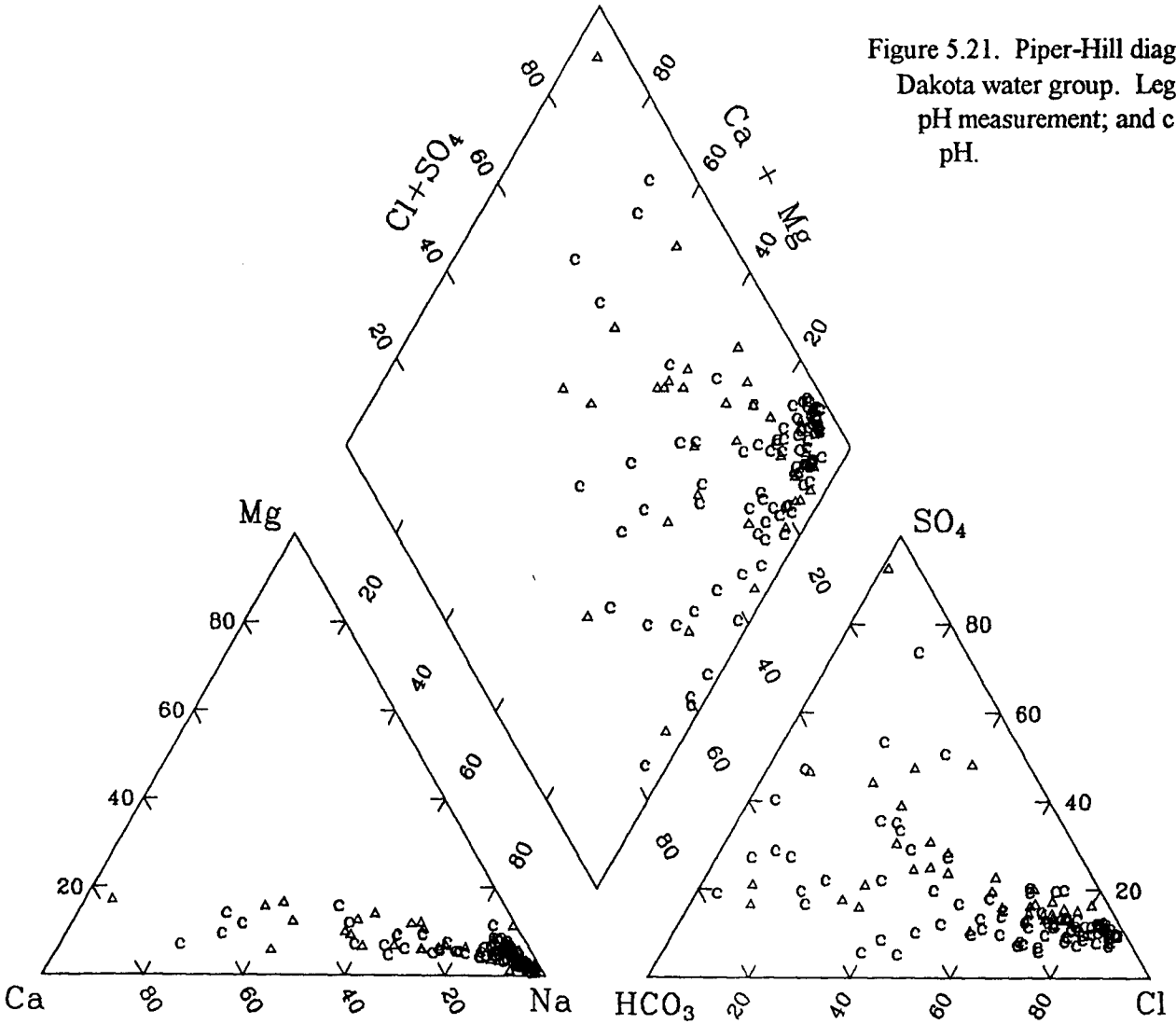

Figure 5.21. Piper-Hill diagram for the east confined Dakota water group. Legend: Δ : water sample with pH measurement; and c : water sample without field pH.

valuable information for examining the coupled flow and chemical reactions occurring in the aquifer system.

A large part of the east confined Dakota water has characteristics similar to that of the west confined Dakota water. Cation exchange and calcite dissolution have controlled the water chemistry to some degree. Figure 5.14 shows that, in the east confined Dakota aquifer, depletion of Ca and dissolution of calcite have produced waters that plot to the left of the 1:1 equivalent ratio line. Generally, HCO_3 concentration in the east confined Dakota water is higher than that in the west confined Dakota water. This is because of the relatively higher salinity and lower pH in the east confined Dakota water.

To understand the characteristics of the ground water in this part of the Dakota aquifer, comparisons to conservative mixing are used to reveal the relationships between the different water groups. Figures 5.22 and 5.23 show that ground water in the confined Dakota aquifer east of the Cedar Hills subcrop is a result of mixing of regional ground-water flow from the west, intruded Cedar Hills saltwater, and surface recharge. Chemical reactions have also altered the waters during the mixing process, especially during the mixing of Cedar Hills water and regional ground-water flow from the west. Figure 5.23 shows that many points representative of the east confined Dakota water group plot below the lower boundary for the zone of conservative mixing between the Cedar Hills water and confined Dakota water from the west. It indicates that there are factors additional to conservative mixing that control the Mg/Cl ratio. Similar phenomena occur for Ca/Cl but they are not as pronounced as for Mg/Cl (Figure 5.22). Cation exchange causes the depletion of Mg and Ca where the Cedar Hills and west confined Dakota water mix together.

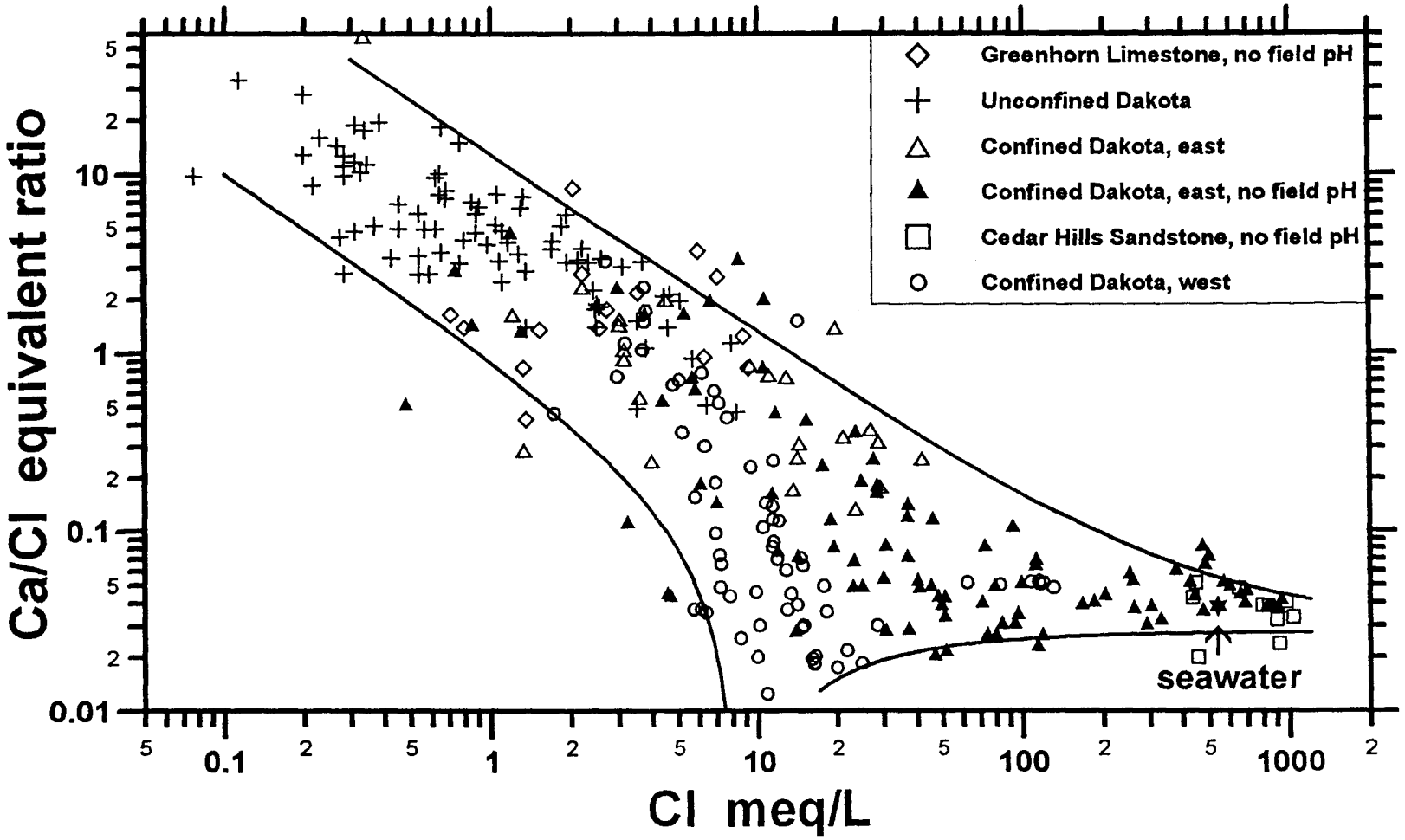

Figure 5.22. Relationship of Ca/Cl ratio versus Cl concentration for different water groups. The solid lines represent the conservative mixing of two end water members of each line and form the boundaries for zones of mixing of the unconfined Dakota, west confined Dakota, and Cedar Hills water groups. Conservative mixing of two or three of the end member waters produces waters that would plot within the mixing boundaries.

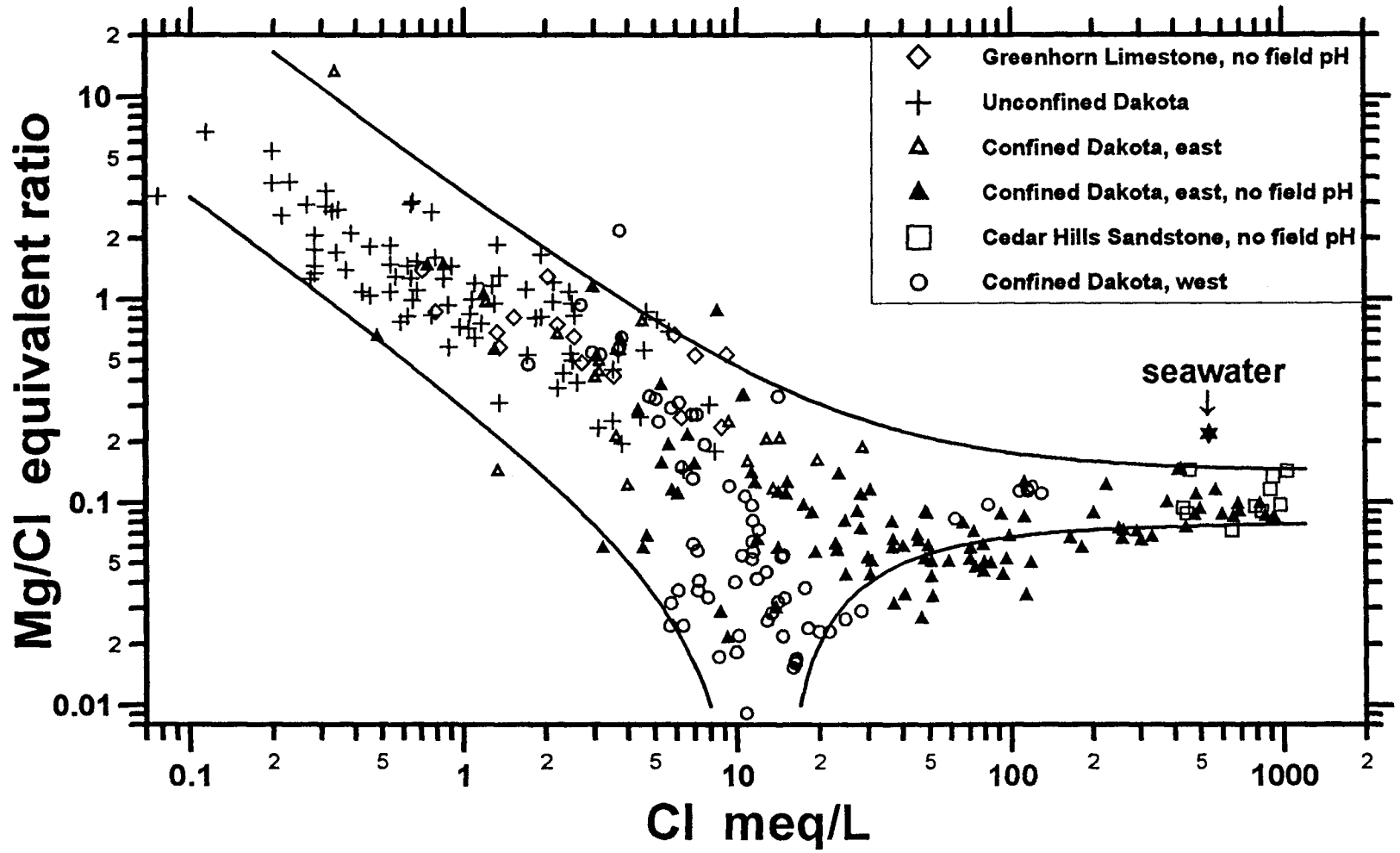

Figure 5.23. Relationship of Mg/Cl ratio versus Cl concentration for different water groups. Refer to the caption of Figure 5.22 for explanation of the mixing lines.

5.3. SUMMARY OF GROUND-WATER EVOLUTION IN THE DAKOTA AQUIFER SYSTEM

The Dakota aquifer system in the study area provides an excellent example of the evolution of ground-water chemistry due to mixing of different water sources and alteration by chemical reactions. Waters with unique chemical characteristics important to the evolution originate in the Permian Cedar Hills Sandstone, regional Dakota ground-water flow from the west, leakage from upper confining layers, and surface recharge in the outcrop zone. Most of the major river valleys in the study area serve as the discharge zones for the Dakota aquifer. Local surface recharge only affects limited areas within the outcrop zone and the subcrops along the edges of river valleys. Intrusion of Cedar Hills saltwater has a major impact on the water chemistry in the Dakota aquifer east of where the Cedar Hills Sandstone hydraulically joins the Dakota aquifer. Leakage from the overlying Upper Cretaceous confining layer also significantly influences the ground-water chemistry at the top part of the confined Dakota aquifer. Overall, the relationships of the major constituents show clearly the influence of mixing of different water sources in the confined parts of the Dakota aquifer.

The solubility of minerals plays an important role in controlling the major constituents of the ground water in different parts of the Dakota aquifer system. Dissolution of calcite occurs mainly in the Greenhorn Limestone and near the recharge area of the Dakota aquifer. Based on geochemical simulation, saturation with respect to calcite is likely to occur in the confined parts of the Dakota aquifer. Dissolution of halite, magnesite, and anhydrite (or gypsum) are the major factors controlling ground-water chemistry in the Cedar Hills Sandstone. Precipitation of gypsum was not found in the subsurface of any part of the system except for the weathered zone in outcrop areas of the Greenhorn Limestone, Graneros Shale,

part of the Dakota Formation, and the Kiowa Formation. Gypsum crystals found in the outcrop area indicate that gypsum solubility controls the sulfate concentration in the upper confining layers and lower part of the Dakota aquifer (Kiowa Formation) despite the absence of gypsum in the subsurface formations.

Water types of Na-Cl, Na-SO_4, and Na-mixed-anion in the west confined Dakota aquifer derive from a combination of cation exchange, mineral dissolution, oxidation-reduction, and mixing of waters. Dissolution of calcite and oxidation of pyrite and organic matter are the major sources of HCO_3 and SO_4, respectively. However, those reactions have occurred earlier in the flow path rather than where the Na-SO_4 and Na-mixed-anion type waters occur. Chemical data shows that reduction of SO_4 could be occurring in the west confined Dakota aquifer.

Cation exchange reactions have greatly influenced the ground-water chemistry in the confined Dakota aquifer and the shallow part of the Cedar Hills Sandstone. For the cation exchange to occur, the Dakota aquifer has to have contained saltwater prior to the current fresher water. The previous saltwater is assumed to have been derived mainly from the underlying Permian strata. The Na and Cl source was primarily from halite dissolution giving a Na/Cl mole ratio close to one. Cation exchange of Ca and Mg for Na in the Dakota aquifer would increase the dissolved Na relative to dissolved Cl content. Hence, the effect of cation exchange can be expressed by the amount of concentration difference between Na minus Cl. Figure 5.24 shows the excess Na in meq/L; the excess Na for the east confined Dakota aquifer and Cedar Hills waters ranges from near 0 up to 46 meq/L, whereas, the excess Na for the unconfined Dakota water is less than 5 meq/L. The excess Na for the west confined Dakota and Greenhorn waters ranges from 5 to 20 meq/L. There is no source of Na that can explain

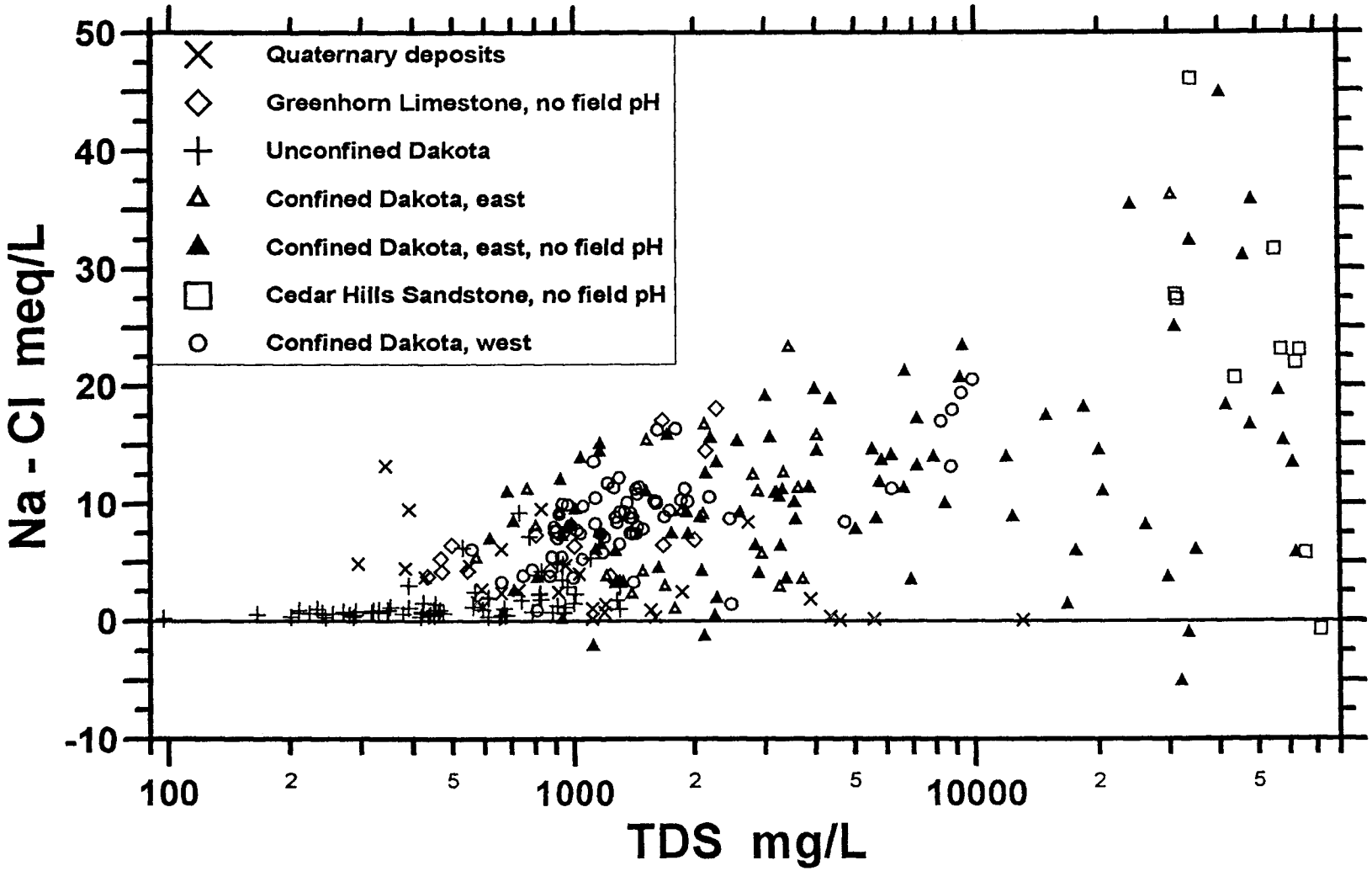

Figure 5.24. Na minus Cl equivalent concentration versus TDS content. The excess Na concentration is considered to be a result of cation exchange of dissolved Ca and Mg for Na on clays.

the excess Na other than cation exchange. The Cedar Hills water with the greatest salinity has equal Na and Cl concentrations. The increasing excess Na concentration with decreasing TDS content for Cedar Hills water suggests that some less saline water has also entered the Cedar Hills Sandstone and caused cation exchange.

An interesting pattern occurs for the Quaternary alluvial water group: excess Na generally increases with decreasing TDS content. This feature suggests that the shallow part of the alluvial aquifers is undergoing a freshening process. However, the freshening process has not yet affected the deeper part of the alluvial aquifers where water is brackish due to saltwater intrusion from below.

The evolution of Dakota water chemistry in central and north-central Kansas is a complex hydrogeochemical process. Water-chemistry data and geochemical simulations can only partially explain the ground-water evolution. The coupled hydrogeochemical simulations described in Chapter 7 provide a more complete explanation of the coupled reaction of mixing of waters, cation exchange, and calcite precipitation/dissolution. Chapter 8 will compare the water-chemistry data with the results of coupled models and give a more complete interpretation of the history of the ground-water chemistry in the Dakota aquifer.

CHAPTER 6

THE COUPLED HYDROGEOCHEMICAL PROGRAM

6.1. INTRODUCTION

In the past decade, the development of numerical models for coupling mass transport and chemical reactions of multi-components in subsurface systems has been growing rapidly. Most of the models have been designed to solve specific problems or contain limited functions for general modeling purposes (Rubin and James, 1973; Grove and Wood, 1979; Valocchi et al., 1981; Jennings et al., 1982, Miller and Benson, 1983; Rubin, 1983; Cedarberg, 1985; Lewis et al., 1986; Appelo and willemsen, 1987; Hostetler and Erikson, 1989; Yeh and tripathi, 1990). Some of the programs are flexible enough to allow incorporation of additional functions if necessary. However, there are still many unclear factors and relationships in many categories known to affect rates of chemical migration. It is still not practical to create a numerical model to cover the entire known set of possible transport and chemical functions occurring in nature. This is primarily because the required computing power is enormous, rather than there being a lack of knowledge concerning some of the phenomena.

Existing models of coupled transport and geochemistry were reviewed for applicability to this study. The review criteria included modeling capability, functions involved, and access to the model code. The model HYDROGEOCHEM (Yeh and Tripathi, 1990) was determined to be the most suitable. According to Yeh and Tripathi (1989), HYDROGEOCHEM is currently practical for the model size of the study in terms of the computing facilities available. A possible drawback of the program was that the chemical module was not thoroughly tested and the program had not yet been widely used.

HYDROGEOCHEM is a 2-D finite-element coupled hydraulic transport and chemical reaction model. This program was first released from the Oak Ridge National Laboratory in 1989 (Yeh and Tripathi, 1990). Since then, this program has been further improved (Yeh, 1992a, b, c). The program was written for general simulation purposes. The hydrological component of the model can be applied to heterogeneous, anisotropic, saturated and unsaturated flow under transient or steady state conditions. For geochemical equilibrium processes, the model includes aqueous complexation, redox, acid-base, adsorption-desorption, ion exchange, and precipitation-dissolution reactions. The model simulates the chemical reactions with the assumption of local chemical equilibrium. This program is designed to allow adaptation of additional advanced functions.

The capability of the original chemical module of HYDROGEOCHEM (EQMOD, Yeh, 1992(a)) was limited in handling dilute solutions due to the Davies convention it used for calculating the activity coefficient of chemical species. Part of the EQMOD was modified to adapt the program for use in this study. The performance of the HYDROGEOCHEM was also improved by programming additions, especially to enhance the input-output routines.

Although the program has been available for a few years and has been further improved since first release, the program was still not yet thoroughly tested. The input and output formats were not clearly documented. Difficulties in understanding the definition of the input parameters and reading the output data required a careful examination of the source code and fundamental theories of the program. Many bugs and defects were found and corrected. The input functions are now clearer and better documented. The output file was improved not only to clarify the data generated but also to allow more output options.

Adaptations for this research included adding the B$^{\bullet}$ method for calculating activity coefficients and the Gaines and Thomas convention for computing cation exchange. The following sections briefly describe the functions and governing equations for the program and the fundamental modifications made in the chemical module. For a detailed discussion of the program, the readers should refer to Yeh and Tripathi (1990, 1991), and Yeh (1992a, b, c).

6.2. MODEL STRATEGY AND GOVERNING EQUATIONS

HYDROGEOCHEM computes the coupled hydrogeochemical solutions by sequentially iterating between transport equations and geochemical equilibrium equations. This approach is currently the best approach for practical 2- and 3-D applications in terms of minimizing computing requirements. One major mathematical concern is the selection of the primary dependent variables (PDVs) which determine how successfully the model can deal with a complete suite of chemical reactions, realistic 2- and 3-D applications, and future expansion for advanced adaptations. The PDVs are solved via primary governing equations, which are mainly the partial differential equations for hydrological transport. Variables that are solved via secondary governing equations, which consist of mainly nonlinear algebraic equations for chemical reactions, are termed secondary dependent variables (SDVs). Once PDVs are obtained, SDVs and their partial derivatives with respect to PDVs can be computed from chemical reaction equations (Yeh and Tripathi, 1990). Figure 6.1 is a flow-chart of the main program. BC and IC stand for boundary and initial conditions, respectively. T is the total analytical concentration, and C is the total dissolved concentration. Tw is the total analytical concentration of the new iteration.

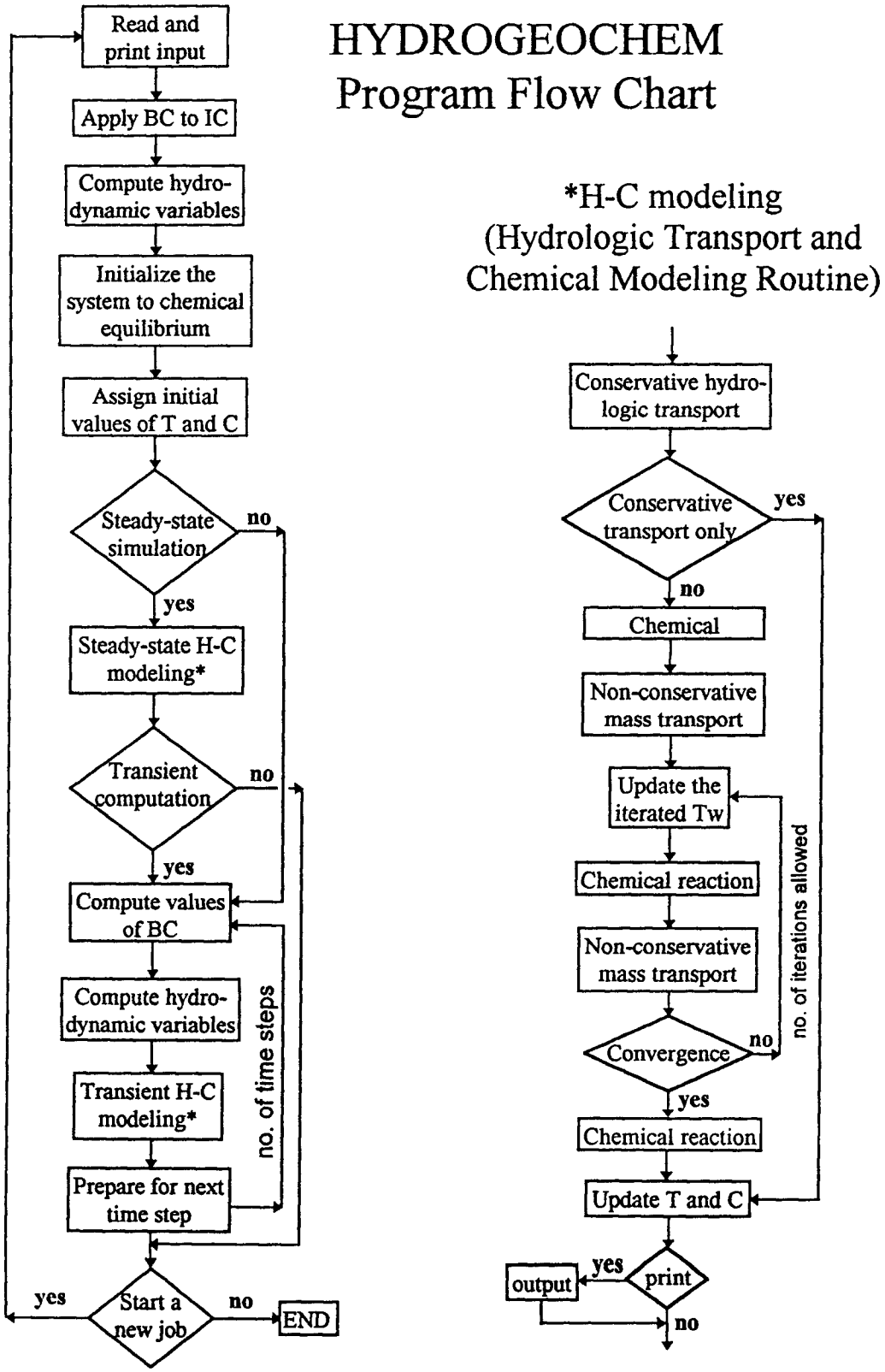

Figure 6.1. Flowchart for the main program of HYDROGEOCHEM.

Two often mentioned nomenclatures by Yeh and Tripathi (1989, 1990, 1991) are *components* and *species* that are used in this discussion. The definitions, based on Yeh and Tripathi (1990), are '*Components are a set of linearly independent "basis" chemical entities such that every species can be uniquely represented as a combination of those components; and no component can be represented by other components than itself. · · · · · A species is the product of a chemical reaction involving the components as reactants.*'

HYDROGEOCHEM employs the total analytical concentration of components as the PDVs. The concentrations of individual species are treated as the SDVs. The total analytical concentration for a component means the sum of the component concentrations in both aqueous and solid phases.

6.2.1. Flow Equations

The first step to simulate solute transport is to determine a flow field for the model. A finite-element flow model, HYDROFLOW (Yeh, 1992b), is used for this purpose. The governing flow equation ignores the compressibility of the media and water and is written as:

$$\frac{\partial\theta}{\partial t}=\frac{d\theta}{dh}\frac{\partial h}{\partial t}=\nabla\cdot[K\cdot\nabla(h+z)]+Q\ , \tag{6.1}$$

$$V=-K\cdot\nabla(h+z) \tag{6.2}$$

where

θ = moisture content (L^3/L^3),

h = pressure head (L),

$d\theta/dh$ = storage coefficient (1/L),

t = time (T),

K = hydraulic conductivity tensor (L/T),

Q = source or sink of water [(L^3/L^3)/T],

z = elevation (L),

V = Darcy's velocity (L/T).

For saturated flow, θ is equal to the porosity and thus $d\theta/dh$ is constant. For unsaturated flow conditions, K is a function of moisture content.

6.2.2. Hydrologic Transport Equations

The general transport governing equation can be derived based on the principle of conservation of mass. As described earlier, the geochemical functions of the model include 1) aqueous complexation, 2) adsorption, 3) ion exchange, 4) redox, 5) acid-base, and 6) dissolution-precipitation reactions. The total analytical concentrations of components are used as the PDVs. The transport governing equations consider all the chemical species involved in the system. Since the model flow field is determined independently, the density effect of dissolved solids on mass transport is not considered in the program.

The governing transport equation for the aqueous component (free ion) species (subscript (a)) can be obtained by applying the principle of mass conservation in integral form as follow:

$$\frac{D}{Dt}\int_v \theta c_j dv = -\int_\Gamma n\cdot(\theta c_j)V_f d\Gamma - \int_\Gamma n\cdot J_j d\Gamma + \int_v \theta r_{(a)j} dv - \int_v \theta t_{(a)j} dv + \int_v m_{(a)j} dv, \qquad (6.3)$$

$$j = 1, 2, \ldots, N_a$$

where

v = material volume containing constant amount of media (L^3),

c_j = concentration of the j-th aqueous component species (M/L^3),

Γ = surface enclosing the material volume v (L^2),

n = outward unit vector normal to the surface Γ,

V_f = V/θ, linear fluid velocity relative to the solid (L/T),

J_j = $\theta c_j(V_j - V_f)$, is the surface flux of the j-th aqueous component species with respect to linear fluid velocity V_f [$(M/T)/L^2$],

$r_{(a)j}$ = production rate of the j-th aqueous component species per unit fluid volume due to all chemical reactions [$(M/L^3)/T$],

$\iota_{(a)j}$ = rate of decay of the j-th aqueous component species [$(M/L^3)/T$],

$m_{(a)j}$ = external source/sink rate of the j-th aqueous component species [$(M/L^3)/T$],

N_a = number of aqueous component species.

Equation (6.3) can be expressed with respect to a differential volume (Yeh and Tripathi, 1990) as

$$\frac{\partial \theta c_j}{\partial t} + \nabla \cdot (c_j V) - \nabla \cdot (\theta D \cdot \nabla c_j) = \theta (r_{(a)j} - \iota_{(a)j}) + m_{(a)j}, \quad j = 1, 2, \ldots, N_a \qquad (6.4)$$

where D is the dispersion coefficient tensor (L^2/T). The first term represents the accumulation rate of mass, the second term represents the advection rate of mass flux, the third term is the net mass flux rate caused by dispersion and diffusion, the fourth term is the rate of mass change due to chemical reactions and radioactive decay, and the fifth term is the source/sink of mass at boundaries.

Equation 6.4 is a mass balance equation written in conservative form. The advection-diffusion form is sometimes more appropriate for numerical simulation of solute transport.

Therefore, an advection-diffusion transport equation is derived by expanding the first term of Equation 6.4 and combining Equations 6.1 and 6.2:

$$\theta\frac{\partial c_j}{\partial t} + V\cdot\nabla c_j - \nabla\cdot(\theta D\cdot\nabla c_j) = \theta(r_{(a)j} - \iota_{(a)j}) + m_{(a)j} - Qc_j\,, \qquad (6.5)$$

$$j = 1, 2, ..., N_a$$

Since all the aqueous complex species (subscript (x)) are subject to the same hydrologic transport mechanism as the aqueous component species, the governing transport equation is identical in form to Equation 6.5.

$$\theta\frac{\partial x_i}{\partial t} + V\cdot\nabla x_i - \nabla\cdot(\theta D\cdot\nabla x_i) = \theta(r_{(x)i} - \iota_{(x)i}) + m_{(x)i} - Qx_i\,, \qquad (6.6)$$

$$i = 1, 2, ..., M_x$$

where

x_i = concentration of the i-th complexed species (M/L^3),

$r_{(x)i}$ = production rate of i-th complexed species per unit fluid volume due to the i-th complexation reaction [$(M/T)/L^3$],

$\iota_{(x)i}$ = rate of decay of the i-th complexed species [$(M/L^3)/T$],

$m_{(x)i}$ = external source/sink rate of the i-th complexed species [$(M/L^3)/T$],

M_x = number of aqueous complexed species.

The program assumes that all the species in the solid phase are immobile, such as adsorbent components (immobile adsorbing site, subscript (s)), adsorbed species(subscript (y)), ion-exchange species (subscript (z)), and precipitated species (subscript (p)). Their governing equations can be obtained by expanding the first term and by dropping the second and the third terms on the left-hand side of Equation (6.4).

$$\theta\frac{\partial s_j}{\partial t}+\frac{\partial \theta}{\partial t}s_j=\theta(r_{(s)j}-\iota_{(s)j})+m_{(s)j}\,,\qquad j=1,\ 2,\ \ldots,\ N_s \tag{6.7}$$

$$\theta\frac{\partial y_i}{\partial t}+\frac{\partial \theta}{\partial t}y_i=\theta(r_{(y)i}-\iota_{(y)i})+m_{(y)i}\,,\qquad i=1,\ 2,\ \ldots,\ M_y \tag{6.8}$$

$$\theta\frac{\partial z_i}{\partial t}+\frac{\partial \theta}{\partial t}z_i=\theta(r_{(z)i}-\iota_{(z)i})+m_{(z)i}\,,\qquad i=1,\ 2,\ \ldots,\ M_z \tag{6.9}$$

and

$$\theta\frac{\partial p_i}{\partial t}+\frac{\partial \theta}{\partial t}p_i=\theta(r_{(p)i}-\iota_{(p)i})+m_{(p)i}\,,\qquad i=1,\ 2,\ \ldots,\ M_p \tag{6.10}$$

where

s_j = concentration of the j-th adsorbent component (M/L^3),

$r_{(s)j}$ = production rate of the j-th adsorbent component species per unit fluid volume due to all sorption reactions [$(M/L^3)/T$],

$m_{(s)j}$ = external source/sink rate of the j-th adsorbent component species [$(M/L^3)/T$],

$\iota_{(s)j}$ = rate of decay of the j-th adsorbent component species [$(M/L^3)/T$],

N_s = number of adsorbent component species,

y_i = concentration of the i-th adsorbed species (M/L^3),

$r_{(y)i}$ = production rate of the i-th adsorbed species per unit fluid volume due to the i-th sorption reaction [$(M/L^3)/T$],

$m_{(y)i}$ = external source/sink rate of the i-th adsorbed species [$(M/L^3)/T$],

$\iota_{(y)i}$ = rate of decay of the i-th adsorbed species [$(M/L^3)/T$],

M_y = number of adsorbed species,

z_i = concentration of the i-th ion-exchanged species (M/L^3),

$r_{(z)i}$ = production rate of the i-th ion-exchanged species per unit fluid volume due to the i-th ion-exchange reaction [(M/L^3)/T],

$m_{(z)i}$ = external source/sink rate of the i-th ion-exchanged species [(M/L^3)/T],

$\iota_{(z)i}$ = rate of decay of the i-th ion-exchanged species [(M/L^3)/T],

M_z = number of ion-exchanged species,

p_i = concentration of the i-th precipitated species (M/L^3),

$r_{(p)i}$ = production rate of the i-th precipitated species per unit fluid volume due to the i-th precipitation reaction [(M/L^3)/T],

$m_{(p)i}$ = external source/sink rate of the i-th precipitated species [(M/L^3)/T],

$\iota_{(p)i}$ = rate of decay of the i-th precipitated species [(M/L^3)/T],

M_p = number of precipitated species.

Equations 6.5 through 6.10 constitute six sets of equations for six sets of unknowns, c_j, x_i, s_j, y_i, z_i, and p_i. Multiplying each equation by the stoichiometric constant of the chemical reaction and summing over all the species for the equation gives:

$$\theta\frac{\partial T_j}{\partial t}+\frac{\partial\theta}{\partial t}(S_j+P_j)+V\cdot\nabla C_j=\nabla\cdot(\theta D\cdot\nabla C_j)-\theta\Lambda_{(s)j}+M_{(s)j}-QC_j\,, \qquad (6.11)$$

$$j=1,\,2,\,...,\,N_s$$

The governing equations for the adsorbent component is

$$\theta\frac{\partial W_j}{\partial t}+\frac{\partial\theta}{\partial t}W_j=-\theta\Lambda_{(s)j}+M_{(s)j}\,,\quad j=1,\,2,\,...,\,N_s\,, \qquad (6.12)$$

The governing equation for the ion-exchange site is obtained similarly to Equation 6.12 but with the assumption that the site is completely occupied:

$$\theta \frac{\partial N_{eq}}{\partial t} + \frac{\partial \theta}{\partial t} N_{eq} = -\theta \Lambda_{eq} + M_{eq} \tag{6.13}$$

in which

$$C_j = c_j + \sum_{i=1}^{M_x} a_{(x)ij}\, x_i\,, \quad j=1, 2, ..., N_a\,, \tag{6.14}$$

$$S_j = \sum_{i=1}^{M_y} a_{(y)ij}\, y_i + \sum_{i=1}^{M_z} a_{(z)ij}\, z_i\,, \quad j=1, 2, ..., N_a\,, \tag{6.15}$$

$$P_j = \sum_{i=1}^{M_p} a_{(p)ij}\, p_i\,, \quad j=1, 2, ..., N_a\,, \tag{6.16}$$

$$T_j = c_j + \sum_{i=1}^{M_x} a_{(x)ij}\, x_i + \sum_{i=1}^{M_y} a_{(y)ij}\, y_i + \sum_{i=1}^{M_z} a_{(z)ij}\, z_i + \sum_{i=1}^{M_p} a_{(p)ij}\, p_i\,, \tag{6.17}$$

$$j = 1, 2, ..., N_a\,,$$

$$M_{(a)j} = m_{(a)j} + \sum_{i=1}^{M_x} a_{(x)ij}\, m_{(x)i} + \sum_{i=1}^{M_y} a_{(y)ij}\, m_{(y)i} + \sum_{i=1}^{M_z} a_{(z)ij}\, m_{(z)i} + \sum_{i=1}^{M_p} a_{(p)ij}\, m_{(p)i}\,,$$

$$j = 1, 2, ..., N_a\,, \tag{6.18}$$

$$\Lambda_{(a)j} = \iota_{(a)j} + \sum_{i=1}^{M_x} a_{(x)ij}\, \iota_{(x)i} + \sum_{i=1}^{M_y} a_{(y)ij}\, \iota_{(y)i} + \sum_{i=1}^{M_z} a_{(z)ij}\, \iota_{(z)i} + \sum_{i=1}^{M_p} a_{(p)ij}\, \iota_{(p)i}\,,$$

$$j = 1, 2, ..., N_a\,, \tag{6.19}$$

$$W_j = s_j + \sum_{i=1}^{M_y} b_{(y)ij}\, y_i\,, \quad j=1, 2, ..., N_s\,, \tag{6.20}$$

$$N_{eq} = \sum_{i=1}^{M_z} \nu_i z_i \qquad (6.21)$$

where

C_j = total dissolved concentration of the j-th aqueous component (M/L^3),

S_j = total sorbed (adsorbed plus ion-exchanged) concentration of the j-th aqueous component (M/L^3),

P_j = total precipitated concentration of the j-th aqueous component (M/L^3),

T_j = total analytical concentration of the j-th aqueous component (M/L^3),

$M_{(a)j}$ = total source/sink rate of the j-th aqueous component ($M/L^3/T$),

$\Lambda_{(a)j}$ = total decay rate of the j-th aqueous component ($M/L^3/T$),

$a_{(x)ij}$ = stoichiometric coefficient of the j-th aqueous component in the i-th complexed species,

$a_{(y)ij}$ = stoichiometric coefficient of the j-th aqueous component in the i-th adsorbed species,

$a_{(z)ij}$ = stoichiometric coefficient of the j-th aqueous component in the i-th ion-exchanged species,

$a_{(p)ij}$ = stoichiometric coefficient of the j-th aqueous component in the i-th precipitated species,

W_j = total analytical concentration of the j-th adsorbent component (M/L^3),

$M_{(s)j}$ = total source/sink rate of the j-th adsorbent component ($M/L^3/T$),

$\Lambda_{(s)j}$ = total decay rate of the j-th adsorbent component ($M/L^3/T$),

N_{eq} = number of equivalents of the ion-exchange site per unit volume of solution (M/L^3),

M_{eq} = total (equivalent) source/sink rate of the ion-exchange site ($M/L^3/T$),

Λ_{eq} = total (equivalent) decay rate of the ion-exchange site ($M/L^3/T$),

$b_{(y)ij}$ = stoichiometric coefficient of the j-th adsorbent component in the i-th sorbed species,

ν_i = charge of the i-th ion-exchanged species.

6.2.3. Chemical Equilibrium Equations

Chemical reactions are described by a set of nonlinear algebraic equations under the assumption of local equilibrium. EQMOD calculates the chemical equilibrium based on the ion association and equilibrium constant approach (compared to the Gibbs free-energy approach). In the equilibrium constant approach, a set of nonlinear algebraic equations is obtained based on the law of mass action and the principle of mole balance. The notations remain consistent with the previous section that subscripts of (a), (x), (s), (y), (z), and (p) represent aqueous species, aqueous complex species, adsorbent, adsorbed species, ion-exchanged species, and precipitated species, respectively. The nonlinear algebraic equations for the chemical equations can be obtained as follows:

6.2.3.1. Aqueous complexation

$$x_i = \alpha_{(x)i} \prod_{k=1}^{N_a} c_k^{a_{(x)ik}}, \quad i = 1, 2, \ldots, M_x \tag{6.22a}$$

in which

$$\alpha_{(x)i} = K_{(x)i} \prod_{k=1}^{N_a} (\gamma_{(a)k})^{a_{(x)ik}} / \gamma_{(x)i}, \quad i = 1, 2, \ldots, M_x \tag{6.22b}$$

Where

$\alpha_{(x)i}$ = the modified stability constant of the i-th complexed species (at ionic strength, $I \neq 0$),

$K_{(x)i}$ = the thermodynamic equilibrium constant of the i-th complexed species,

$\gamma_{(x)i}$ = the activity coefficient of the i-th complexed species (L^3/M),

$\gamma_{(a)k}$ = the activity coefficient of the k-th aqueous component species (L^3/M).

6.2.3.2. Adsorption

$$y_i = \alpha_{(y)i} \left(\prod_{k=1}^{N_a} c_k^{a_{(y)ik}} \right) \left(\prod_{k=1}^{N_s} s_k^{b_{(y)ik}} \right), \quad i = 1, 2, \ldots, M_y \tag{6.23a}$$

in which

$$\alpha_{(y)i} = K_{(y)i} \left[\prod_{k=1}^{N_a} (\gamma_{(a)k})^{a_{(y)ik}} \right] \left[\prod_{k=1}^{N_s} (\gamma_{(s)k})^{b_{(y)ik}} \right] \Big/ \gamma_{(y)i}, \tag{6.23b}$$

$$i = 1, 2, \ldots, M_y$$

where

$\alpha_{(y)i}$ = the modified stability constant of the i-th adsorbed species (at $I \neq 0$),

$K_{(y)i}$ = the thermodynamic equilibrium constant of the i-th adsorbed species,

$\gamma_{(y)i}$ = the activity coefficient of the i-th adsorbed species (L^3/M),

$\gamma_{(s)k}$ = the activity coefficient of the k-th adsorbent component species (L^3/M).

6.2.3.3. Ion exchange

Equilibrium models of ion exchange reaction follow three principles: electroneutrality, filled exchange sites, and an equilibrium law relating the concentrations in solution to those on the solid matrix (Rubin and James, 1973; Charbeneau, 1981). One common aspect of all cation exchange selectivity equations is that the ratio of the dissolved cation activity is important rather than the individual cation activity. Among the proposed equations for calculating cation selectivity coefficients, Vanselow (Vanselow, 1932), Gaines and Thomas (Gaines and Thomas, 1953), and Gapon (Gapon, 1933) conventions are the most commonly used. All three conventions have been applied to transport models with cation exchange (Valocchi et al., 1981; Miller and Benson, 1983; Van Ommen, 1985; Cederberg et al., 1985; Charbeneau, 1988). Originally, in EQMOD, activities of ion-exchanged species are calculated by their mole fractions, which is the Vanselow convention.

Appelo et al. (1993) applied the three cation exchange conventions to a multicomponent, heterovalent system to calculate the mixing front of mass transportation. They concluded that both Gaines and Thomas and Vanselow conventions give near-identical

results. The Gapon equation can easily lead to selectivity reversal when the aqueous fractions of a solute change, a situation not found in experimental data.

The Gaines and Thomas convention was chosen over the Vanselow equation and adapted to the EQMOD module for the ion-exchange calculations. There are two reasons for the preference. First, there are more data for selectivity coefficients for the Gaines and Thomas equation in the literature than for other conventions. Second, the use of the equivalent fraction for the calculation of the selectivity coefficient corresponds to the conventional unit, equivalent per unit weight of dry solid mass, for laboratory determined CEC. Therefore, an extra computation procedure can be omitted that is necessary when using the Vanselow convention (Griffioen, 1993). Furthermore, the author uses SOLMINEQ.88 to verify the modified program and to prepare chemical data for the coupled simulation. SOLMINEQ.88 calculates the selectivity coefficient using the equivalent fractions of adsorbed ions.

A general Gaines and Thomas ion-exchange reaction equation is given as

$$\tfrac{1}{a}A^{a+} + \tfrac{1}{b}B\text{–}X_b \Leftrightarrow \tfrac{1}{b}B^{b+} + \tfrac{1}{a}A\text{–}X_a, \qquad K_{A/B}^{GT} = \frac{[B^{b+}]^{1/b}[A\text{–}X_a]^{1/a}}{[A^{a+}]^{1/a}[B\text{–}X_b]^{1/b}} \tag{6.24}$$

where

a = charge of ion-exchange species A,

b = charge of ion-exchange species B,

X = surface ion-exchange site,

$i\text{-}X_{v_i}$ = adsorbed species i, i represents A or B, and v_i is the charge of i,

$K_{A/B}^{GT}$ = selectivity coefficient between species A and B.

Equation 6.24 uses the exchangeable cations as the basis for their activity. Due to lack of data for the activity of adsorbed species, an ideal solution was proposed by Gaines and Thomas

(1953) assumed that the activity of adsorbed species equals their equivalent fractions on the surface sites. Thus,

$$\beta_i = q_i / N_{eq} \ , \quad i = 1, 2, \ldots, M_z \ , \tag{6.25a}$$

in which

$$q_i = \nu_i z_i \ , \tag{6.25b}$$

where

β_i = equivalent fraction of adsorbed species per unit solution volume for ion exchange,

q_i = equivalent concentration of adsorbed species per unit solution volume for ion exchange (M/L^3)

Rather than from Equation 6.21, the total amount of ion exchange sites is normally determined from

$$N_{eq} = \frac{\rho}{\theta} CEC \tag{6.26}$$

where

ρ = bulk density per unit volume of aquifer materials (M/L^3),

CEC = equivalents of cation exchange capacity per unit weight of dry solid (M/M).

The selectivity coefficient of Equation 6.24 then becomes

$$K_{A/B}^{GT} = \frac{[B^{b+}]^{1/a} \beta_A^{\ 1/b}}{[A^{a+}]^{1/b} \beta_B^{\ 1/a}} \tag{6.27}$$

Instead of using the form of Equation 6.24 in EQMOD, the chemical reaction is treated as

$$bA^{a+} + aB\text{–}X_b \Leftrightarrow aB^{b+} + bA\text{–}X_a \ , \quad K'_{A/B} = \frac{[A\text{–}X_a]^b [B^{b+}]^a}{[A^{a+}]^b [B\text{–}X_b]^a} \tag{6.28}$$

With some manipulation, the selectivity coefficient for Equation 6.28 can be expressed as

$$K'_{A/B} = \left(\frac{a z_A / N_{eq}}{\gamma_A(A^{a+})}\right)^b \left(\frac{\gamma_B(B^{b+})}{b z_B / N_{eq}}\right)^a \tag{6.29}$$

The concentration of adsorbed species A can be obtained by

$$z_A = \left[K'_{A/B} \frac{b^a}{a^b} \frac{\left(\gamma_A(A^{a+})\right)^b}{\left(\gamma_B(B^{b+})\right)^a} z_B^a (N_{eq})^{b-a} \right]^{1/b} \tag{6.30}$$

A general form of Equation 6.30 is used as the governing equation of the ion-exchange reaction for the program as shown below

$$z_i = \left[K'_{iJ} \frac{\nu_J^{\nu_i}}{\nu_i^{\nu_J}} \frac{(\gamma_i a_i)^{\nu_J}}{(\gamma_J a_J)^{\nu_i}} z_J^{\nu_i} (N_{eq})^{\nu_J - \nu_i} \right]^{1/\nu_J}, \quad i = 1, 2, \ldots, M_z \tag{6.31}$$

where

K'_{iJ} = the selectivity coefficient ($K_{JJ} = 1$) of the i-th species with respect to the J-th species for equation (6.29),

γ_i = the activity coefficient of the i-th aqueous species denoting either $\gamma_{(x)i}$ or $\gamma_{(a)i}$ (L^3/M),

a_i = the mole concentration of the i-th aqueous species denoting either c_j or x_i (M/L^3).

The fortran subroutine including the modified code is listed in Table B.1 of Appendix B.

6.2.3.4. Precipitation-dissolution

$$1 = \alpha_{(p)i} \prod_{k=1}^{N_s} c_k^{a_{(p)ik}} , \quad i = 1, 2, \ldots, M_p , \tag{6.32a}$$

in which

$$\alpha_{(p)i} = K_{(p)i} \prod_{k=1}^{N_s} (\gamma_{(a)k})^{a_{(p)ik}} , \quad i = 1, 2, \ldots, M_p , \tag{6.32b}$$

where

$\alpha_{(p)i}$ = the modified stability constant of the i-th precipitated species (at ionic strength, $I \neq 0$),

$K_{(p)i}$ = the thermodynamic equilibrium constant of the i-th precipitated species,

No concentration of precipitated mineral is contained in Equation 6.32b because its activity is assumed to be 1.

6.2.3.5. Redox reactions and electron activity

Redox reactions involve transfer of electrons. The "operational" electron can be considered as an aqueous component and no special mathematical treatment is needed for redox reactions (Reed, 1982; Yeh and Tripathi, 1990). A redox reaction can also be considered as a complexation, precipitation, adsorption, or ion-exchange reaction if the resulting species is involved in such kinds of reactions.

6.2.3.6. Acid-base reactions and proton activity

Similar to the redox reaction, the acid-base reaction involves transfer of protons. For the coupled model, the total concentration of the excess proton ($\Sigma H^+ - \Sigma OH^-$) must be known before the pH can be computed. A negative total analytical concentration of excess protons can occur if the total OH^- concentration is greater than the total H^+ concentration in the system. An acid-base reaction can be considered as an aqueous complexation, precipitation, adsorption, or ion-exchange reaction if the resulting species containing H^+ or OH^- ions are involved in such kind of reactions.

6.2.3.7. Activity coefficient

Solute concentrations are expressed as activities in the law of mass action. The activities of all aqueous species are related to their mole concentrations by the concept of activity coefficient. Thus,

$$A_i = \gamma_i a_i \tag{6.33}$$

where A_i is the activity of aqueous species i, a_i the molality, and γ_i the activity coefficient. The activity coefficients of aqueous species depend considerably on the salt content, which is expressed by the ionic strength of the solution. Ionic strength I is defined as

$$I = \frac{1}{2}\sum_{i=1}^{M_a} a_i \nu_i^2 \tag{6.34}$$

where M_a is the number of aqueous species equal to the number of aqueous component species plus the number of complexed species. The ionic strength of freshwater is normally less than

0.02, while seawater has an ionic strength of about 0.7. For an uncharged species the salt effect is relatively small for the usual range of possible salt concentrations.

Activity coefficients of charged aqueous species are determined experimentally. Many semi-empirical formulae, usually based on electrostatic Debye-Hückel theory, have been proposed to estimate activity coefficients from the ionic strength. The Davies equation is used in the original EQMOD geochemical model and is valid up to I = 0.5 M (Kotrly and Sucha, 1985; Appelo and Postma, 1994). However, for the Dakota aquifer study, the coupled model must deal with ground water with TDS up to 70,000 mg/L and an ionic strength of more than 1.2 M. A modified Debye-Hückel equation - the $B^{\bullet}$ method (Helgeson, 1969) was adapted for HYDROGEOCHEM to handle the high TDS water. In fact, the $B^{\bullet}$ option is only valid for solutions with ionic strength up to about 1 M (Kharaka et al., 1988). However, the ionic strength of solutions in most of the model domain is less than the maximum criterion for the $B^{\bullet}$ method. Information is seldom obtained for the Permian brine because it is not of interest for use as a water resource. It is tolerable to have a less accurate result for the area in the model of extremely high salinity due to the lack of data.

The $B^{\bullet}$ method is a modified Debye-Hückel equation shown as

$$\log \gamma_i = \frac{-A_\gamma z_i^2 \sqrt{I}}{1 + \mathring{a}_i B_\gamma \sqrt{I}} + B^{\bullet} I \ , \qquad (6.35a)$$

in which

$$A_\gamma (T) = \frac{1.8248 \times 10^6 \sqrt{\rho_w}}{(\varepsilon T)^{3/2}} \ , \qquad (6.35b)$$

and

$$B_\gamma(T) = \frac{50.29 \times 10^8 \sqrt{\rho_w}}{\sqrt{\varepsilon T}} \quad , \tag{6.35c}$$

where

$\mathring{a}_i$ = ion size parameter for the i-th species,

T = temperature ($^\circ$K),

A_γ = molar Debye-Hückel coefficient, which is a function of temperature T,

B_γ = molar Debye-Hückel coefficient, which is a function of temperature T,

ρ_w = density of water at temperature T,

ε = dielectric constant at temperature T,

$B^\bullet$ = deviation function.

Currently, the $B^\bullet$ method in the program is only valid for a temperature range of 0 - 50 $^\circ$C and one atmosphere of pressure. The Dakota aquifer in the study area occurs at relatively shallow depths, thus pressure differences are not important and aquifer temperature is also well within the temperature range allowed for valid chemical calculations. The ion size parameters are given in the database of the user's manual for SOLMINEQ.88. The values used for molar Debye-Hückel coefficients A_γ and B_γ are from Helgeson et al. (1981), and the values for the $B^\bullet$ deviation function were obtained from Helgeson (1969) and Kharaka et al. (1988). These values are listed in Table 6.1. The fortran source code for the adapted $B^\bullet$ method is listed in Table B.2.

Table 6.1. Values for Debye-Hückel parameters (Helgeson et al., 1981) and $B^{\bullet}$ deviation function (Helgeson, 1969) for temperatures between 0 to 50 °C and one atmosphere of pressure.

Temperature (°C)	A_γ	B_γ	$B^{\bullet}$
0	0.4913	0.3247	0.038
5	0.4943	0.3254	--
10	0.4976	0.3261	--
15	0.5012	0.3268	--
20	0.5050	0.3276	--
25	0.5091	0.3283	0.041
30	0.5135	0.3291	--
35	0.5182	0.3299	--
40	0.5231	0.3307	--
45	0.5282	0.3316	--
50	0.5336	0.3325	0.043

Examples of activity coefficients simulated by the modified EQMOD at different ionic strengths for selected ion species are presented in Figure 6.2. The modified chemical module was verified by comparing results with SOLMINEQ.88. The deviation between results of these two models is within 3%. The deviation is mainly caused by a different number of chemical species involved in the test problems for SOLMINEQ.88, which includes a database with a large number of equilibrium constants for aqueous species and minerals, compared to the modified EQMOD.

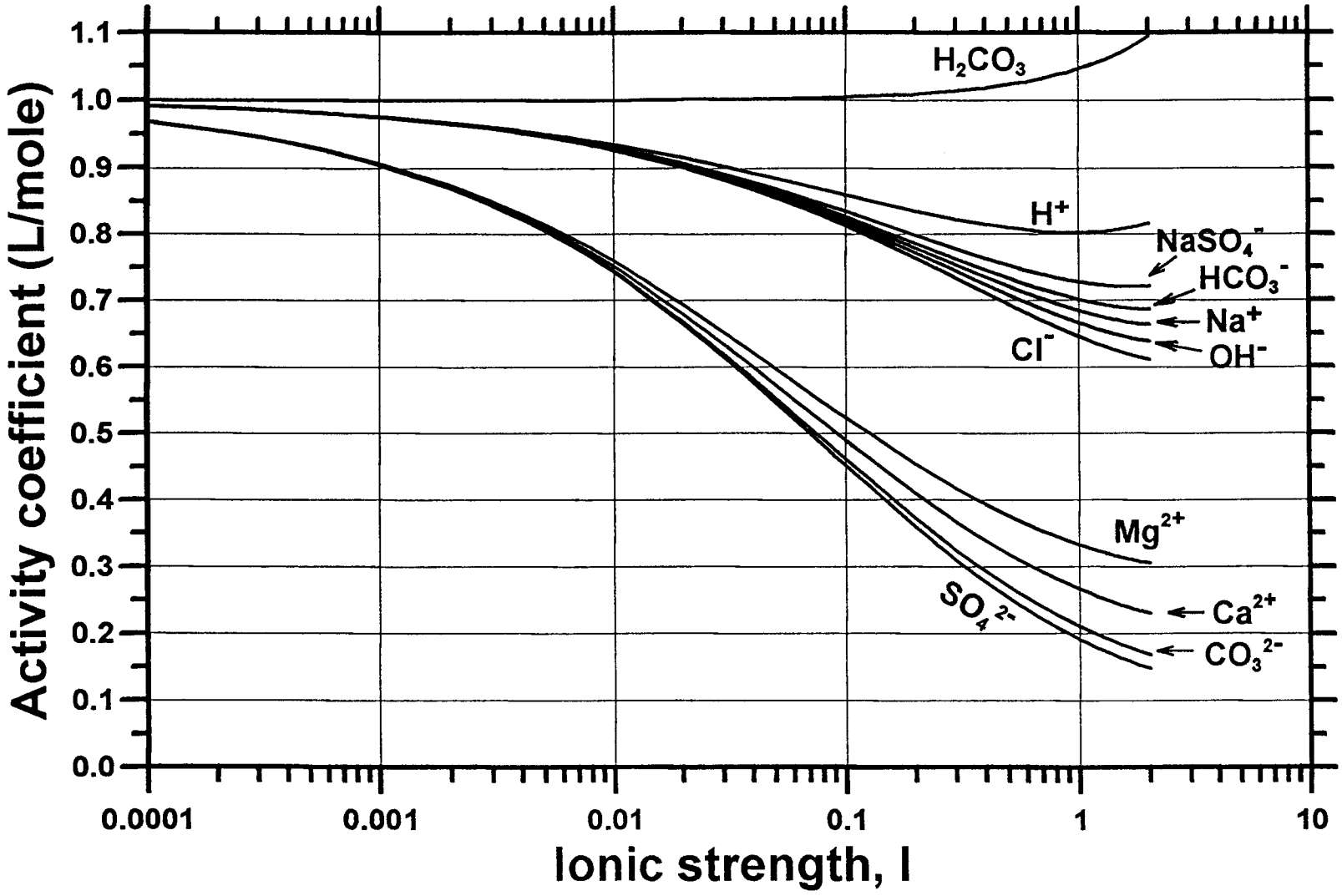

Figure 6.2. Relations of EQMOD simulated activity coefficients for selected aqueous sepcies to ionic strength of solution (15 °C).

CHAPTER 7

ONE-DIMENSIONAL COUPLED MODEL

7.1. SCOPE

The purpose of the 1-D model is to improve the understanding of the fundamental concepts of coupled hydrogeochemical processes occurring in the Dakota aquifer. Transitions in water types are caused mainly by salinity changes and cation exchange and concomitant reactions. As described earlier, mixing of waters in the Dakota aquifer has caused chemical reactions to occur, i.e., cation exchange reactions, precipitation/dissolution of calcite, and dissolution of gypsum, that control major constituent concentrations. Previous studies indicate that Na-SO_4-HCO_3 and Na-mixed-anion type waters in western and central Kansas are produced by cation exchange due to freshening of the aquifer (Macfarlane et al., 1988, 1991). However, it is unclear how the concomitant reactions interact with each other during flow through the aquifer. A simple 1-D model can help to explain the fundamental concept of the flow and chemical interactions along a flow path.

Other reactions also occur due to changes in chemical environment, i.e., oxidation of pyrite and organic matter, and possibly reduction of sulfate. There is insufficient data for systematically defining redox conditions for the Dakota aquifer, thus no attempt was made to simulate the redox reactions. Moreover, because of the local equilibrium assumption (LEA) for HYDROGEOCHEM, dissolution of gypsum was not modeled because geochemical simulation indicates that the Dakota water is undersaturated with respect to gypsum (Figure 5.10). The LEA will force the simulated water to be in equilibrium with gypsum if the mineral is given to the model, and therefore, the water chemistry in the model would be greatly altered.

Suggested approaches for overcoming the deficiency of LEA include supplying the products of gypsum as external sources or reducing the equilibrium constant of gypsum to account for conditions of unsaturation (Tripathi, 1994, personal communication). No attempt was made to include these approaches in the models because they would induce more uncertainty and a better result is not assured if the operation is not well planned. However, the LEA should be valid for the cation exchange and precipitation/dissolution of calcite because these reactions reach equilibrium in a few hours to a few days (Langmuir, 1971; Bahr and Rubin, 1987; Bahr, 1990; Griffioen, 1993) compared to the duration of years for ground water in the Dakota aquifer.

Previous studies of ion exchange have often assumed that exchange occurs among free ions. This assumption has been applied in almost all the numerical simulations. Recently, exchange with complex species has been considered to have a major impact on cation exchange and water chemistry (Sposito et al., 1983a, 1983b; Suarez and Zahow, 1989; Griffioen and Appelo, 1992; Griffioen, 1992, 1993). However, data for the properties of adsorbed complexes are sparse. In addition, little is known about the properties of cation exchange reactions in the Dakota aquifer. Both reasons prohibit the application of a complicated model of ion exchange. Only exchange among the free ions of Ca^{2+}, Mg^{2+}, and Na^{+} was simulated to elucidate observed chemical transitions in the Dakota aquifer.

As described in Chapter 3, a significant portion of some of the major dissolved constituents exist in the form of ion pairs and ion complexes. Sulfate complexes are the most important. Aqueous complexes can have an important effect on cation exchange if only the free ions are involved in the exchange reactions. This means that the larger the fraction of the

exchanging cation in ion complexes, the smaller the free-ion concentration available for cation exchange.

Variations in the depleted Ca and Mg concentrations in the Dakota water to the west of the Cedar Hills subcrop indicate that multiple factors control the intensity of cation exchange. The occurrence of cation exchange is related to the mixing of waters and surface properties of formation materials. Factors related to these two reactions are believed to be the major controls. Numerical sensitivity analyses were performed to determine the factors controlling the intensity of the cation-exchange reactions. The tests were carried out in six different categories (Table 7.1). The first three analyses test the effect of the properties of the aquifer materials. The last three examine the individual effect of the chemistry of initial and incoming waters and the effect of the concentration difference between the mixing waters. The incoming waters of the sixth category have already undergone some degree of cation exchange. This category examines the effect of cation exchange on water chemistry after the water has passed through several different chemical environments with increased intensity of cation exchange along the flow path.

7.2. MODEL SETUP

The 1-D model simulates the chemical interactions occurring as a result of mixing of waters, ion exchange, ion complexing, and calcite dissolution/precipitation. The model grid was carefully designed so that the retardation and conservative mixing front of the incoming freshwater and initial saltwater can all be represented at a particular simulation time with a significant number of nodes for each stage. There are 201 nodes along a seven-kilometer (4.38

Table 7.1. Categories for sensitivity analyses of the effect of properties of the formation materials and the salinities of initial and incoming waters on cation exchange.

Category	Test values	Model name	Remarks
I. Selectivity coefficient for Mg $K_{Mg/Ca}$*	0.5	1D11	The simulation time for all the models is 567 years.
	0.7	1D00	
	1.0	1D13	
II. Selectivity coefficient for Ca $K_{Ca/Na}$*	2.0	1D21	Conditions for standard model input other than the test values: $K_{Ca/Na}$*= 3.2, $K_{Mg/Ca}$*= 0.7
	3.2	1D00	
	5.0	1D23	
III. Cation exchange capacity meq/kg of solid	10	1D31	CEC = 25 meq/kg, initial water = 14S-14W-14CD incoming water = 6S-3W-11ADAA
	25	1D00	
	100	1D33	
	500	1D34	
IV. Initial saltwater TDS mg/L	6883	1D41	14S-14W-21CD1 (Table A.6)
	33410	1D42	13S-14W-19D1 (Table A.6)
	71410	1D00	14S-14W-14CD (Table A.8)
V. Incoming water TDS mg/L Na ≈ Cl	450	1D00**	6S-3W-11ADAA (Table A.3)
	2112	1D52	14S-14W-25BB1 (Table A.6)
	6883	1D53	14S-14W-21CD1 (Table A.6)
VI. Incoming water TDS mg/L (Na - Cl meq/L)***	450 (-0.7)	1D00	6S-3W-11ADAA (Table A.3)
	955 (7.87)	1D62	6S-5W-6CB (Table A.6)
	2119 (16.7)	1D63	15S-12W-14ADD (Table A.5)

* : Refer to Equation 6.24 for definition.
** : The incoming water for the model is saturated with respect to calcite.
*** : The value in parentheses is the concentration difference of Na minus Cl.

miles) long flow path for the model (Figure 7.1). The grid size varies from 10 to 50 m (33 - 164 ft) in horizontal distance.

The aquifer properties and flow condition for the model imitate the Dakota aquifer. The reported porosity for the Dakota sandstone ranges from 0.20 to 0.35 (Macfarlane et al., 1990). However, to account for the 60 to 70% of siltstone and shale in the formation, an effective porosity of 0.2 for the lumped material was assigned to the model. A bulk density of 2.0 g/cm^3 was given to the lumped material. The constant Darcy's flow velocity, 5×10^{-3} m/day from west to east, is based on the regional hydraulic gradient and hydraulic conductivity

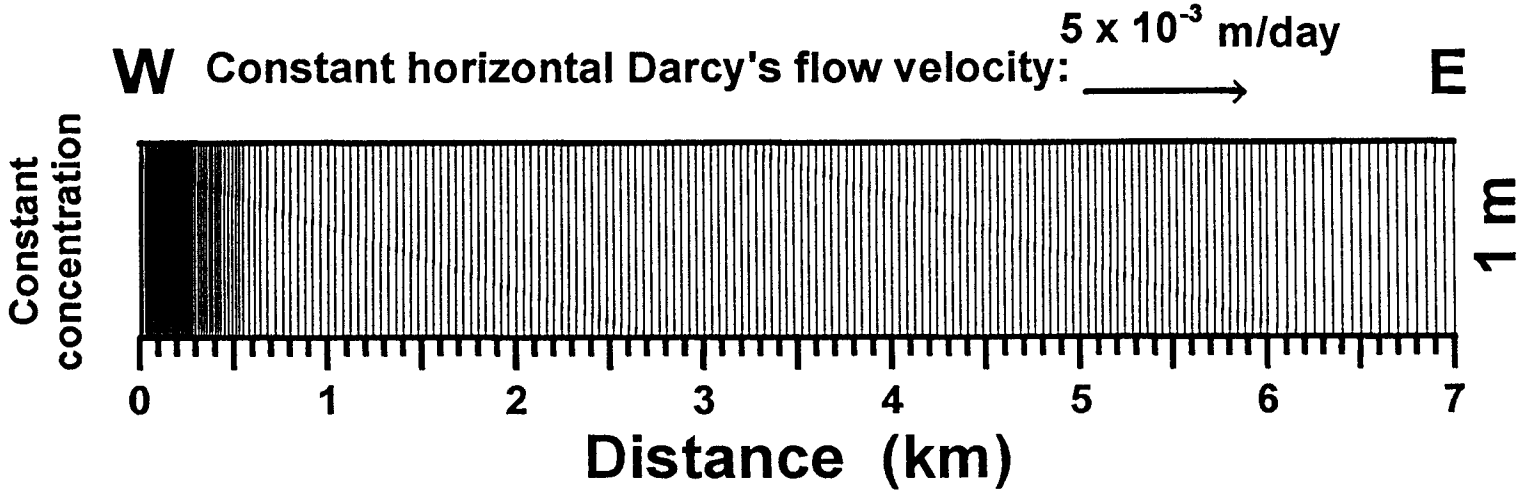

200 elements, 402 nodes

Porosity = 0.20
Longitudinal dispersivity = 25 m
Cation Exchange Capacity = 25 meq/kg

Figure 7.1. The 1-D model grid and its hydrological parameters.

values obtained from the available pumping-test data. There is no field dispersivity data available for the Dakota aquifer. A reasonable value of 25 m (82 ft) was assigned based on a knowledge of the geology, the scale of the model, and a review of previous research (Gelhar et al., 1992).

The CEC's were determined for samples from the KGS #1 Jones Core from north-central Lincoln County (Table 7.2). Except for the sample of Kiowa marine shale, the CEC's for the samples from the Dakota aquifer range from 0.5 to 8 meq/100g, with an average of 3.2 meq/100g. The values are comparable to those from previous studies for aquifers of similar materials (Table 3.1). There is no significant difference between the average CEC's of the Dakota Formation and the Longford Member of the Kiowa Formation. However, the CEC's for samples of grain sizes coarser than fine sand are in a range of 0.5 to 3.7 meq/100g and average 1.73 meq/100g. Table 2.1 indicates that kaolinite and illite are the dominant clay minerals in the Dakota aquifer. Organic matter in the sediments does not seem to affect the CEC values based on the data in Table 7.2. High illite and montmorillonite content in the Kiowa marine shale is the reason for its relatively high CEC.

The CEC's of the Dakota aquifer samples from the Jones core do not vary greatly compared to the possible range of CEC for clay minerals, although the sediment materials and associated depositional environments are quite different in different core sections. The laboratory results are considered to be satisfactory and applicable to other parts of the Dakota aquifer system. Most of the water flow in the aquifer is through coarser materials; only a small amount of water flows in the fine-grained sediments between sandstone bodies. However, the effect of fine-grained sediments on cation exchange is still significant because the CEC is large. Thus a value of 2.5 meq/100g was selected as the constant CEC for the model.

Table 7.2. Cation exchange capacity of sediments collected from KGS #1 Jones core. The number on the left side of the sample ID indicates the core depth in feet from which the sample was taken. A detailed geological description of the core is given in Macfarlane et al. (1991b) and in Combes and Feldman (1993).

Sample ID	Geological formation	Remarks	CEC meq/100 g
71-1 71-2	Dakota	fine sandstone, rare pyrite concretions, plant debris	3.7 3.6
81-1 81-2	Dakota	fine sandstone, plant debris, iron oxides	3.5 3.4
122-1 122-2	Dakota	mudstone to siltstone, abundant hard brown sand-sized grins, probably weathered pyrite	5.4 5.1
154-1 154-2	Dakota	silty fine sandstone, poor sorted, many plant debris	4.4 4.4
172-1 172-2	Dakota	medium sandstone, clean, well sorted, pyrite crystals scattered	2.0 1.9
200-1 200-2	Dakota	fine to medium sandstone, clean, well sorted	0.52 0.57
284-1 284-2	Longford Member of Kiowa	sandy shale, red-filled crusts and root tubes, paleosoils	5.3 4.9
319-1 319-2	Longford Member of Kiowa	mudstone with sand-sized pyrite crystals	7.8 9.2
354-1 354-2	Longford Member of Kiowa	fine sandstone with thin clay lamina	0.86 0.90
418-1 418-2	Longford Member of Kiowa	fine sandstone, clean, well sorted	0.55 0.57
435-1 435-2	Longford Member of Kiowa	medium to fine sandstone, glauconite up to 10%, pyrite concretions	1.1 1.0
470-1 470-2	Kiowa	dark gray marine shale	32.8 32.8
475-1 475-2	Permian	green siltstone	6.1 5.9

The value is nearly halfway between the overall average (3.2 meq/100g) and the average value for fine to medium sandstone (1.73 meq/100g). With the above parameters, the cation exchange capacity with respect to one unit volume (one liter) of water can be calculated by Equation 6.26

$$N_{eq} = \frac{\rho}{\theta} CEC = \frac{2.0}{0.2} \times 25 = 250 \text{ meq / L of water} \quad (7.1)$$

To minimize numerical dispersion and instability, the Peclet number and Courant number for the 1-D model are limited as below.

$$Pe = \Delta x/\alpha_L \leq 2 \quad (7.2)$$

$$Cr = V_f \Delta t/\Delta x \leq 3.5 \quad (7.3)$$

where Pe = Peclet number, dimensionless

Δx = grid size in horizontal direction, m

α_L = longitudinal dispersivity, m

Cr = Courant number, dimensionless

V_f = average linear velocity, m/day

$V_f = v/n$ v = Darcy's velocity, m/day, n = porosity

Δt = time step, day

A sensitivity analyses of the limit of the Peclet number for HYDROGEOCHEM was made with a 2-D model of conservative mass transport before the 1-D model was run. The results showed that no numerical instability (oscillation) for conservative mass transport was observed until the Peclet number was greater than about 11. However, later study indicated that a smaller Peclet number is necessary when the model includes cation exchange because of the occurrence of sharpening fronts. Nevertheless, the numerical instability problem can be reduced by applying an upstream weighting function to the numerical calculation. To reduce numerical dispersion, the grid sizes and time steps were set small so that the Courant number is limited to less than one for the early part of the simulation (Bear and Verruijt, 1987). Both the grid size and time step were increased when the transport front passed the first kilometer of the

model. With the above modeling strategy, no numerical instability was observed in any of the simulations.

The field chemistry data indicate that the Dakota aquifer is undergoing a freshening process. The salinity of the saline water in the Dakota aquifer before flushing is unknown. However, the upper limit of the saltwater concentration should probably not have substantially exceeded that presently in the underlying Permian strata. The input water chemistry used in the simulations is listed in Table 7.1. The values selected are based on chemical analyses listed in Appendix A.

There are seven basic chemical components, six aqueous complex species, and one mineral involved in the models. Hydrogen (H^+), calcium (Ca^{2+}), magnesium (Mg^{2+}), sodium (Na^+), carbonate(CO_3^{2-}), sulfate(SO_4^{2-}), and chloride(Cl^-) ions are the basic components. The aqueous complex species include OH^- (decomposition of water), H_2CO_3, HCO_3^-, $CaSO_4^\circ$, $MgSO_4^\circ$, and $NaSO_4^-$. Calcite ($Ca_{0.95}Mg_{0.05}CO_3$) is the only mineral involved in the models. Ca^{2+}, Mg^{2+}, and Na^+ are the three free ions involved in the cation exchange. The equilibrium constants for the complex species and calcite are from the SOLMINEQ.88 geochemical model at 15 °C and one atmosphere pressure. The selectivity coefficients for the cation exchange reactions are based on Bruggenwert and Kamphorst (1979) and the literature review described in Chapter 3. The chemical reactions in the models are listed in Table 7.3. The concentrations and equivalent fractions of adsorbed cations for the incoming and initial waters in model 1D00 (Table 7.4) were calculated by SOLMINEQ.88; the same results were also obtained from EQMOD - the chemical module of HYDROGEOCHEM. An example of a 1-D model (1D00) input file is listed in Appendix C.

Table 7.3. Chemical species and equations used in the 1-D models. The chemical equilibrium constants are from the SOLMINEQ.88 model for a temperature of 15 °C and one atmospheric pressure. Note the difference in definition of the selectivity coefficients used in this table in comparison with Table 7.1.

Chemical model species	Chemical species	Equilibrium constant or solubility products
Component free ion species	H^+, Ca^{2+}, Mg^{2+}, Na^+, CO_3^{2-}, SO_4^{2-}, Cl^-	
Aqueous complex species	$H_2O \Leftrightarrow H^+ + OH^-$	$\log K_{H_2O} = -14.37$
	$H^+ + CO_3^{2-} \Leftrightarrow HCO_3^-$	$\log K_{HCO_3^-} = 10.44$
	$H^+ + HCO_3^- \Leftrightarrow H_2CO_3$	$\log K_{H_2CO_3} = 6.43$
	$Ca^{2+} + SO_4^{2-} \Leftrightarrow CaSO_4^0{}_{(q)}$	$\log K_{CaSO_4^0} = 2.285$
	$Mg^{2+} + SO_4^{2-} \Leftrightarrow MgSO_4^0{}_{(q)}$	$\log K_{MgSO_4^0} = 2.37$
	$Na^+ + SO_4^{2-} \Leftrightarrow NaSO_4^-$	$\log K_{NaSO_4^-} = 1.133$
Cation-exchange species*	$Na^+ + X^- \Leftrightarrow Na\text{-}X$	$\log K_{Na} = 0.0$ (reference)
	$Ca^{2+} + 2Na\text{-}X \Leftrightarrow 2Na^+ + Ca\text{-}X_2$	$\log K'_{Ca/Na} = 1.0103$
	$Mg^{2+} + 2Na\text{-}X \Leftrightarrow 2Na^+ + Mg\text{-}X_2$	$\log K'_{Mg/Na} = 0.7005$
Mineral	$0.95Ca^{2+} + 0.05Mg^{2+} + CO_3^{2-} \Leftrightarrow Ca_{0.95}Mg_{0.05}CO_3$	$\log K_{calcite} = 8.4$

* : X^- represents one negatively-charged exchange site on the solid surface. The values of the selectivity coefficients are for model 1D00. Data were selected or modified as described in text.

Table 7.4. Concentrations computed for exchanging cations at the boundary (freshwater, 6S-3W-11ADAA) and initial (saltwater, 14S-14W-14CD) conditions of model 1D00.

Ion	$K'_{i/Na}$	Aqueous, mmole/L		Adsorbed, mmole/L of water# (%)*	
		Initial	Boundary	Initial	Boundary
Na^+	1.0	1108	1.63	204.5 (81.8)	2.58 (1.0)
Mg^{2+}	5.0176	79.55	0.44	16.5 (13.2)	9.30 (7.5)
Ca^{2+}	10.24	18.49	2.43	6.26 (5.0)	114.4 (91.5)

i : represents the exchangeable cations , i.e., Na^+, Mg^{2+}, and Ca^{2+}

: see Equation 7.1 for definition

* : equivalent fraction on exchange site, N_{eq} = 250 meq/L of solution

7.3. RESULTS AND INTERPRETATION

7.3.1. An Example of Conservative Mixing

A simulation of simple conservative mixing of two waters sampled, and the adsorbed cation ratios for the mixed waters, from the Dakota aquifer demonstrates changes in the system without the coupled flow simulation. Figure 7.2 shows the activity and adsorbed cation ratios for the conservative mixing of two waters sampled from wells at 5S-5W-4AAB2 (saltwater, Table A.6) and 6S-3W-11ADAA (freshwater, Table A.3). Cation exchange among Ca^{2+}, Mg^{2+}, and Na^{+} was assigned to the geochemical mixing model. The activities and adsorbed concentrations of the cations were obtained from geochemical simulations of SOLMINEQ.88. Ion pairs and ion complexes were also simulated by SOLMINEQ.88. The results show that, although the Ca concentration in the freshwater is two times lower than that in the saltwater (Figure 7.2a), the Ca^{2+} activity of the freshwater is higher than that of the saltwater (Figure 7.2b). This phenomenon indicates that the effects of ion complexes and ionic strength of the solution are important for waters of high salinity. The Na concentration decreases greatly from the saltwater end to the freshwater end, therefore the activity ratios of Ca^{2+}/Na^{+} and Mg^{2+}/Na^{+} increase two and one orders of magnitude, respectively, in the same direction (Figure 7.2c). Figure 7.2d shows that in a mixture of 85% freshwater and 15% saltwater the adsorbed Ca^{2+} concentration is about the same as that of Na^{+} and becomes the dominant adsorbed cation on the clay surfaces in mixtures with a greater freshwater percentage. The adsorbed concentration of Mg^{2+} on clay surfaces does not vary much, despite a concentration in the saltwater of more than 40 times that in the freshwater. The adsorbed concentration of Mg^{2+} reaches a maximum when the adsorbed Ca^{2+} and Na^{+} are equal.

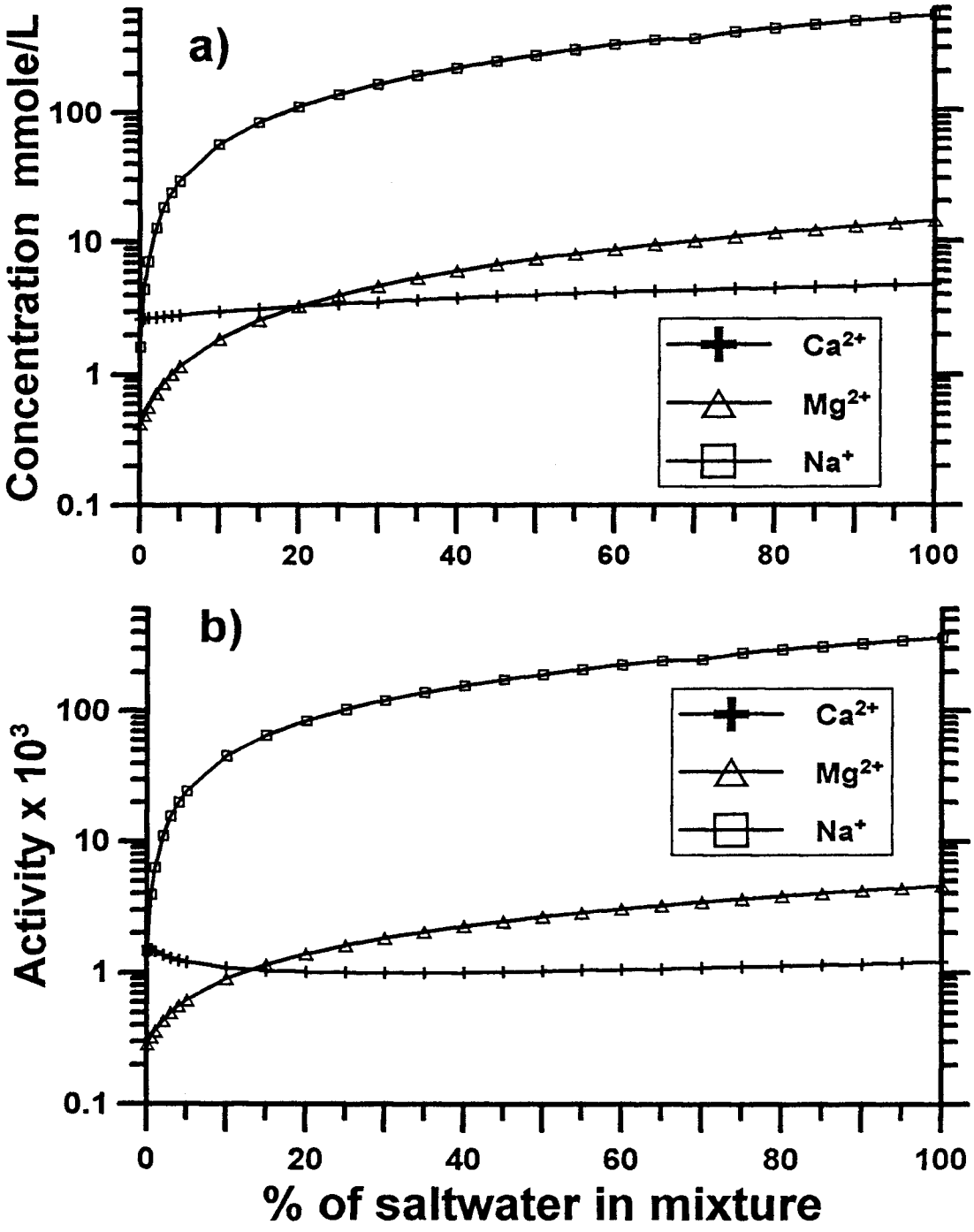

Figure 7.2. Conservative mixing of a freshwater and a saltwater from the Dakota aquifer. The percent of saltwater from 5S-5W-4AAB2 increases from left to right along the X axis, and the percent of freshwater from 6S-3W-11ADAA decreases in the same direction. a) mole concentrations of exchanging cations, b) activities of exchanging cations, c) activity ratios of $Ca^{2+}/Na^{+}$and Mg^{2+}/Na^{+}, d) adsorbed fractions of exchanging cations.

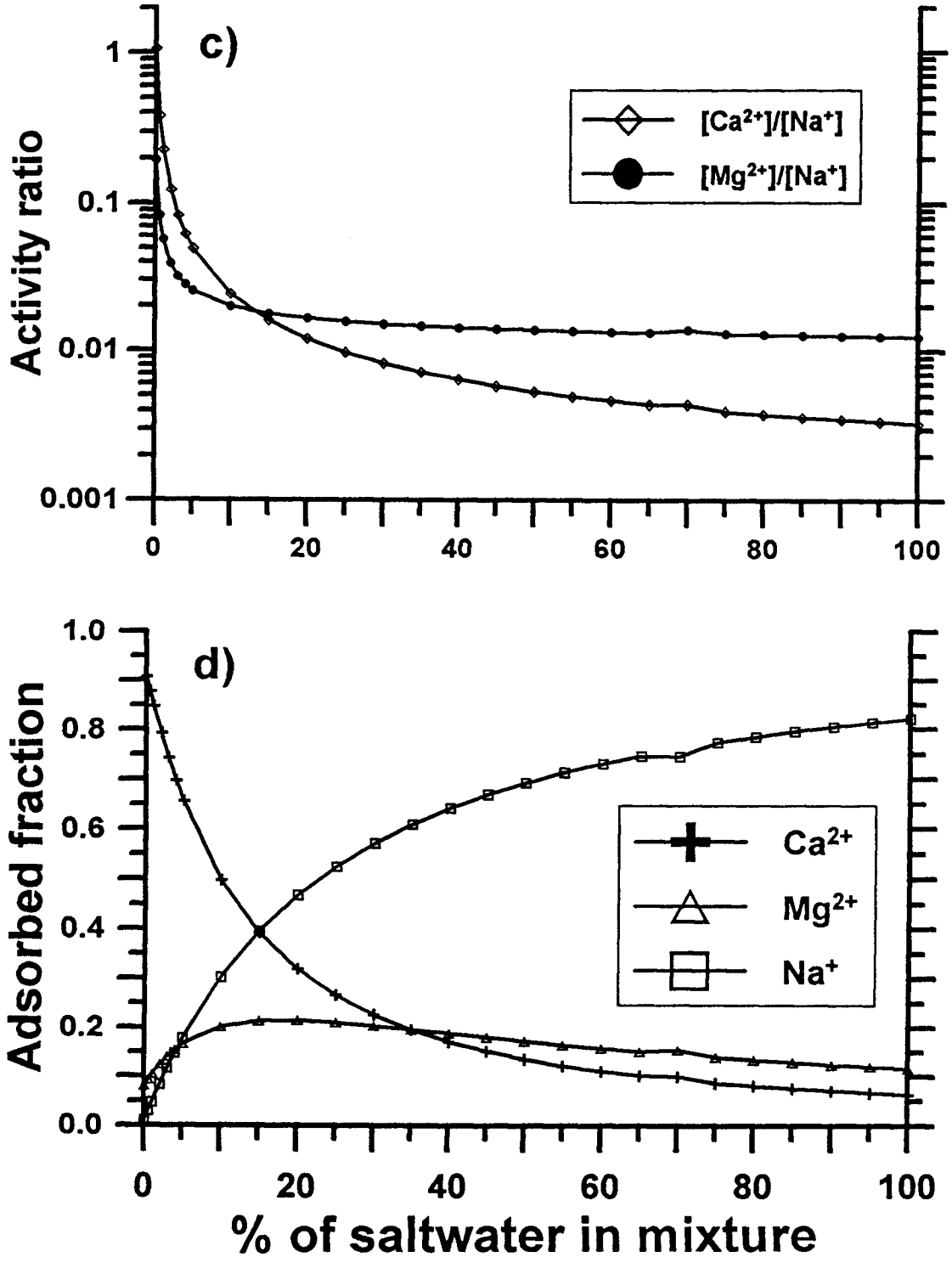

(Figure 7.2. Continued...)

7.3.2. The Effect of Coupled Mixing and Chemical Reactions on Water Chemistry - Ion Chromatography Caused by Cation Exchange

The discussion of the 1-D model results is divided into two sections. This section presents the effect of mixing and chemical reactions on water chemistry with focus on the simulation of model 1D00 and its related variations. The variations include simulations of conservative transport of the component species, of transport with aqueous complexation and cation exchange but without precipitation/dissolution of calcite, and with longer transport time for the same flow and chemical conditions for model 1D00. The next section describes the results of the sensitivity analyses listed in Table 7.1.

Conservative transport of Cl shows that the center of the breakthrough curve is at 5,170 m after 2.07×10^5 days (about 567 years) of travel time (Figure 7.3). The breakthrough curve caused by dispersion extends from about 3.1 km to slightly outside of the model at the east end. Figure 7.4 shows the model results for Ca, Mg, and Na in simulation 1D00. There are three distinct zones of dissolved cations along the flow path. Two fronts appear in the Na profile, one conservative mixing front with the center at 5,170 m and one sharp front near the west end of the model. As described in Chapter 3, the area of constant concentration in between the two fronts is a "plateau zone". The sharpening front of Ca and Mg between zones II and III on Figure 7.4 is actually a combination of two fronts because the simulation time is too short to separate them. Figure 7.5 is a result of a simulation with the same physical and chemical conditions but with a longer simulation time of 1.079×10^6 days (2,956 years). Three fronts occur for Ca and Mg. Two of those fronts are on Figure 7.5; the other is the dilution front which has passed the right end of the model in Figure 7.5. Figures 7.5a and b depict that zone III for Ca and Mg can be further divided into two zones, zones III_1 and III_2,

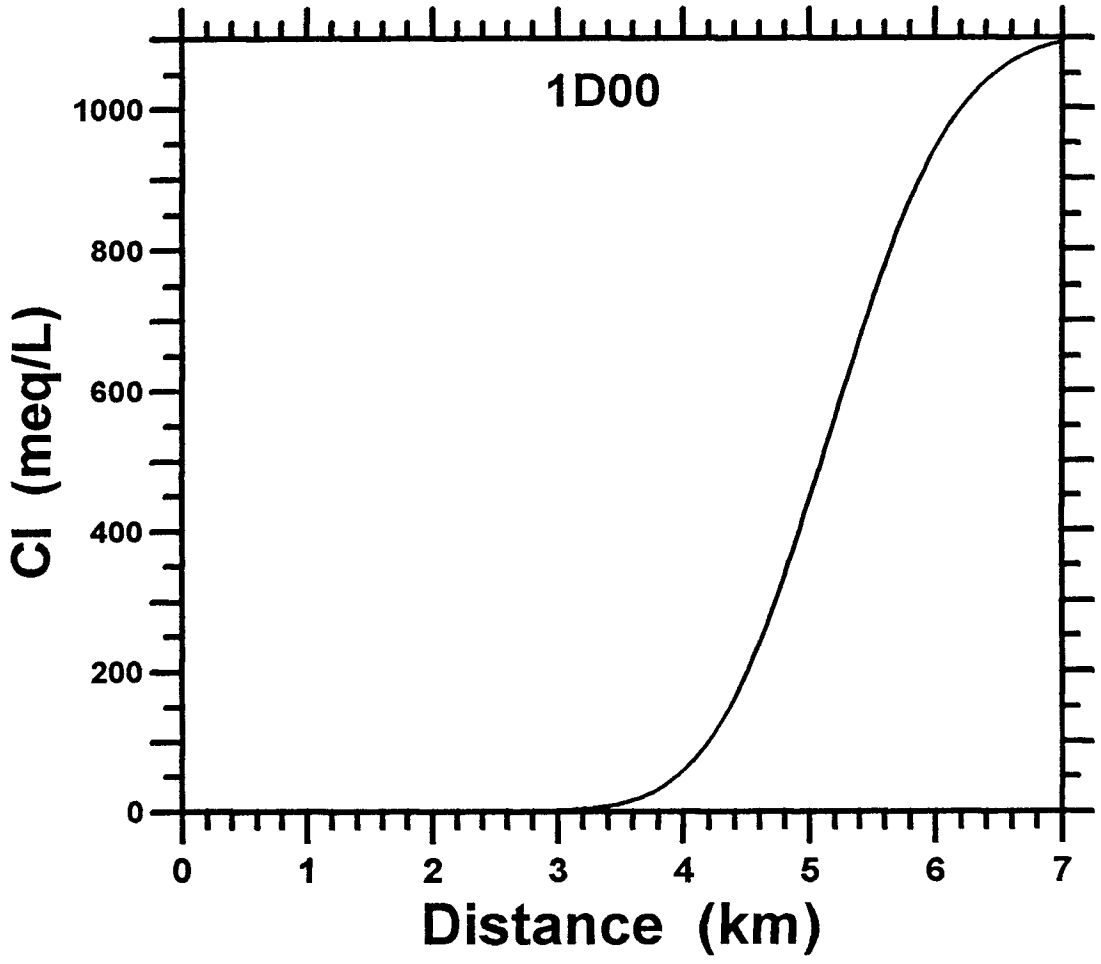

Figure 7.3. Conservative transport of Cl for the 1-D coupled model at 567 years.

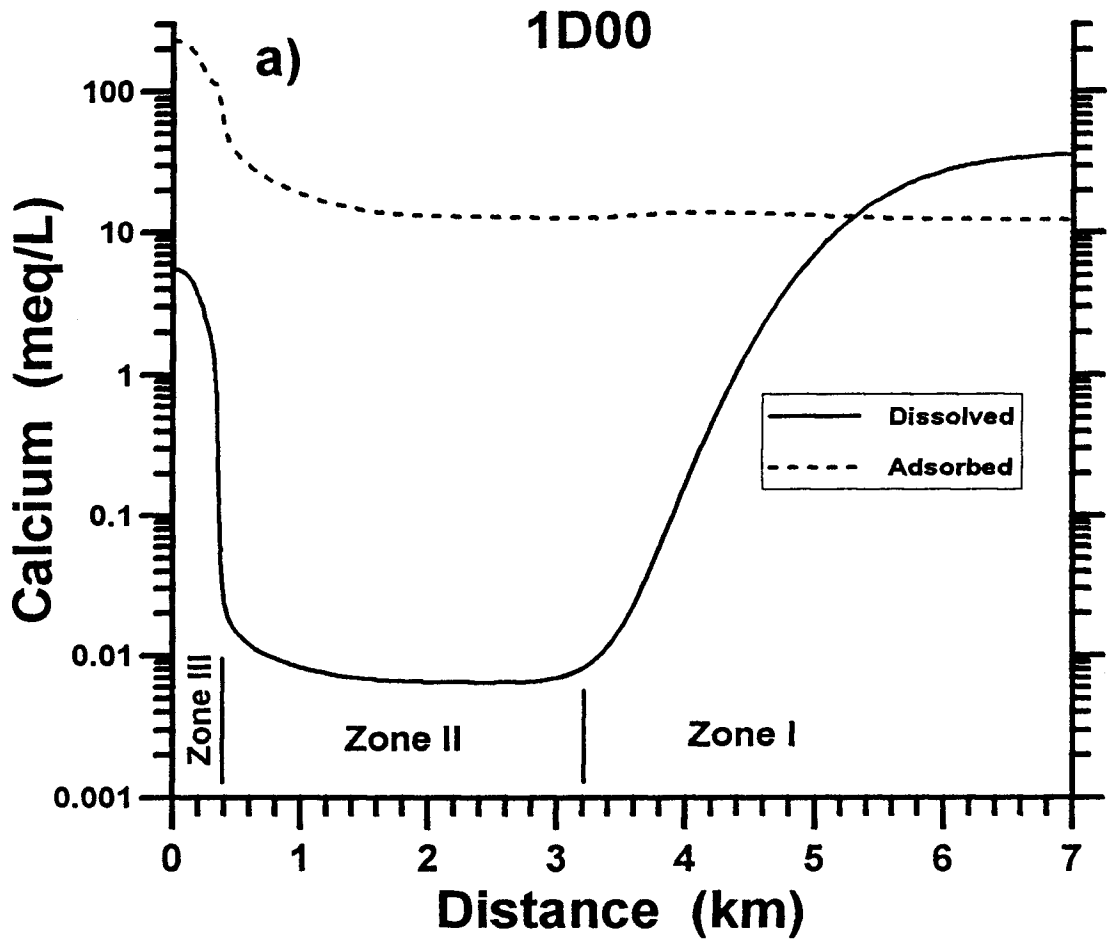

Figure 7.4. Model results of 1D00 with calcite precipitation/dissolution at 567 years. a) Ca, b) Mg, and c) Na. The concentration profiles are divided into three distinct zones.

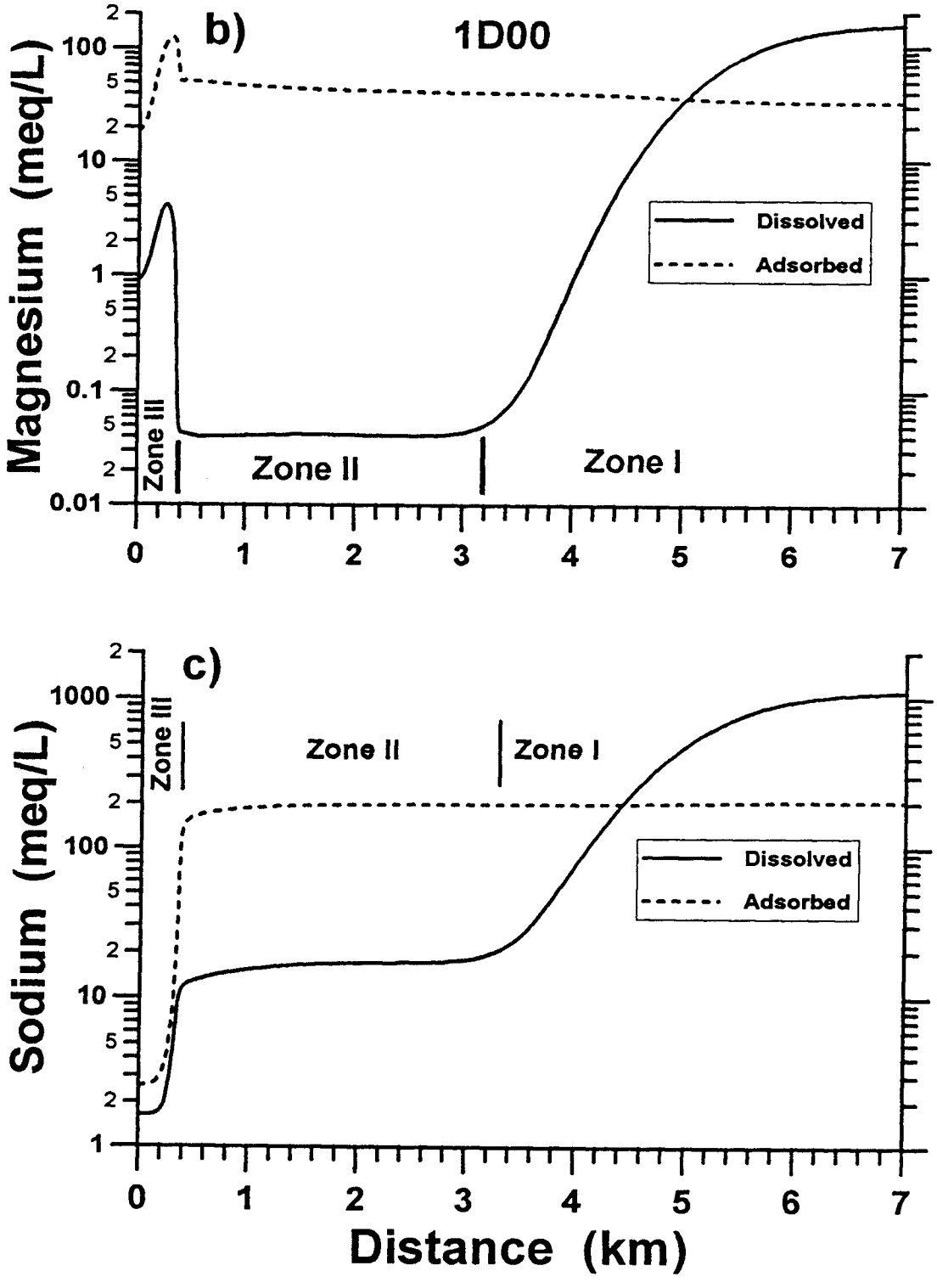

(Figure 7.4. Continued...)

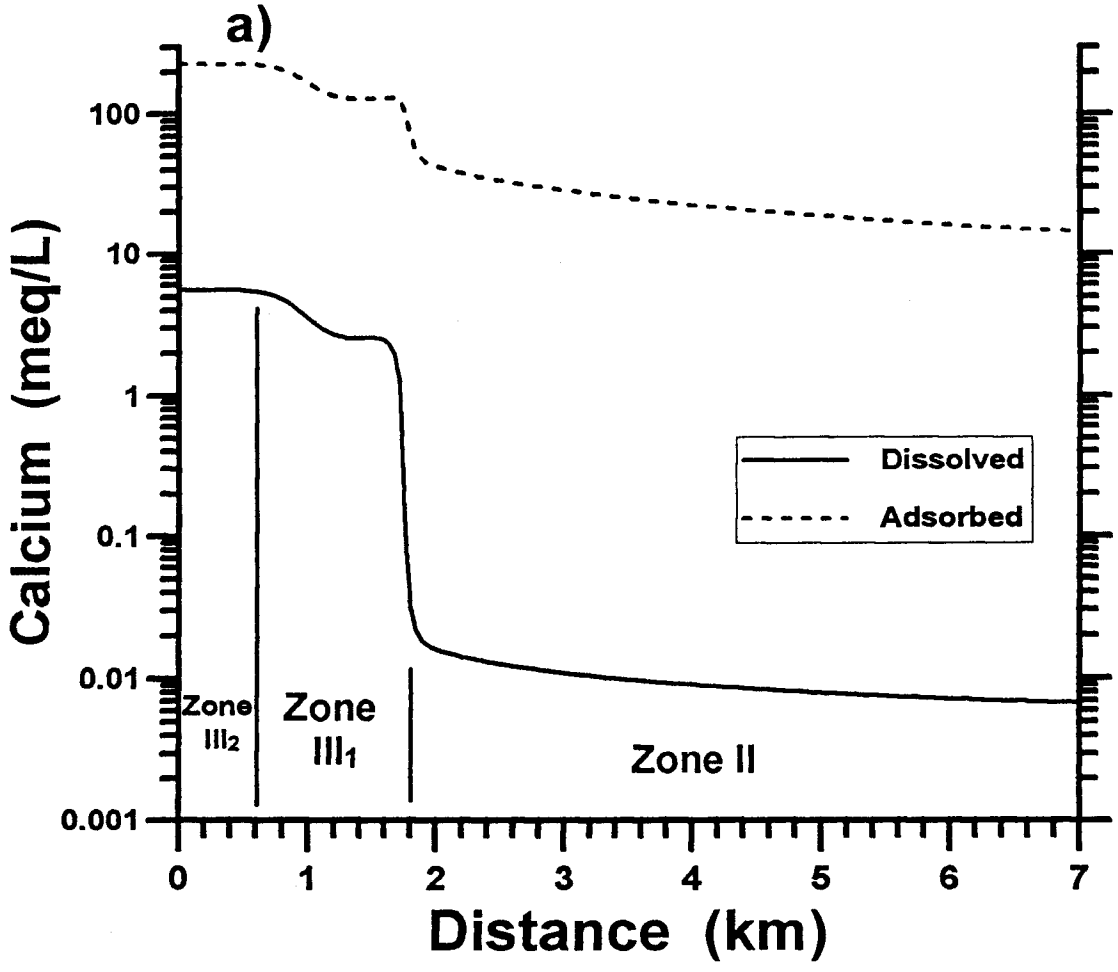

Figure 7.5. Model results for 1D00 at 2,956 years. a) Ca, b) Mg, and c) Na. The discussion of the zonation is presented in the text.

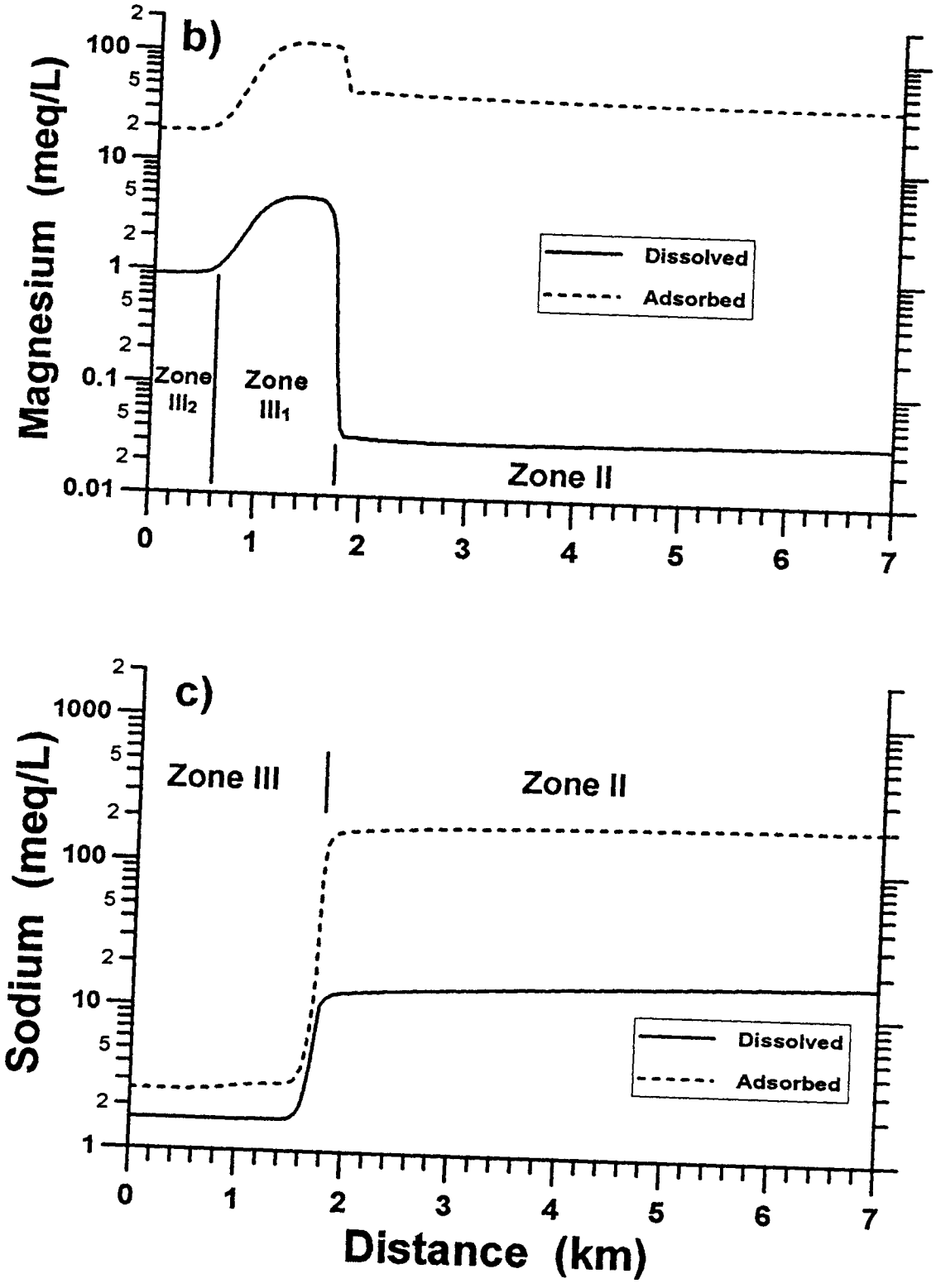

(Figure 7.5. Continued...)

according to their concentration patterns. The two subdivided zones are separated by a front with a relatively gentle slope.

The model results shown in Figures 7.4 and 7.5 can be interpreted by applying the principle of ion chromatography discussed in Chapter 3. Based on the conceptual diagram of Figure 3.1, zone I at the right side of model 1D00 includes the unaltered initial saltwater and the conservative salinity front. Zone III_2 at the left side of the curves is where the solid matrix is in equilibrium with the incoming freshwater. Zone II in the middle of the model is the "plateau zone" resulting mainly from cation exchange of Ca^{2+} and Mg^{2+} for Na^+ on clays. In zone III, all the exchangeable Na^+ on exchange sites with respect to the incoming freshwater is replaced by Ca^{2+} and Mg^{2+}. Zone III_1 is a result of different velocities of the Ca and Mg retardation fronts and required charge balance between dissolved anions and cations. As Table 7.4 shows, in order for the aquifer materials to change from equilibrium with the initial saltwater to equilibrium with the incoming freshwater, 108 mmole/L of Ca^{2+} and 7.2 mmole/L of Mg^{2+} are required. Although the Ca concentration in the incoming water is four times the Mg concentration, much more water is needed to saturate the surface sites with Ca^{2+} than with Mg^{2+}. Therefore, the retardation front for Ca moves slower than that for Mg. The cation charge deficiency in zone III_1 caused by the slow movement of the Ca retardation front is compensated by the increased Mg concentration. The sequence of evolution is also shown in the profile of adsorbed cations (Figure 7.6a).

The relationship between the exchanging divalent and monovalent cations is clearly shown in Figure 7.6b. The nearly constant $(Ca + Mg)^{1/2}/Na$ mole ratio in zone III, despite the variation of the individual concentrations of Ca and Mg in the zone, is an ideal indication for studying divalent-monovalent exchange reactions. However, the effect of cation exchange on

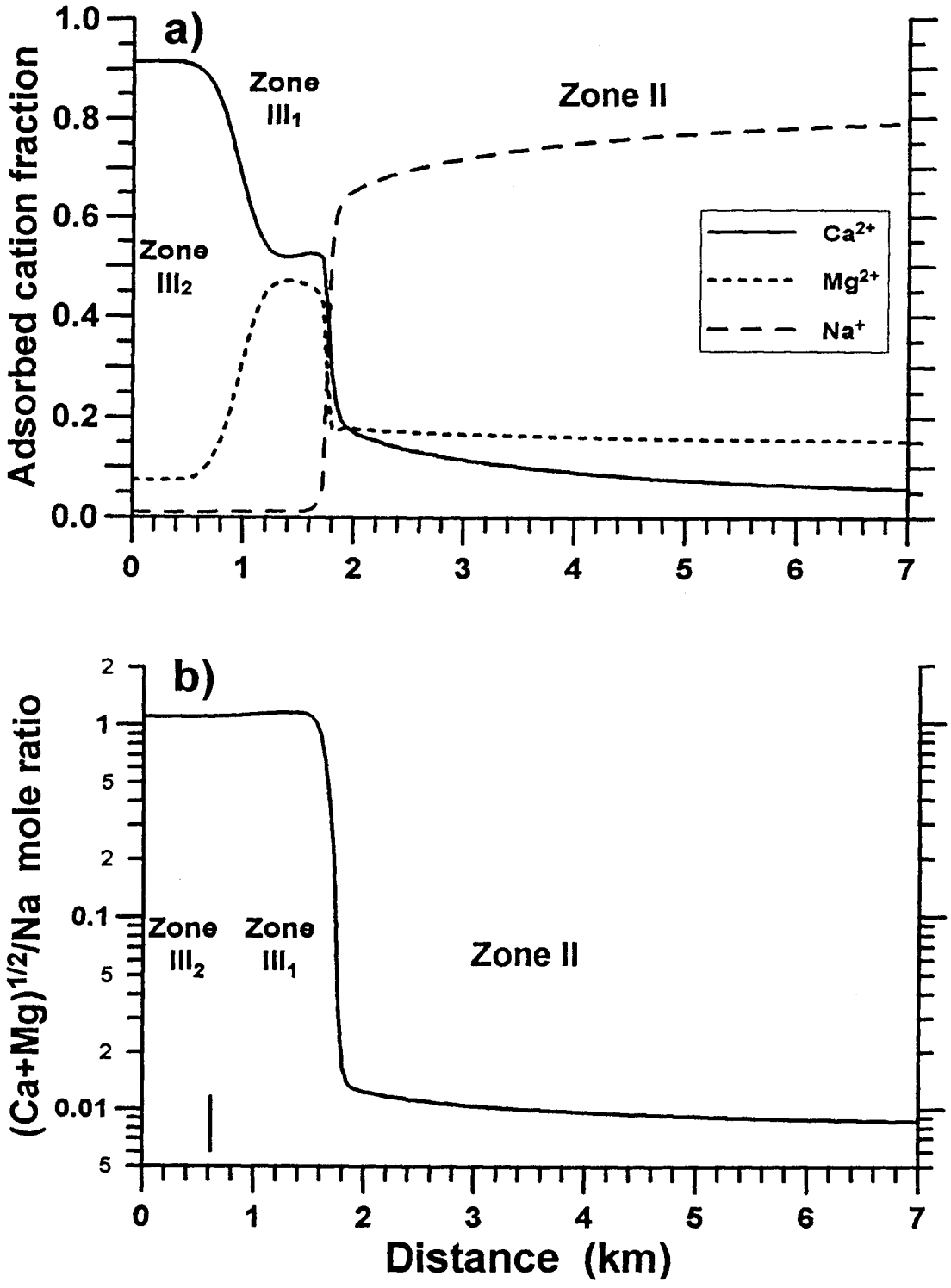

Figure 7.6. Model results for 1D00 at 2,956 years. a) adsorbed cation fractions, and b) $(Ca + Mg)^{1/2}/Na$ mole ratio.

the individual concentrations of Ca and Mg is difficult to determine in actual systems because the cations are also affected by other chemical reactions.

Table 7.4 indicates that the exchangeable cation concentrations in the sediment are much greater than the dissolved concentrations in the incoming freshwater. Because of the large buffering capacity of the exchange medium, the adsorbed cation ratios are not easily changed until a large enough volume of freshwater flows through the system. The cation ratios in the incoming freshwater quickly adapt to the composition on the surface sites, which are still in equilibrium with the previous saltwater (Valocchi et al., 1981b; Appelo et al., 1993; Appelo, 1994b). The exchangeable cation concentrations on the clay surfaces do not change appreciably across the salinity front (Figure 7.4).

The length and exchanging cation concentrations of the plateau zone (zone II) can be estimated by applying the principle just mentioned (Appelo, 1994b). The 1-D model can be used as an example to demonstrate an analytical solution by considering only the cation exchange reactions without dispersion. The mole concentrations are assumed to be equal to the activities for the exchanging cations in the freshwater. With this assumption, the adsorbed fractions of exchangeable cations in equilibrium with the incoming freshwater are recalculated as $\beta_{Ca,III_2} = 0.912$, $\beta_{Mg,III_2} = 0.081$, and $\beta_{Na,III} = 0.007$. To calculate the cation concentrations in zone II, the exchange reactions in Table 7.3 are recalled

$$K'_{Ca/Na} = \frac{[Na^+]_{II}^2 \beta_{Ca,II}}{[Ca^{2+}]_{II}\, \beta_{Na,II}^2} = 10.24 \tag{7.4}$$

$$K'_{Mg/Na} = \frac{[Na^+]_{II}^2 \beta_{Mg,II}}{[Mg^{2+}]_{II}\, \beta_{Na,II}^2} = 5.0176 \tag{7.5}$$

The brackets represent activity. Based on the principle mentioned in the last paragraph, the

plateau zone is assumed to maintain the same adsorbed cation ratios as the initial condition (Table 7.4). After the saltwater is flushed out, the total cation activity equals that in the freshwater and is represented by

$$[Na^+]_{II} + 2([Ca^{2+}]_{II} + [Mg^{2+}]_{II}) = N \ meq / L \tag{7.6}$$

N is the total cation concentration for the incoming water and is equal to 7.37×10^{-3} meq/L for this case. Solving Equations 7.4 to 7.6 gives $(Na^+) = 7.365 \times 10^{-3}$ mmole/L, $(Mg^{2+}) = 2.12 \times 10^{-6}$ mmole/L, and $(Ca^{2+}) = 3.9 \times 10^{-7}$ mmole/L, where parentheses represent mole concentration. The results show that (Na^+) comprises almost the entire concentration of cations. Compared to the incoming water, the ratios of $(Ca^{2+})/(Na^+)$ and $(Mg^{2+})/(Na^+)$ decrease 28140 and 940 times in zone II, respectively. This is because the fixed composition on the exchange medium requires the aqueous cation ratios to adapt to those of the initial saltwater while the total cation concentration is diluted two orders of magnitude to match the total anion concentration of the incoming freshwater. This feature is called the "salinity effect" (Valocchi et al., 1981b; Appelo, 1994a, 1994 b). The salinity effect is particularly clear when saline water is flushed by freshwater. When the analytical solution is compared with the numerical model results of Figure 7.7 in which calcite is not included, it appears that the depleted Ca and Mg concentrations in Figure 7.7 are not as low as in the analytical solution. This is caused by a decrease in the free ion concentrations of cations available for exchange as a result of the formation of dissolved complex species which are not available for cation exchange.

The sharpening effect on the retardation front is due to a greater velocity for the trailing-end than for the fore-end of the front. The velocity of the fore-end of the sharp front is reduced by ion exchange while the concentration at the tail-end travels at the water flow

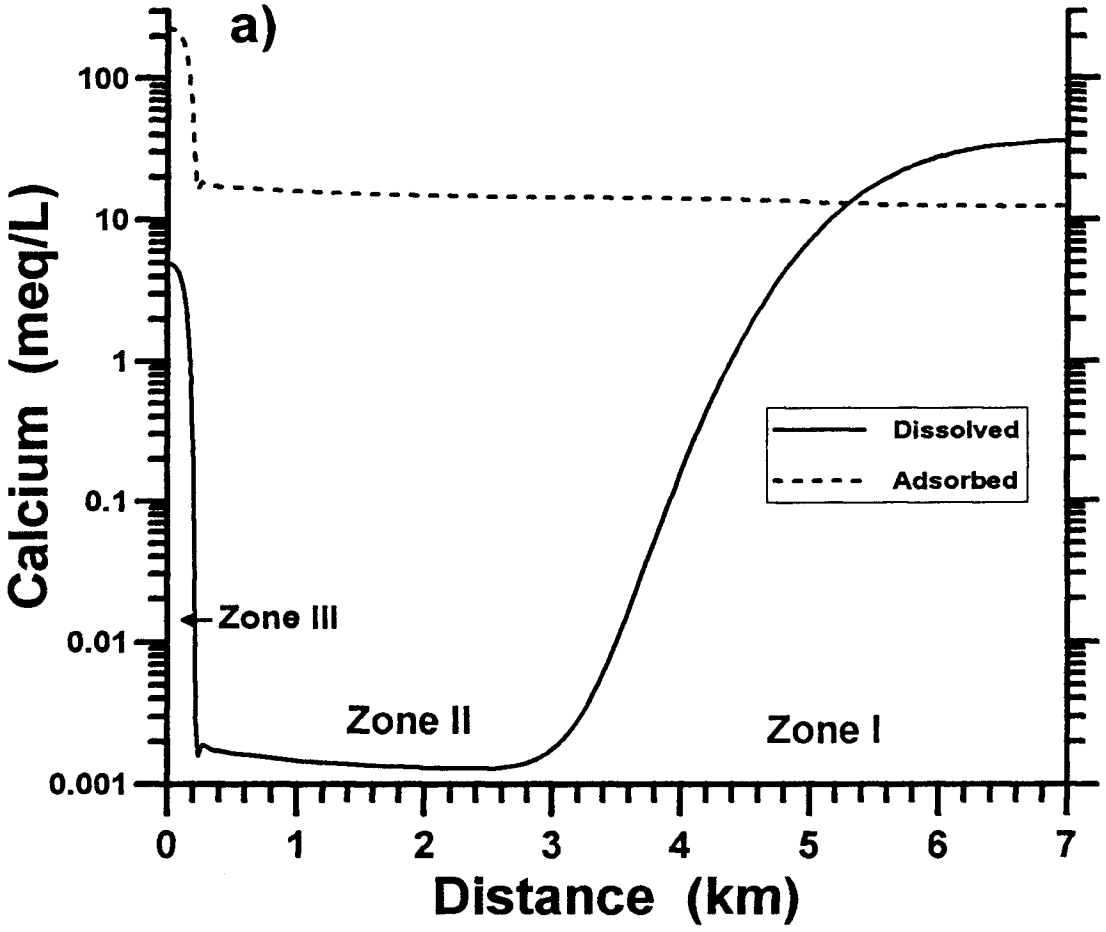

Figure 7.7. Model results for 1D00 without calcite precipitation/dissolution at 567 years. a) Ca, b) Mg, and c) Na.

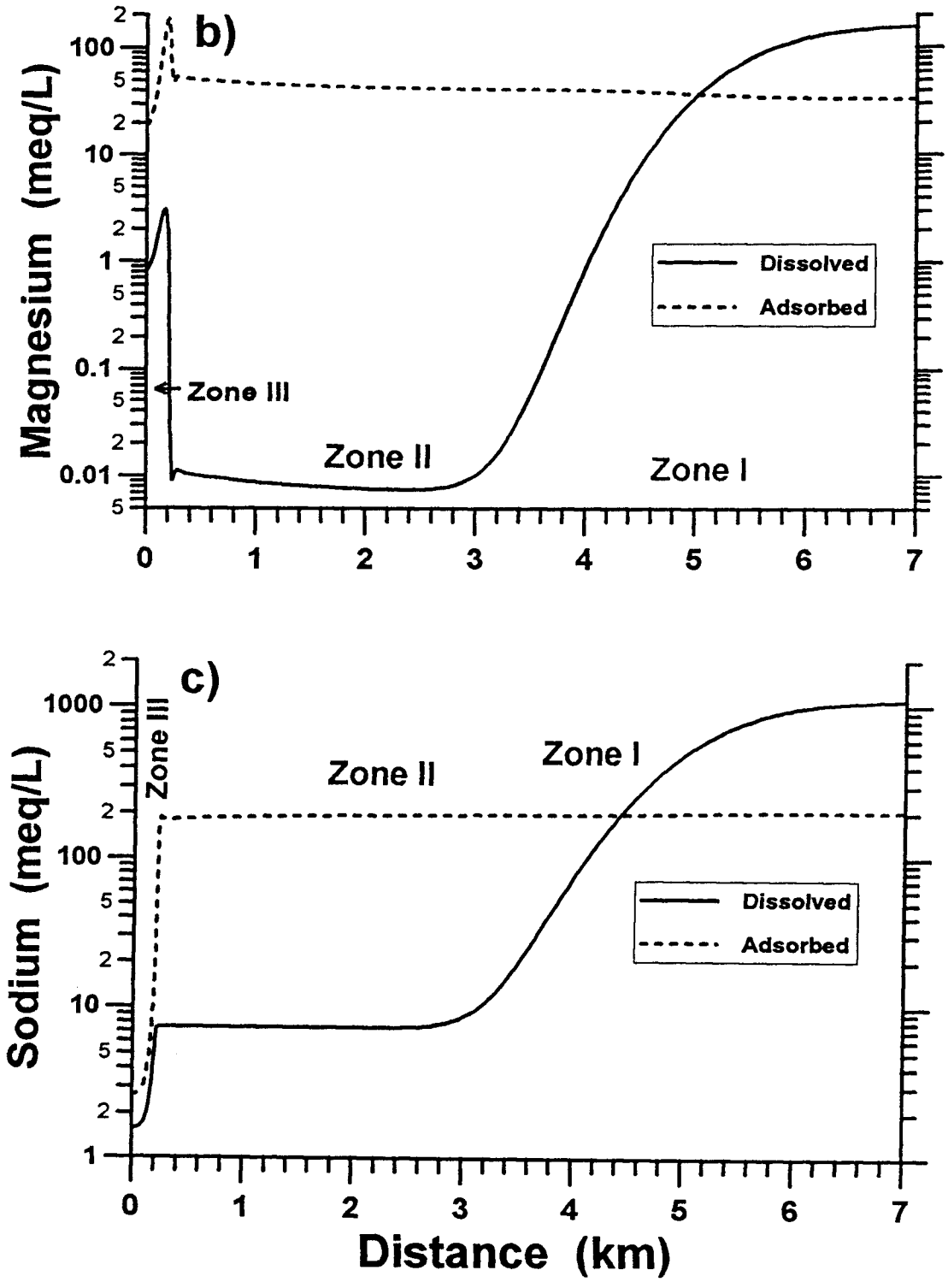

(Figure 7.7. Continued...)

velocity. On the other hand, a broadening effect is caused by a greater velocity for the fore-end than for the trailing-end. No broadening front occurs in the 1-D models.

The sharpening front between zones II and III indicates that cation exchange can intensively change water chemistry in a very short distance even if dispersivity is applied to the model. The front between zone III_1 and III_2 in Figure 7.5 (a and b) is not as sharp as the sharpening front between zones II and III because of a smaller selectivity coefficient of $K_{Ca/Mg}$ compared to $K_{Ca/Na}$ and $K_{Mg/Na}$ (Table 7.1). However, the slope is still much steeper than the conservative mixing front. This indicates that the evolution of water chemistry in a freshening aquifer system can be defined relatively easily if cation exchange is the major factor controlling cation concentrations.

The representation of cation exchange in the form of the $(Ca + Mg)^{1/2}/Na$ mole ratio is based on Equation 6.24 (assuming that the ion concentrations are equal to their activities). Equations 7.4 and 7.5 indicate that $[Ca^{2+}]/[Na^{+}]^2$ and $[Mg^{2+}]/[Na^{+}]^2$ are proportional to their adsorbed ratios. Therefore, the above relationships can be used to represent the adsorbed cation ratios. Since the exchange reaction equations in Table 7.3 are just another form of Equation 6.24, the adsorbed cation ratios can also be expressed by $[Ca^{2+}]^{1/2}/[Na^{+}]$ and $[Mg^{2+}]^{1/2}/[Na^{+}]$. The pattern of relative ratios along the flow path for both expressions are exactly the same. The ratio of $(Ca + Mg)^{1/2}/Na$ is used to represent the combined effect of the bivalent cations exchanging with Na. A detailed discussion of the issue is presented in Chapter 8.

The derivation of the analytical solution for calculating the velocity of the retardation fronts and consequently the required pore volume of incoming water to equilibrate the sediment has been presented in several articles (Pope et al, 1978; Charbeneau, 1981; Novak et al., 1988;

Appelo, 1994b). The same principle also has been applied to the chromatographic pattern caused by precipitation/dissolution of minerals (Bryant et al., 1987; Novak et al., 1988; Helfferich, 1989). The travel velocity of the retardation front can be expressed as a function of the water flow velocity:

$$V_{ci} = \frac{V_f}{1 + dq_i / dc_i} \tag{7.7}$$

where

V_{ci} = travel velocity of retarded front of species i,

q_i = adsorbed concentration of species i,

c_i = dissolved concentration of species i.

The terms dq_i and dc_i represent the concentration differences of the opposite sides of the front to be calculated. The velocity given by the last equation can be related to pore volume (Φ) by

$$\Phi = \frac{V_f}{V_{ci}} = 1 + \frac{dq_i}{dc_i} \tag{7.8}$$

The term "1" on the very right-hand side indicates that one pore volume of incoming water is needed to flush out the initial water before the cation exchange starts. The retardation front lags the conservative front by a pore volume of dq_i/dc_i. Appelo et al. (1993) used "sharp front flushing factor Φ_s" to define the relative column pore volumes needed for the sharpening front to appear after the salinity front.

$$\Phi_s = \frac{\Phi}{\Phi_0} = \frac{\Delta q_i}{\Delta c_i} \tag{7.9}$$

where Φ_0 is the column length through which the retardation front has traveled. This equation explains why the salinity effect is more pronounced when saltwater is replaced by freshwater

because the value of Δc between zones II and III is small for freshwater. Equation 7.9 illustrates that the spatial length of the plateau in zone II will extend with the extension of zone III if the CEC remains constant throughout the flow length.

The analytical example is again useful for explaining changes in the system. The first sharpening front appears when the exchangeable Na^+ (with respect to the incoming freshwater) in sediments is exhausted. The flushing factor for the first sharpening front can be obtained from the Na concentration

$$(\Phi_s)_1 = \frac{\Delta q_{Na}}{\Delta c_{Na}} = \frac{q_{Na\,III} - q_{Na\,II}}{c_{Na\,III} - c_{Na\,II}} = \frac{2.58 - 204.5}{1.63 - 7.365} = 35.21$$

And the velocity of the first sharpening front is

$$(V_{CNa})_1 = \frac{V_f}{1 + (\Phi_s)_1} = \frac{5 \times 10^{-3} / 0.2}{1 + 35.21} = 6.9 \times 10^{-4} \ \text{m/day}$$

To clearly show each of the waves in the diagram, a longer travel time is used for the demonstration. The mixing front is located at 6,500 m after 2.6×10^5 days (about 712 years) of transport. The location of the sharpening front of Na is then at $6.9 \times 10^{-4} \times 2.6 \times 10^5 =$ 179.4 m. If the location of the salinity front (X_0) and the flushing factor $(\Phi_s)_1$ are known, the location of the first sharpening front $(X_i)_1$ can be calculated by

$$(X_i)_1 = \frac{X_0}{1 + (\Phi_s)_1} = \frac{6500}{1 + 35.21} = 179.5 \text{ m}$$

The calculation of the cation concentrations in zone III_1 is much more complicated. The estimated dissolved and adsorbed concentrations of Mg in the zone were obtained from Figure 7.8 and are $q_{Mg\,III_1}$ = 108.1 mmole/L and $c_{Mg\,III_1}$ = 2.60 mmole/L. The location of the second sharp front of Mg between zones III_1 and III_2 can be calculated. First, the flushing

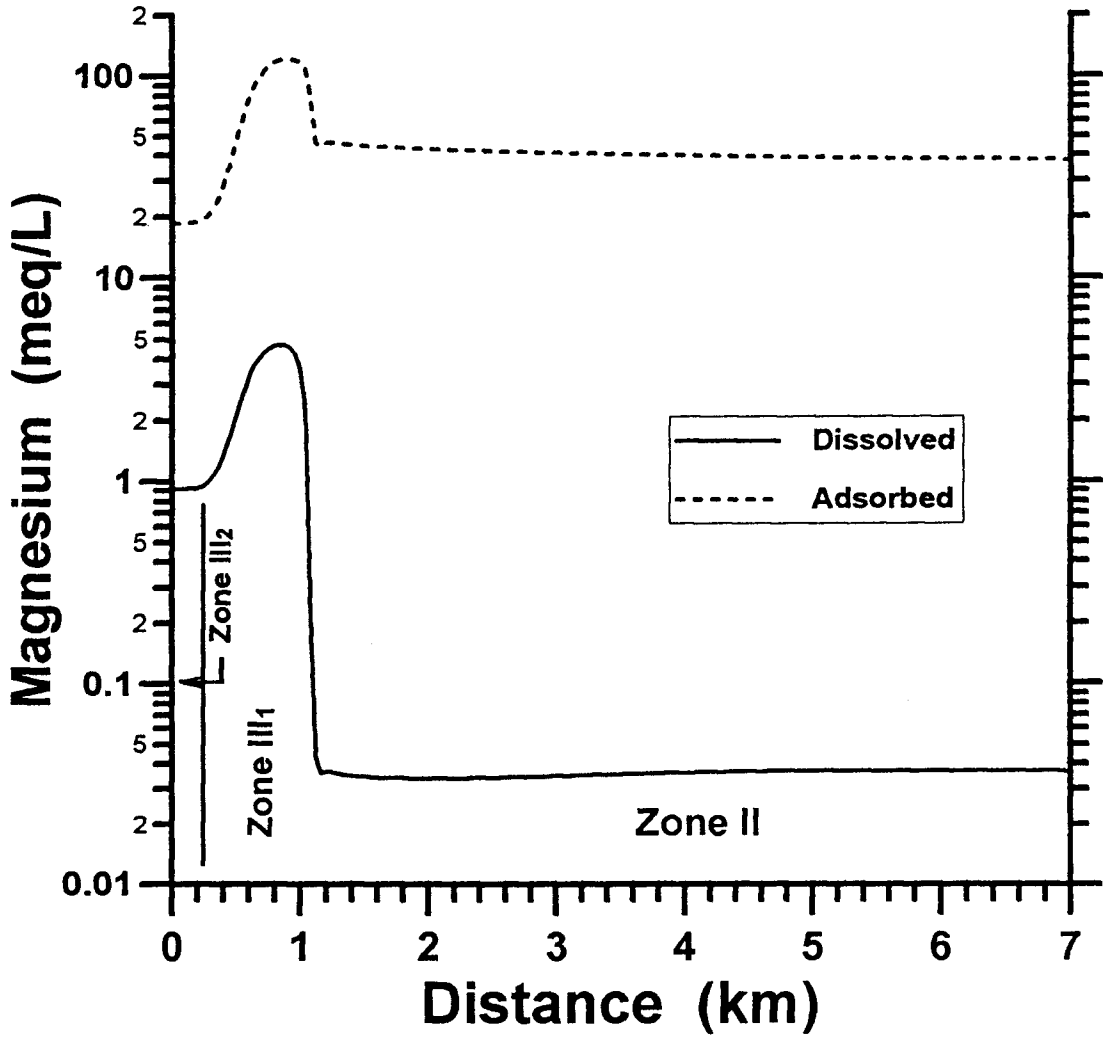

Figure 7.8. Simulated Mg concentrations for model 1D00 without calcite at 3,642 years.

factor $(\Phi_s)_2$ is obtained by

$$(\Phi_s)_2 = \frac{q_{MgIII_2} - q_{MgIII_1}}{c_{MgIII_2} - c_{MgIII_1}} = \frac{108.1 - 10.13}{2.60 - 0.44} = 45.36$$

Values of q_{MgIII_2} and c_{MgIII_2} are obtained from Table 7.4. The location of the second retardation front is

$$(X_{Mg})_2 = \frac{X_0}{1 + (\Phi_s)_2} = \frac{6500}{1 + 45.36} = 140.2 \text{ m}$$

The flushing factor of the first retardation front can also be calculated via the Mg concentration.

$$(\Phi_s)_1 = \frac{q_{MgIII_1} - q_{MgII}}{c_{MgIII_1} - c_{MgII}} = \frac{108.1 - 16.5}{(2.60 - 2.12 \times 10^{-3})} = 35.23$$

The value is essentially the same as that obtained using Na. The example shows that the location of the first retardation front can be obtained from the distribution of both Na and Mg. Similarly, the retardation fronts can also be calculated from the Ca distribution. Results for the analytical example are shown in Figure 7.9.

Figure 7.10 shows that calcite dissolution mainly occurs in zone III where the major cation exchange has occurred and moves through the zone with the retardation front. More precisely, most of the calcite dissolution occurs in the vicinity of the retardation fronts and a minor amount of calcite dissolution occurs at the conservative mixing zone. Calcite dissolution occurs at the mixing front mainly due to the change in ionic strength. In zone II, in spite of the low dissolved concentration of Ca, no further calcite dissolution occurs because the water is saturated with respect to calcite due to the high CO_3 concentration and solution pH that has been transported to this zone (Figure 7.11). The increased CO_3 concentration and pH come

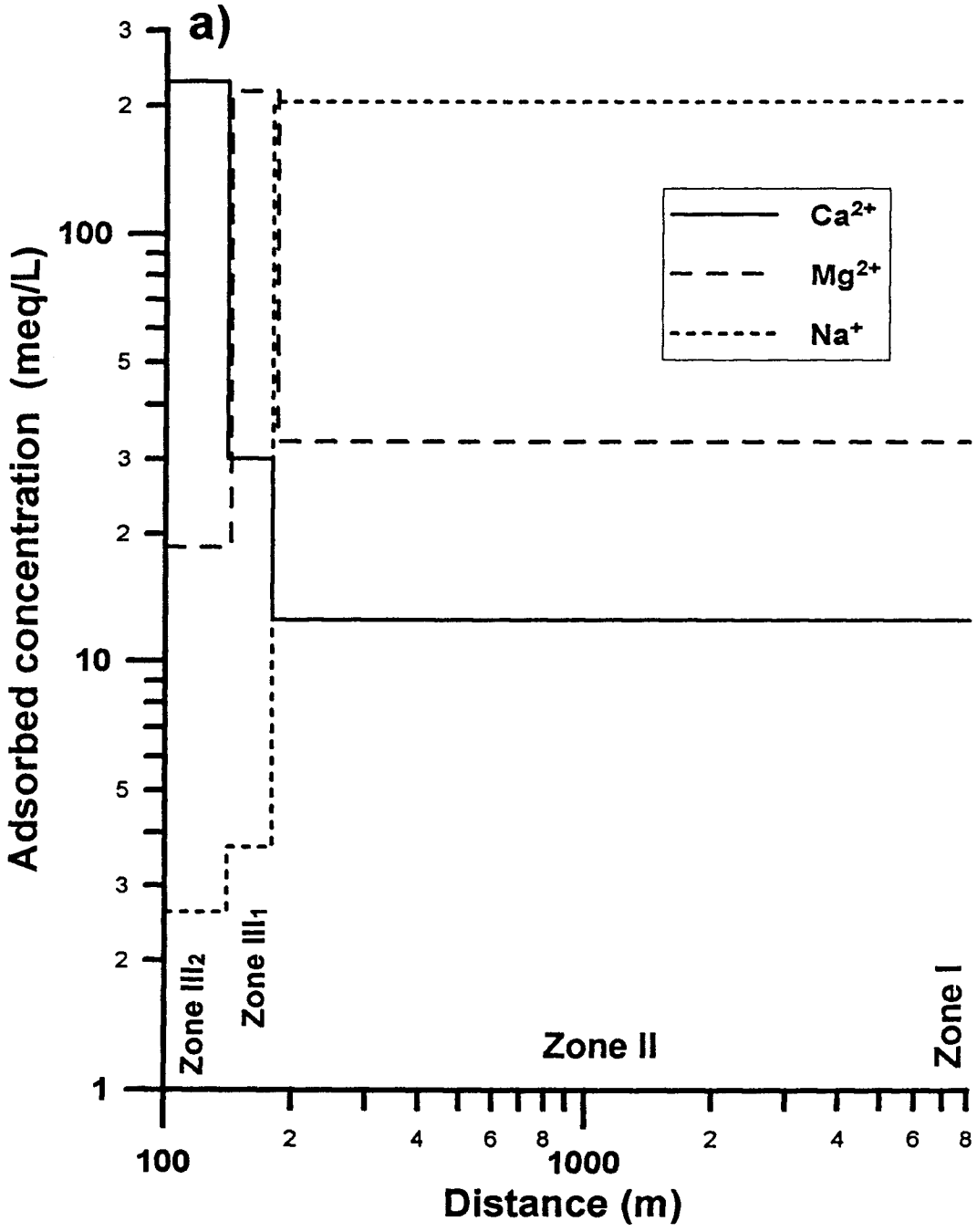

Figure 7.9. Distribution of cation concentrations obtained from the analytical calculation. a) adsorbed concentrations, and b) dissolved concentrations. The flow and chemical conditions are same as those for model 1D00. The results are calculated at about 712 years.

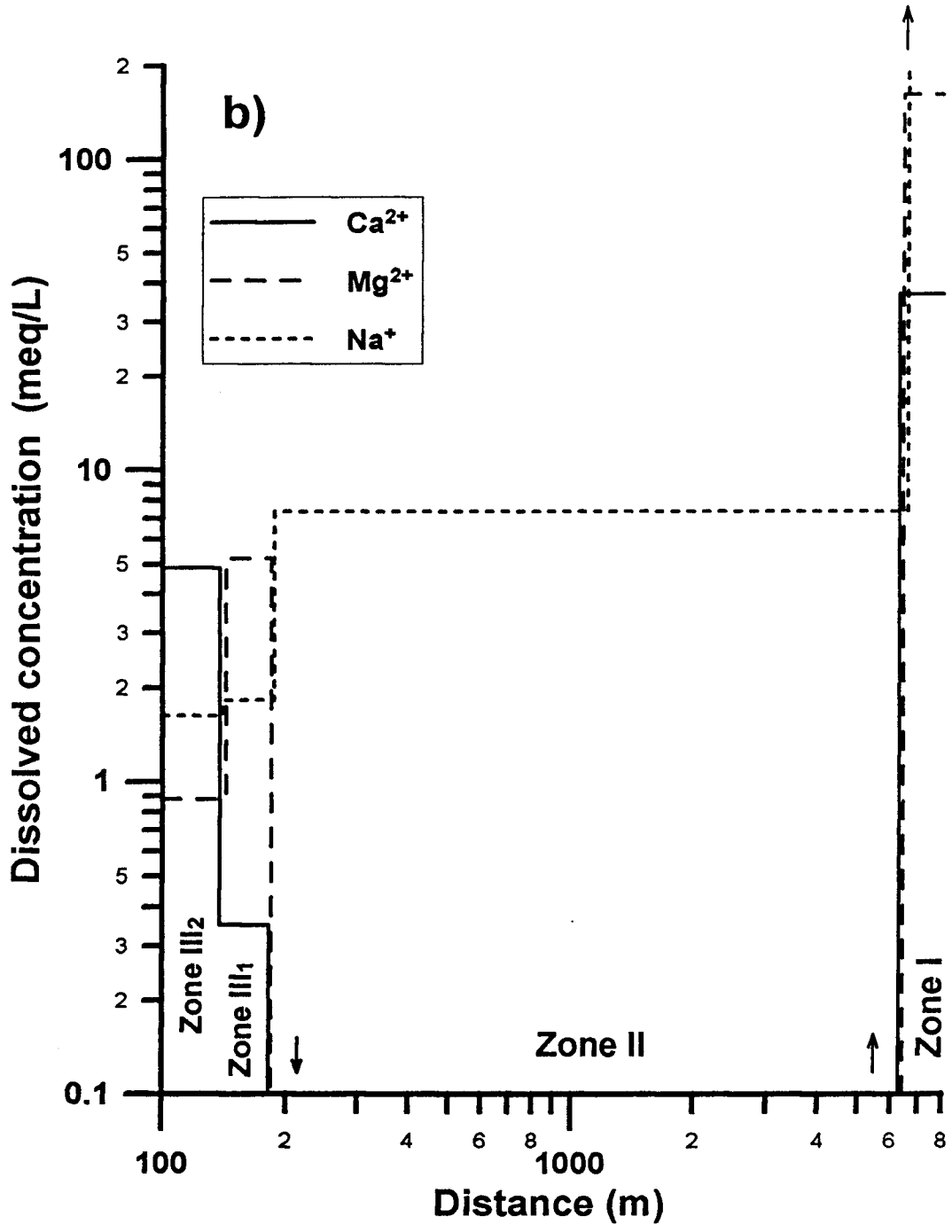

(Figure 7.9. Continued...)

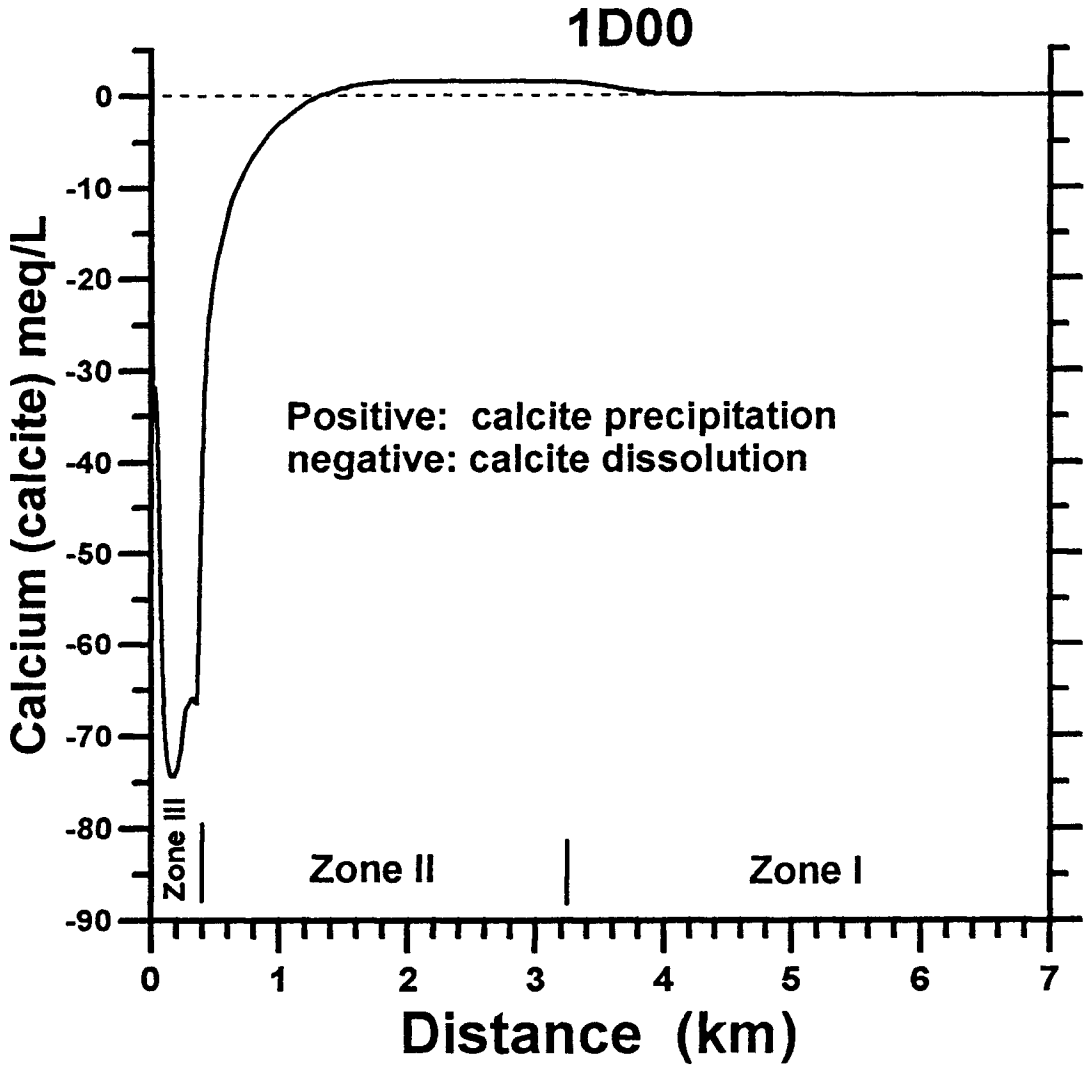

Figure 7.10. Dissolution and precipitation of calcite for model 1D00 at 567 years. The Y axis represents the amount of Ca for calcite.

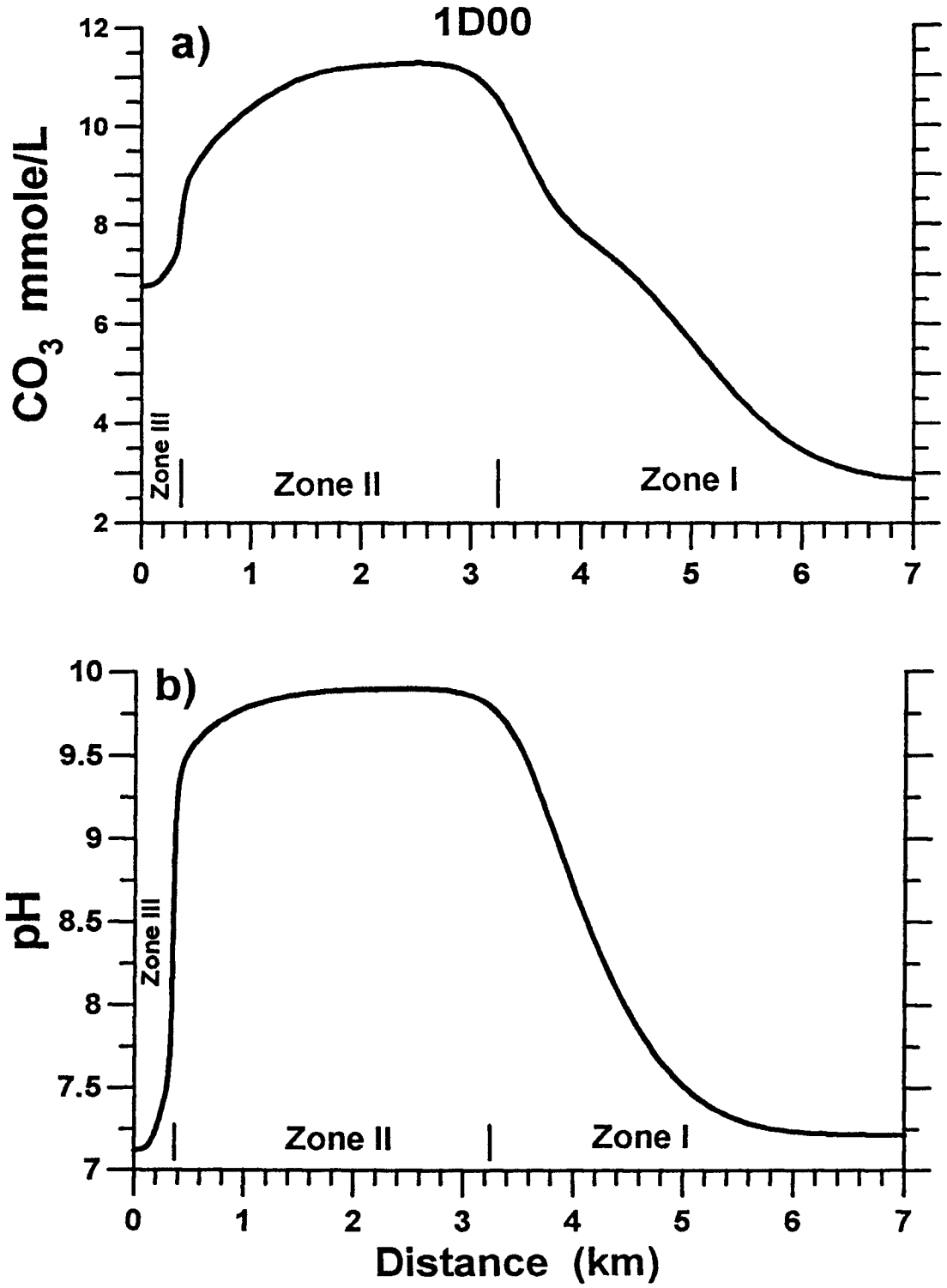

Figure 7.11. Simulated results for model 1D00 at 567 years.
a) total dissolved CO_3 concentration, b) pH.

from the calcite dissolved upstream and are carried along with the ground-water flow. Walsh et al. (1984) referred to this phenomenon as the "downstream equilibrium" condition. Dissolution of calcite raises the pH up to 9.8 in zone II (Figure 7.11b). Another effect of calcite dissolution on water quality in zone II is an increase in TDS due to the additional dissolved carbonate and also Ca^{2+} and Mg^{2+} exchanged for Na^{+} (Figure 7.12).

The effect of calcite dissolution can be seen by comparing the results in figures 7.4 and 7.7. The sharpening fronts are apparently moving faster for the model with calcite dissolution. Figure 7.13a shows that the greatest amount of dissolved Ca added to solution from the calcite dissolution occurs in zone III. The little peak located in between 4 to 5 km indicates that a minor amount of calcite dissolution also occurs in the conservative mixing front. The small amount of excess Mg in the mixing front is another indication of calcite ($Ca_{0.95}Mg_{0.05}CO_3$) dissolution in this area (Figure 7.13b). The original incoming water is undersaturated with respect to calcite. The incoming freshwater in the model without calcite (Figure 7.7) remains undersaturated with respect to calcite. In comparison, the incoming freshwater in model 1D00 becomes calcite saturated after reacting with calcite. Calcite dissolution in zone III does not substantially increase the dissolved Ca and Mg concentrations in zone II because the additional Ca and Mg are adsorbed onto clay surfaces shortly after they are added to the solution. The adsorption is indicated by the large increase of dissolved Na concentration in zone II which was desorbed by exchange with the added Ca^{2+} and Mg^{2+} (Figure 7.13c). The positive and negative peaks near the west end of the diagrams are a result of different locations for the retardation fronts in the two models. A faster movement of the sharpening front occurs in the model with calcite dissolution.

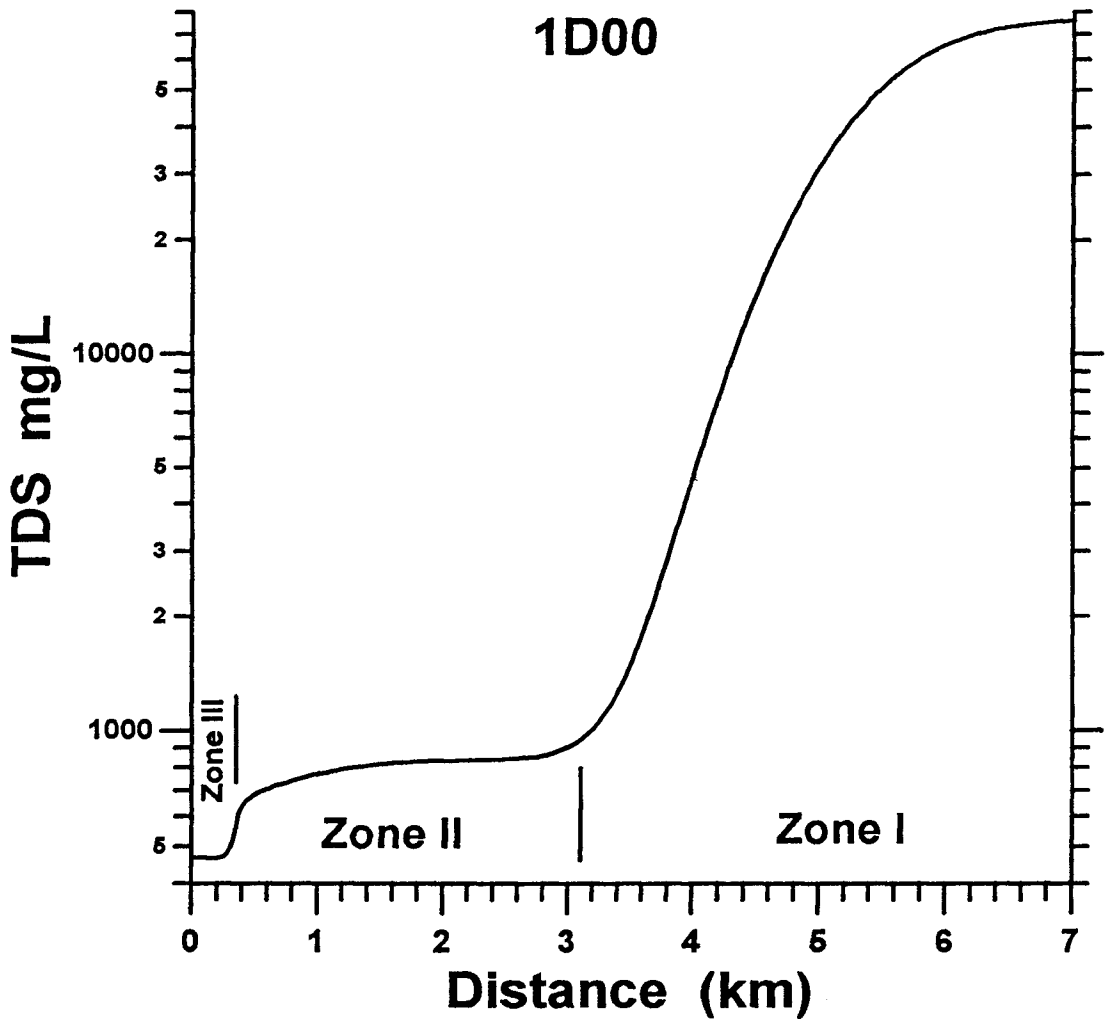

Figure 7.12. Simulated TDS concentration for model 1D00 at 567 years.

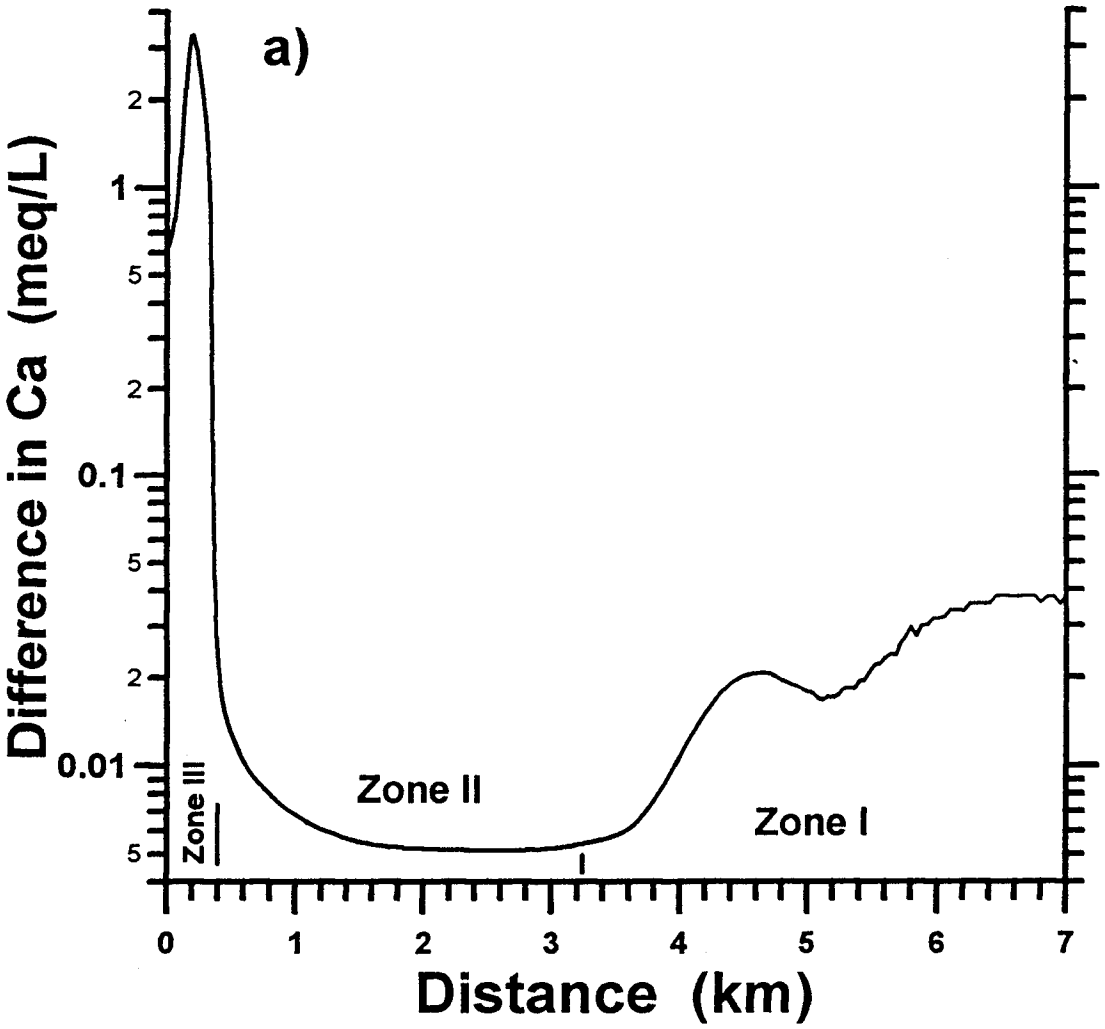

Figure 7.13. The effect of calcite dissolution on dissolved cation concentrations in model 1D00 at 567 years. a) Ca, b) Mg, and c) Na. These diagrams are a result of subtracting values of Figure 7.7 from Figure 7.4.

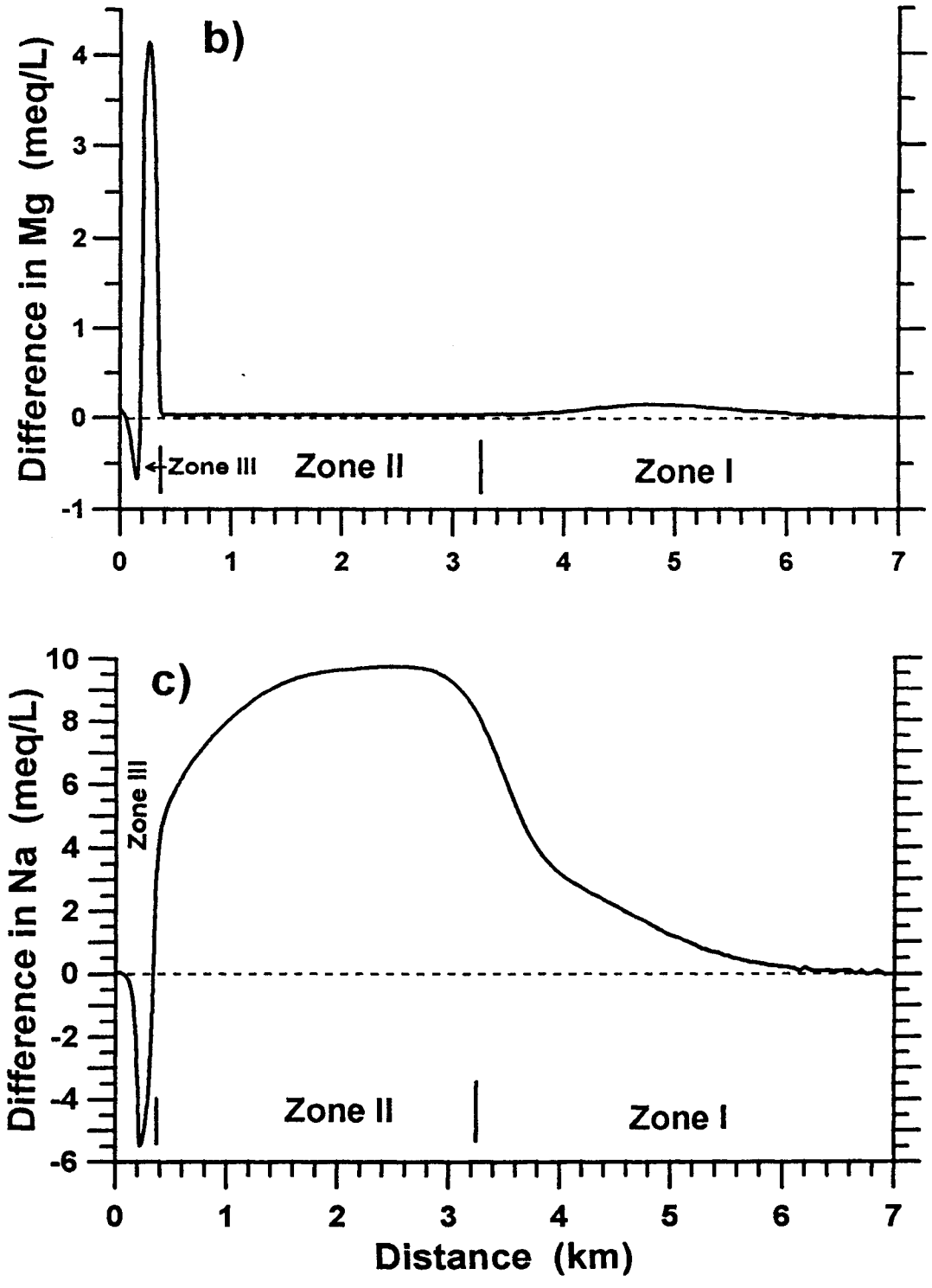
b)
Difference in Mg (meq/L)
4
3
2
1
0
-1
Zone III
Zone II
Zone I
0
1
2
3
4
5
6
7
c)
Difference in Na (meq/L)
10
8
6
4
2
0
-2
-4
-6
Zone III
Zone II
Zone I
0
1
2
3
4
5
6
7
Distance (km)

(Figure 7.13...)

As described in Chapter 3, ion exchange is an action that occurs in non-steady state conditions when an aquifer system undergoes freshening or salinization. After the conservative mixing front passes, the system reaches a temporary stable condition in zone II. Only a small amount of cation exchange takes place between Mg^{2+} and Na^{+} through this zone (Figure 7.14). At this stage, the concentration of Ca^{2+} is too low to have any significant effect until close to the first sharpening front where the additional Ca from dissolution of calcite provides the cause for exchange between Ca^{2+} and Na^{+}. Other pronounced features are that pH and carbonate concentrations reach their maximum levels in zone II.

Figure 7.15 illustrates that cation exchange occurs immediately when the freshwater and saltwater mix. The chromatographic separation follows the imposed selectivity order and shows clearly that Na^{+} is displaced first and Mg^{2+} next. The displaced Na^{+} is exchanged for Mg^{2+} and Ca^{2+}, and later the rejected Mg^{2+} is replaced only by Ca^{2+}. In zone II, the increase in Na concentration is greater than the sum of the decreased Ca and Mg concentrations. This indicates that additional Ca and Mg are supplied for cation exchange by calcite dissolution. Similar chromatographic patterns have been reported for laboratory experiments (e.g., Appelo et al., 1990), field injections (e.g., Grove and Wood, 1979; Valocchi et al., 1981b), and natural ground water systems (e.g., Thorstenson et al., 1979; Chapelle, 1983; Boyle, 1992).

The major process in zone I is the mixing of initial saltwater with the water from zone II. Although the TDS concentrations of the waters from the two zones are quite different, their exchanging cation activity ratios are required to fit the adsorbed concentration ratios in the sediment that is still in equilibrium with the initial saltwater. Only minor cation exchange (relative to the adsorbed concentration) occurs in the mixing front (Figure 7.14). The origin of the plateau in zone II is caused by cation exchange and the cation concentrations in zone II are

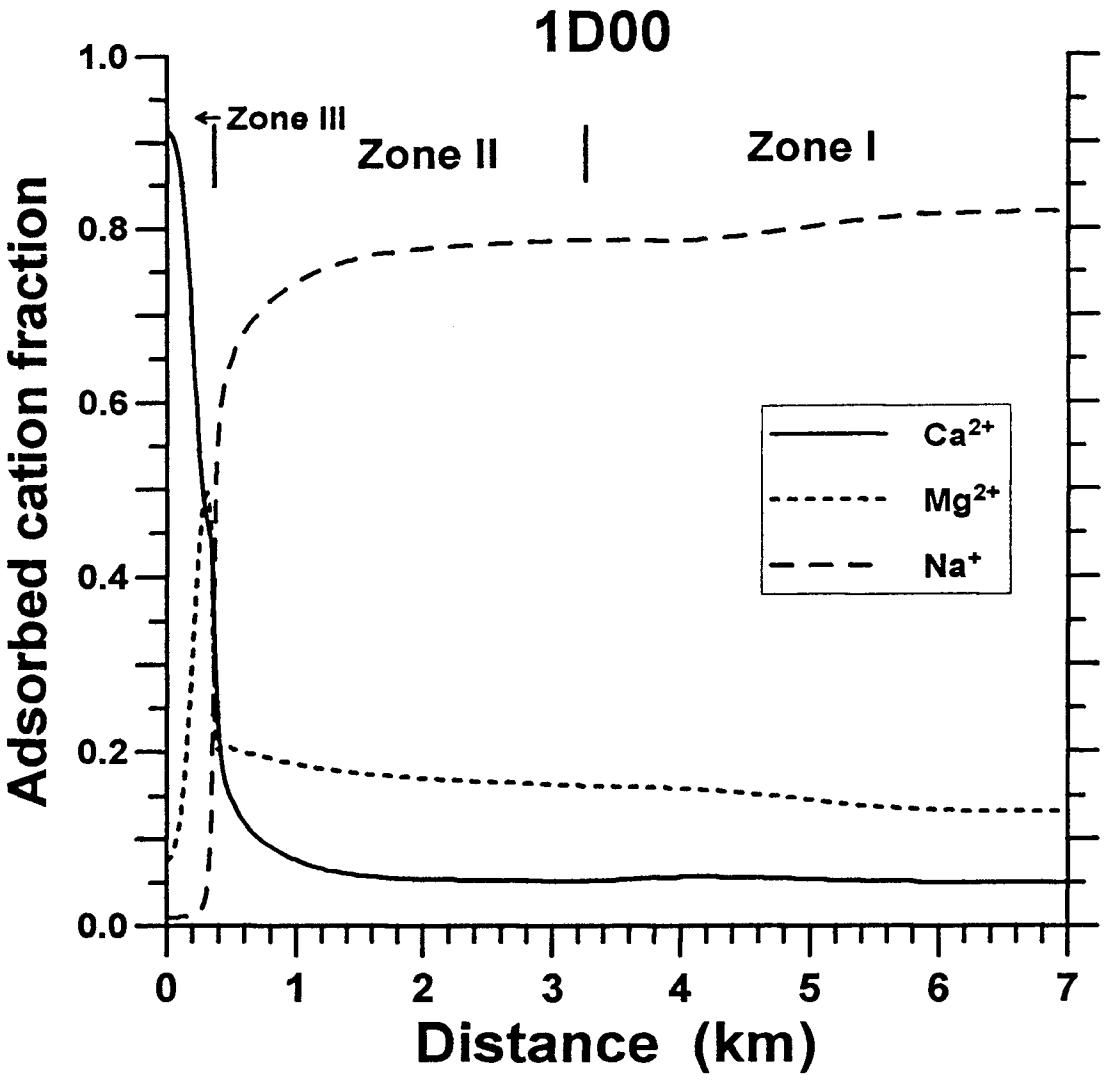

Figure 7.14. Adsorbed fractions of exchanging cations for model 1D00 at 567 years.

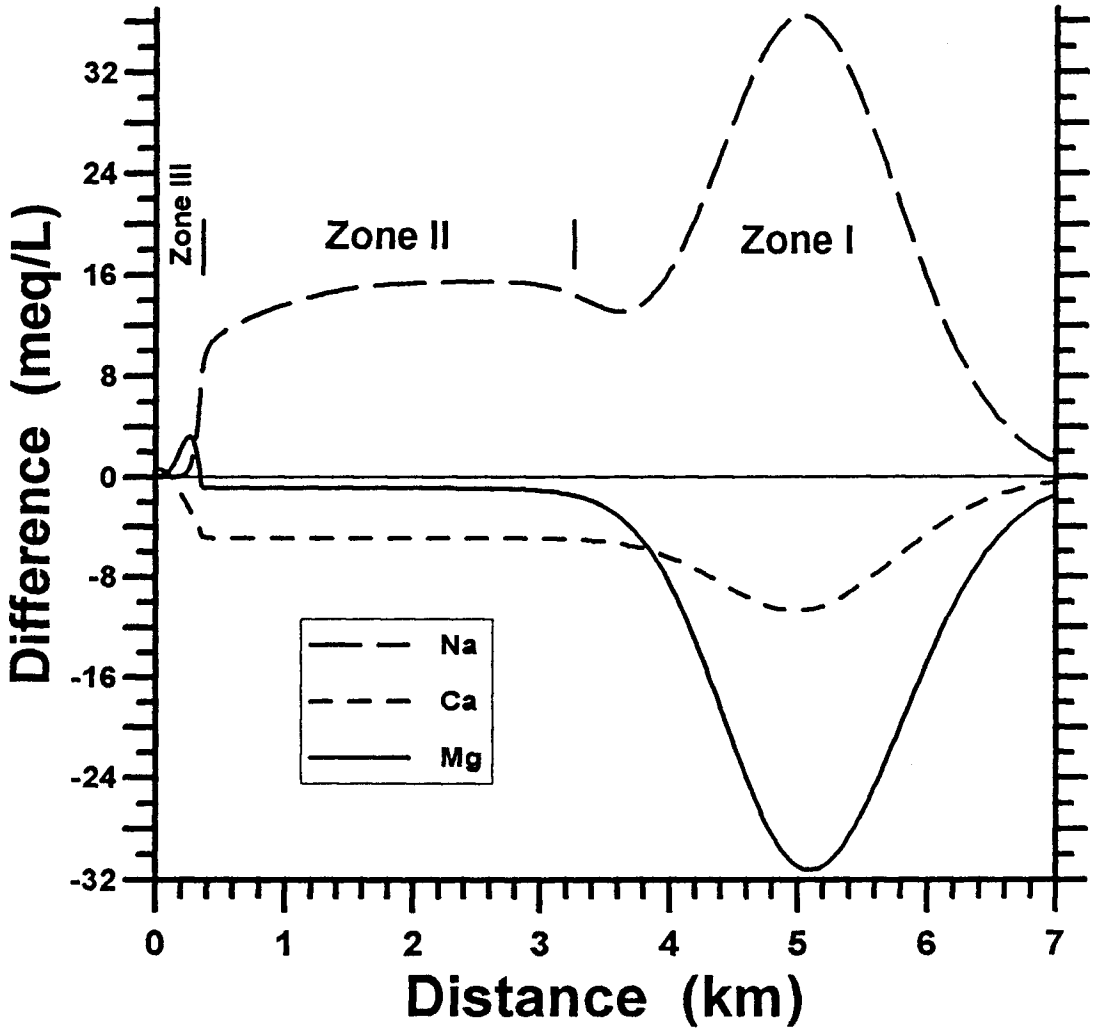

Figure 7.15. The dissolved concentration difference of exchangeable cations between model 1D00 and simulated conservative transport along the flow path at 567 years with the same initial and boundary water compositions.

controlled by the incoming freshwater (salinity effect). The exchange reaction of Ca^{2+} and Mg^{2+} for Na^{+} is enhanced at the mixing front because the TDS contents of waters at this location are higher than in zone II. The effect can be calculated analytically by Equations 7.4 to 7.6. Further discussion is given in Section 7.3.3.3.

The evolution of the water chemistry is shown on a trilinear diagram in Figure 7.16. The initial saltwater is Na-Cl type and the incoming freshwater is Ca-HCO_3 type. In zone I, water starts as Na-Cl type then changes to Na-HCO_3 type when mixed with water from zone II. In zone II, the water chemistry is in a temporary stable condition as the dense distribution of data points indicates at the lower corner of the diamond. Na-HCO_3 is the dominate water type in zone II. In zone III, the water changes from the mixed-cation-HCO_3 type in zone III_1, to the Ca-HCO_3 type of the incoming water in zone III_2. The mixed-cation-HCO_3 type water is not commonly found in actual aquifers because of its short transient character along the flow path.

Comparing the coupled model results with the example illustrated in section 7.3.1 for the geochemical modeling of conservative mixing, it is clear that a conventional geochemical model is not able to describe the chromatographic pattern observed in aquifers. The occurrence of zones II and III_1 and sharpening fronts is not shown in the geochemical model. On the other hand, the traditional mass transport models with a single retardation coefficient can not explain the occurrence of the plateau zones, or differentiate the sharpening fronts and the conservative mixing front. Only coupled models which consider both flow and chemical reactions can relevantly describe the transport of chemically active species.

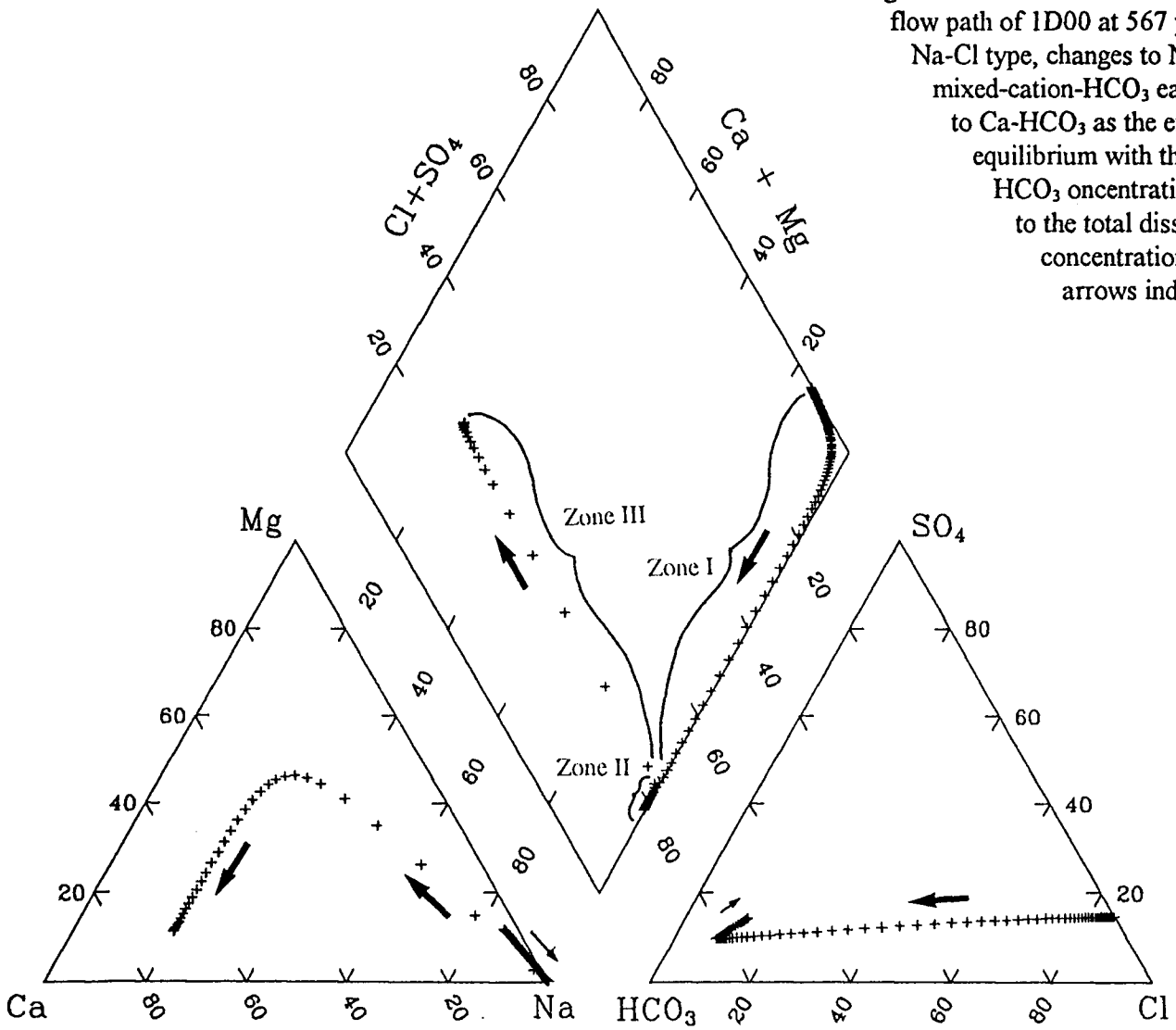

Figure 7.16. The evolution of water chemistry along the flow path of 1D00 at 567 years. The water starts as Na-Cl type, changes to Na-HCO_3 in zone II, to mixed-cation-HCO_3 early in zone III, and finally, to Ca-HCO_3 as the exchange sites approach equilibrium with the incoming freshwater. The HCO_3 oncentrations are assumed to be equal to the total dissolved carbonate concentrations regardless of pH. The arrows indicate the evolution direction.

7.3.3. Sensitivity Analyses

The purpose of the sensitivity analyses is to examine the factors controlling the intensity of cation exchange. As described previously, three of the six categories for sensitivity analyses involve the effects of the formation properties on the water chemistry (Table 7.1). The other three categories are used to examine the individual effects of the initial and incoming water chemistry. The influence on the intensity of cation exchange by the contrast in ionic concentrations between the two mixing waters is also discussed.

7.3.3.1. Selectivity Coefficients

The definition of the selectivity coefficient is given in Chapter 6. For category I in Table 7.1, based on the previous studies discussed in Chapter 3, reasonable $K_{Mg/Ca}$ ranges from 0.5 to 1 for most clay minerals. With fixed $K'_{Ca/Na}$ (10.24), the variation of $K'_{Mg/Na}$ (from 2.56 to 10.24) does not significantly affect the water chemistry in any stage nor the traveling velocity of the sharpening front (Figure 7.17). The most notable effect of this category is on the adsorbed fractions of Mg^{2+} and Na^{+} on the clays (Figures 7.14 and 7.18). The adsorbed proportion of Mg varies from less than 0.1 to more than 0.2 in zone I with the variation of $K'_{Mg/Ca}$ from 0.5 to 1. Most of the surface sites for the increase in adsorbed Mg^{2+} concentration are taken from Na^{+}. The proportion of adsorbed Ca^{2+} is slightly reduced when $K'_{Mg/Ca}$ increases from 0.5 to 1. Those changes, in turn, affect the amount of calcite dissolution. The smaller the $K'_{Mg/Ca}$, the higher is the relative affinity of Ca^{2+} on the surface sites. Therefore, as more Ca^{2+} is required on the clay surfaces during cation exchange, more calcite is dissolved (Figure 7.19). However, the effect of the selectivity coefficient on the

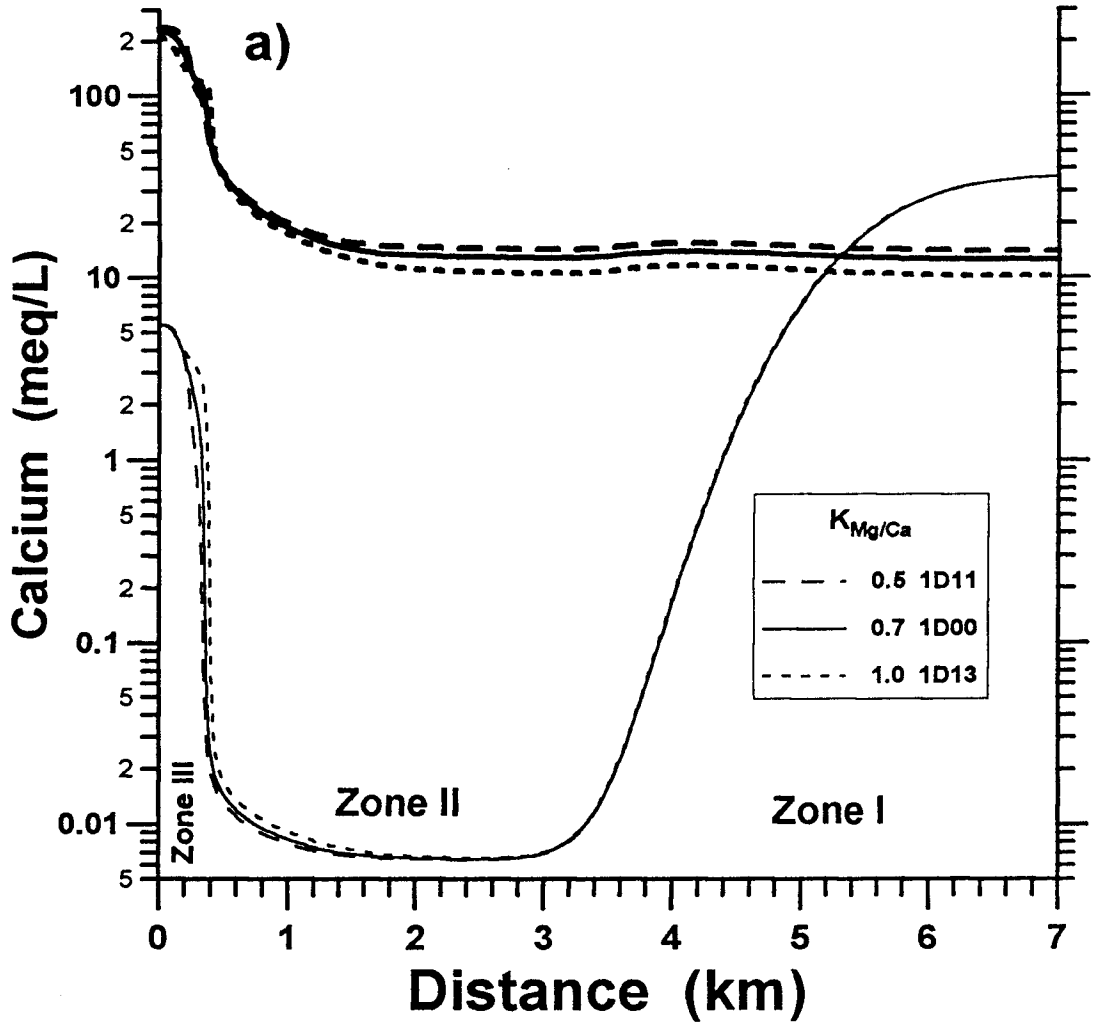

Figure 7.17. Simulated cation concentrations for sensitivity analyses of three $K_{Mg/Ca}$ values at 567 years. a) Ca, b) Mg, and c) Na. The thick lines represent the adsorbed concentrations and the thin lines indicate the dissolved concentrations.

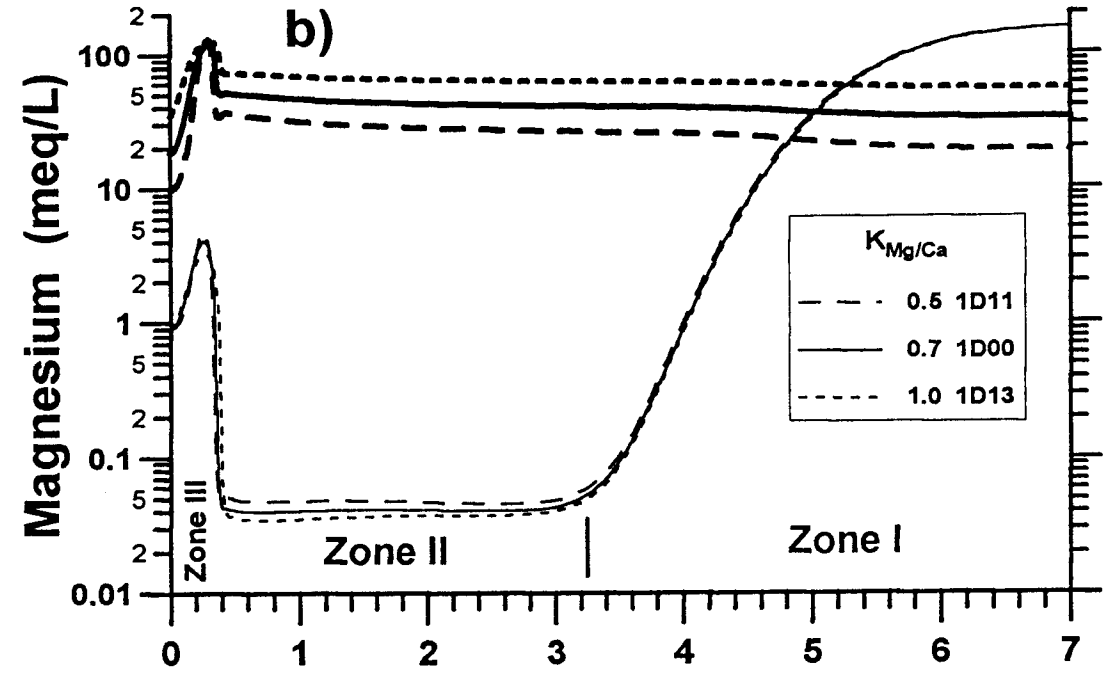

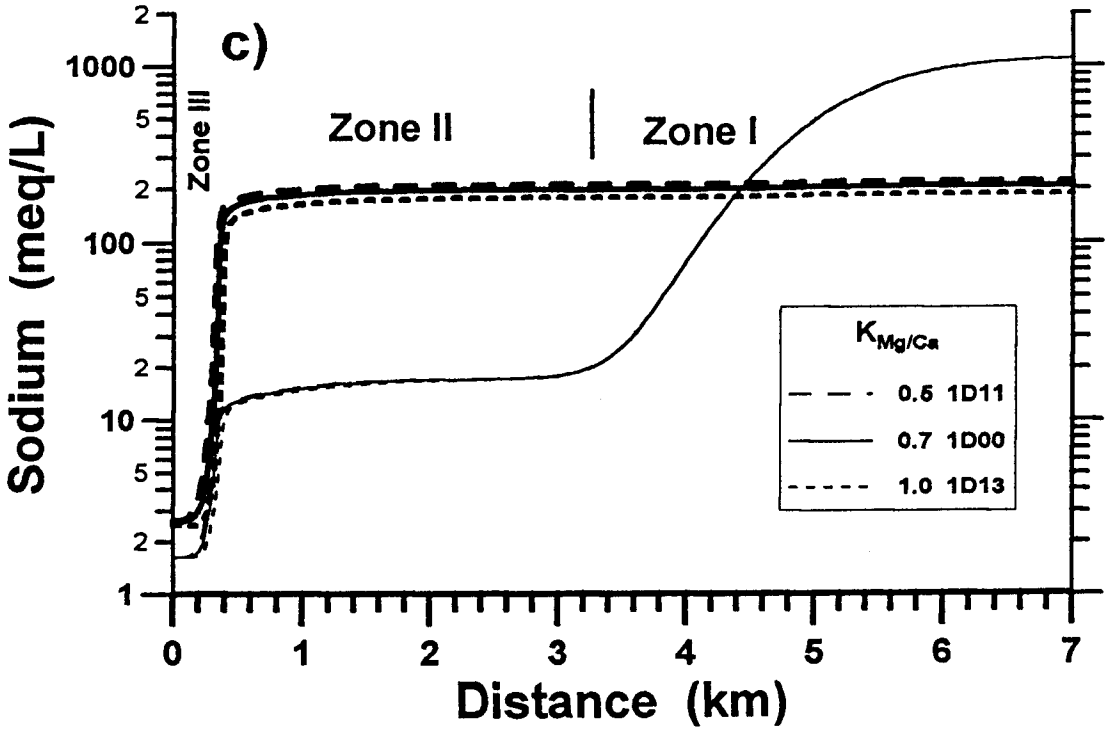

(Figure 7.17. Continued...)

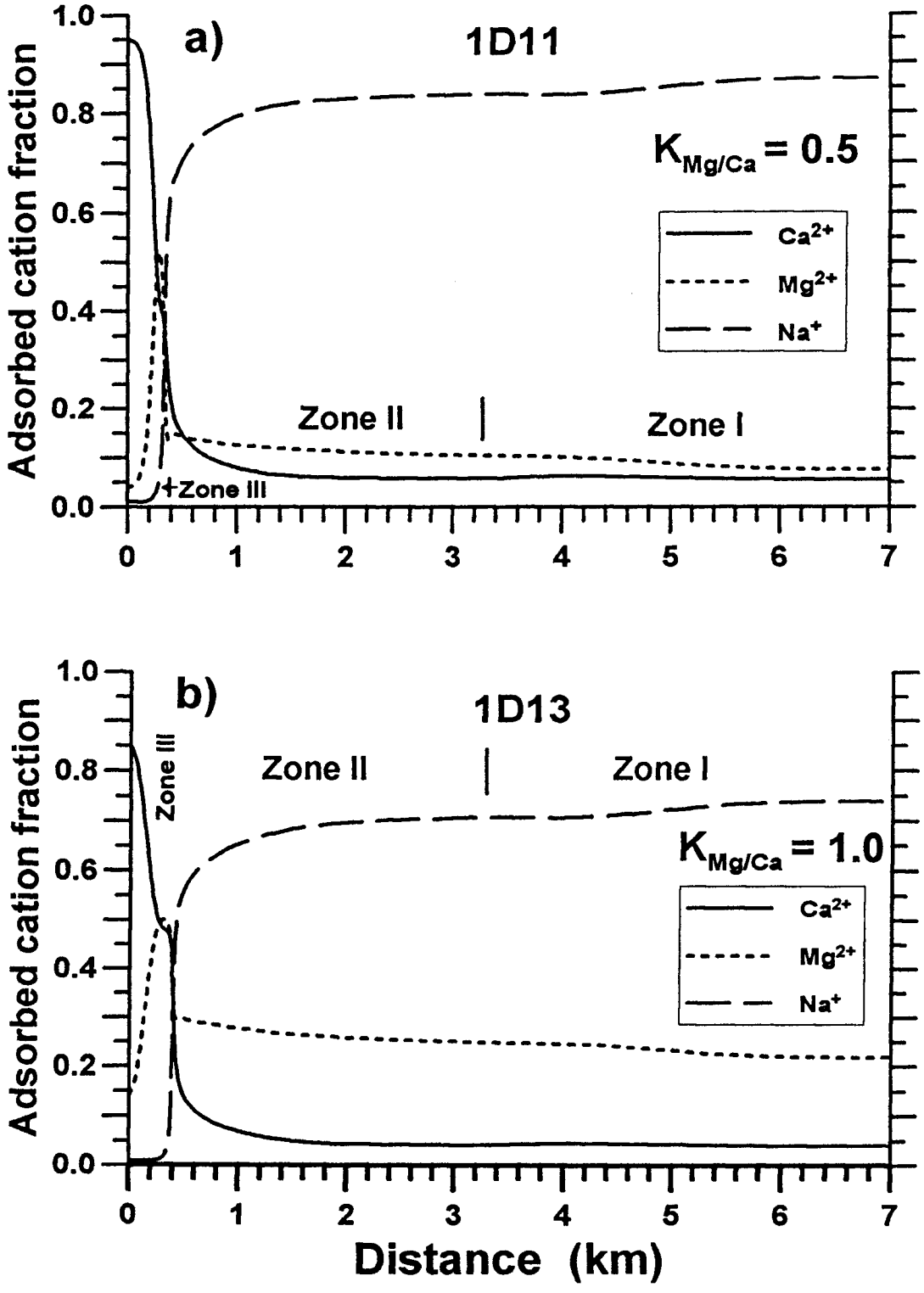

Figure 7.18. Simulated adsorbed cation proportions for sensitivity analyses of two $K_{Mg/Ca}$ values at 567 years. a) $K_{Mg/Ca}$ = 0.5, and b) $K_{Mg/Ca}$ = 1.0.

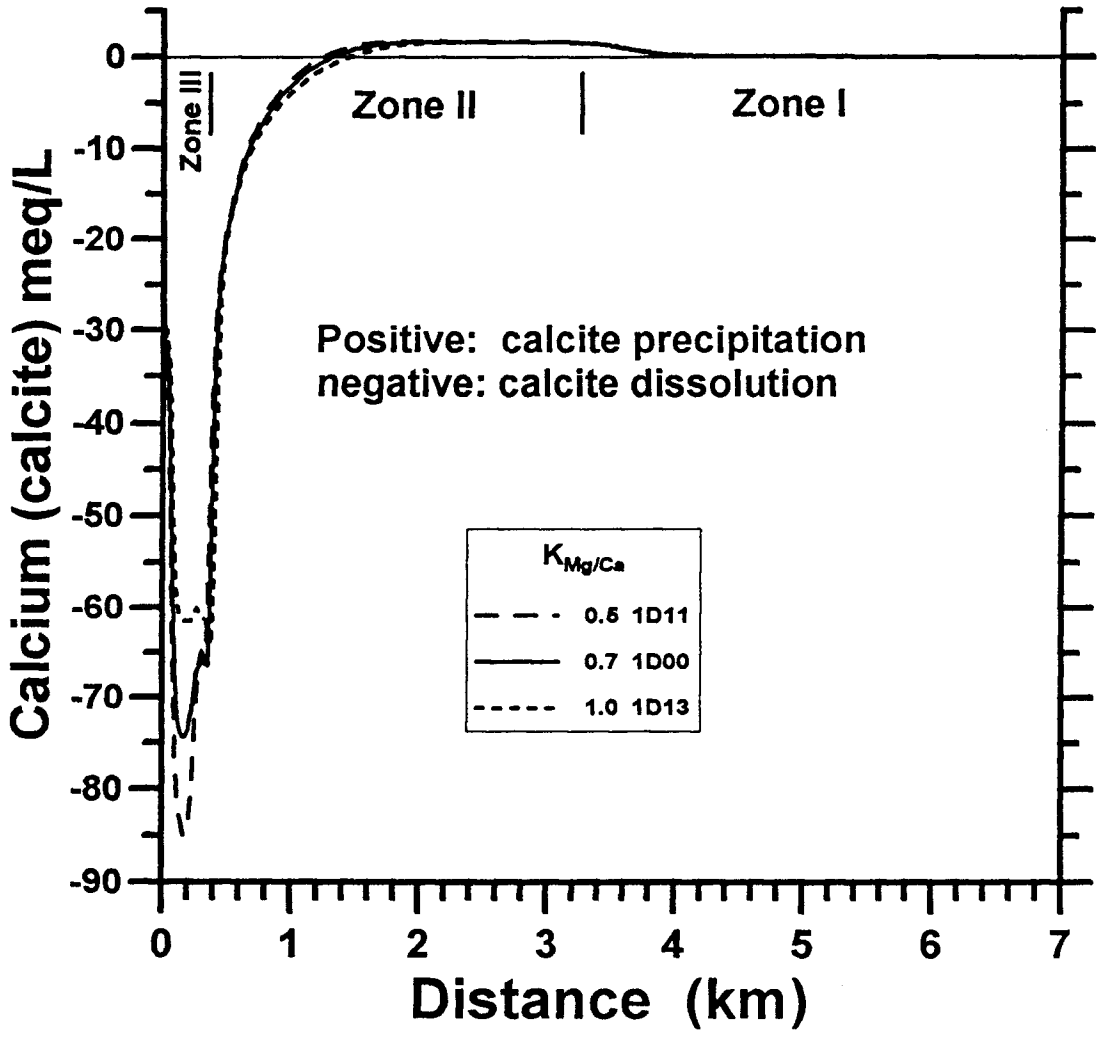

Figure 7.19. Simulated calcite dissolution for sensitivity analyses of three $K_{Mg/Ca}$ values at 567 years. The Y axis represents the amount of Ca for calcite.

adsorbed cations for the Dakota sediments can not be well determined due to the lack of data for the exchangeable fractions of each individual cation in the aquifer materials.

For category II (Table 7.1), the $K_{Ca/Na}$ varies from 2.0 to 5.0 and $K_{Mg/Ca}$ is fixed at 0.7. Previous studies of cation exchange indicate that there are wide ranges in $K_{Ca/Na}$ for different varieties of geological materials. However, with ternary exchange of Ca^{2+}, Mg^{2+}, and Na^{+}, the $K_{Mg/Ca}$ is normally within a certain range as indicated in the previous paragraph. In the test strategy for this category, $K_{Mg/Na}$ changes with the variation of $K_{Ca/Na}$. Similar to the result of category I, the effect of $K_{Ca/Na}$ variation on water chemistry in zone II is insignificant (Figure 7.20). The velocities of the retardation fronts are slightly affected. Rather than adsorbed Ca^{2+}, the initial adsorbed Mg^{2+} fraction is the most sensitive variable in this test (Figures 7.14 and 7.21). This is because the dissolved Mg concentration in the initial saltwater is much higher than the Ca concentration, and the variation in selectivity coefficients affects the adsorbed Mg^{2+} concentration more than the adsorbed Ca^{2+}.

In summary, the first two categories (I and II in Table 7.1) of sensitivity analyses reveal that the variation in selectivity coefficients within a reasonable range does not substantially affect the aqueous chemistry in zone II. However, the buffering capacity of the exchange medium for each cation varies significantly with the variation in selectivity coefficient. The effect causes a variation in the velocity of the retardation front. Magnesium, which has the intermediate selectivity coefficient, changes the most in the two sensitivity analyses due to its higher concentration relative to Ca in the initial saltwater.

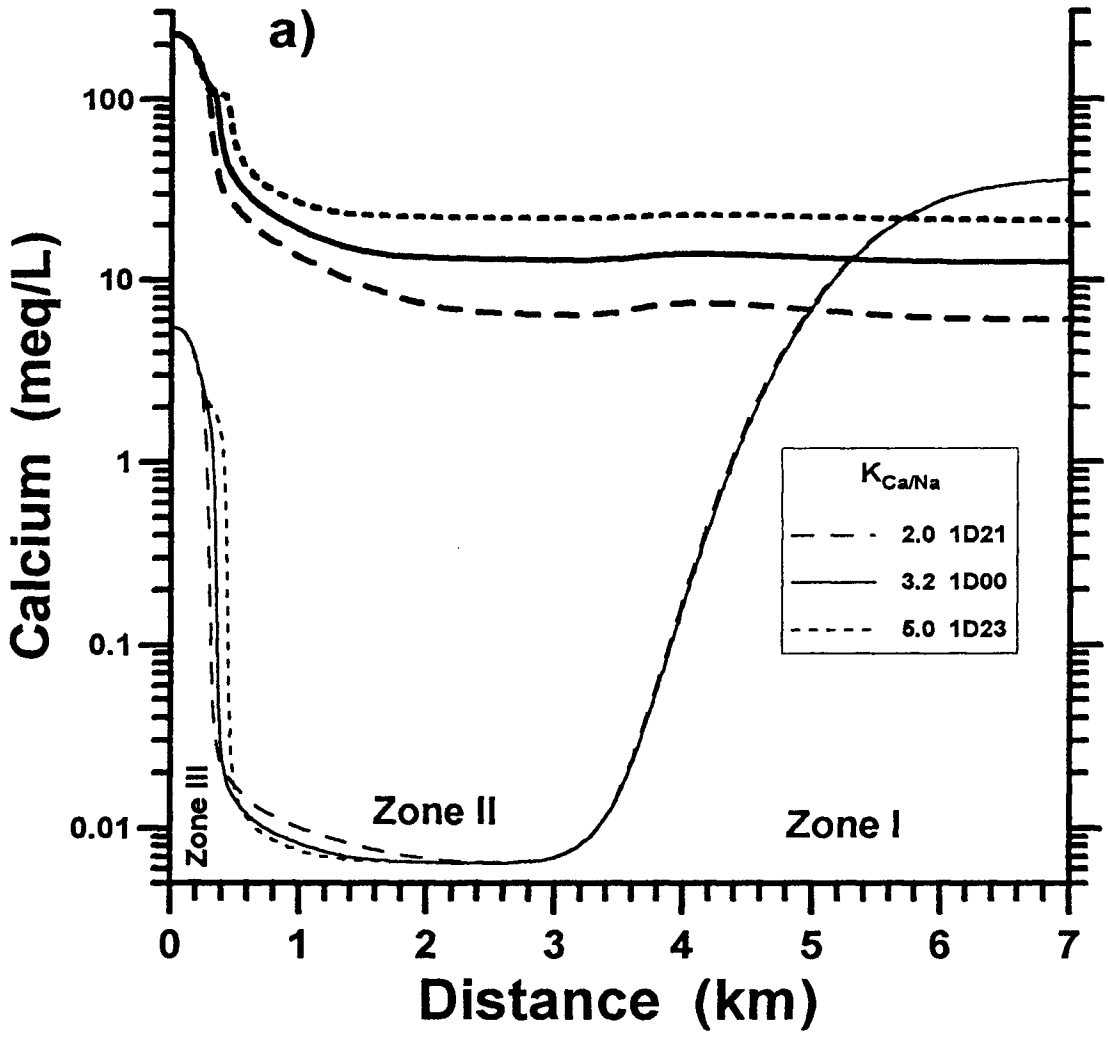

Figure 7.20. Simulated cation concentrations from the sensitivity analyses of three $K_{Ca/Na}$ values at 567 years. a) Ca, b) Mg, and c) Na. The thick lines represent the adsorbed concentrations and the thin lines represent the dissolved concentrations.

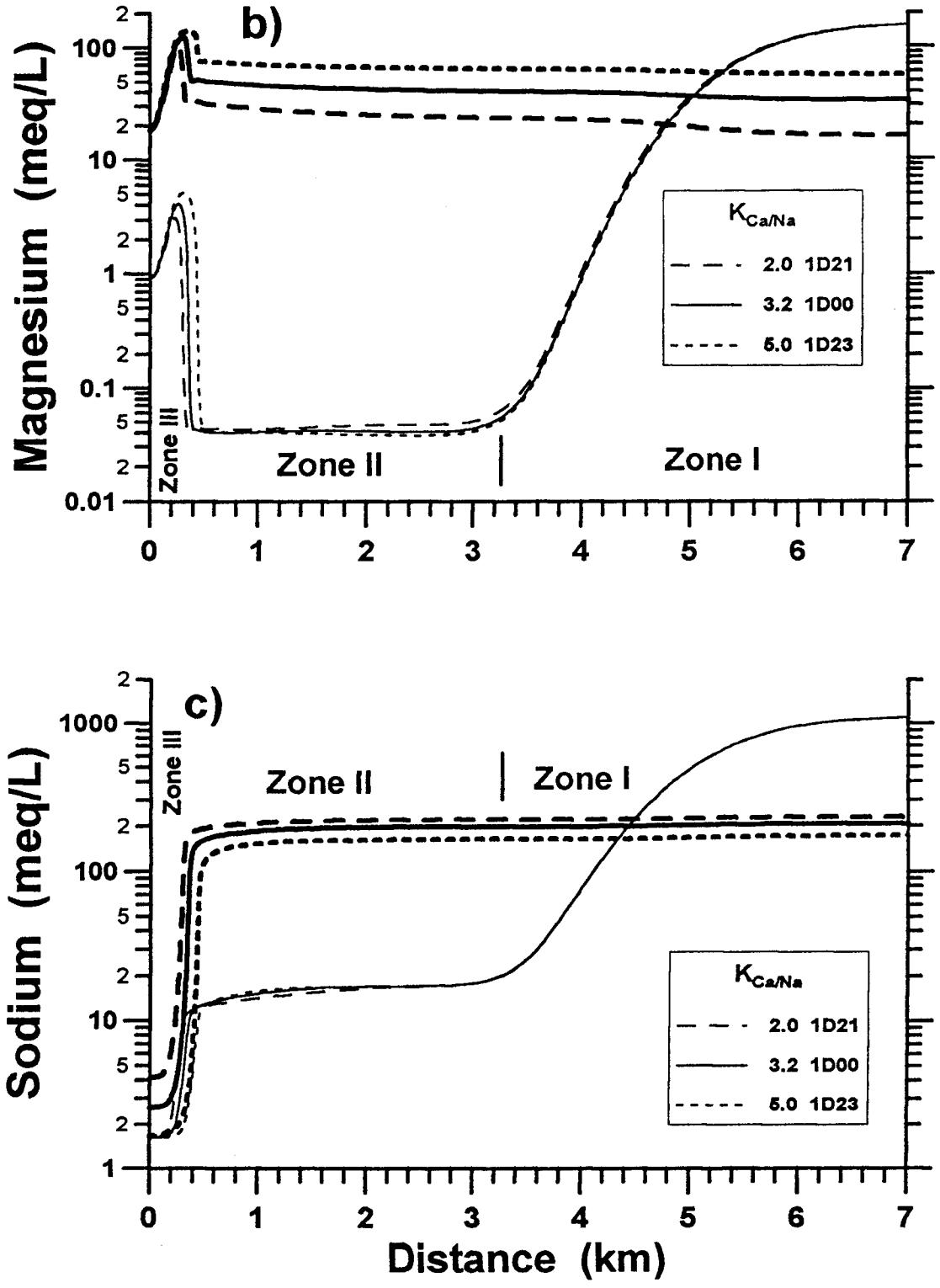

(Figure 7.20. Continued...)

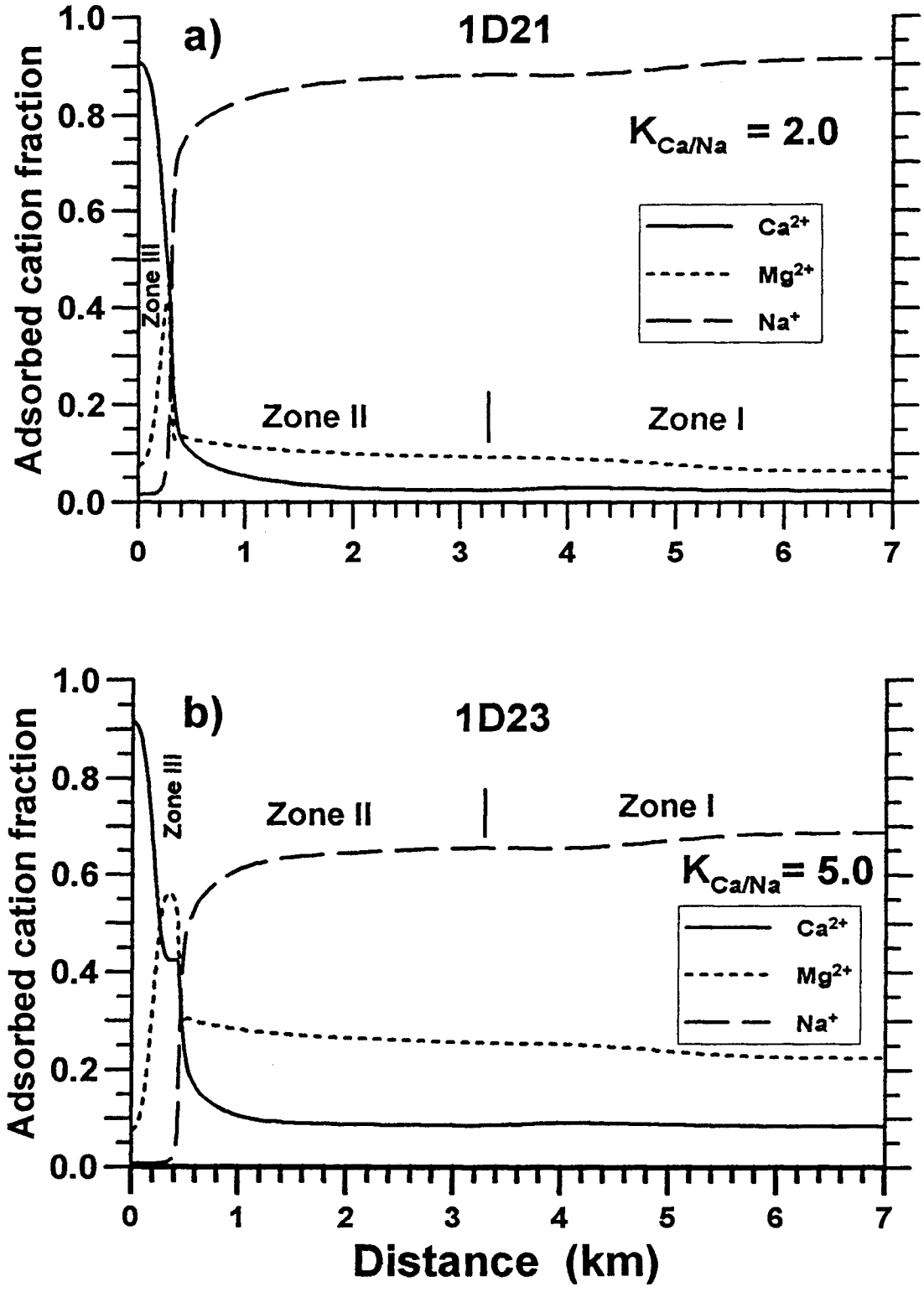

Figure 7.21. Simulated adsorbed cation fractions from the sensitivity analyses of two $K_{Ca/Na}$ values at 567 years. a) $K_{Ca/Na}$ = 2.0, and b) $K_{Ca/Na}$ = 5.0.

7.3.3.2. Cation Exchange Capacity

A wide range of CEC values was tested for category III of the sensitivity analyses. The exchange capacity of 1 L of pore water is equal to CEC times a bulk density over a porosity factor of 10 kg/L as indicated in Equation 7.1. This produces exchange capacities of 100, 250, 1,000, and 5,000 meq/L of solution for the tested models in this category. Table 7.2 indicates that an CEC of 10 to 30 meq/kg is reasonable for the Dakota aquifer when the amount of argillaceous sediments present in the system is considered.

The higher the CEC of the formation materials, the more freshwater is necessary to change the surface sites from in equilibrium with the residual saltwater to in equilibrium with the incoming freshwater. This is because the buffering capacity of the exchange medium increases with increasing CEC due to the greater amount of exchangeable cations on the surface sites (Figure 7.22). The greatest effect of CEC other than altering adsorbed cation concentrations is to change the velocities of the retardation fronts. The model with the highest velocities for the retardation fronts is the one with the lowest CEC. This means that the flushing factor and the length of the plateau zones increase with increasing CEC (Equations 7.8 and 7.9).

There are several different aspects of the CEC effects on water chemistry. At high CEC's of 100 meq/kg or greater, the Ca and Mg concentrations in zone II reach a minimum such that the water chemistry of the plateau zones is similar for different CEC values higher than 100 meq/kg (Figure 7.22). Changes in CEC are not as important for controlling cation exchange intensity in such conditions. Rather, CEC is more a factor in controlling the velocity of the retardation front and the length of the plateau zone. The concomitant calcite dissolution is very sensitive to CEC because the velocity of the Ca retardation front depends heavily on

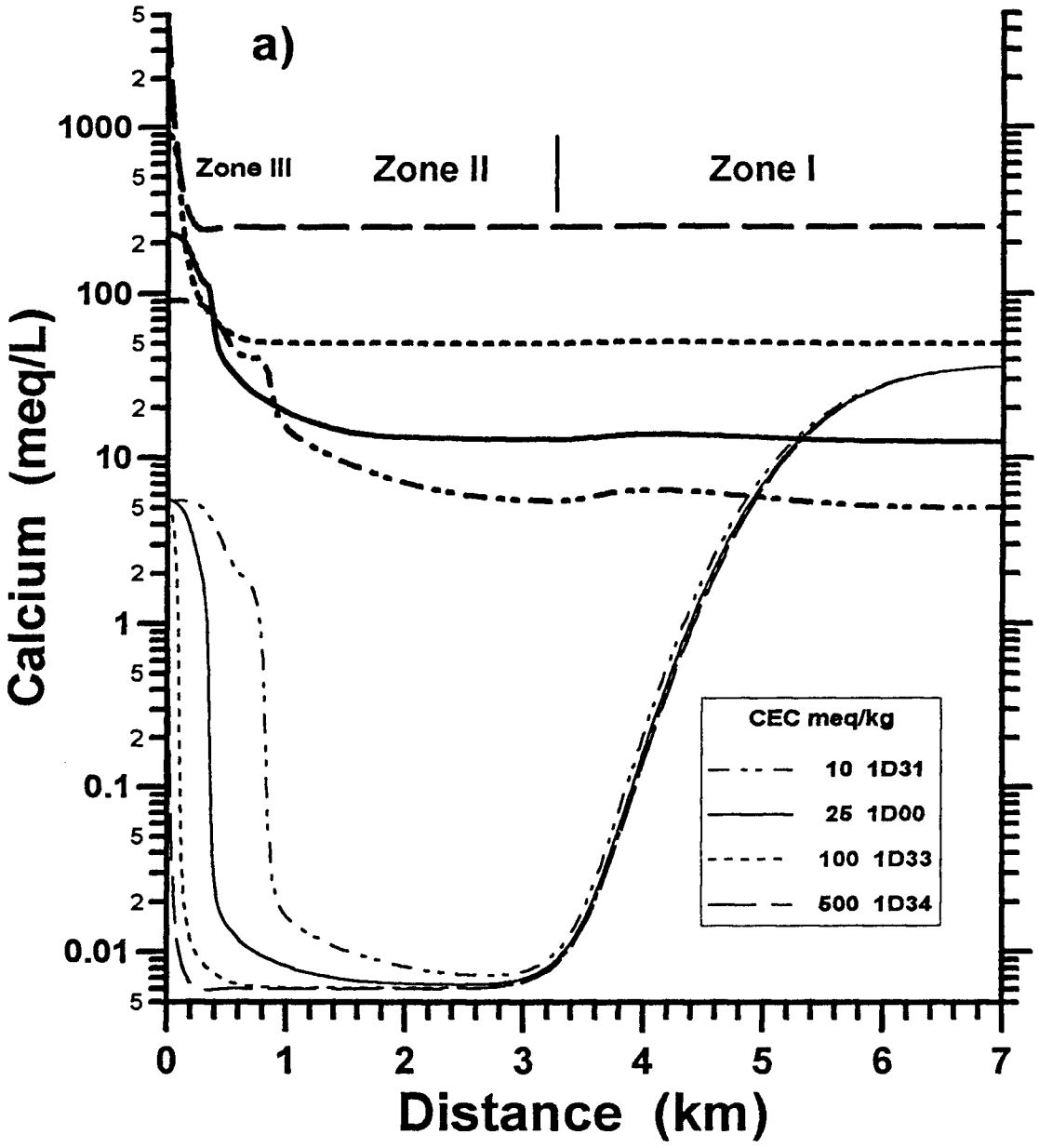

Figure 7.22. Simulated cation concentrations from the sensitivity analyses of four CEC values at 567 years. a) Ca, b) Mg, and c) Na. The thick lines represent the adsorbed concentrations and the thin lines represent the dissolved concentrations.

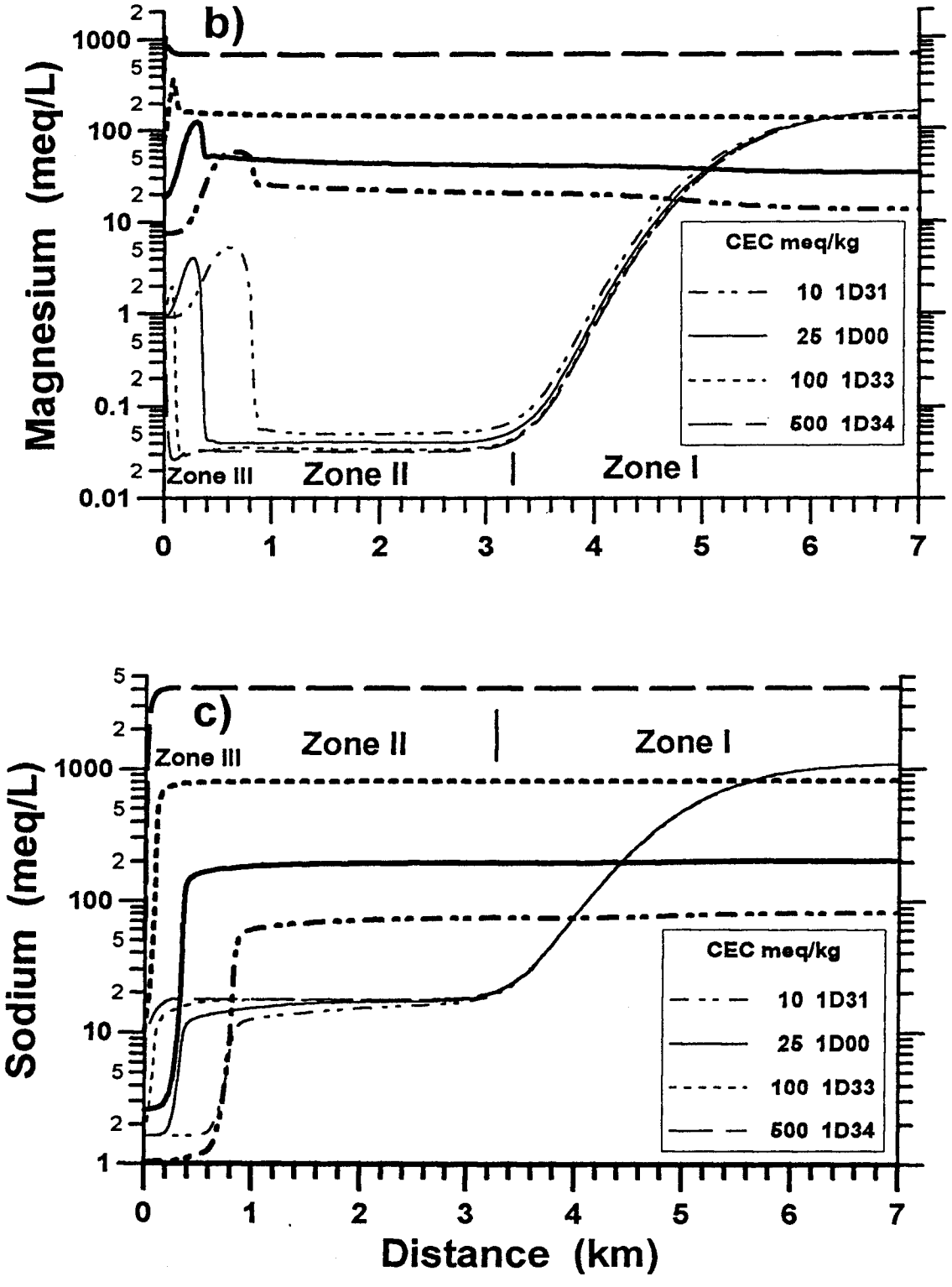

(Figure 7.22. Continued...)

CEC. As the CEC increases, the velocity of the Ca retardation front decreases. Thus, more calcite will be dissolved per unit length of flow path (Figure 7.23) because more Ca is required for exchange. However, variation of calcite dissolution caused by the variation of CEC does not substantially affect the maximum solution pH and CO_3 concentration in zone II (Figure 7.24). Figure 7.25 shows that at lower CEC values, the sediments have a smaller capacity to keep the dissolved cation ratios at the original adsorbed composition. This fact is particularly clear for the model with a CEC of 10 meq/kg. A smaller buffering capacity of low CEC sediments also decreases the magnitude of the Na peak in the salinity front (Figure 7.26). Based on the test results for sensitivity analyses in category III, the exchange buffering effect of sediments on water chemistry can not reach a maximum strength for the model condition when the CEC is lower than 10 meq/kg.

7.3.3.3. Salinity Contrast of Incoming and Initial Waters

As described in Chapter 5, the initial saltwater is assumed to have come from the underlying Permian strata and its Na and Cl derived from halite dissolution. Therefore, the mole ratio of Na over Cl for the saltwater is close to 1. The initial waters (Na/Cl = 0.999) used in the models represent such kind of water. The incoming freshwater also has only a small difference in the Na and Cl molar concentrations. As a result, any excess of Na relative to Cl concentration for water in the simulations is a result of cation exchange. Comparison of Na and Cl contents are convenient for representing exchange effects along the flow path because Cl is considered as a conservative species in the model.

The last three categories of sensitivity analyses test the effect of different constituent concentrations in the initial and incoming waters on the intensity of cation exchange.

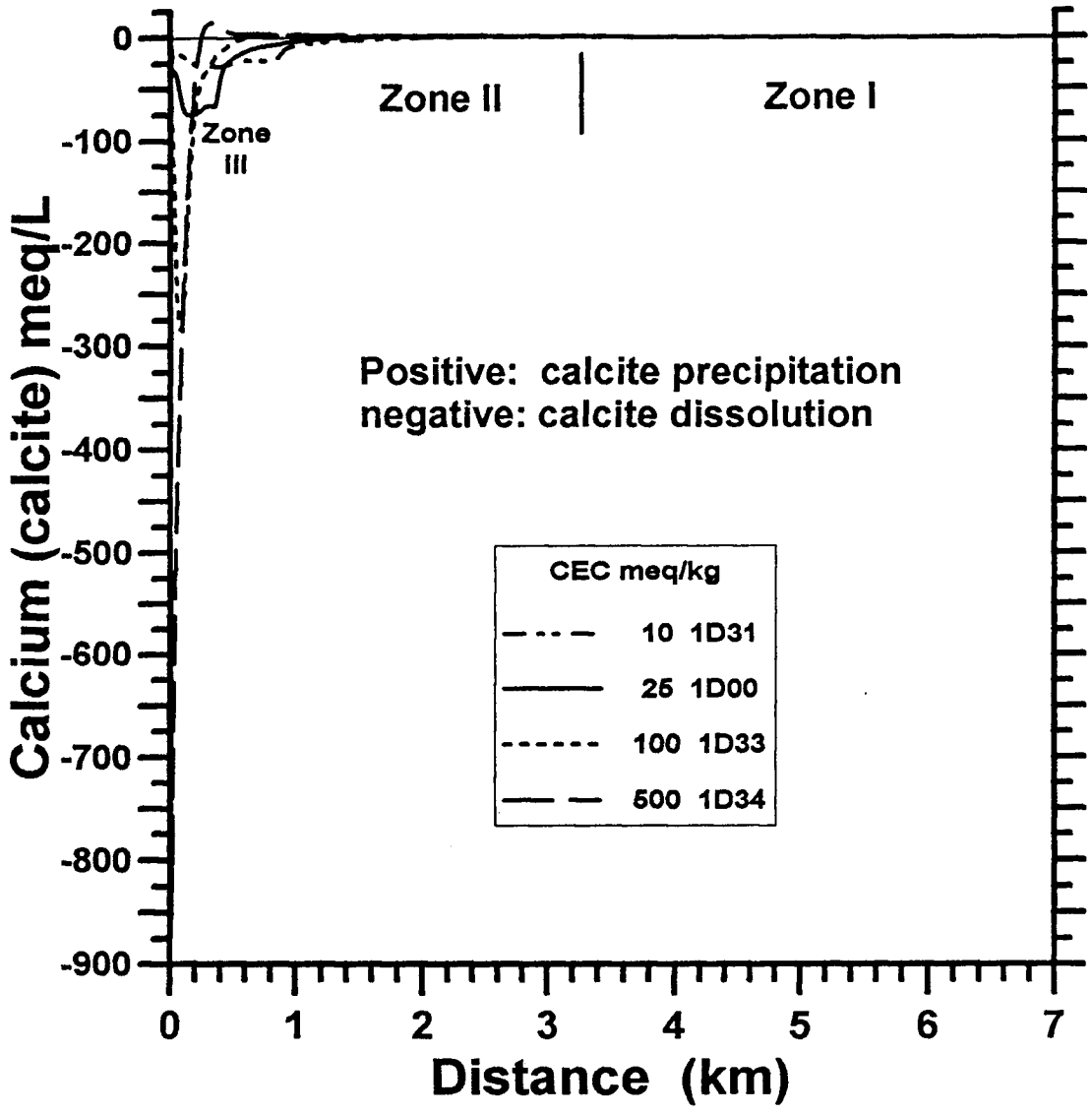

Figure 7.23. Simulated calcite dissolution from the sensitivity analyses of four CEC values at 567 years. The Y axis represents the amount of Ca added or removed by calcite.

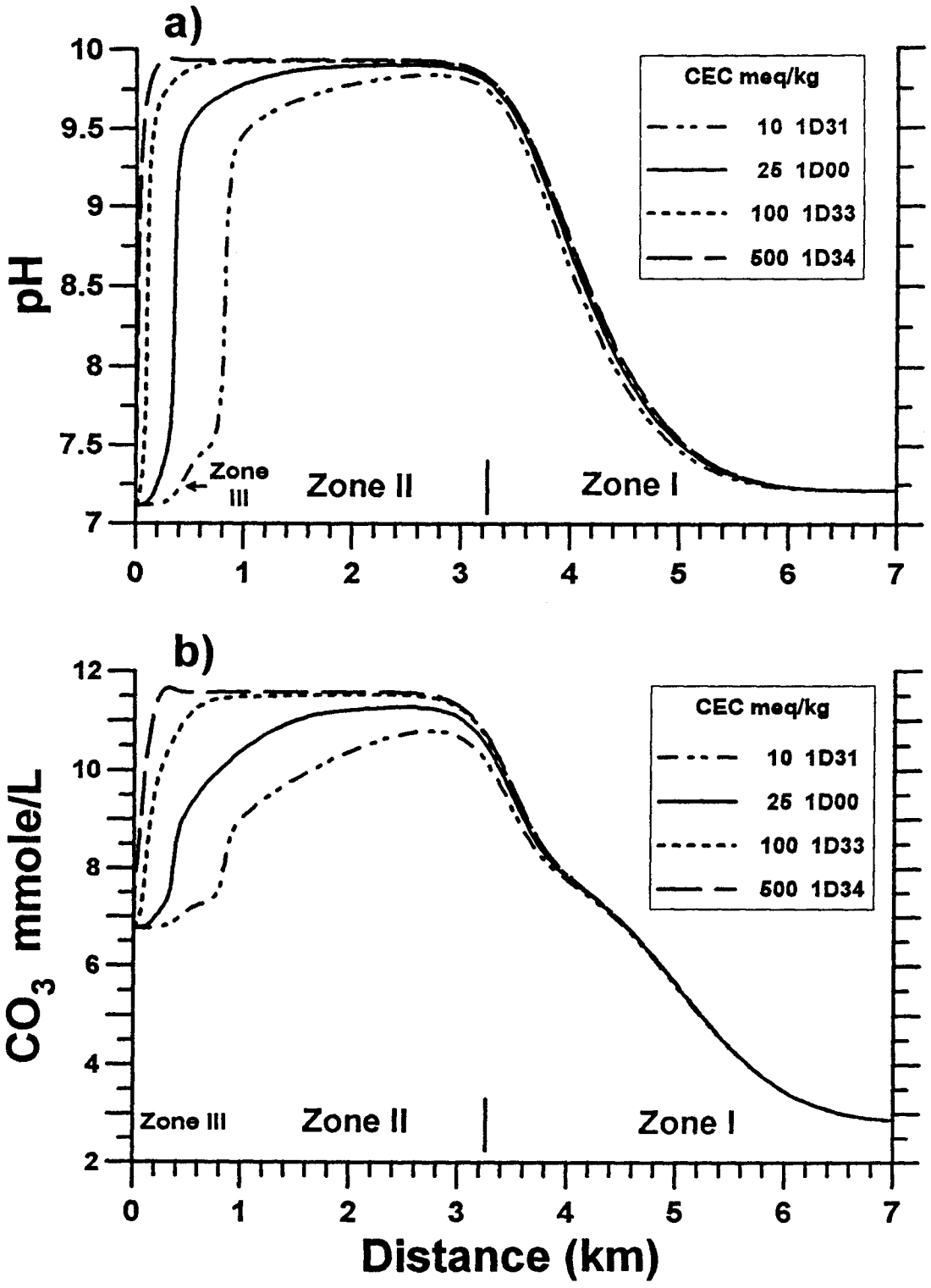

Figure 7.24. Simulated a) pH, and b) total dissolved carbonate concentration from the sensitivity analyses of four CEC values at 567 years.

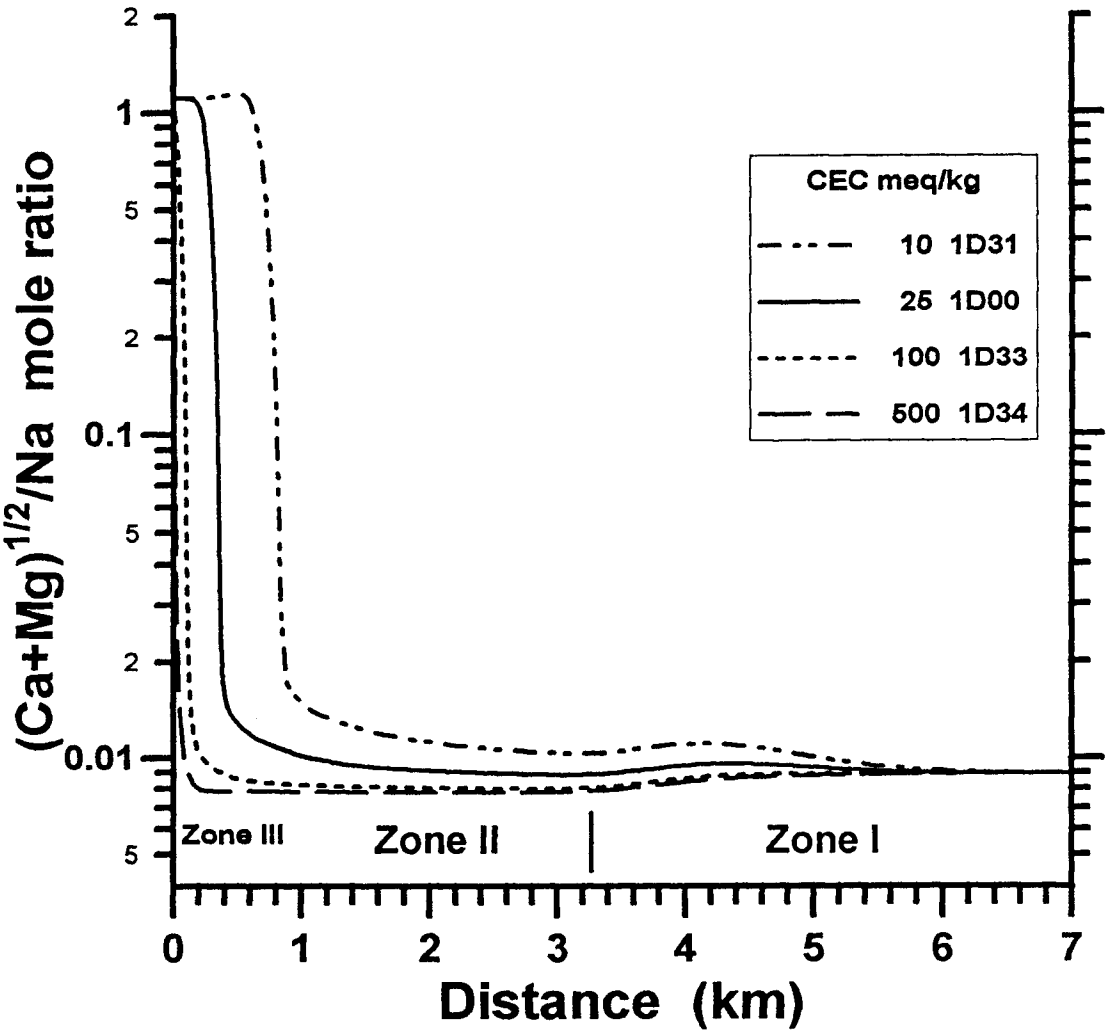

Figure 7.25. Simulated dissolved $(Ca + Mg)^{1/2}/Na$ mole ratios from the sensistivity analyses of four CEC values at 567 years.

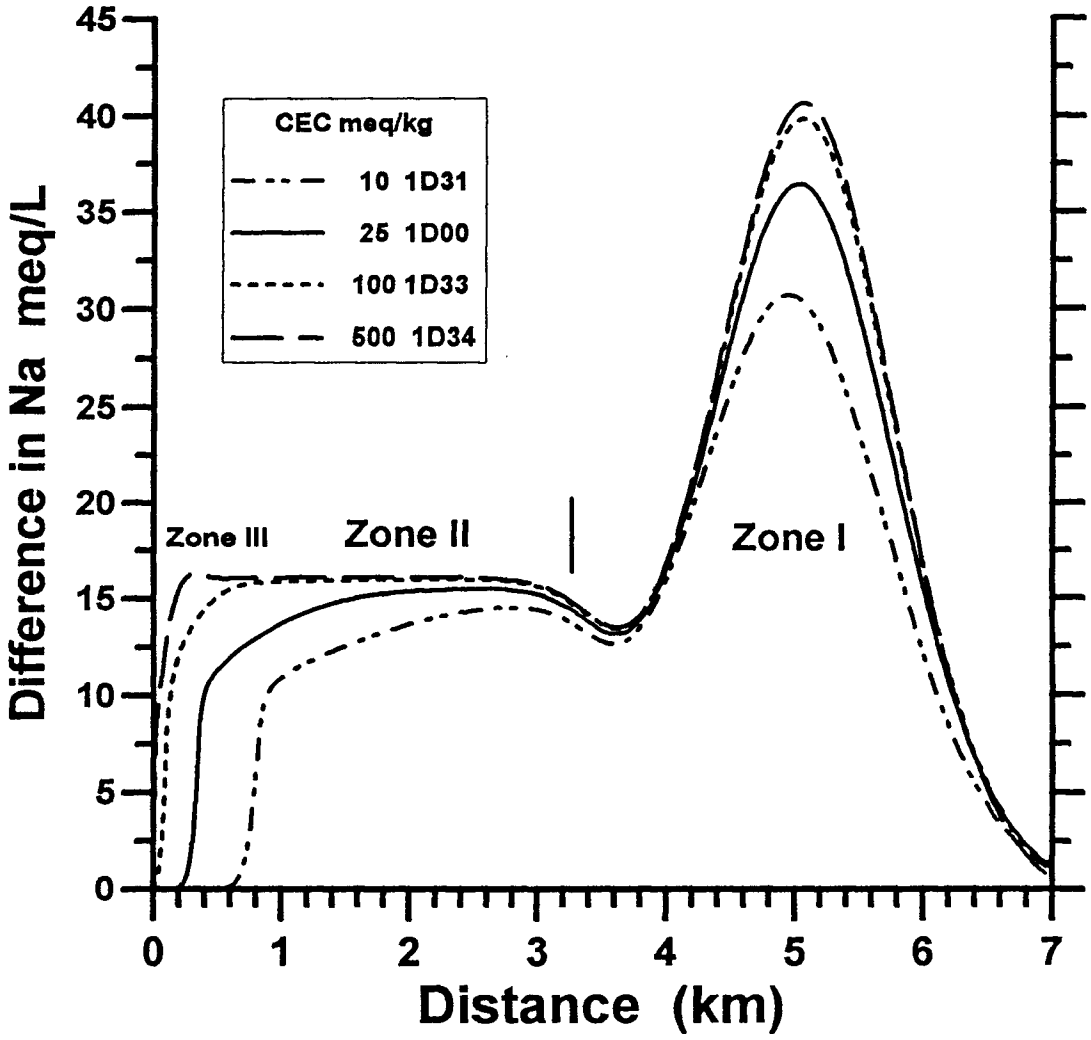

Figure 7.26. Deviations of Na from conservative transport curve along the flow path from the sensitivity analyses of four CEC values at 567 years.

Equations 7.4 to 7.6 show that the intensity of cation exchange depends on the Δq_i. Because the dissolved cation ratios are controlled by the adsorbed cation fractions on the exchange medium, the greater the Δq_i, the more intensive the cation exchange must be to regulate the aqueous composition. In the Dakota aquifer, Na and Cl are the major contributions to the TDS content of saline water. This implies that the mole percentage of Na increases with increasing salinity. On the other hand, the importance of divalent cations, especially Ca, increases when the water becomes fresher. In these conditions, a general assumption for the last three categories of sensitivity analyses is that the higher the solution salinity, the lower is the $(Ca + Mg)^{1/2}/Na$ mole ratio. Figure 7.27 illustrates the relationship and shows that the intensity of cation exchange increases with the TDS concentration of the initial saltwater.

Figure 7.28 shows the effect of different initial TDS contents on the Ca concentration distribution. The Ca concentrations in zone II indicate that greater cation exchange intensity occurs when the two mixing waters have a larger salinity difference and thus, greater contrast in cation ratios. The greater cation exchange intensity also increases the amount of calcite dissolved thereby appreciably affecting the solution pH and carbonate (mainly HCO_3) concentration (Figure 7.29). The values for both pH and carbonate concentration in zone II follow the trend of the salinity difference between the initial and incoming waters regardless of the initial pH and HCO_3 concentration. If the relationship of pH and cation exchange is as simple as above, the pH distribution can be used as a simple representative of the intensity of cation exchange because pH in zone II is mainly affected by the relative intensity of cation exchange.

The cation concentrations in zone II are not only affected by Δq_i but also by the salinity of the incoming water (Equation 7.6). Category V of the sensitivity analyses, in which

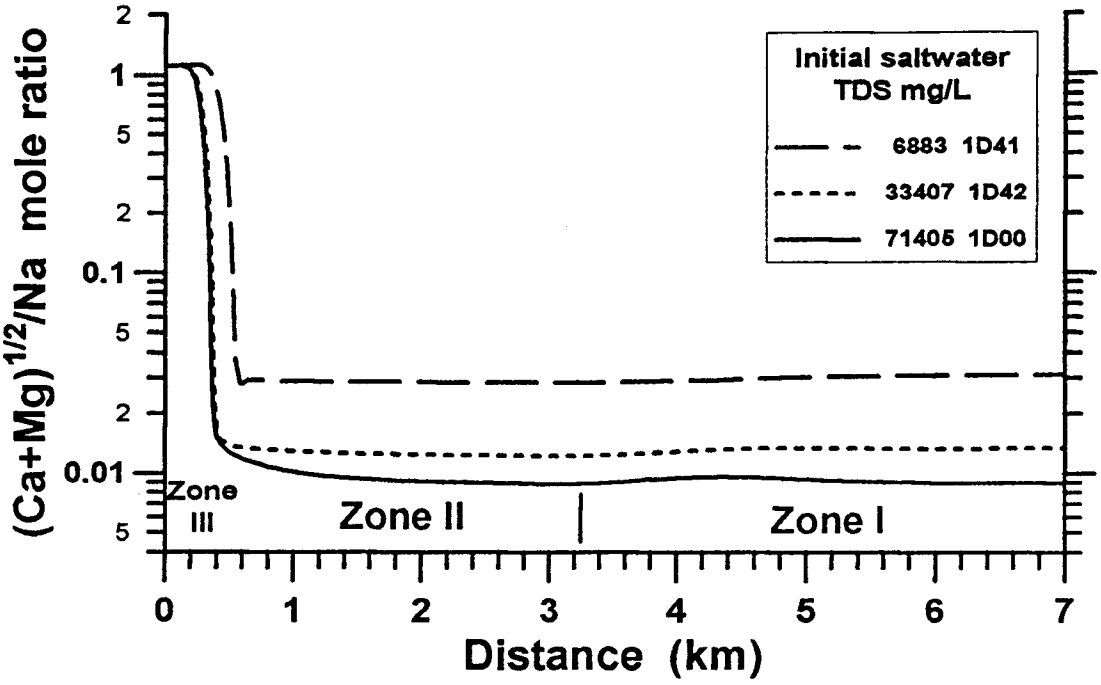

Figure 7.27. Simulated $(Ca + Mg)^{1/2}/Na$ mole ratio from the sensitivity analyses of three TDS contents of the initial saltwater at a simulation time of 567 years.

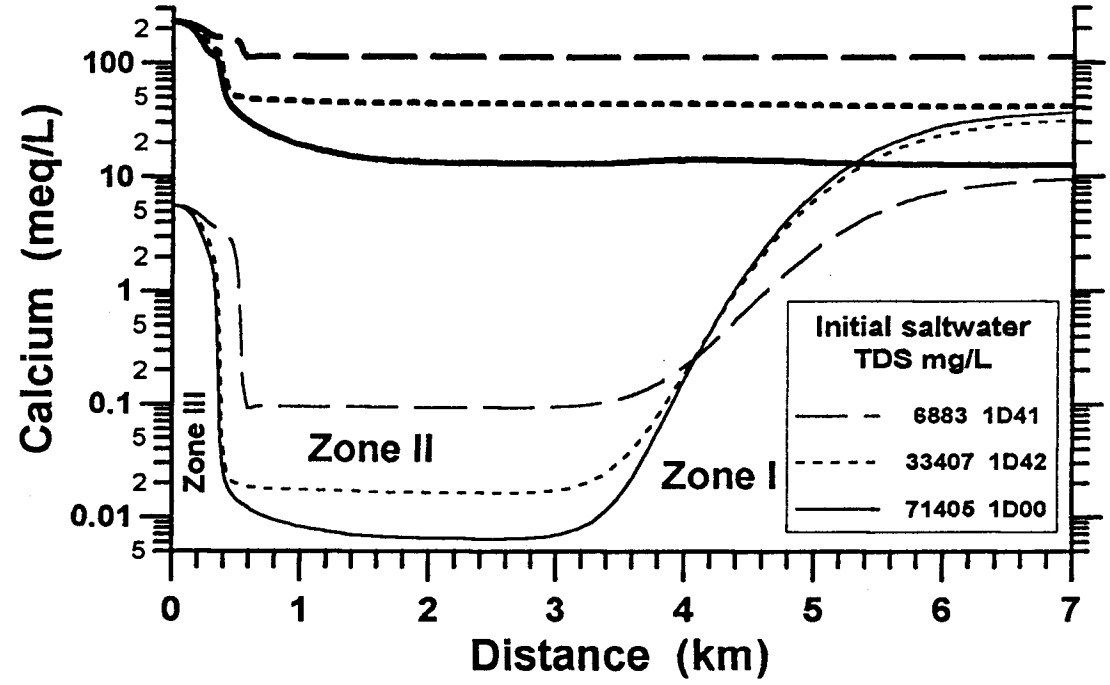

Figure 7.28. Simulated Ca concentrations from the sensitivity analyses of three TDS concentrations of the initial saltwater. The thick lines represent the adsorbed concentrations and the thin lines indicate the dissolved concentrations.

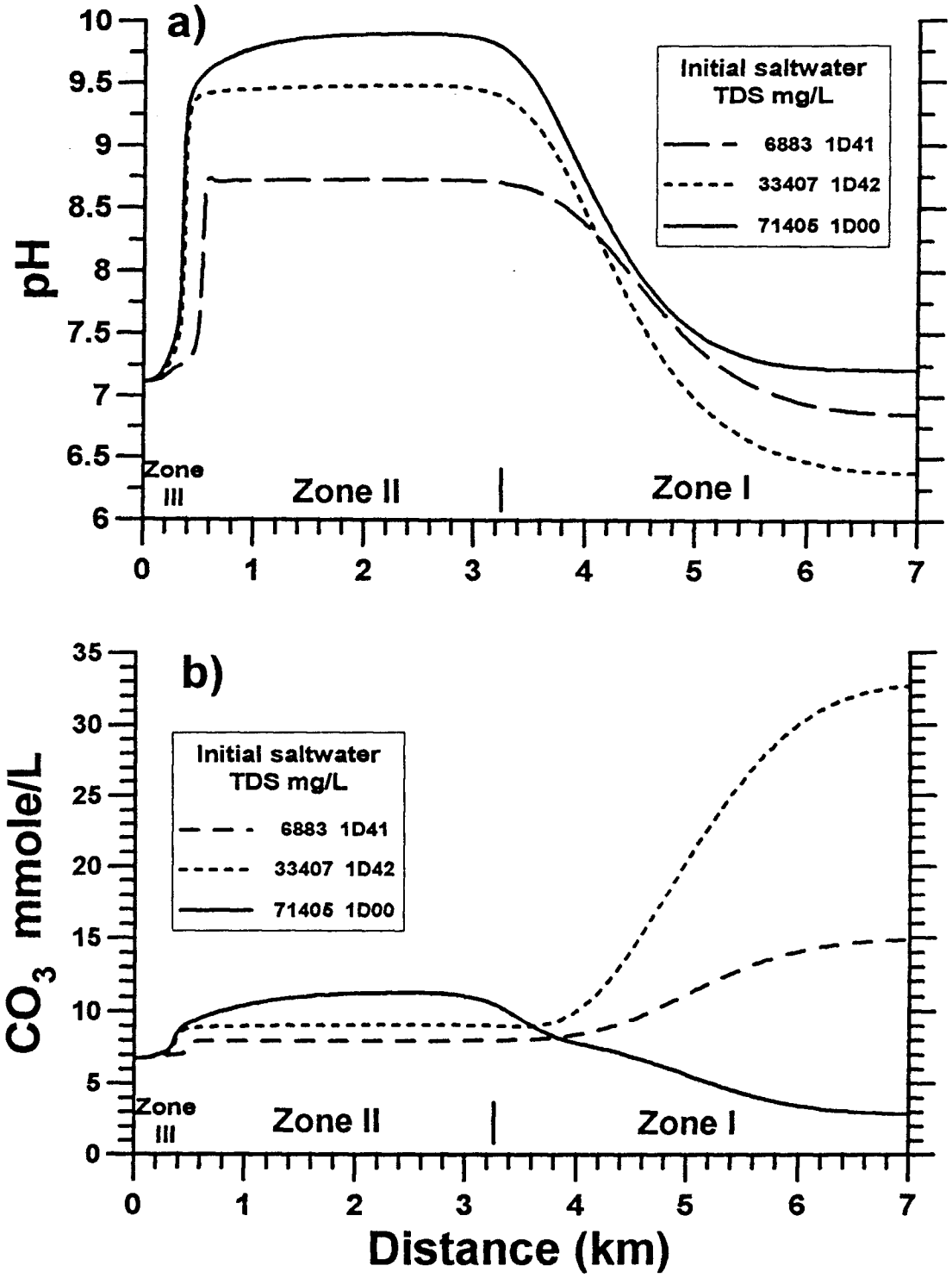

Figure 7.29. Simulated results from the sensitivity analyses of three TDS concentrations of the initial saltwater. a) pH, and b) total dissolved carbonate concentration.

the incoming waters have approximately equal Na and Cl concentration, represents recharge water entering the model without previous cation exchange. The incoming waters examined in category VI of the sensitivity analyses represent recharge water that has undergone some degree of cation exchange before entering the model. The simulated pH's show that, in general, the intensity of cation exchange for both categories V and VI also follow the principle of salinity contrast (Figure 7.30). Despite the fact that pH's for the incoming freshwaters are slightly different in models 1D52 and 1D63, the maximum pH values in zone II for these two models are about the same because the TDS contents of the incoming waters for these two models are very similar.

For sensitivity analyses of categories V and VI, the concentration level of exchanging cations in zone II is mainly affected by the salinity contrast of the two mixing waters. However, the ionic concentration of the incoming water is a more important factor than the salinity contrast as Equation 7.6 shows. A smaller salinity effect and salinity contrast for the incoming water with a higher TDS concentration allows higher Ca and Mg concentrations to occur in zone II (Figure 7.31). The depleted Ca concentrations in zone II for models 1D52 and 1D63 are about the same because the TDS concentrations of the incoming waters are about the same although their cation ratios are different. The explanation is that the exchange medium strongly controls the dissolved cation ratios no matter what the ratios are in the incoming water. The results are consistent with the results for pH in Figure 7.30.

Another approach for examining the intensity of cation exchange is the concentration difference between Na and Cl as described earlier in this section. Figure 7.32a shows that the salinity contrast considerably affects the amount of exchanged Na in the plateau zone. This is because the $(Ca + Mg)^{1/2}$/Na mole ratios on the clays are different for different initial

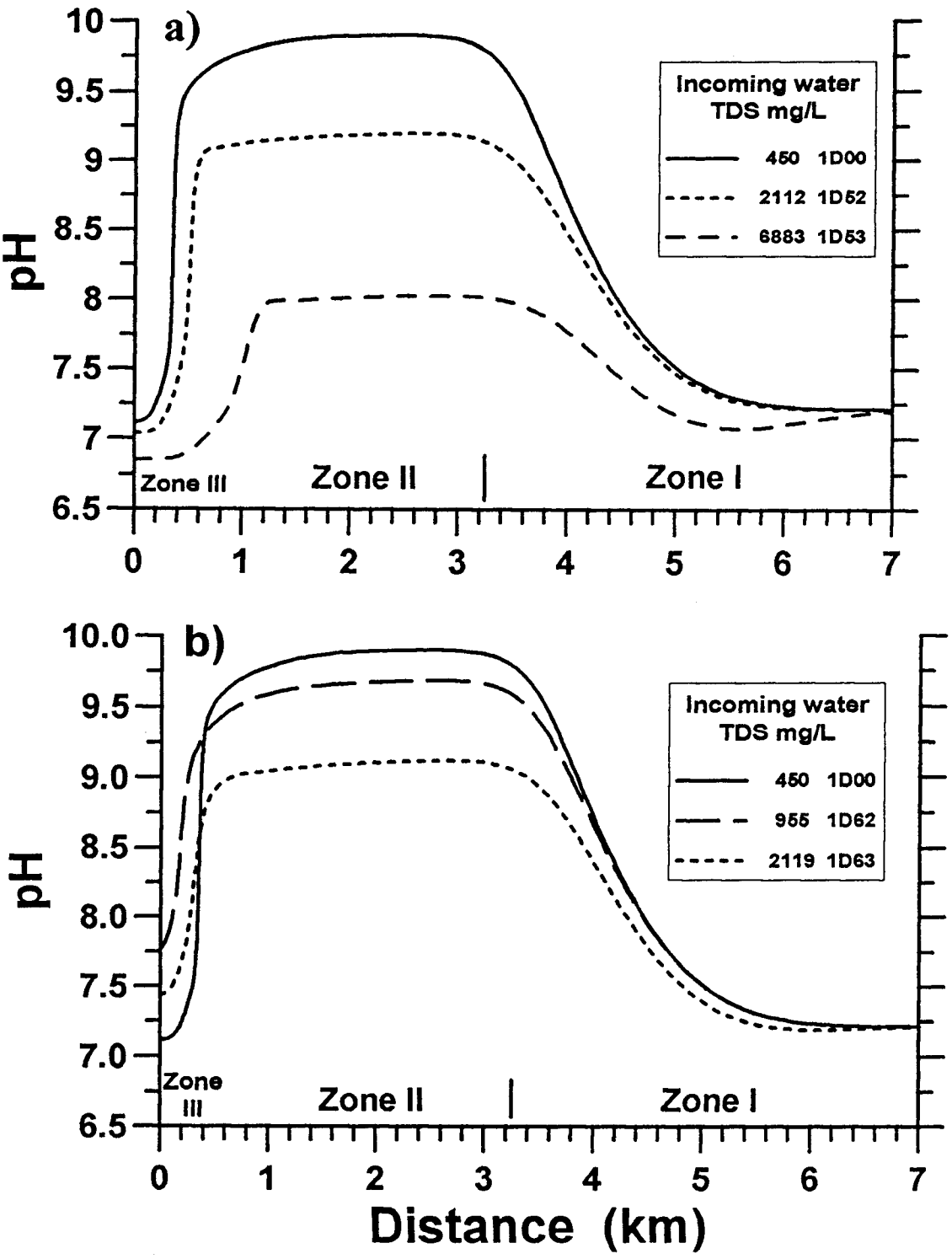

Figure 7.30. Simulated pHs from the sensitivity analyses of three TDS concentrations of the incoming water at 567 years. a) category V, and b) category VI.

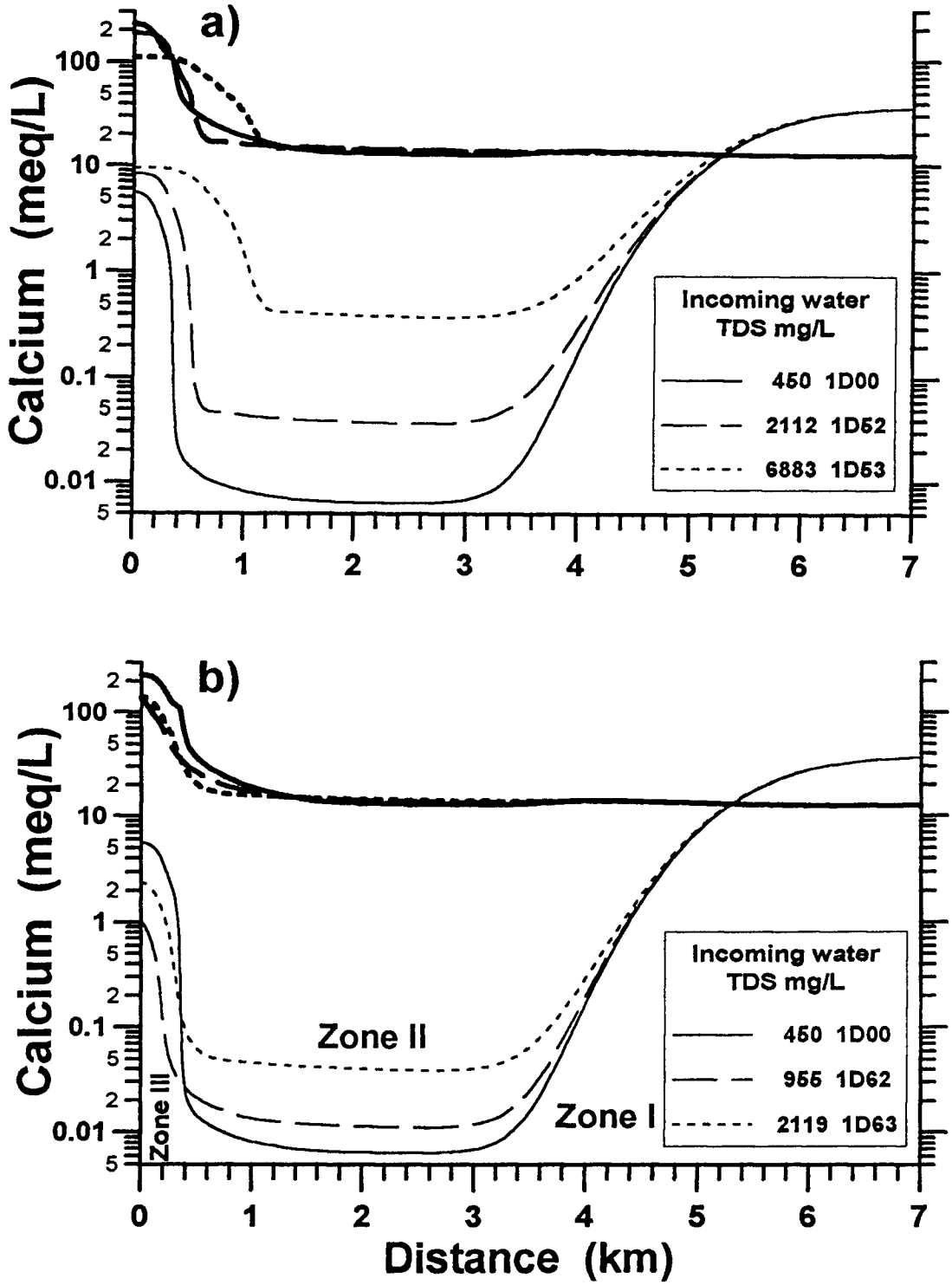

Figure 7.31. Simulated Ca concentrations from the sensitivity analyses of three TDS contents of the incoming water. a) category V, and b) category VI. The thick lines represent the adsorbed concentrations and the thin lines indicate the dissolved concentrations.

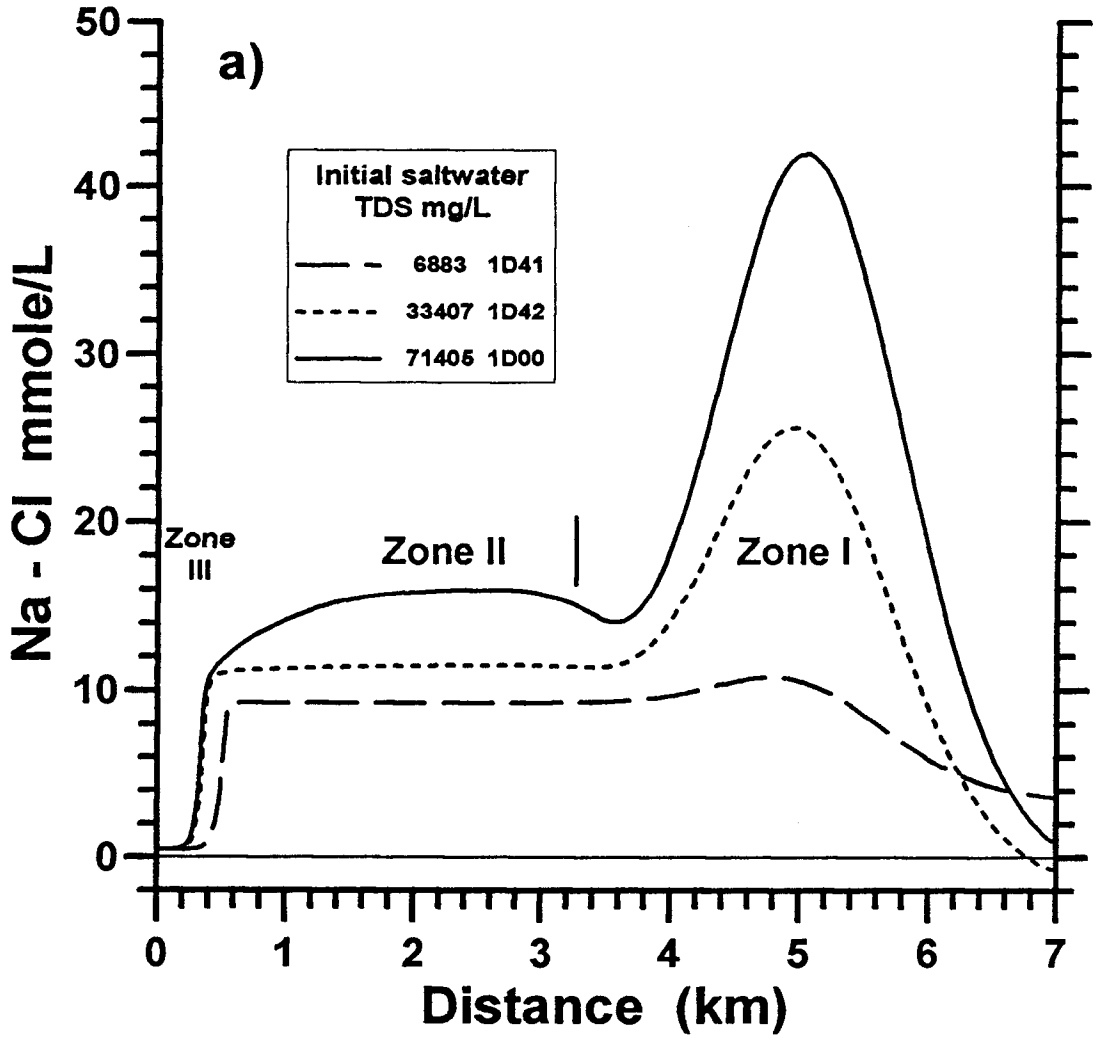

Figure 7.32. Simulated mole difference of Na minus Cl from the sensitivity analyses of three TDS concentrations of a) initial saltwater, b) incoming water (category V), and c) incoming water (category VI).

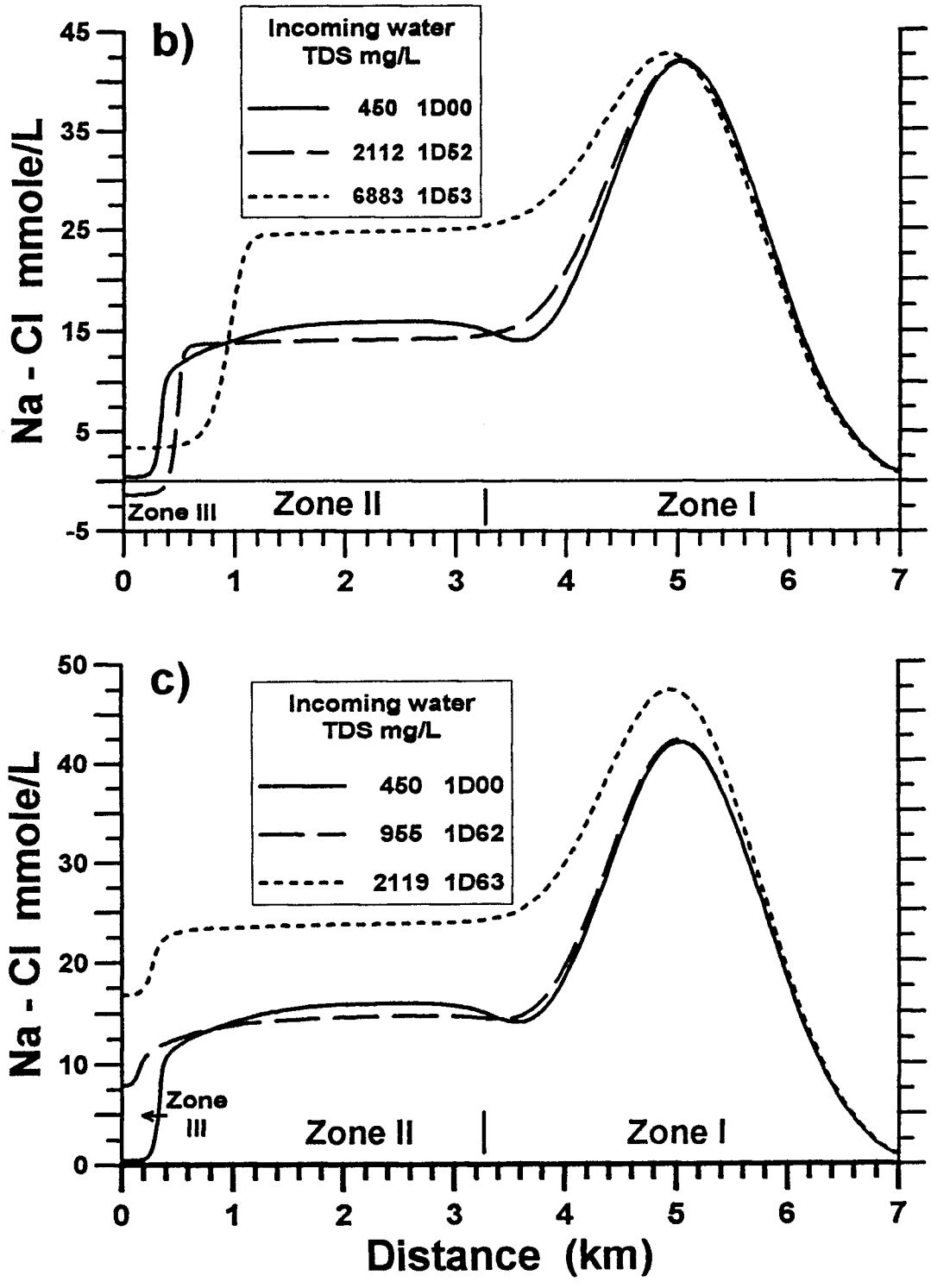

(Figure 7.32. Continued...)

saltwaters (Figure 7.27). The effect of the incoming water salinity on the exchanged Na can be explained by Equation 7.6. However, the salinity effect can be counter-balanced by the relatively smaller salinity contrast of the mixing waters (Figures 7.32b and c). For example, the excess Na in zone II for 1D00, 1D52, and 1D62 are about the same. The TDS content of the incoming water is lowest in model 1D00, but the salinity contrast of the mixing waters is the greatest. The TDS concentration of the incoming water in model 1D52 is about five times that of 1D00. The higher salinity of the incoming water potentially allows higher cation concentrations and absolute amounts of exchange in zone II. However, the salinity contrast of the two mixing waters is smaller and therefore less intensive cation exchange occurs in the system. The counter-balance effects are probably the reason for the similar amount of excess Na in zone II for models 1D00, 1D52 and 1D62. In model 1D53, the high excess Na is due to the high TDS concentration of the incoming water (Figure 7.32b).

The heterogeneity of the Dakota aquifer could allow a variety of cation exchange effects on water chemistry because water could pass through several different chemical environments with step-wise cation exchange processes along a flow path. The incoming waters for models in category VI have undergone some degree of cation exchange as the concentration difference of Na and Cl shows. Figure 7.32c indicates that the excess Na accumulates for water encountering more than one cation-exchange environment. The accumulation of excess Na is particularly evident for model 1D63 as compared to model 1D52 with a similar TDS content of the incoming water (Figure 7.32). This implies that if a recharge water flows through an aquifer system in which the cation exchange environment varies along the flow path, the individual chemical environment effect might not be distinguishable from the final result.

The sensitivity analyses of the last two categories also provide information about the factors that affect the retardation front velocity. The two major factors are the concentrations of divalent exchanging cations (Ca^{2+} and Mg^{2+}) and the contrast of the cation ratios between the incoming and initial waters. Figure 7.31a shows that the Ca concentrations of the incoming waters for models 1D52 and 1D53 are very similar. However, the retardation front velocities for the two models are quite different (Figure 7.33a). Apparently the contrast of cation ratios between the two mixing waters is a major factor. Models in category VI show that despite the lower contrast of cation ratios between the recharge and initial waters for models 1D62 and 1D63, the velocities of their retardation fronts are smaller than for model 1D00 (Figure 7.33b). The lower concentrations of divalent cations in the incoming water for models 1D62 and 1D63 are the main control on the retardation front velocity (Figure 7.31b). This result implies that a unique retardation factor is not appropriate for transient chemical sources in a system involving cation exchange or adsorption.

Another notable feature is the magnitude of the enhanced peak of excess Na in the conservative mixing front. The change in the Na peak illustrates the importance of the ionic concentration of the initial saltwater in Figure 7.32a. The appearance of the excess Na peak at the center of the mixing front is caused by the combined effect of factors controlling cation exchange. The factors include the salinity of the initial saltwater and the contrast of cation ratios between the mixing waters. Cation exchange occurs during dilution of the initial saltwater. This is because the activity coefficients of the exchanging cations change due to dilution, and, thus, activities of the cations and their ratios in the diluted saltwater also change. For waters in the downstream direction (right-hand side) of the mixing front, mixed water with higher percentages of the initial saltwater is located toward the east side. Thus, less

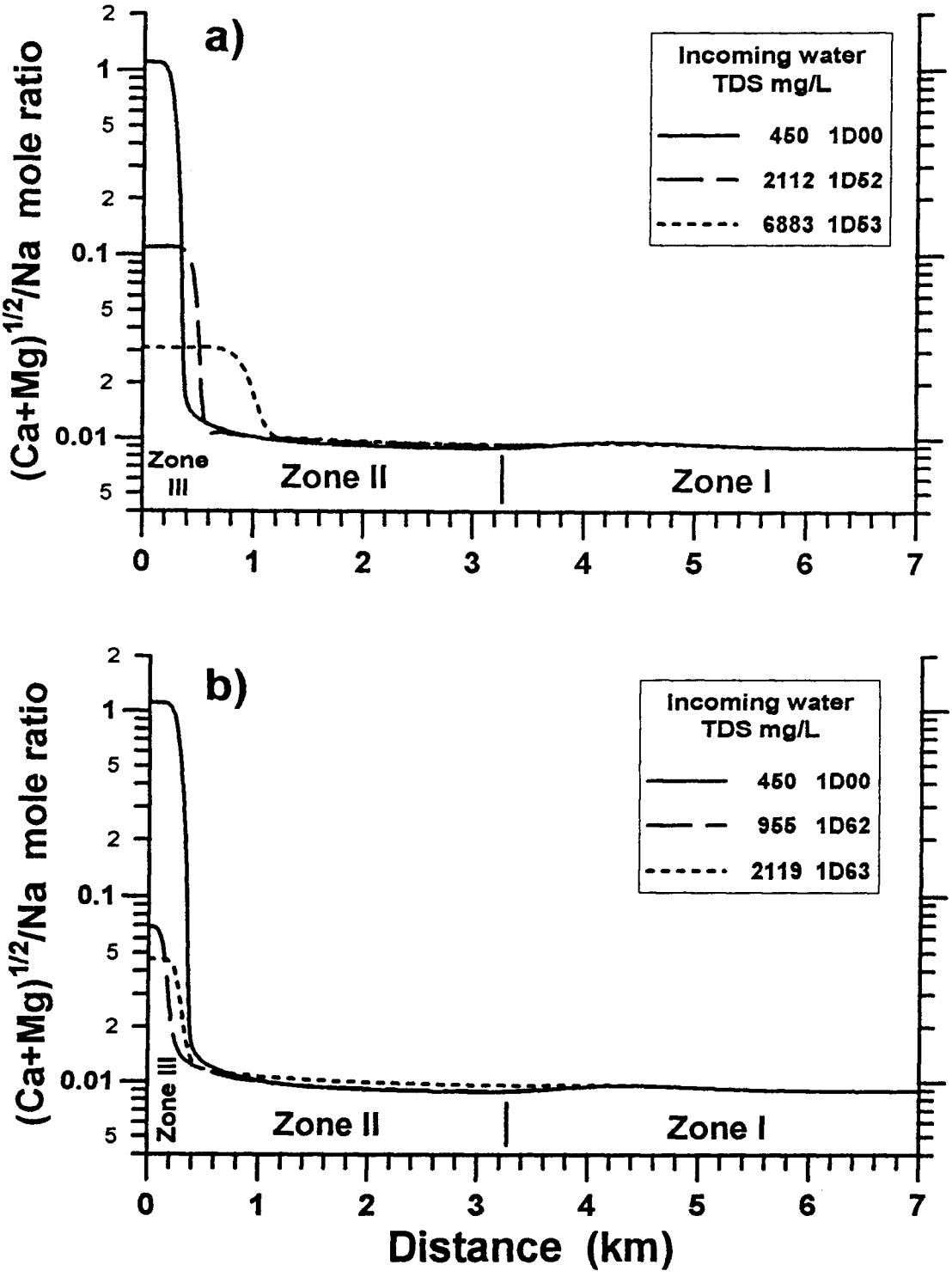

Figure 7.33. Simulated mole ratios of $(Ca + Mg)^{1/2}/Na$ from the analyses of three TDS concentrations of the incoming water. a) category V, and b) category VI.

adjustment for the mixed water with higher saltwater content is required for being in equilibrium with the exchange sites. The adjustment increases toward the upstream direction (left-hand side) when the freshwater content increases. In the upstream half of the mixing front, the mixed waters contain more water from the incoming recharge. In spite of the westward increase in the intensity of cation exchange, the ion concentration of the water decreases and so limits the absolute amount of exchange that can occur (Equation 7.6). This combined effect on excess Na concentration reaches a maximum at the center of the mixing front. In general, the decrease in the excess Na in the downstream (east) side of the mixing front is due to the decrease in exchange intensity. On the west side of the peak, the decrease in the excess Na is caused by the decreased salinity although the intensity of cation exchange increases. Figure 7.32 supports this hypothesis. Based on the above explanation, the magnitude of the enhanced Na peak is mainly dependent upon the concentration of the initial water and, to a less degree, the salinity difference between the two mixing waters.

CHAPTER 8

COMPARISON OF GROUND-WATER CHEMISTRY DATA AND THE 1-D COUPLED MODEL RESULTS

8.1. ESTIMATION OF THE ADSORBED ION COMPOSITION FOR PREDICTED PREVIOUS SALTWATER FROM THE GROUND-WATER CHEMISTRY DATA

The 1-D model results can be used to partially interpret the geochemical evolution of the ground water in the Dakota aquifer. Instead of a complex mixing scenario of waters described in Chapter 5, a flushing of a saltwater aquifer by freshwater is proposed that is similar to the 1-D model. The study area does not cover an entire regional flow path in the Dakota aquifer, thus, the Dakota water groups described in Chapter 5 are not in a continuous sequence of chemical evolution and are affected by different water sources. However, the water-chemistry data are still valuable for the interpretation of the ground-water evolution in the Dakota aquifer if the following assumptions are made to adapt the water groups to a conceptual 1-D flow path. First, the chemistry of the fresh unconfined Dakota water in north-central Kansas is assumed to be similar to the water in the recharge zone in southeastern Colorado and southwestern Kansas. Second, the Dakota aquifer is assumed to have contained saltwater from the underlying Permian strata immediately prior to being flushed by the present fresher water. Third, the confined Dakota waters are assumed to be in the intermediate stages of the geochemical evolution in the same regional ground-water flow path. Based on the chemical characteristics of the ground water, the west confined Dakota water is in zone II of the 1-D model. The east confined Dakota waters range across the conservative mixing front and part of zone II. The relative position of the water groups in the conceptual flow path is shown in Figure 8.1. This conceptual evolution sequence does not necessarily mean the actual

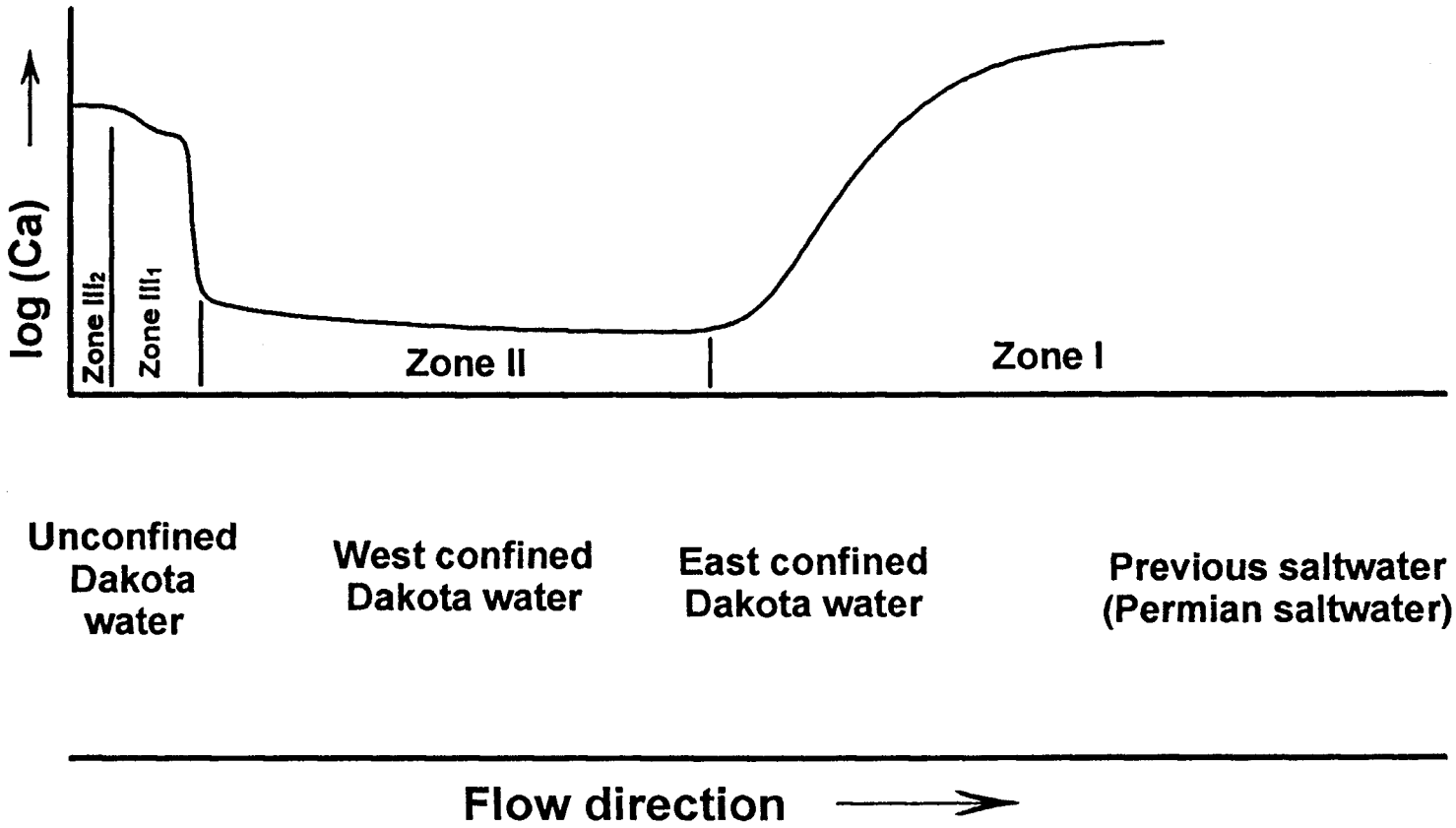

Figure 8.1. 1-D conceptual model for the Dakota aquifer and the relative positions for the water groups along the ideal flow path. Calcium concentration is used to show the ground-water evolution along the conceptual flow path.

relationship among those water groups. Nevertheless, it provides valuable information for interpreting the geochemical evolution in the aquifer system.

As the 1-D model results indicate in Chapter 7, the ratios of dissolved exchanging cations in zone II must equilibrate with the adsorbed cation ratios on the exchange medium which retains essentially the same ratios as when in contact with the initial saltwater (Figures 7.9 and 7.27). This principle can be used along with an examination of the current ground water undergoing cation exchange to estimate the adsorbed cation ratios on the exchange sites and cation ratios of the previous saltwater in zone II. Ground water from the confined Dakota aquifer west of the Cedar Hills subcrop provides a good example for the estimation of the previous saltwater in the west confined Dakota aquifer. An assumption needed is that the CEC and all the selectivity coefficients for the exchange reactions are constant for the ionic strength and pH ranges of the solutions in the aquifer system. An additional assumption is that free ions of Ca^{2+}, Mg^{2+}, and Na^{+} are the only exchanging cations involved.

With the above assumptions, the exchange reactions, based on Equation 6.24, can be written as

$$Na^{+} + X^{-} \Leftrightarrow Na\text{-}X \qquad K_{Na} = \frac{[Na - X]}{[Na^{+}][X^{-}]} \tag{8.1}$$

$$\tfrac{1}{2}Ca^{2+} + Na\text{-}X \Leftrightarrow Na^{+} + \tfrac{1}{2}Ca\text{-}X_2 \qquad K_{Ca/Na} = \frac{[Na^{+}][Ca - X_2]^{1/2}}{[Ca^{2+}]^{1/2}[Na - X]} \tag{8.2}$$

$$\tfrac{1}{2}Mg^{2+} + Na\text{-}X \Leftrightarrow Na^{+} + \tfrac{1}{2}Mg\text{-}X_2 \qquad K_{Mg/Na} = \frac{[Na^{+}][Mg - X_2]^{1/2}}{[Mg^{2+}]^{1/2}[Na - X]} \tag{8.3}$$

$$\tfrac{1}{2}Mg^{2+} + \tfrac{1}{2}Ca\text{-}X_2 \Leftrightarrow \tfrac{1}{2}Ca^{2+} + \tfrac{1}{2}Mg\text{-}X_2 \qquad K_{Mg/Ca} = \left(\frac{[Ca^{2+}][Mg - X_2]}{[Mg^{2+}][Ca - X_2]}\right)^{1/2} \tag{8.4}$$

Where

X^- = one negatively-charged surface exchange site

$I\text{-}X_i$ = adsorbed cation, I represents exchangeable cation, and i is the charge of I

K_{I_1/I_2} = selectivity coefficient between cations I_1 and I_2

The hyphen used for the adsorbed cations is to distinguish the adsorptive relationship from actual complex species. The brackets represent activity. The activities of adsorbed cations are often considered equal to the equivalent fractions of total adsorbed cations (Gains and Thomas, 1953). The equivalent fraction is obtained from $\beta_I = i\times(I\text{-}X_i)/CEC$, where i is the charged valence of cation I. Thus

$$\beta_{Na} + \beta_{Ca} + \beta_{Mg} = 1 \tag{8.5}$$

In giving $[I\text{-}X_i] = \beta_I$, the activity coefficient of the adsorbed cation is assumed to be equal to 1.

Equation 8.1, the adsorption of Na, is used as the reference for the selectivity coefficient, which means $K_{Na} = 1$. Selectivity coefficients of Ca^{2+} and Mg^{2+} for model 1D00 (Table 7.1) are applied to Equations 8.2 and 8.4.

$K_{Ca/Na} = 3.2$

$K_{Mg/Ca} = \dfrac{K_{Mg/Na}}{K_{Ca/Na}} = 0.7$, thus

$K_{Mg/Na} = 2.24$

From Equations 8.2 and 8.3, the adsorbed cation ratios can be expressed by the dissolved cation activities as

$$\frac{\beta_{Ca}^{1/2}}{\beta_{Na}} = K_{Ca/Na}\frac{[Ca^{2+}]^{1/2}}{[Na^+]} = 3.2\times\frac{[Ca^{2+}]^{1/2}}{[Na^+]} \tag{8.6}$$

$$\frac{\beta_{Mg}^{1/2}}{\beta_{Na}} = K_{Mg/Na}\frac{[Mg^{2+}]^{1/2}}{[Na^{+}]} = 2.24 \times \frac{[Mg^{2+}]^{1/2}}{[Na^{+}]} \qquad (8.7)$$

The activities of the free cations of Ca^{2+}, Mg^{2+}, and Na^{+} for all the water samples are obtained from the SOLMINEQ.88 geochemical simulation.

As discussed at the beginning of this chapter, the west confined Dakota waters fit in zone II of the conceptual 1-D flow model (Figure 8.1) in which the water chemistry is dominated by cation exchange. The water is an excellent example for estimation of the salinity of the previous saltwater. Equations 8.6 and 8.7 indicate that the activity ratios of $[Ca^{2+}]^{1/2}/[Na^{+}]$ and $[Mg^{2+}]^{1/2}/[Na^{+}]$ can be used to represent the adsorbed cation fractions. Figures 7.15 and 7.27 show that the ratio of $[Ca^{2+} + Mg^{2+}]^{1/2}/[Na^{+}]$ is a more relevant indication of the cation exchange reaction because both the bivalent cations exchange with Na^{+} on the exchange medium at the same time. Values for the three different activity ratios were calculated from data for ground-water samples (Figures 8.2 to 8.4). The figures show that the $[Ca^{2+}]^{1/2}/[Na^{+}]$ and $[Mg^{2+}]^{1/2}/[Na^{+}]$ ratios for the west confined Dakota water are generally greater than those for the Cedar Hills water. This indicates that the previous saltwater in the west confined Dakota aquifer was different from the current Cedar Hills water. Previous studies indicate that the current ground-water salinity of the Dakota aquifer is mainly derived from intruded Permian saltwater rather than residual seawater (Macfarlane et al., 1988, 1990). Thus, the previous saline water in the Dakota aquifer is a mixture of intruded Permian saltwater and ground-water flowing within the Dakota aquifer which had a TDS concentration lower than the current Cedar Hills water.

The isolated point at the lowest $[Ca^{2+}]$ and $[Mg^{2+}]$ on Figures 8.2 to 8.4 represents a Dakota water sampled from the northwest corner of Trego County (Figure 5.1). The other

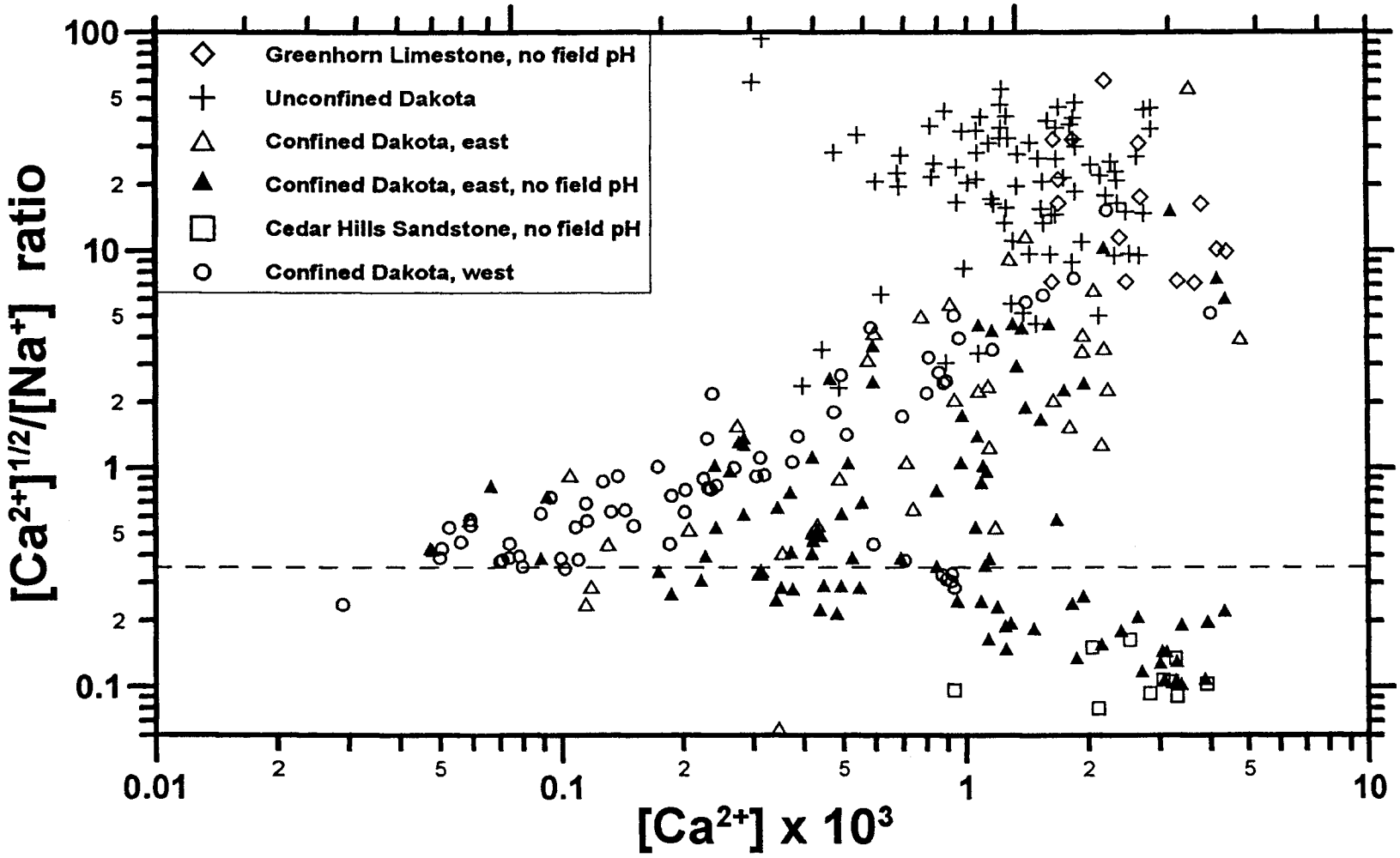

Figure 8.2. $[Ca^{2+}]/[Na^{+}]$ ratio versus $[Ca^{+}]$ for ground-water samples. The dashed line represents the minimum activity ratio for most of the west confined Dakota water estimated from the chemical data.

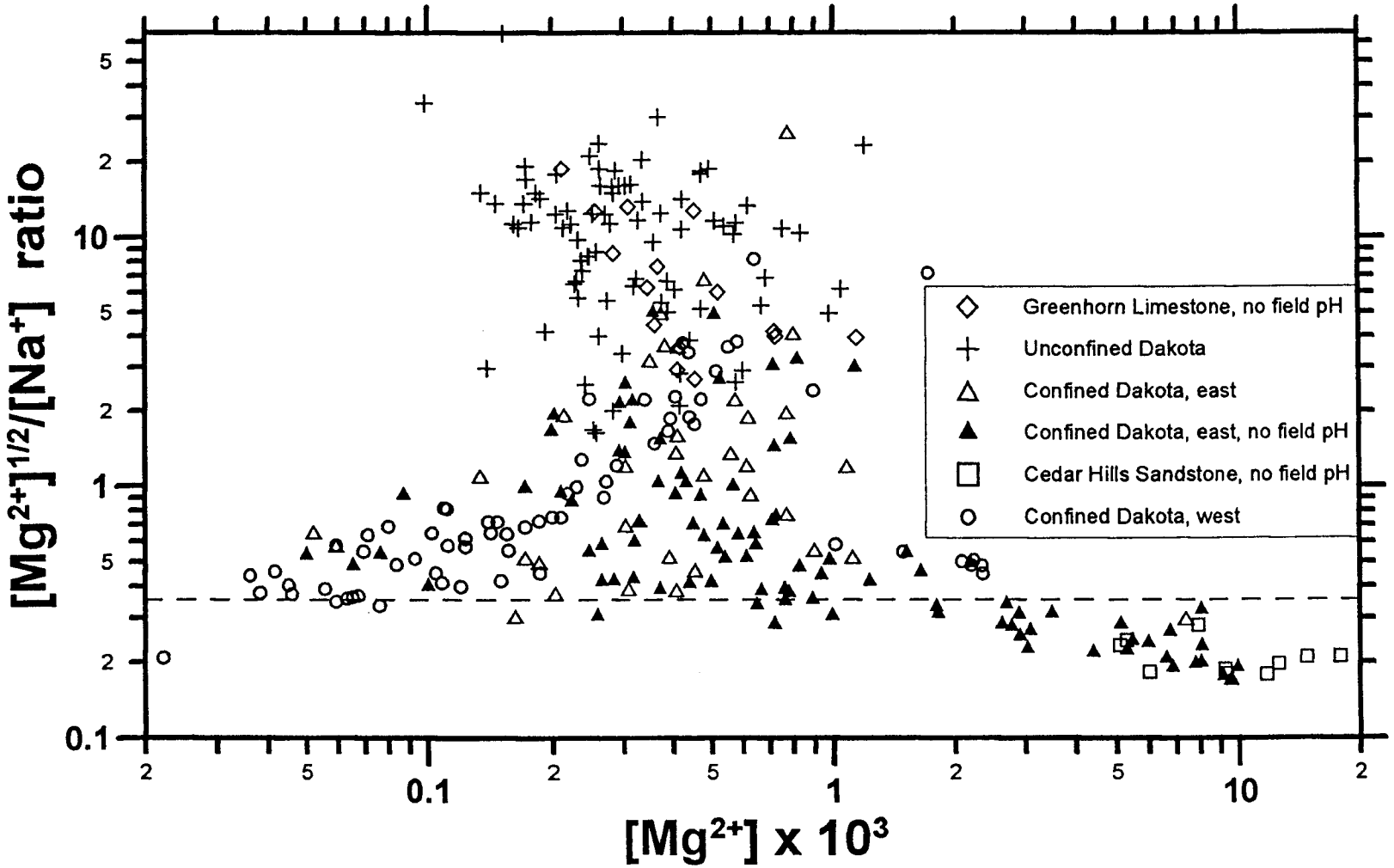

Figure 8.3. $[Mg^{2+}]^{1/2}/[Na^{+}]$ ratio versus $[Mg^{2+}]$ for ground-water samples. The dashed line represents the minimum activity ratio for most of the west confined Dakota water estimated from the chemical data.

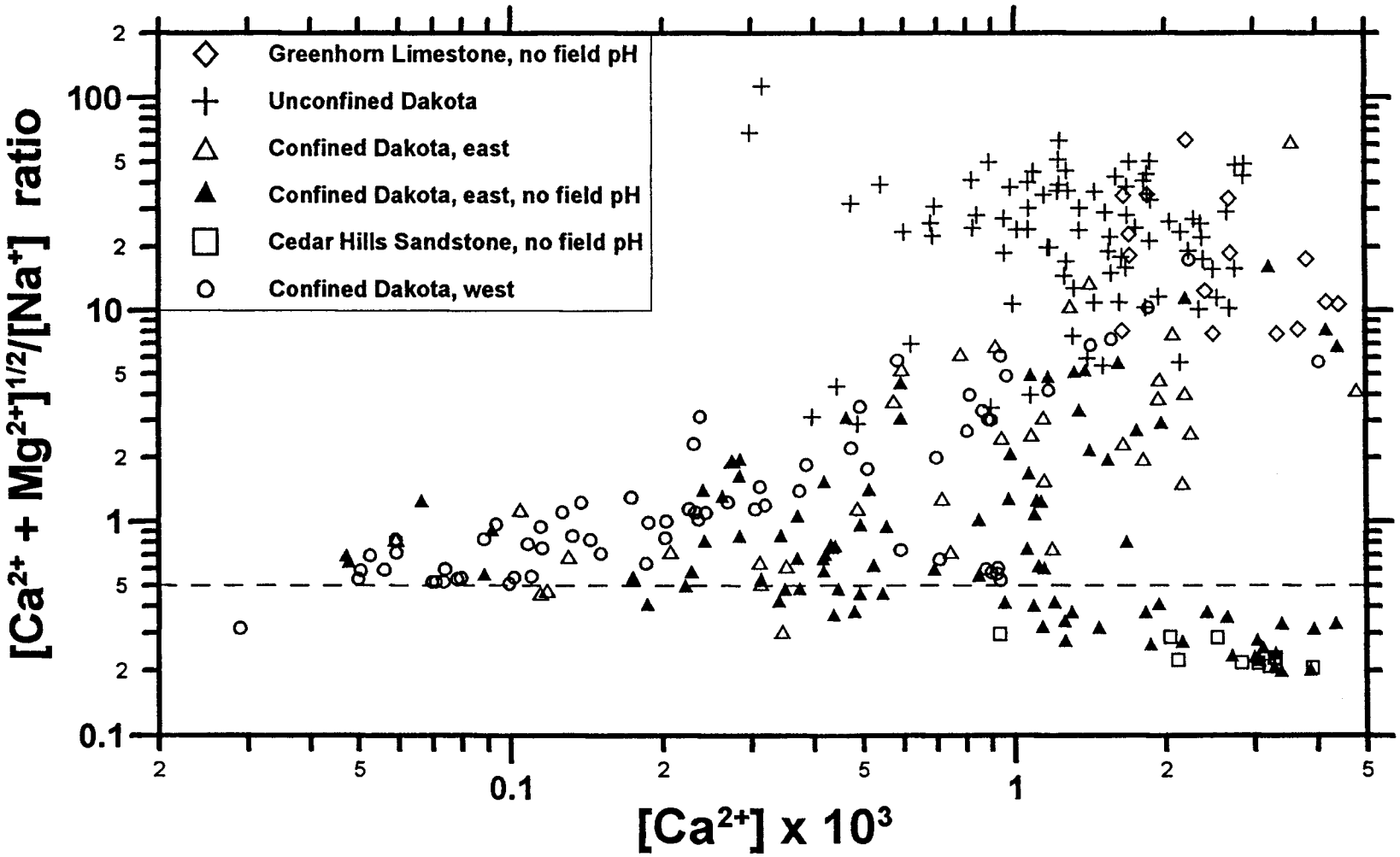

Figure 8.4. $[Ca^{2+} + Mg^{2+}]^{1/2}/[Na^{+}]$ ratio versus $[Ca^{2+}]$ for ground-water samples. The dashed line represents the minimum activity ratio for most of the west confined Dakota water estimated from the chemical data.

waters in the west confined Dakota group were collected from eastern and southern Trego and western Ellis counties. The cation ratios for the isolated point are lower than for the other west confined Dakota waters. This suggests that there was saltier water in the Dakota aquifer in the northwestern part of Trego County than in eastern Trego and western Ellis counties. This is consistent with the current TDS distribution in the Dakota aquifer in which salinities generally increase from central Trego County towards northwestern Kansas. Therefore, the following discussion does not include the northwest Trego County water, but focuses on the waters from eastern and southern Trego and western Ellis counties which have similar chemical characteristics and are statistically more representative.

The activity ratio values of the exchanging cations obtained from Figures 8.2 to 8.4 for the previous saltwater (represented by the dashed lines) are

$[Ca^{2+}]^{1/2}/[Na^{+}] = 0.36, \quad [Mg^{2+}]^{1/2}/[Na^{+}] = 0.34, \quad [Ca^{2+} + Mg^{2+}]^{1/2}/[Na^{+}] = 0.5$

The possible adsorbed cation fractions on the exchange sites can be calculated using these data. From Equation 8.6

$$\frac{\beta_{Ca}^{1/2}}{\beta_{Na}} = K_{Ca/Na}\frac{[Ca^{2+}]^{1/2}}{[Na^{+}]} = 3.2 \times 0.36 = 1.152 \tag{8.8}$$

From equation 8.7

$$\frac{\beta_{Mg}^{1/2}}{\beta_{Na}} = K_{Mg/Na}\frac{[Mg^{2+}]^{1/2}}{[Na^{+}]} = 2.24 \times 0.34 = 0.762 \tag{8.9}$$

Combining Equations 8.5, 8.8, and 8.9 allows calculation of the adsorbed fractions of the exchangeable cations

$\beta_{Na} = 0.508, \quad \beta_{Ca} = 0.342, \quad \beta_{Mg} = 0.15$

These values can be used with results from the 1-D coupled model to estimate the chemistry of

the previous saltwater in the upper part of the Dakota aquifer in western Ellis and eastern and southern Trego counties as discussed in the next section.

8.2. COMPARISON OF THE DAKOTA WATER CHEMISTRY AND THE 1-D COUPLED MODEL RESULTS

It is impossible to determine the relative spatial position of water samples along an idea flow path in the Dakota aquifer because of the physical and chemical heterogeneities and lack of detailed knowledge of the geohydrological history. Instead of displaying the data in terms of spatial location, the conservative species Cl is initially used as an indication of the stage of chemical evolution in the 1-D model. However, as Figure 7.3 indicates, the Cl concentration cannot distinguish the incoming freshwater from the water undergoing cation exchange in the plateau zone. An alternate approach is to use the Na concentration for the X axis to identify the zone position of the waters. The approach is appropriate only when cation exchange is the sole heterogeneous chemical reaction in which Na^+ is involved. Simulation results for model 1D00 form the principle basis on which the field data are interpreted. The relationship of Na concentration distribution and relative spatial location can be approximately assessed from Figure 7.4c.

Figure 8.5 compares the numerical simulation from model 1D00 with field data for the Na minus Cl concentration in waters from the Dakota aquifer, Greenhorn Limestone, and Cedar Hills Sandstone. The spatial stage of the simulated chemical evolution represented by the thick line in Figure 8.5 can be identified from Figure 7.15. The small peak occurring between 10 and 20 meq/L Na corresponds to the plateau zone (zone II) and the large peak corresponds to the large excess Na peak in the mixing front. The saddle between the two peaks is located at the boundary between zones II and I. The curve to the left of the small peak

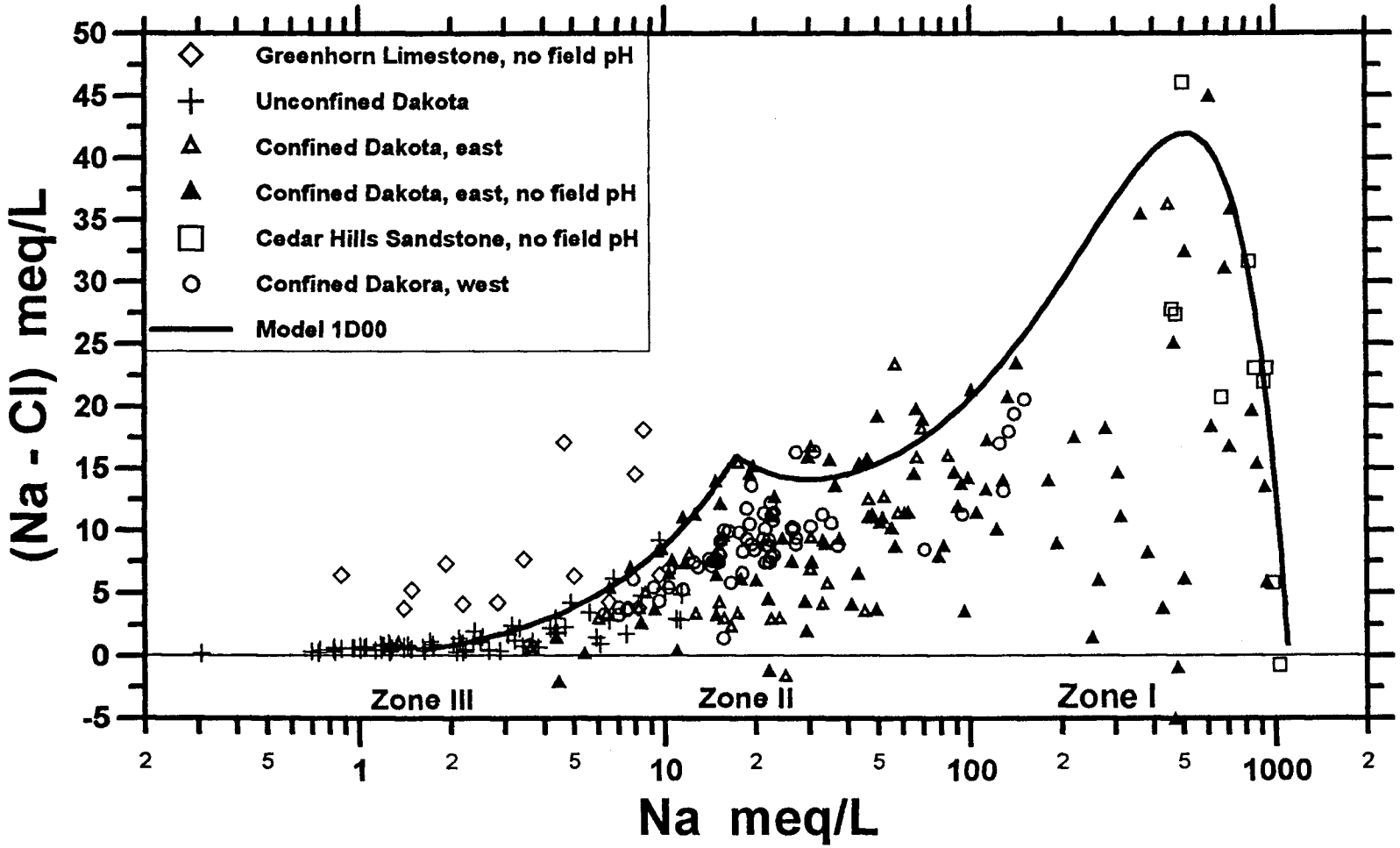

Figure 8.5. Comparison of Na minus Cl concentration versus Na concentrations for field data and model 1D00 results. The excess Na concentration results mainly from the cation exchange of Ca and Mg for Na on clay surfaces. The Na concentration also represents the relative position of a water sample along a conceptual flow path.

represents the incoming freshwater in zone III and the retardation front. The model result forms an upper boundary which matches relatively well the maximum (Na - Cl) difference in actual Dakota aquifer waters.

Waters from both the Cedar Hill Sandstone and east confined Dakota aquifer contain the highest excess Na concentration. Based on Figure 7.15, this indicates that the center of the salinity mixing front is near where the Cedar Hills Sandstone aquifer is hydraulically interconnected with the Dakota aquifer. A short distance after the Cedar Hills saltwater enters the bottom of Dakota aquifer, the mixed water is diluted to less than 50% of Permian saltwater.

The chemistry of the two waters with the highest (Na - Cl) concentration could be caused by three reasons. First, the previous intruded Permian saltwater could have had a higher TDS content than the initial saltwater used for model 1D00. However, the cation ratio evidence does not support the occurrence of saltier water in the near past (Figures 8.2 to 8.4). Second, the dissolution of magnesite in the Cedar Hills Sandstone might have supplied extra Mg^{2+} for cation exchange. The third possibility is that the waters might have encountered several different chemical environments with increased cation exchange intensity along the flow path. The effect of each cation exchange step might have accumulated to produce a higher excess Na concentration as indicated by model 1D63 (Figure 7.32c).

More complicated reactions could have caused deviation of the field data from the model line between the two peaks. Data points below the curve indicate that, rather than an ideal mixing of waters and cation exchange, the reactions have been affected by the heterogeneity of the physical and chemical properties of the Dakota aquifer system. The majority of Dakota waters from west of the Cedar Hills subcrop are located under the small

peak. This suggests that the intensity of cation exchange in the west confined Dakota aquifer is less than what model 1D00 shows. As Figure 7.32a indicates, the lower excess Na concentration in the west confined Dakota aquifer is because the formation materials were in equilibrium with a previous saltwater of lower TDS content than that of the initial saltwater used in model 1D00.

Figure 8.5 indicates that the Greenhorn water generally has a higher excess Na concentration than Dakota water of similar Na concentration. The reason for the striking characteristics of the Greenhorn Limestone waters is not clear. A possible explanation is that the limestones and shales in the Greenhorn have different exchange characteristics than the sandstone and siltstones of the Dakota aquifer. Comparison of Figure 8.5 with Figure 5.24 indicates a relatively lower Na/TDS ratio for the Greenhorn waters than for the Dakota waters (Figure 5.3). A relatively higher $(Ca + Mg)^{1/2}/Na$ concentration ratio in shallow Greenhorn water (Figures 8.6 and 8.7) might have enhanced the intensity of cation exchange deeper in the Greenhorn Limestone while Cl was being flushed by downward recharge flow.

Figure 8.6 illustrates the relationship of the $(Ca + Mg)^{1/2}/Na$ ratio for the field data and the 1D00 model simulation. The field data shows a similar evolution pattern as the numerical model result. The horizontal part of the numerical curve at a low cation ratio represents zones I and II along the flow path. The Dakota waters from west of the Cedar Hills subcrop correspond to zone II of the 1-D model and generally have a lower $(Ca + Mg)^{1/2}/Na$ mole ratio near the low Na part of the horizontal line than for other water groups with the same Na concentration range. Cation exchange is an important factor in controlling the cation ratios of the water in the western part of the study area. Generally, the $(Ca + Mg)^{1/2}/Na$ mole ratios of the west confined Dakota waters approach a low limit of approximately 0.61 (dashed line in

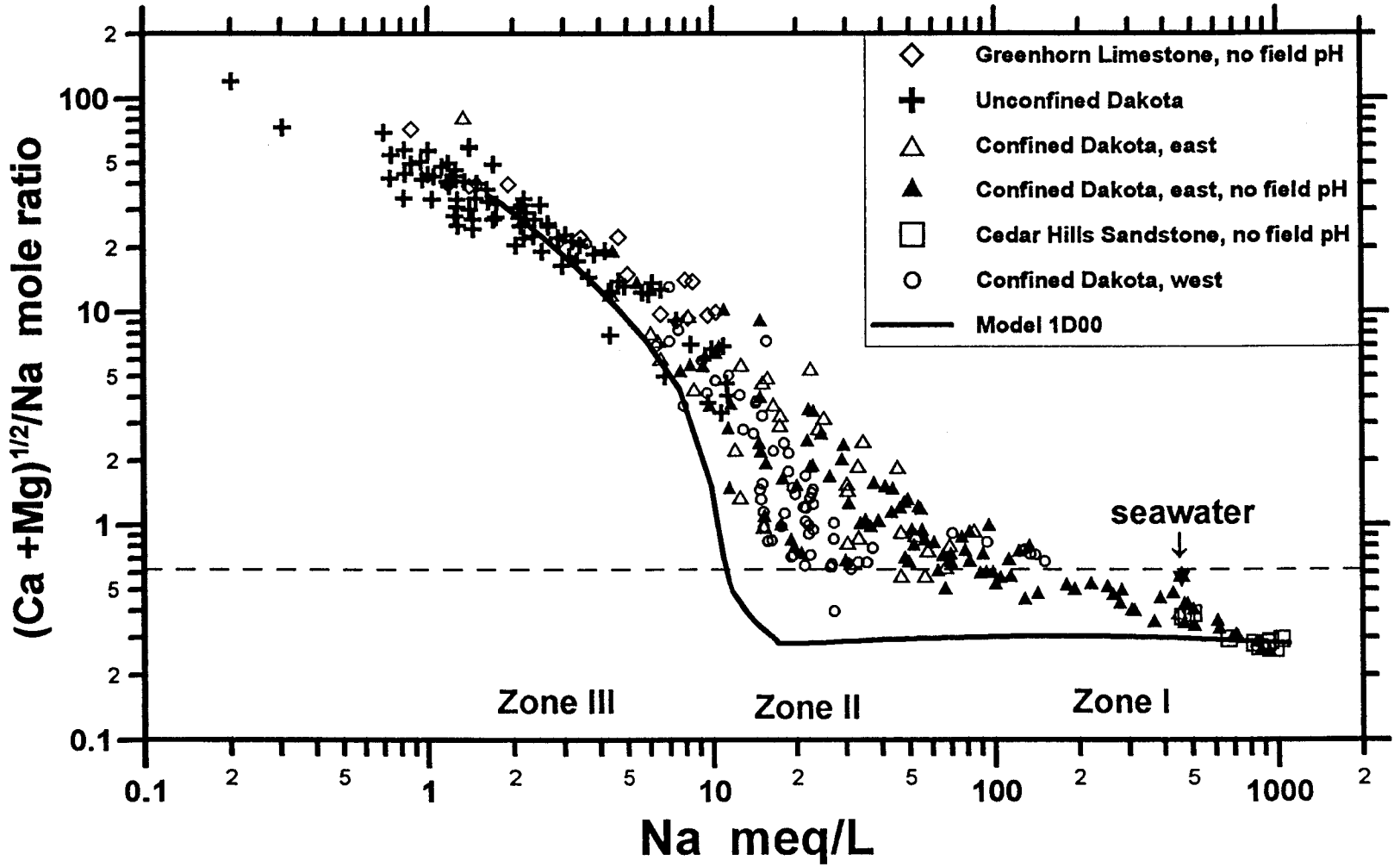

Figure 8.6. Comparison of $(Ca + Mg)^{1/2}/Na$ mole ratio for field data and model 1D00 results. The Na concentration also represents the relative position of a water sample along a conceptial flow path. The dashed line represents the estimated cation ratio for the previous saltwater in the upper part of the west confined Dakota aquifer.

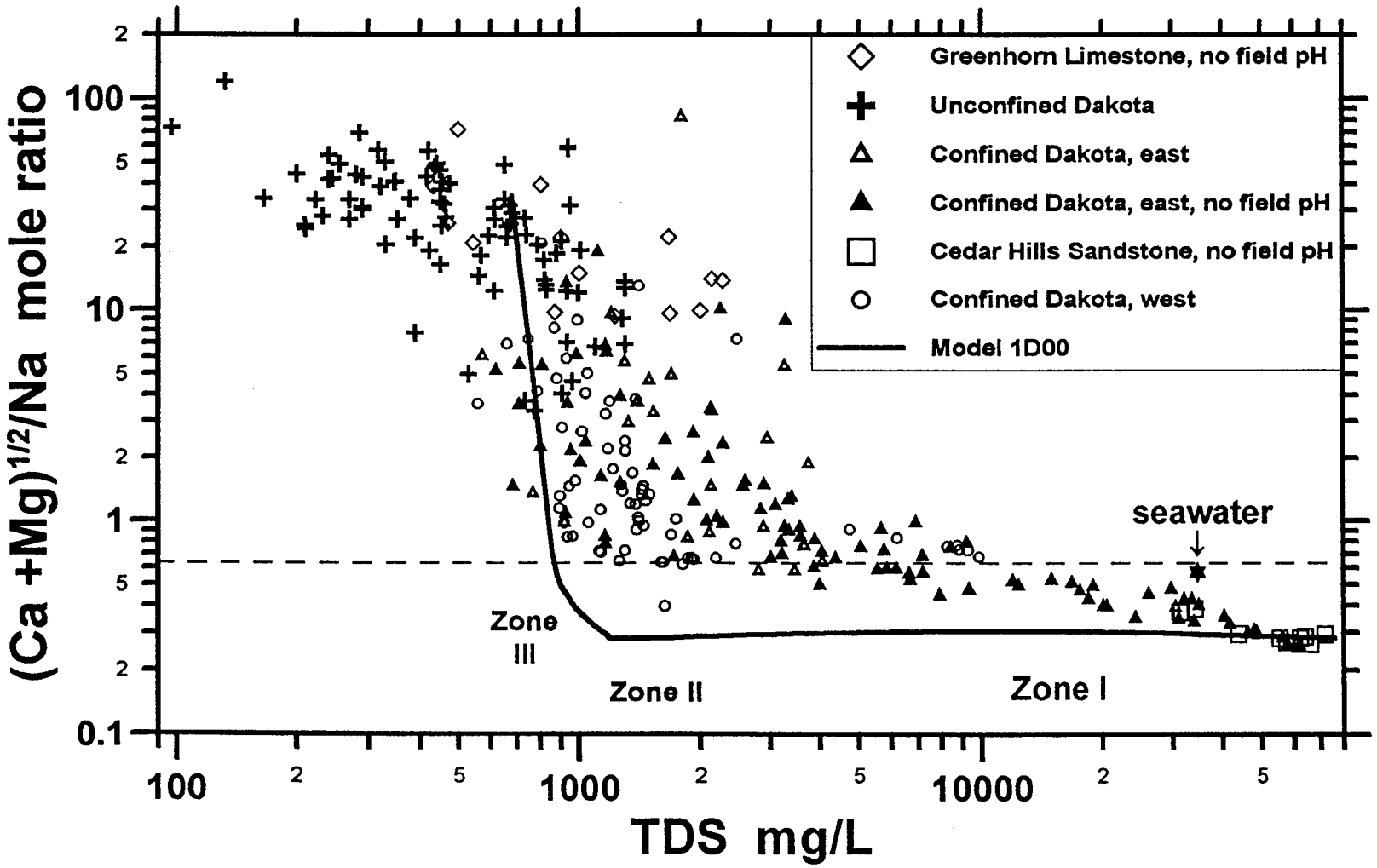

Figure 8.7. $(Ca + Mg)^{1/2}/Na$ mole ratio versus TDS concentration for field data and model 1D00 results. The dashed line represents the estimated cation ratio for the previous saltwater in the upper part of the west confined Dakota aquifer.

Figure 8.6). This number is slightly higher than estimated value from Figure 8.4 because cation concentrations, rather than cation activities, are used to calculate the $(Ca + Mg)^{1/2}/Na$ ratio in Figure 8.6.

Again, as discussed earlier in this chapter, the data suggests that the previous saltwater in the upper part of the west confined Dakota aquifer had a lower salinity than that of the initial saltwater used in the numerical model. The previous saltwater in that part of the aquifer can be estimated by the intersection of the dashed line with the zone of data points for the east confined Dakota waters that are affected by the intruded Cedar Hills saltwater (Figure 8.7). The previous saltwater that was in equilibrium with the Dakota aquifer matrix materials in eastern Trego and western Ellis counties is estimated to have a TDS concentration in the range of 5,000 to 10,000 mg/L. The diagram also suggests that the incoming freshwater that generated the waters in the west confined Dakota aquifer may have had a TDS content of about 700 to 800 mg/L. Furthermore, Figures 8.5 to 8.7 suggest that the front of fresh recharge has passed central Kansas (Trego and Ellis counties) in the upper Dakota Formation. However, the available chemical data can not be used to determine whether the freshwater came laterally from the west or vertically from top leakage.

Field data shows that the salinity of Dakota water in Kansas generally increases with depth and laterally northwestward (Macfarlane et al., 1990; Whittemore et al., 1995). A similar salinity distribution probably was also present in the Dakota aquifer within the last several million years. The highest TDS water generally occurs at the bottom of the aquifer and fresher water toward the top. This concept implies that in the past the Dakota aquifer materials had reacted with water of different quality in different locations, both in the vertical and lateral directions, rather than a homogeneous reaction between a freshwater and an

extremely salty water. Mixing of different waters in both vertical and lateral directions complicates the geochemical evolution process and also masks the effect of cation exchange on the water chemistry. This explains why the majority of the field data plot below the simulated curve and spread widely for the excess Na concentration in Figure 8.5. The salinity change in the vertical direction explains why the previous saltwater in the upper Dakota aquifer in Trego and western Ellis counties was not as salty as the Permian water.

As mentioned before all of the water groups are not in the flow-path sequence as Figure 8.1 shows. The west confined Dakota water group is not affected by the intruded Cedar Hills water that flows eastward to the Dakota outcrop zone. Figures 8.5 to 8.7 reveal that the intensity of cation exchange is limited in the confined Dakota east of the Cedar Hills subcrop due to the short flow path and consistent source of saltwater from the Cedar Hills Sandstone. In contrast, in the Dakota aquifer to the west of the Cedar Hills subcrop, the smaller amount of current saltwater intrusion and longer flow path from western to central Kansas allow more development of cation exchange effects.

Additional factors that may have affected ground-water chemical evolution in the Dakota aquifer system and that might explain the deviation of the field data and numerical simulation include the following:

1. The heterogeneity of the aquifer causes different rates of flow and chemical reactions in different layers. Waters of different quality can mix with each other through dispersion and diffusion. The chemical characteristics of water influenced by this non-ideal mixing process will be different from the numerical model results for homogeneous media. The gradual change of the $(Ca + Mg)^{1/2}/Na$ ratio for the field data in comparison with the

sharp curve and constant horizontal tail of the model curve in Figure 8.7 indicates the effect of continuing mixing of different TDS waters in the system.

2. Vertical leakage from the underlying Permian strata and the top confining layer have disturbed the temporary equilibrium condition of cation exchange (zone II). The intruded waters change the concentration and cation ratios in the Dakota system. Waters of relatively high Ca and Mg concentrations provide additional sources of Ca and Mg that decrease the rate of calcite dissolution, and, therefore, produces a lower pH in the water than given by the simulation.

3. Other factors may explain why the maximum pH observed in the Dakota aquifer system is ≤ 8.5 in comparison with 9.8 in model 1D00 (Figure 7.12b). These include oxidation of pyrite and organic matter which can reduce solution pH as indicated in Chapter 3. Reduction of SO_4 by organic matter in the west confined Dakota aquifer can generate HCO_3 and also lower the solution pH. Ion exchange involving protons and cation-bicarbonate complexes could also affect the solution pH (Griffioen, 1993; Appelo, 1994a).

4. Selectivity coefficients should ideally be determined for a ternary exchange system since that is the case for the model study. However, such data are rare. Selectivity coefficients from binary exchange systems cannot exactly represent the condition in a multi-component exchange system and therefore contribute some error to the model.

5. Chemical simulation indicates that dissolution of magnesite has occurred in the Cedar Hills Sandstone and functions as a continuing source of Mg and HCO_3. Dissolution of sulfate minerals in the Permian sediments provides additional dissolved Ca. The effect of those minerals are not simulated in the model and probably significantly affect the chemistry of water affected by Permian saltwater intrusion.

6. Other more complicated chemical reactions in the aquifer system, including minor aqueous complexes, dissolution/precipitation of other minerals (for example oxides and apatites), and surface reactions (such as exchange of OH^- for F^- on clays and apatites) could contribute to the deviation between the field data and model results.

7. The method of calculating activity coefficients and the equilibrium constants applied in the model may not exactly simulate the field conditions and also contribute to the field-model deviations.

CHAPTER 9

TWO-DIMENSIONAL SEMI-EMPIRICAL COUPLED MODEL FOR THE CHEMICAL TRANSITION ZONE IN CENTRAL KANSAS

9.1 MODEL SETUP

The 1-D model described in Chapter 7 demonstrates the effect of mixing and cation exchange on ground-water chemistry. A 2-D profile model was designed to incorporate the complexities of the hydrogeological system of the Dakota aquifer in the simulation of a chemical transition zone. The 2-D model profile approximately follows the west to east regional ground-water flow in the Dakota aquifer across Ellis and western Russell counties. The west end of the model starts at R18W in west-central Ellis County, extends across the Cedar Hills subcrop zone, and ends at the Saline River valley in northwestern Russell County (Figure 1.2). The cross-section length is 48 km (30 miles). The model simulates the mixing of regional Dakota freshwater from the west, intruded saltwater from the Cedar Hills Sandstone, and fresh leakage from the overlying Upper Cretaceous confining layer.

The regional hydrogeological heterogeneity of the Dakota aquifer has been more systematically studied in recent years (Macfarlane et al., 1991 and 1994). However, the geological information along the particular model profile is not detailed enough to define the individual layers at the scale of the model grid. The information necessary for determining the geohydrological parameters in each individual geological layer is also not available. Therefore, a 2-D heterogeneous profile model would be difficult to develop at present because of the lack of data and complex three-dimensional characteristics of the aquifer system. The difficulty of assigning boundary and initial chemical conditions increases substantially when

the model includes physical complexities. A numerical simulation becomes impracticable when the model hydrogeology becomes too detailed because of the complication of determining the exact chemical compositions at nodes for boundary and initial conditions. As a result of the restrictions, a conceptual model was developed to explain the hydrogeochemical processes in the Dakota aquifer. The cross-section was simplified by using homogeneous hydrogeological units in the 2-D model.

The 2-D profile model consists of 1,848 nodes and 1,700 quadrangular elements (Figure 9.1). The horizontal distance between nodes ranges from 100 to 500 m (330 - 1,650 ft). The vertical nodal distance ranges from 2 to 15 m (6.6 - 49.5 ft). The model thickness ranges from 227 m (749 ft) at the west boundary to 102.4 m (338 ft) at the east end. There are six different hydrogeological units used in the model: an alluvial aquifer, the upper Dakota aquifer, the lower Dakota aquifer, a combined unit of Kiowa marine shale and Cheyenne Sandstone, the upper Permian aquitard, and the Cedar Hills Sandstone (Figure 9.2). The geohydrological parameters for each unit were determined from a sensitivity analyses of conservative transport of Cl. The values for the geohydrological parameters are summarized in Table 9.1. Detailed discussion of the sensitivity analyses is presented later in this chapter.

The geological setting in the model domain was constructed based on Macfarlane et al. (1988). The alluvial aquifer represents the alluvial deposits in the Saline River valley. The upper Dakota unit is approximately equal to the Dakota Formation. The lower Dakota unit represents the Longford Member of the Kiowa Formation. The thickness of the marine shale of the Kiowa Formation becomes significant in affecting the vertical flow to the west of the Cedar Hills subcrop. The marine shale is lumped with the underlying Cheyenne Sandstone to form a single unit to reduce the model complexity. The Upper Permian aquitard is located

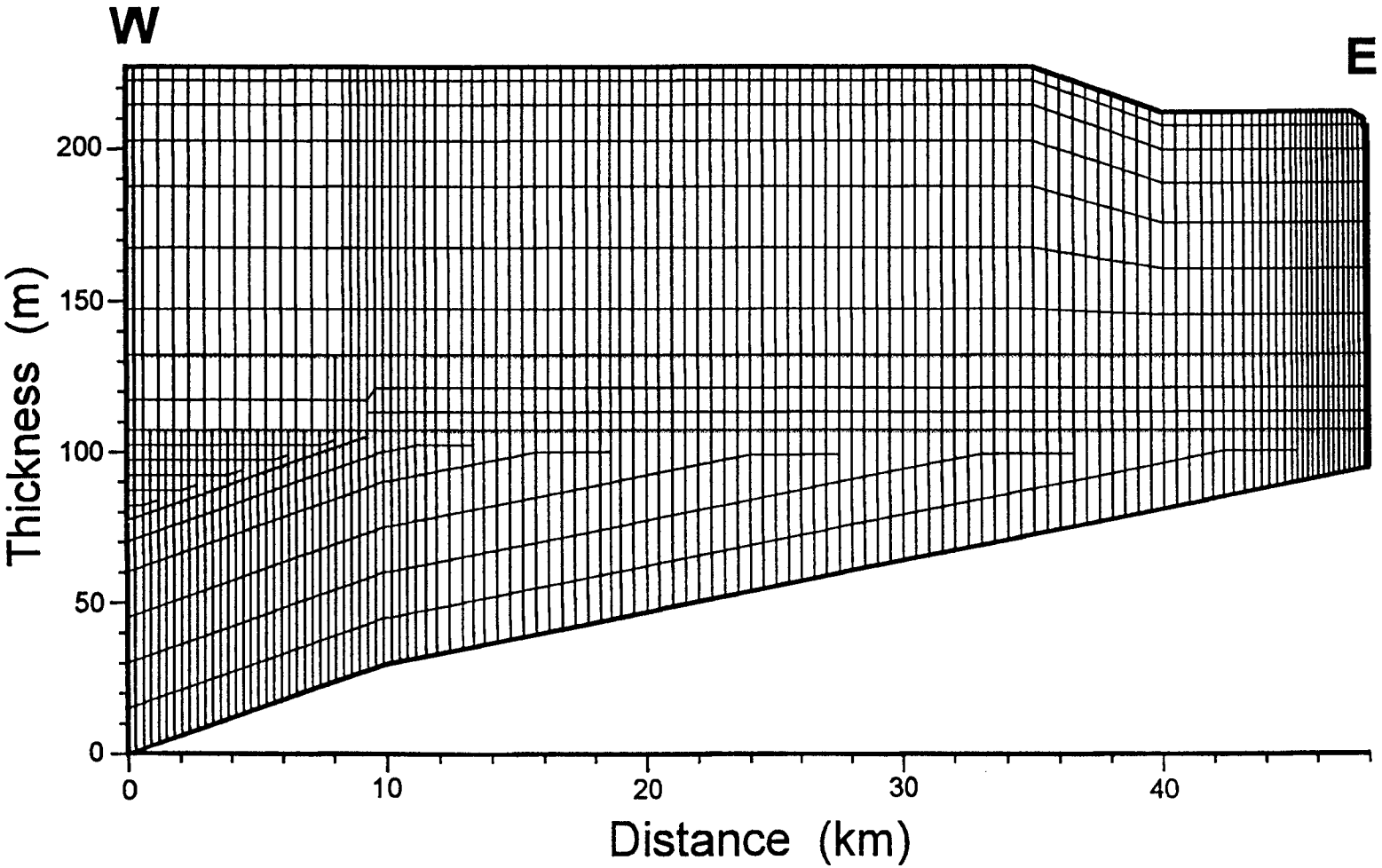

Figure 9.1. Finite element grid for the 2-D coupled profile model. The model was used to simulate the chemical transition zone in the Dakota aquifer system in central Kansas. The location for the model is shown in Figure 1.2.

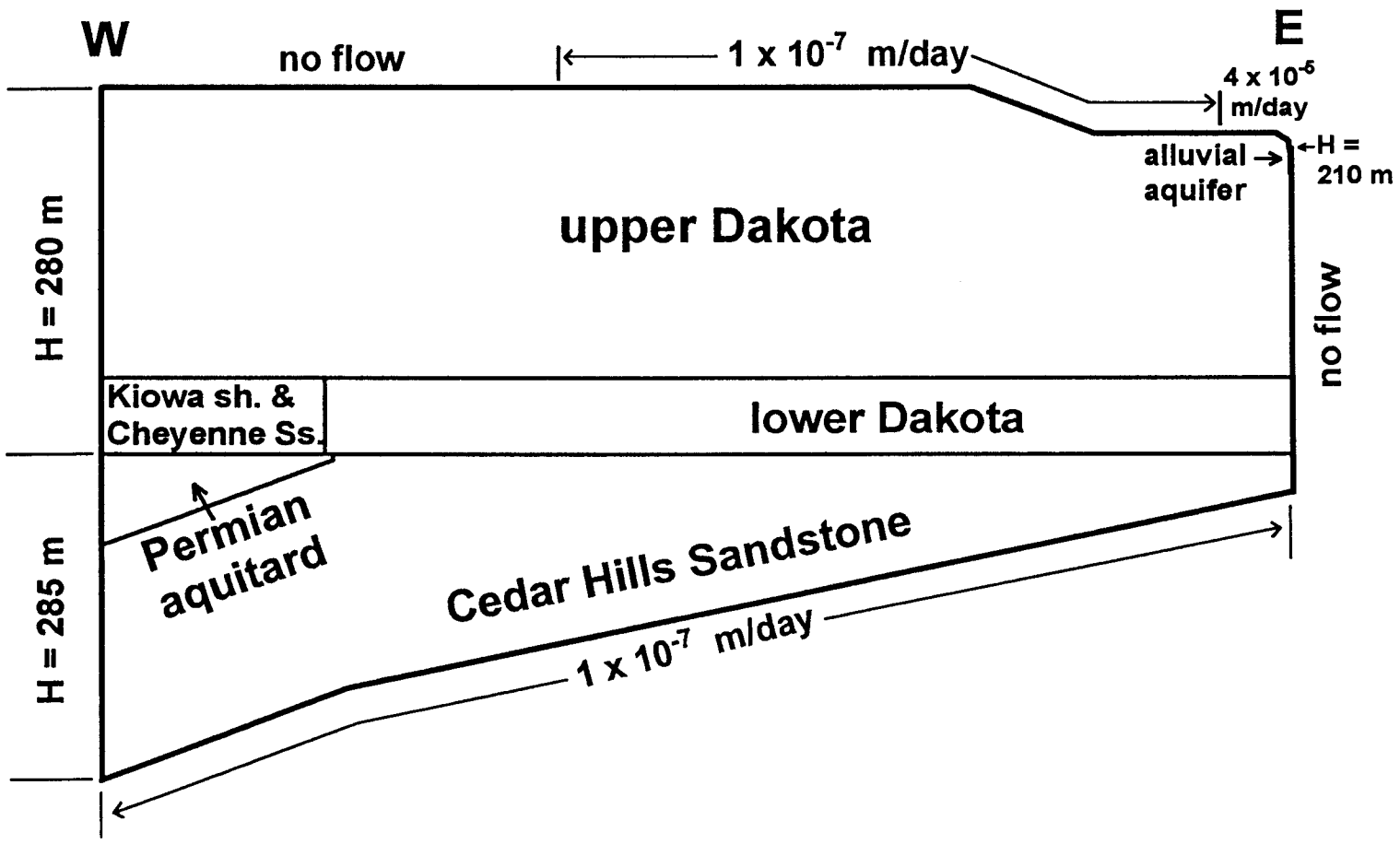

Figure 9.2. Hydrogeologic units and flow boundary conditions for the 2-D semi-empirical profile model. Constant heads (H) were assigned to the west side boundary and river bottom nodes at the upper-right corner of the model. Constant fluxes were given to the top and bottom boundaries.

between the Kiowa/Cheyenne unit and the Cedar Hills Sandstone west of the Cedar Hills subcrop. The dip, thickness, and subcrop zone of the Cedar Hills Sandstone was selected based on previous studies and test-hole log records (Macfarlane et al., 1988, 1990).

Table 9.1. Geohydrological parameters for the hydrogeological units used in the 2-D profile model.

Unit	Hydraulic conductivity (m/day) K_x	K_z	Dispersivity (m) α_l	α_v	Diffusion coefficient (m^2/day)	Bulk density (g/cm^3)	CEC (meq/100g)	Porosity
Alluvial aquifer	30	5	20	0.3	0	1.8	2.5	0.30
Upper Dakota	3	0.001	20	0.3	0	2.0	2.5	0.20
Lower Dakota	1	0.0005	15	0.2	0	2.1	5.4	0.18
Kiowa shale & Cheyenne Sandstone	1	1×10^{-5}	10	3×10^{-3}	5×10^{-7}	2.2	20	0.15
Upper Permian aquitard	1×10^{-5}	1×10^{-6}	1	1×10^{-3}	3×10^{-7}	2.4	10	0.05
Cedar Hills Sandstone	1	0.05	15	0.2	0	2.2	3.0	0.15

K_x and K_z are the horizontal and vertical hydraulic conductivities, respectively.
α_l and α_v are the longitudinal and vertical dispersivities, respectively.

As mentioned in Chapter 6, a flow domain must be determined prior to the coupled hydrogeochemical simulation. A steady-state flow model was used for the coupled hydrogeochemical simulation. The flow boundary conditions for the steady-state model are shown in Figure 9.2. The east boundary of the model is located at the hydraulic divide under the Saline River and no cross-flow occurs. Constant heads were assigned to the west side and the river bottom nodes at the top of the east side boundary. The river bottom nodes are the discharge points for the model. The west constant-head boundary was divided into two

sections to represent the head difference between the confined Dakota and the Permian strata. The top boundary is a constant flux boundary with different recharge rates in different sections. The different recharge rates indicate the variation of the top leakage due to a decrease in thickness of the Upper Cretaceous confining layer from west to east. Constant flux was assigned to the bottom boundary to indicate continuous diffusion of saltwater from below.

The Dirichlet (constant concentration) chemical boundary conditions are referenced in Figure 9.3 and listed in Table 9.2. The chemistry of the initial saltwater intruded from the Permian in the 2-D model is represented by a sample analysis that is similar to the initial condition for model 1D00 in Chapter 7. Despite the different recharge rates and changes in geology along the top boundary, a constant water chemistry was assigned to the entire top boundary. It was assumed that the top recharge is Ca-SO_4-HCO_3 type water derived from the Greenhorn Limestone and does not change substantially after passing through the Graneros Shale. The basic chemical components and the chemical reactions in the model are the same as those in Table 7.3. In addition, dissolution of magnesite is included in the model because magnesite occurs in the Permian units (the Cedar Hills Sandstone and the upper Permian aquitard).

$$Mg^{2+} + CO_3^{2-} \Leftrightarrow MgCO_{3(s)} \qquad K_{magnesite} = [Mg^{2+}][CO_3^{2-}] = 10^{-7.952}$$

The time step used during simulation increased from one year to one hundred years. The total simulation time was 3,000 years. Output results were examined for various intermediate time steps to determine the progress of chemical evolution. Numerical instability for the model results occurred in the upper Permian aquitard and along sharp fronts, particularly for species involved in heterogeneous chemical reactions, i.e. cation exchange and

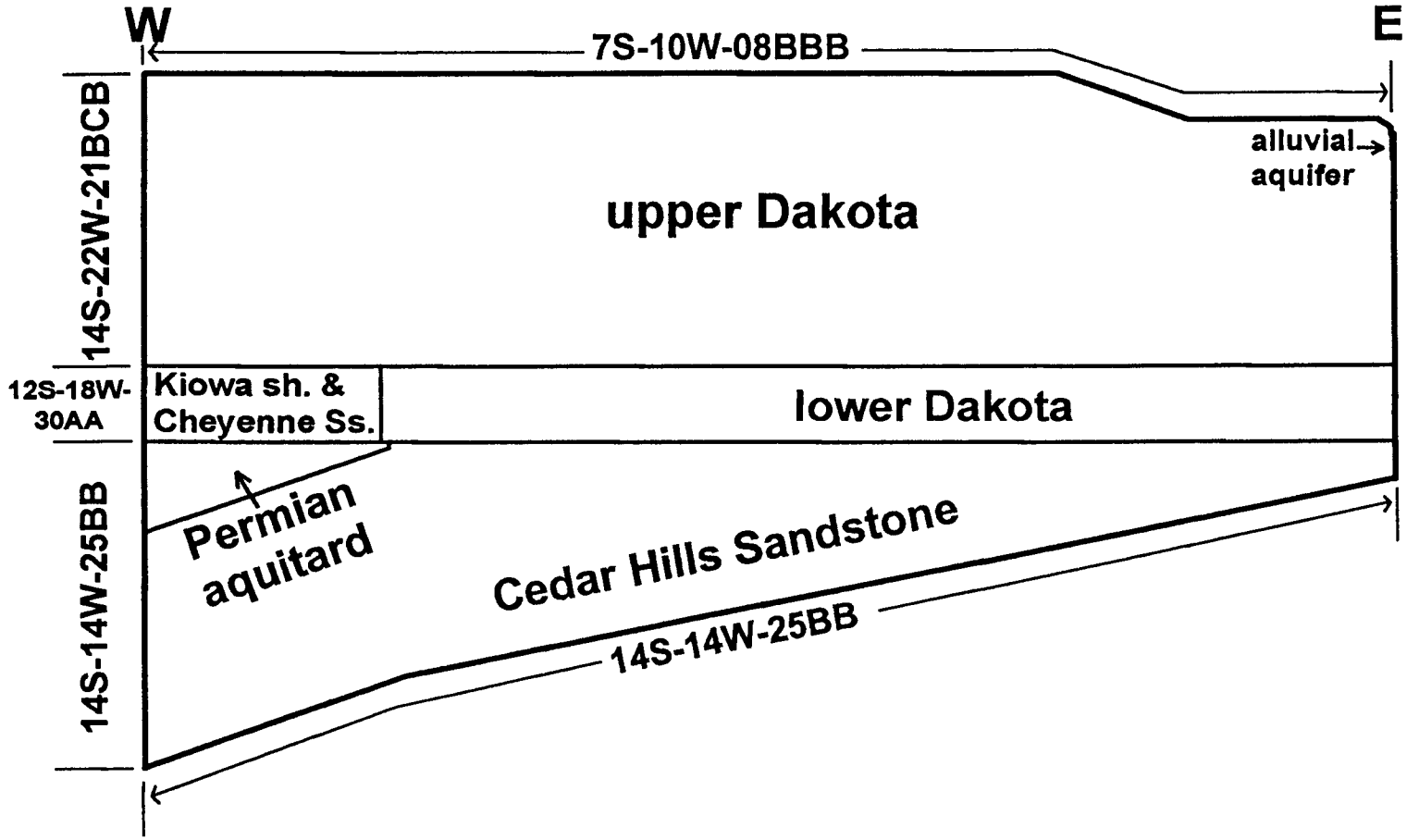

Figure 9.3. Dirichlet chemical boundary conditions for the 2-D semi-empirical profile model. The boundary identifiers are well locations for which sample analyses are listed in Table 9.2.

precipitation/dissolution. However, reasonable results were obtained for describing the geochemical evolution in the aquifer system.

Table 9.2. The ground-water chemistry used as the initial and boundary conditions in the 2-D profile model.

Location	7S-10W-08BBB	12S-18W-30AA	14S-14W-25BB	14S-22W-21BCB
Geology	Greenhorn Limestone	Cheyenne Sandstone	Cedar Hills Sandstone	Dakota Formation
pH	7.02	7.45	6.56	8.45
Ca meq/L (mg/L)	9.88 (198)	3.19 (64)	39.4 (790)	0.210 (4.2)
Mg meq/L (mg/L)	1.49 (18)	58.9 (716)	94.3 (1146)	0.182 (2.2)
Na meq/L (mg/L)	5.00 (115)	448 (10300)	976 (22440)	19.4 (446)
HCO_3 meq/L (mg/L)	4.88 (298)	17.5 (1068)	11.4 (696)	7.93 (484)
SO_4 meq/L (mg/L)	7.72 (371)	85.6 (4110)	128 (6150)	4.00 (192)
Cl meq/L (mg/L)	3.53 (125)	412 (14600)	970 (34400)	5.70 (202)
TDS mg/L	1002	30410	65610	1122

9.2. ESTIMATION OF HYDROGEOLOGICAL PARAMETERS

Each hydrogeological unit in the numerical model is associated with only one set of hydrological properties. In actual systems, the geohydrological properties vary within a lithologic unit and change abruptly between different lithologic layers, such as sands and shales. Nearly all sandstone aquifers contain an appreciable amount of shale. In many aquifers and oil reservoirs, the most dominant nonuniformity is due to the clayey layers rather than fluctuations in the intrinsic sand properties (measured on a macroscopic scale). For field-scale simulations, each grid block usually contains more than one actual lithologic layer.

Thus, the effective properties of the apparently homogeneous blocks have to be obtained by averaging the values of individual layers involved in the block.

As indicated in Chapter 2, the Dakota Formation contains about 60 to 70% silt and clay materials, and 30 to 40% sandstone. The depositional environments of the Dakota Formation vary from braided-streams to deltas. The Longford Member of the Kiowa Formation comprises mainly paralic deposits. Cores obtained from the study area show that the Dakota aquifer contains mostly interbedded sandstone and claystone, and some thick clay layers and sandstones (Macfarlane et al., 1991b). The shales in the Dakota Formation surround ribbon-like sandstone bodies rather than occurring in a stochastic form in sandstones as normally assumed in characterizing aquifer (or reservoir) properties. However, stochastic studies of the effect of clay layers on aquifer hydraulic properties are still valuable for determining model parameters. Figure 9.4 shows shale length in relation to depositional environment based on a statistical study of Weber (1982). The diagram implies that in marine and barrier bar sands, shale layers tend to split the sand bodies into separate zones with little connection. Vertical crossflow is severely restricted in the delta fringe and between distributary channel fills. Fluvial sand bodies rarely show internal separation on a scale greater than 100 m. However, the hydraulic communication between channel-filled sand bodies is restricted by fine-grained overbank deposits.

The original permeability anisotropy caused by texture and bedding in a sand body is usually very low, ranging between 1 and 2 for horizontal to vertical permeability if clay intercalations are excluded (Haldorsen, 1983; Hutchinson et al., 1961; Rose, 1983; Weber, 1982). The permeability difference is enhanced by diagenetic and lithification processes and may exceed 100:1. However, the primary factor for permeability anisotropy is the existence of

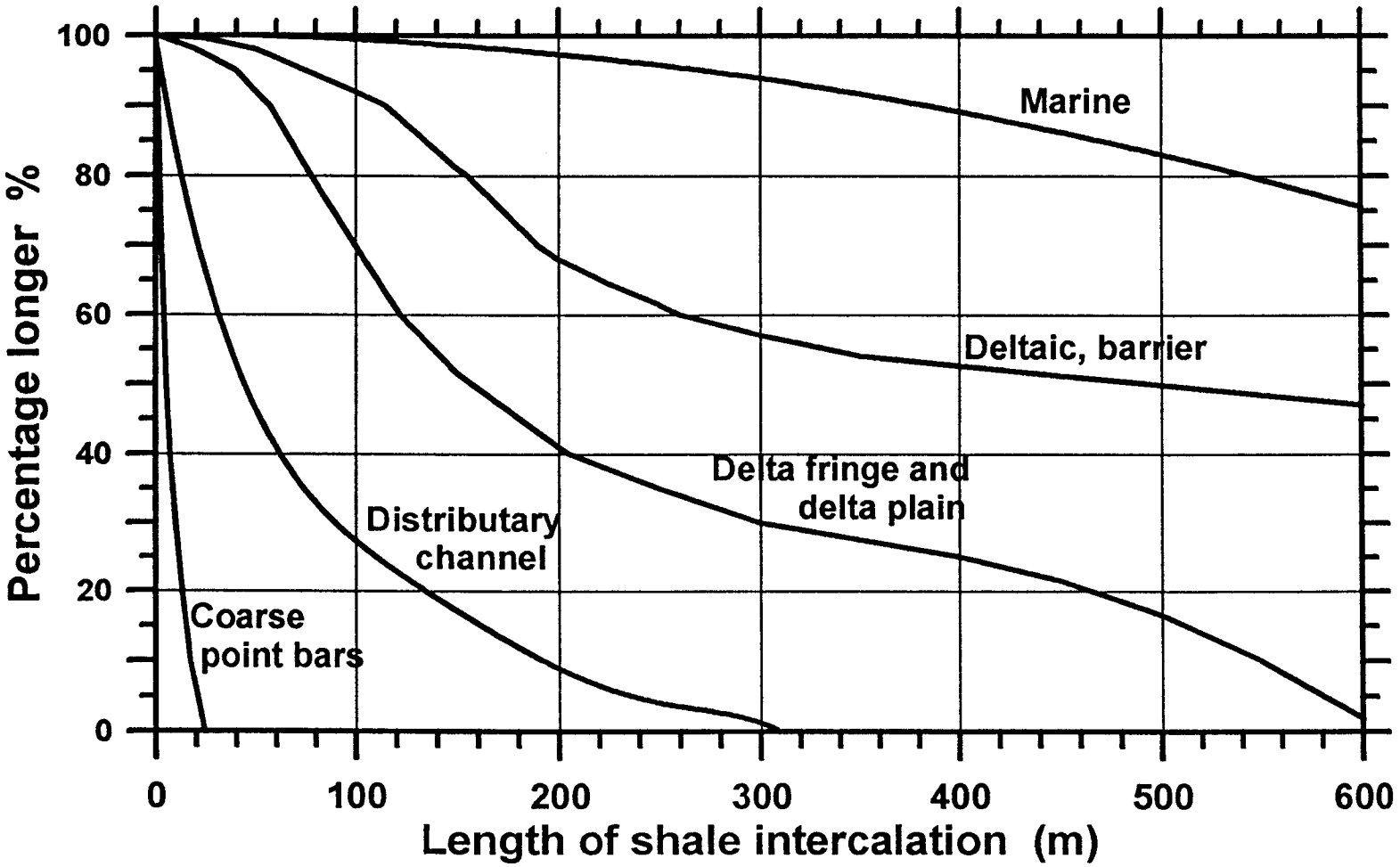

Figure 9.4. Continuity of shale (silt) intercalations as a function of depositional environment (modified from Weber, 1982).

intercalated clay layers in sand bodies. The clay layers reduce the effective porosity and horizontal and vertical permeabilities, and increase the rate of dispersion. Equations 9.1 and 9.2 illustrate the effect of clay layers on horizontal and vertical hydraulic conductivities, respectively (Freeze and Cherry, 1979).

$$K_x = \sum_{i=1}^{n} \frac{K_i d_i}{d} \tag{9.1}$$

$$K_z = \frac{d}{\sum_{i=1}^{n} d_i / K_i} \tag{9.2}$$

where

K_x = averaged horizontal hydraulic conductivity

K_z = averaged vertical hydraulic conductivity

K_i = horizontal or vertical hydraulic conductivity of layer i, i = 1,2,...,n

d_i = thickness of individual layer i, i = 1,2,...,n

d = total thickness of the system of layers

The equations show that clay layers have only a small effect on horizontal hydraulic conductivity by reducing the available flow area for fluid transport. The barrier to vertical hydraulic conductivity created by clay layers is the most important factor causing anisotropy of hydraulic properties.

The degree to which clay layers affect the hydrogeological properties depends upon the density and length of the internal clay layers (Haldorsen, 1983). The relationship of shale length, density, and thickness is not well known. Many numerical studies have been conducted to determine the effect of stochastic shales on both horizontal and vertical permeabilities

(Delhomme and Giannesini, 1979; Haldorsen, 1983; Prats, 1977; Richardson et al., 1978; Weber, 1982). They found that a reduction in vertical permeability is dependent on: 1) the number of shale breaks encountered in a vertical traverse of the block, and 2) the ratio between the length of a shale and the horizontal dimension of the grid block.

The conventional approach for selecting vertical hydraulic conductivity in numerical simulations is to assume that the bulk flow in the vertical direction is in effect traveling along a straight line. Haldoren (1983) pointed out that this assumption violates the real situation and the actual flow-path length should be considered. He confirmed this both analytically and numerically using models with simple shale break configurations. However, determining the flow-path length in a megascopic scale in a complex system is very difficult.

The existence of clay layers in sand bodies tends to increase dispersivity. However, the lateral dispersion in the Dakota aquifer is more likely to be limited by the confining materials because the channel sandstones are confined in clayey and silty overbank deposits. Thus, large longitudinal and small lateral dispersivities are expected in the Dakota aquifer.

9.3. SENSITIVITY ANALYSES OF GEOHYDROLOGICAL PARAMETERS AND BOUNDARY CONDITIONS

The geohydrological parameters for the hydrogeological units used in the model were initially taken from previous numerical simulations in the same region (Wade, 1992; Whittemore et al., 1993). Some of the parameters were tested by a steady-state conservative transport model for Cl. The advantage of using a transport model to test model parameters is that in addition to the calibration of hydraulic head, the shape of the solute plume provides additional information for further adjustment of the model parameters. The sensitivity

analyses included tests for the horizontal and vertical hydraulic conductivities (K_x and K_z), vertical dispersivity(α_v), hydraulic head difference between Dakota and Cedar Hills aquifers at the west boundary, and vertical recharge rates from the top and bottom boundaries. No calibration was attempted because the model is only semi-empirical. The parameter values were selected based on the aquifer properties and the distribution of the water chemistry in the general area along the profile model. Figures 9.5 and 9.6 are the steady-state results for the simulated flow field and Cl concentration distribution, respectively.

In spite of the wide range of K_x values obtained from aquifer tests in the Dakota aquifer, the distribution of values defines the K_x relatively well. Previous Dakota aquifer studies show that the permeability of the Cedar Hills Sandstone is smaller than that of the Dakota aquifer. Based on this relationship, the average K_x of the (upper) Dakota aquifer was selected to be within a possible range of 0.3 to 3 m/day, except for local extremes for channel sandstones. A smaller K_x value was assigned to the Cedar Hills Sandstone. The concentration of the intruded saltwater plume depends on the relative amount of saltwater coming from the Permian aquifer. The relative ratio of K_x for the Dakota and Cedar Hills aquifers is one of the major factors controlling the intruded saltwater plume concentration. For a constant K_x in the Cedar Hills Sandstone, an increase in K_x for the Dakota aquifer will increase the flow from the west and the dilution of the intruded saltwater. However, changing the K_x within the reasonable range of K_x, does not significantly alter the flow pattern and Cl concentration plume. A higher K_x than used in previous numerical simulations was assigned to the Cedar Hills Sandstone to allow enough saltwater to flow to the Dakota aquifer to fit the field data. The higher K_x for the Cedar Hills Sandstone is also supported by the continuity of the

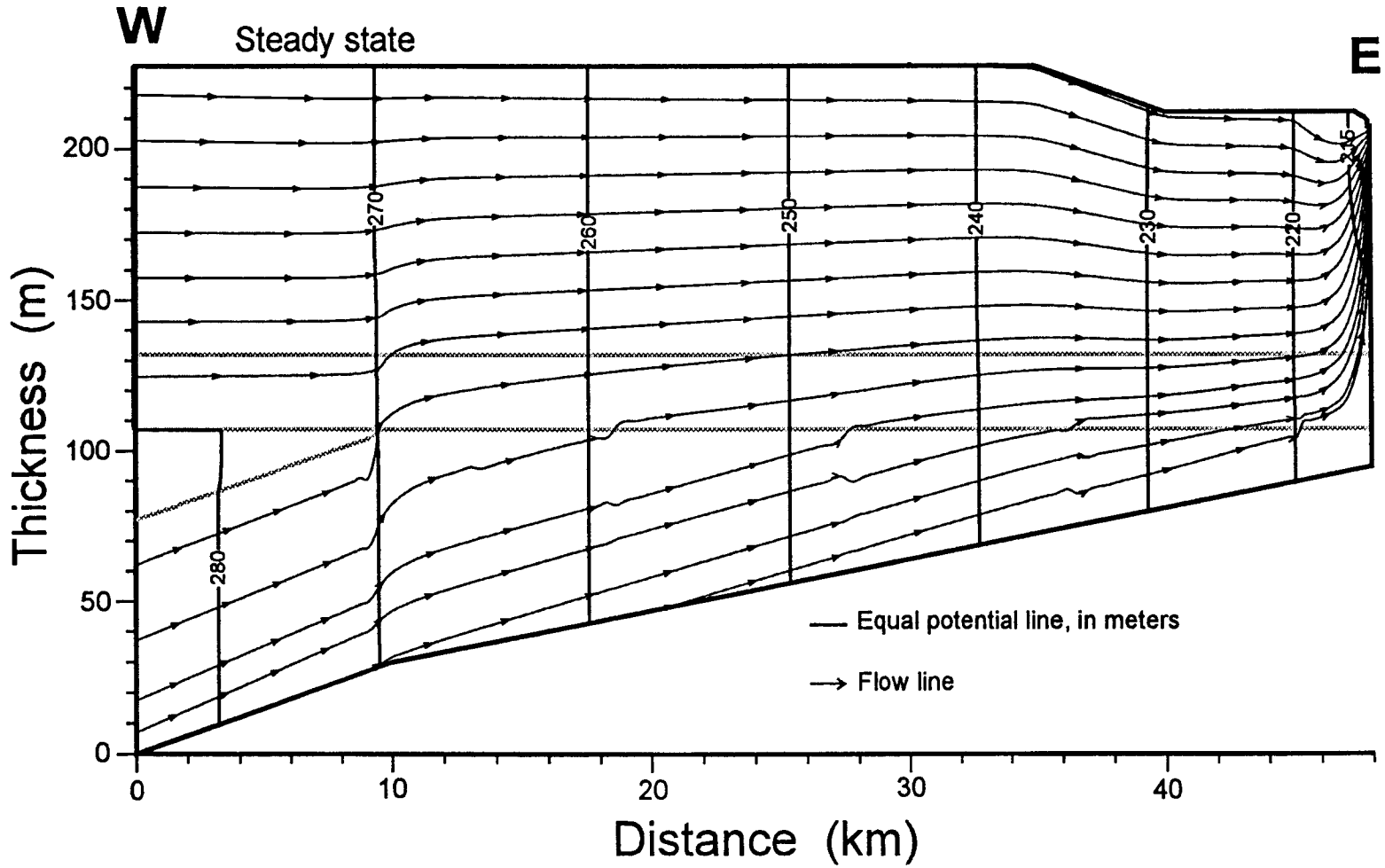

Figure 9.5. Simulated steady-state flow field of the 2-D coupled profile model.

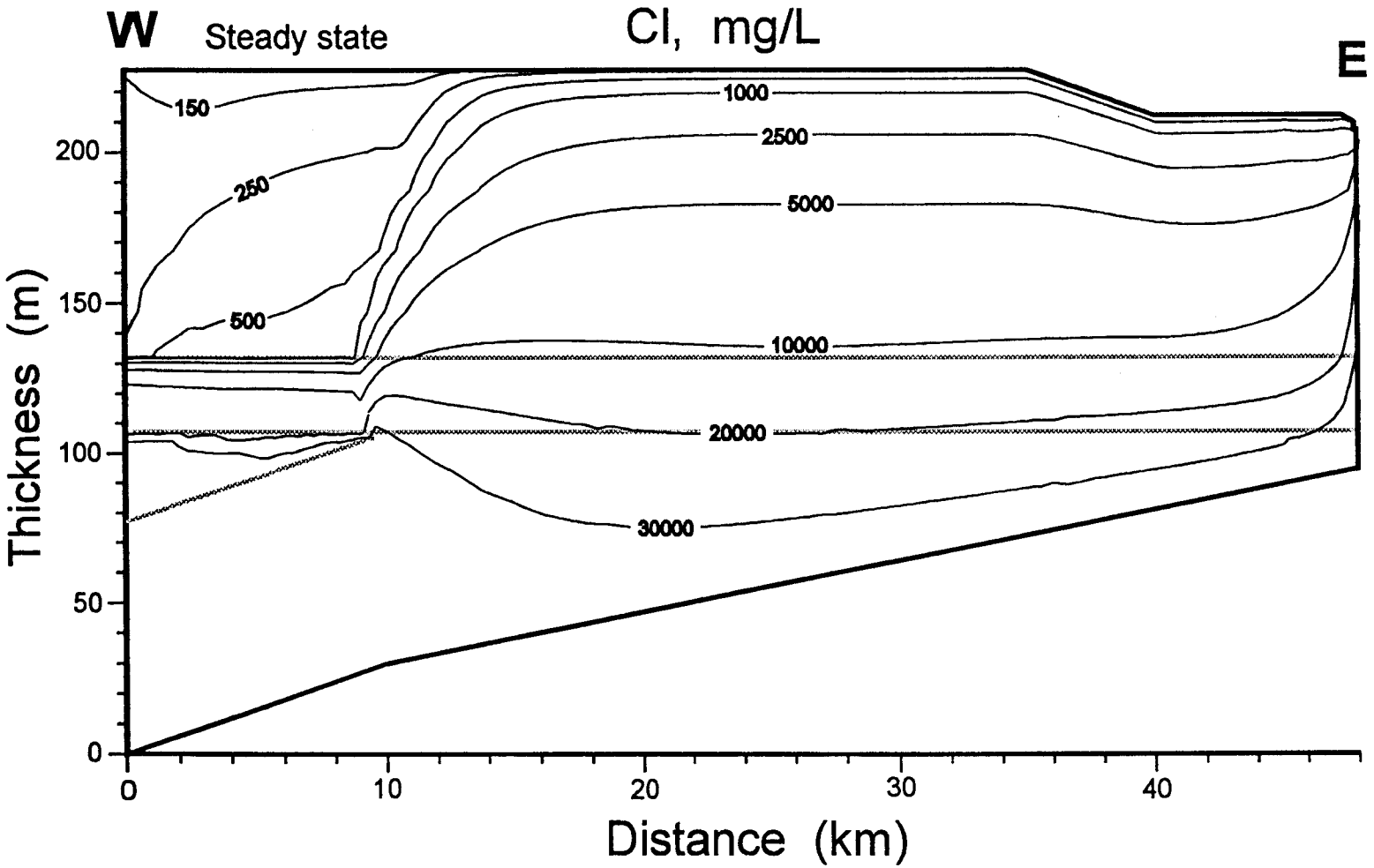

Figure 9.6. Simulated steady-state condition of Cl concentration distribution for the 2-D coupled profile model.

sandstone body shown in the gamma-ray log intensity image of Macfarlane et al. (1994, p. 470, Fig. 6).

The west boundary of the model is more than 9 km to the west of the contact of the Dakota aquifer and Cedar Hills Sandstone. There is a 30 m thick Permian aquitard between the two aquifers at the west boundary; the aquitard pinches out at the contact of the two aquifers. The hydraulic head difference between the two aquifers at the west boundary was examined relative to its effect on the saltwater intrusion. As Figure 9.5 indicates, the head difference at the west boundary is transmitted only through the confined part of the Cedar Hills Sandstone and damps out shortly after the two aquifers join together. The damping effect is caused by a greater hydraulic connection along the Cedar Hills subcrop and by the driving force of the top recharge. The almost evenly distributed hydraulic head in the vertical direction in the model east of the Upper Permian aquitard is not sensitive to the head difference at the west boundary.

The vertical components of hydrologic parameters are rarely available for the Dakota aquifer in Kansas. Almost all of the values available for vertical permeability in the Dakota aquifer are from numerical flow models. Thus, there are uncertainties in the vertical flow conditions in the Dakota aquifer system. The sensitivity analyses indicate that the aquifer system is very sensitive to any change in the vertical geohydrological components. The effects are normally difficult to detect in the flow field but become distinct in solute transport. In general, the K_z of the upper Dakota and the recharge rates at the top boundary are the major controls on the intensity of the effect caused by the top leakage in the Dakota aquifer. In comparison, the K_z's of the lower Dakota and Cedar Hills Sandstone are essential to the intruded Permian saltwater plume.

Along the model profile, the recharge rates at the top boundary become greater from west to east because of the decreased thickness of the Upper Cretaceous confining layer. However, the increased top recharge rate toward the east end of the model does not appreciably change the regional ground-water quality. This is because recharge toward the east end only forms a shallow local flow system and does not substantially affect the regional ground-water flow system. However, the ground-water quality in the upper part of the Dakota aquifer is very sensitive to the amount of recharge from the western part of the top boundary. The top boundary was divided into three sections. The locations of the divide were determined based on the sensitivity analyses. The flow boundary conditions shown in Figure 9.2 indicate that even a trace amount of recharge from the west-end section (0 to 18.4 km) of the top boundary greatly impacts the regional water chemistry in the Dakota aquifer. Therefore, no flow was assigned to this section but a constant chemistry boundary condition was given. In the next top boundary section (18.4 to 45.1 km), a recharge rate of 1×10^{-7} m/day (1.44×10^{-3} inch/year) gives a Cl distribution in the upper Dakota closest to that expected. The top recharge rate for the east-end section is 4×10^{-5} m/day (0.43 inch/year). The top confining layer in this section becomes very thin or disappears and allows a large recharge rate to the Dakota aquifer. However, the recharge is limited to a local flow system and discharges to the Saline River after a relatively short flow path. A previous large-scale, cross-sectional flow model estimated the overall average recharge rate from the Upper Cretaceous aquitard in central Kansas to be about 3.6×10^{-6} m/day (0.052 inch/year) (Whittemore et al., 1993). Considering the much greater recharge rates near the river valleys and the Dakota outcrop zone, the value obtained from the 2-D model is reasonable compared to the previous regional model.

The K_z of the upper Dakota unit determines how readily the top leakage can penetrate into the Dakota aquifer. Generally, if the K_z of the upper Dakota unit is too small to allow the assigned recharge rate to enter the system, the numerical model collapses. A large K_z allows the top leakage to penetrate into the aquifer readily and suppresses the saltwater plume coming from below.

The K_z of the Cedar Hills Sandstone is a major factor controlling the upward discharge of the Permian saltwater into the Dakota aquifer. The ratio of the K_z/K_x for the Permian aquifer is expected to be higher than the Dakota aquifer because of the relatively homogeneous sandy characteristics. However, due to the effects of stratification, the ratio should not be much more than 0.1 (Domenico and Schwartz, 1990). This ratio allows a limited range of values for K_z in the Cedar Hills Sandstone.

There are two possible scenarios of flow in the zone where the Dakota and Cedar Hills aquifers are hydraulically connected. The Cedar Hills saltwater will intrude to the Dakota aquifer if the pressure head in the Permian aquifer is higher than the overlying Dakota aquifer. In contrast, if the sum of the driving force of the top leakage and the potential in the Dakota aquifer exceeds the pressure head in the Cedar Hills aquifer, the Dakota water will flow downward into the Cedar Hills Sandstone and flush out the formation water near the subcrop zone. The sensitivity analyses indicate that the K_z of the lower Dakota unit is the most important factor controlling the flow direction. As described previously, the hydraulic head difference between the two aquifers damps out soon after the aquifers join together. In order to drive the Cedar Hills water upward into the Dakota aquifer, a higher hydraulic pressure must occur in the Cedar Hills Sandstone. Maintaining the pressure head in the Permian aquifer depends on the degree of hydraulic connection between the two aquifers. The better the

connection, the faster the pressure difference disappears. Downgradient to the east, the combined force of the top recharge and the potential head of the Dakota water eventually drives the Dakota water down to the Permian aquifer. A small K_z for the lower Dakota unit not only maintains the pressure head in the Cedar Hills aquifer, it also restricts the movement of the intruding saltwater from below. The two-way limit provides a well defined range for the K_z of the lower Dakota unit. However, an absolute range of the K_z for the lower Dakota unit depends on many other factors and can not be determined with current knowledge of the aquifer system.

As described in Chapter 6, HYDROGEOCHEM does not take into account the density effect on flow. However, due to the very high TDS content of the Permian saltwater, density effect will greatly influence the flow pattern in the 2-D model, particularly the plume shape of the intruded Permian saltwater. Anyhow, the sequence of geochemical evolution pattern is not affected by the density effect on flow field. The spatial location of the different water types in the geochemical evolution pattern along the flow path will be shift if density effect is considered.

No reliable dispersivity data for the Dakota aquifer in Kansas has ever been reported. The longitudinal dispersivities for the different hydrogeological units in the 2-D profile model were mainly selected from a knowledge of the aquifer system, values reported in previous studies for similar types of aquifers, and the numerical stability of the model. As mentioned in the last section, the lateral dispersivity is expected to be small because of the characteristics of the geographic configuration of the sandstone bodies in the Dakota aquifer. The sensitivity analyses of the dispersivities show that higher α_v for the upper and lower Dakota units and Cedar Hills Sandstone increase the spread of the saltwater plume.

9.4. 2-D COUPLED MODEL RESULTS AND INTERPRETATION

Cation exchange reactions occur as part of the ground-water geochemical evolution process when recharge of different salinity replaces the residual water in an aquifer. In the process of mixing, a conservative dissolved constituent reaches a steady state condition in a relatively short time in comparison with the constituents involved in heterogeneous chemical reactions, such as cation exchange. It takes much longer time for a entire aquifer system to reach the steady-state condition in which the formation materials become in equilibrium with the incoming water. The Dakota aquifer system is currently in a transient state and will not reach a chemical steady-state condition with the incoming recharge for a considerable length of time even if the hydrogeological condition remains constant. The water given at the west boundary of the upper Dakota unit is a product of cation exchange occurring upgradient to the west near the regional recharge area. The constant chemical boundary condition selected for the model can only describe part of the transient processes that have occurred in recent geological history in the Dakota aquifer. The representativeness of the hydrogeochemical model results to the natural system is described below, and is followed by a discussion of the major features occurring in the simulation.

Cation exchange and the concomitant reactions are continuous reactions when they occur in an aquifer system. In the HYDROGEOCHEM model, chemical reactions only occur once every time step for iterations between the hydraulic and chemical reaction modules. A problem caused by the discrete numerical calculation is that the numerical model usually underestimates the total effect of chemical reactions which actually would occur during the simulated period. For example, no matter how small the time steps are in a given time period,

the amount of calcite precipitation/dissolution for the 2-D chemical transition profile model is underestimated compared to the natural system simulated. However, a better estimation is achieved by using small time steps. For practical purposes, the balance between model accuracy and capability for the available computer facility has to be considered. Therefore, an attempt to quantitatively describe a chemical transition model with a coupled program may not be appropriate, especially not with large time steps. Most of the time steps for the 2-D numerical simulation were 100 years except for some short periods with smaller time steps. Thus, the amount of calcite precipitation/dissolution was calculated only once every 100 years for most of the simulation period. Although the model shows where the calcite precipitation/dissolution occurs, the simulation result does not indicate the true results for actual reactions. Nevertheless, the coupled simulation still provides valuable information about the general events occurring in the aquifer system.

The conservative transport of Cl in a steady-state condition provides a guideline for adjusting the model parameters. The adjustment is based on the assumption that the Cl distribution in the Dakota aquifer has reached a steady-state condition. The Cl model shows that a strong upward saltwater flow occurs near the western edge of the Cedar Hills subcrop which forms a saltwater "barrier" right on the top of the subcrop zone (Figure 9.6). However, dispersion allows Dakota water to seep into the Cedar Hills Sandstone along the subcrop zone. The dilution effect in the Cedar Hills Sandstone is so strong that the saltwater in the lower eastern part of the model is appreciably diluted. This suggests that a no-flow bottom boundary is not appropriate for the model. A small leakage was given to the bottom boundary to maintain the salinity along the bottom part of the model.

Recharge from the upper confining layer, particularly along the western part of the top boundary, has a great impact on the quality of the regional Dakota water. The result is consistent with the conclusion of a previous geochemical study of the Dakota aquifer in Kansas (Macfarlane et al., 1990). The impact of a top recharge rate of 1×10^{-7} or 1×10^{-6} m/day has only a small effect on ground-water flow in the model but substantially affects the ground-water chemistry.

As discussed earlier, the water in the west confined Dakota aquifer has already been affected by cation exchange reactions. Therefore, there is not much cation exchange expected when the incoming Dakota water from the west mixes with the intruded Permian saltwater. The transient model results for Cl concentration indicate that the top recharge is a major water source in the upper part of the Dakota Formation (upper Dakota unit). The impact of the top recharge is especially important for diluting the saltwater in the Dakota Formation during the early stages of the transient simulation (Figure 9.7) because the water in the Dakota Formation to the west has not had time to completely flow across the cross section. Later in the transient simulation, the combined effect of the regional Dakota water flow from the west and the top recharge further dilutes the Permian saltwater plume. Figure 9.6 shows that in the steady-state condition, Cl concentrations greater than 10,000 mg/L only occur in and just below the lower Dakota unit.

The movement of the low Ca concentration water from the west boundary in the upper Dakota unit is very slow. Leakage with higher Ca concentrations from above and below limit the apparent movement of the low Ca water from the west (Figure 9.8). Figure 9.8 also shows the influence of the top recharge on the water quality in the top portion of the Dakota aquifer.

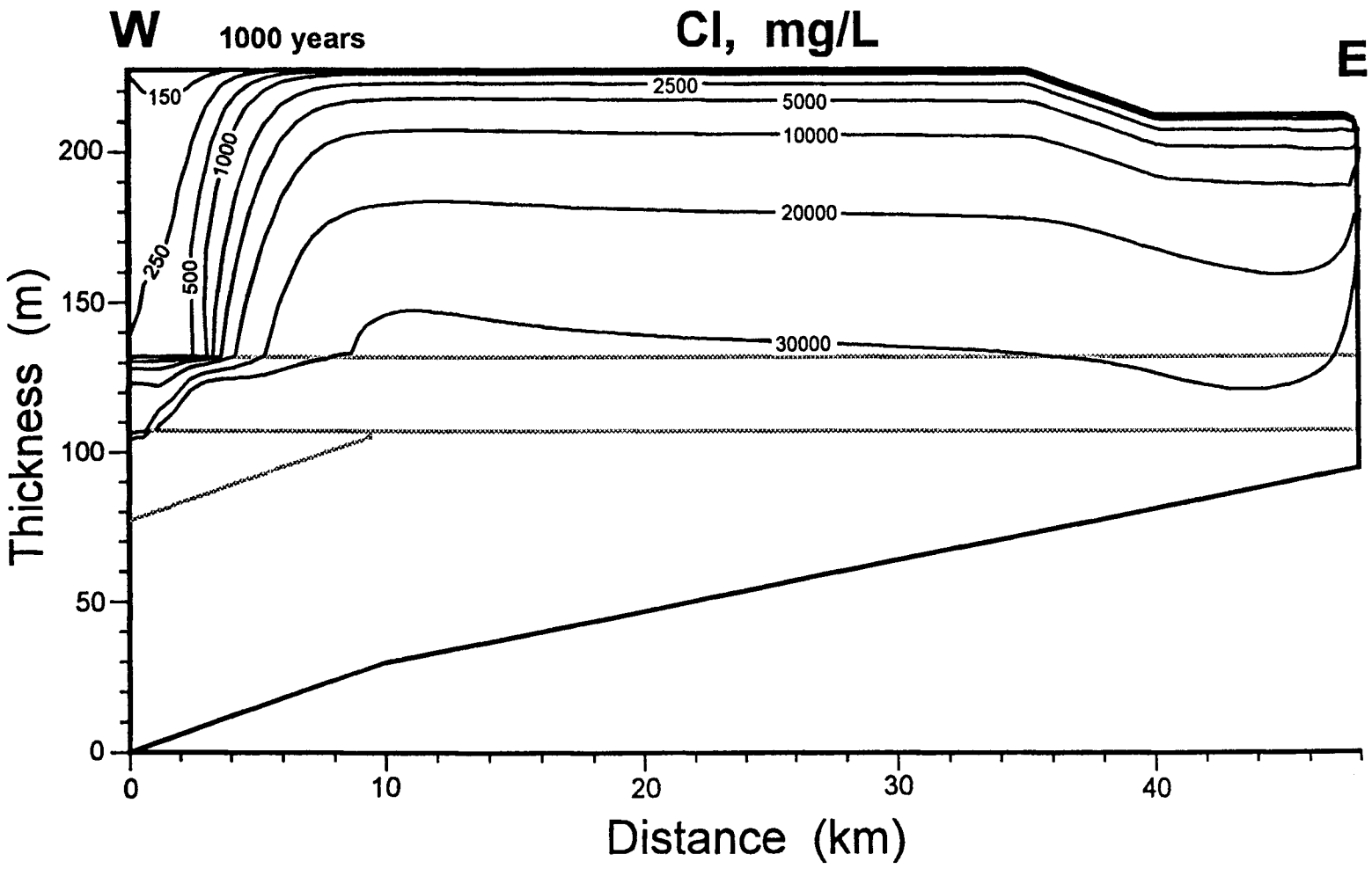

Figure 9.7. Simulated distribution of Cl concentration for the 2-D coupled profile model at 1000 years.

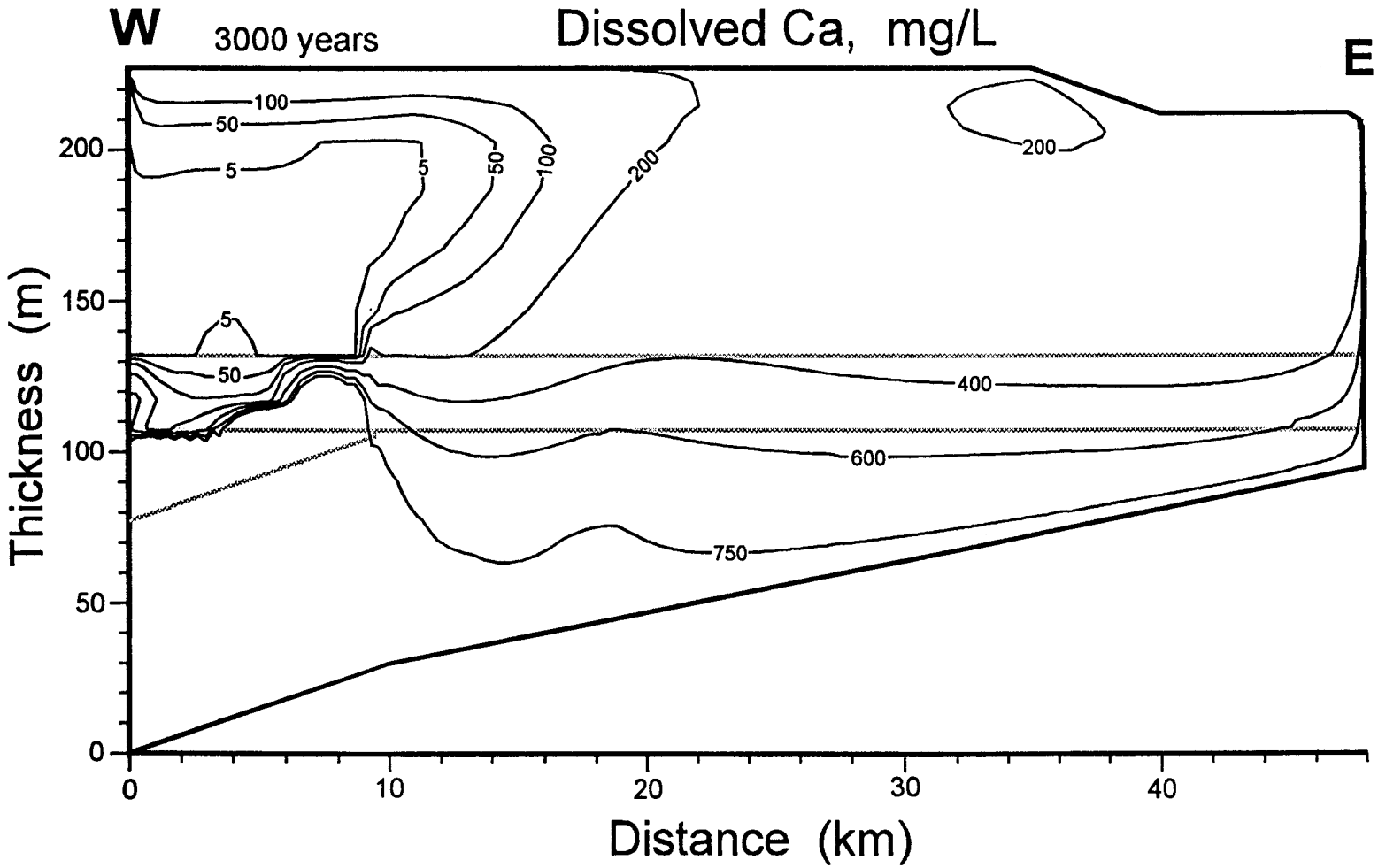

Figure 9.8. Simulated dissolved Ca distribution for the 2-D coupled profile model at 3000 years.

Cation exchange affecting the mixture of overlying recharge from the Upper Cretaceous confining layer and Dakota water occurs in the top part of the Dakota aquifer. The associated reaction is calcite dissolution. Figure 9.9 indicates that dissolution of calcite occurs near the top of the Dakota aquifer where cation exchange is relatively intensive. A small amount of calcite dissolution also occurs across the entire thickness of the Dakota aquifer and extends into the Cedar Hills Sandstone. This might be a result of mixing of all the three different waters. Dissolution of calcite cement caused by cation exchange can be one of the reasons why uncemented sandstone is commonly found in parts of the Dakota aquifer.

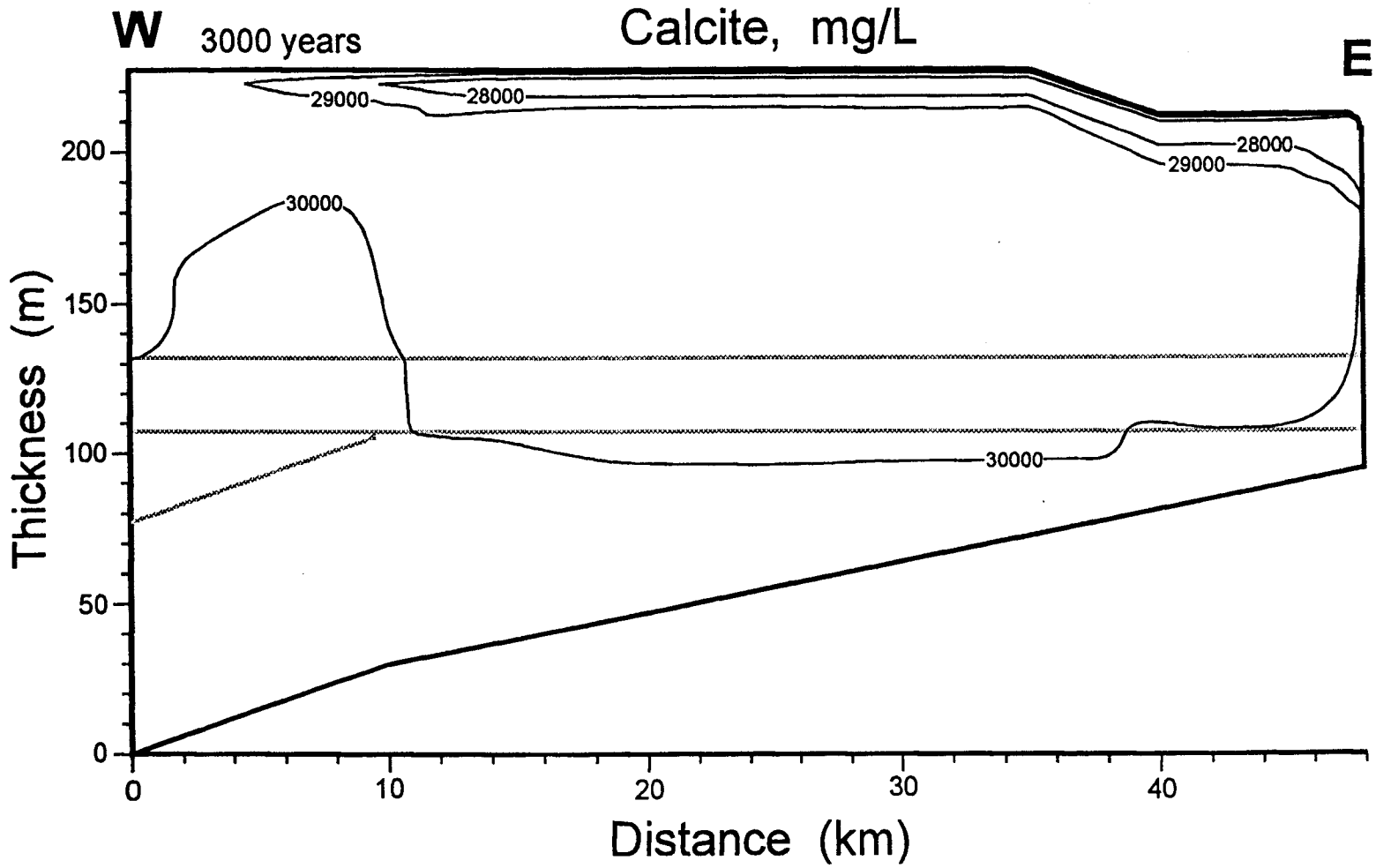

Figure 9.9. Simulated amount of calcite dissolution for the 2-D coupled profile model. The initial calcite concentration is 30,000 mg/L. Contour values smaller than 30,000 mg/L indicate dissolution of calcite has occurred. The unit mg/L for calcite represents the weight of calcite present relative to the pore water volume.

CHAPTER 10
CONCLUSIONS

There are distinct chemical characteristics in different parts of the Dakota aquifer system in central and north-central Kansas (the study area). Saltwater intrusion from the Cedar Hills Sandstone affects the confined Dakota water east of the Cedar Hills subcrop, whereas unconfined Dakota water in the outcrop area is mainly influenced by surface infiltration. Dakota water of Na-mixed-anion type to the west of the Cedar Hills subcrop is generated by cation exchange of Ca^{2+} and Mg^{2+} for Na^{+} on clays and concomitant chemical reactions. Calculations based on a geochemical equilibrium model indicate that most of the confined Dakota and Cedar Hills waters are saturated with respect to calcite. Dissolution of magnesite and anhydrite also occurs in the Cedar Hills Sandstone. Chemical data indicate that oxidation of pyrite occurs near the surface recharge area. Sulfate reduction occurs in the deep confined Dakota aquifer.

Saltwater from the Dakota Formation discharges to the overlying alluvial aquifers of the major river valleys in the study area. Chemical data suggest that the alluvial aquifers are undergoing freshening at shallow depths. Since there is no conspicuous evidence for increasing surface recharge in recent history, it is more likely that the freshening is caused by dilution of the saline water or a decrease in the discharge rate from the Dakota aquifer. Ground-water chemistry in the Greenhorn Limestone in the study area is controlled mainly by calcite dissolution and oxidation of pyrite. Although a small amount of leakage occurs from the Greenhorn Limestone to the underlying Dakota aquifer, the Greenhorn waters do not appear to substantially affect the chemistry of major portions of the aquifer.

The field data and geochemical model calculations provide insufficient information to adequately explain the complex hydrogeochemical reactions that cause changes in the water chemistry. A one-dimensional (1-D) model of coupled flow and chemical reactions shows that the principle of ion chromatography caused by ion exchange can be applied to interpret the chemical evolution of ground waters in the Dakota aquifer system. The chromatographic pattern for cation exchange is more distinct for an aquifer undergoing freshening than salinization because of the relatively large buffering capacity of the exchange media in relation to the salinity of the incoming water. The 1-D model indicates that the chromatographic pattern occurring in the Dakota aquifer due to freshening can be described by three distinct zones. Zone I in the downgradient (east) end contains the initial saltwater and waters in the conservative mixing front. Zone II in the middle of the model contains Na-HCO_3 type water which is a result of cation exchange of Ca^{2+} and Mg^{2+} for Na^+ on clays and calcite dissolution. Zone III in the upstream (west) end can be further divided into two subzones, III_1 and III_2. In zone III, the exchangeable Na^+ is completely desorbed by exchanging with Ca^{2+} and Mg^{2+} and is carried downgradient. In zone III_2, the formation materials are in equilibrium with the incoming freshwater. In zone III_1, the charge balance requires the dissolved Mg concentration to increase to compensate the charge deficiency due to the slow movement of the Ca retardation front.

Numerical sensitivity analyses show that the water chemistry is not substantially affected by the properties of formation materials relative to cation exchange. Variation in selectivity coefficients of the exchanging cations does not significantly affect the water chemistry but does change the adsorbed cation concentrations. The cation exchange capacity

(CEC) affects the velocities of the sharp fronts and the length of zone II. However, when the CEC is large enough to provide sufficient buffering capacity, variation of CEC does not appreciably affect the dissolved chemical composition in the plateau zone (zone II).

The concentrations of exchanging cations in zone II are mainly controlled by the salinity of the flushing (incoming) water and the difference between the salinities of the incoming water and initial saltwater. In contrast, the cation ratios in the same zone are primarily regulated by the adsorbed composition of the surface sites which were in equilibrium with the previous saltwater. Since the cation ratios in zone II must adapt to the chemical conditions of the exchange medium surfaces produced when in contact with the previous saltwater regardless of the salinity of the incoming water, the fresher the incoming water, the lower are the dissolved Ca and Mg concentrations in the softened water. If the adsorption properties of the aquifer materials remain relatively constant in a ground-water system, the salinity of the previous water can be estimated by using the dissolved cation ratios in zone II and water chemistry data with a salinity range extending above and below that of the possible previous saltwater. The estimated TDS content for the former brackish water in the upper part of the west confined Dakota aquifer ranges from 5,000 to 10,000 mg/L.

Both field data and 1-D model results indicate that more Mg than Ca is adsorbed at the early stage of mixing in zone I. Dilution of the initial saltwater causes the ionic strength of the solution to change which affects the activity coefficient of the exchanging cations differently. Therefore, the cation activity ratios change and cation exchange occurs in the diluted solution. In the first half of the mixing front, the Mg concentration is greater than Ca in the mixed water because the concentration of Mg is larger than Ca in the initial saltwater. Despite the lower

selectivity coefficient of Mg than Ca, Mg is able to replace most of the Na on surface exchange sites because of its higher dissolved concentration than Ca. As a result, Mg is adsorbed at a greater rate in the mixing front. The magnitude of the maximum amount of cation exchange at the center of the mixing front depends upon the salinity of the initial water and the intensity of cation exchange caused by the salinity contrast of the two mixing waters.

The 1-D conceptual model is valuable for explaining major hydrogeochemical processes in the Dakota aquifer, particularly the relationships of mixing, cation exchange reactions, and calcite dissolution/precipitation. The numerical model indicates that most chemical reactions, i.e., cation exchange and calcite dissolution, occur along the conservative mixing front and in the vicinity of the retardation front. The plateau zone between these two fronts is in a temporary stable condition where little cation exchange occurs to affect major constituent chemistry. The model also suggests that cation exchange is the dominant factor controlling the cation ratios of water in zone II despite the simultaneous occurrence of calcite dissolution.

Chemical data based on ground-water samples from the Dakota aquifer show that the mixing process in the aquifer system is more complicated than simulated by the numerical model. The chemistry data suggest that the previous saltier water in the Dakota aquifer was not uniformly distributed. A concentration gradient is believed to have existed in the past analogous to that in the current aquifer. In a large part of the confined Dakota to the east of the Cedar Hills subcrop, a freshening process is not prominent due to a continuous supply of saltwater from the Cedar Hills aquifer. In comparison, water in the west confined Dakota aquifer is substantially affected by the cation exchange of Ca^{2+} and Mg^{2+} for Na^{+} on clays.

The two-dimensional semi-empirical model, simulating chemical changes across the zone of saltwater intrusion from the Cedar Hills Sandstone, can be used to further explain the chemical changes in the Dakota aquifer, especially in the vertical direction. The intrusion of Cedar Hills saltwater is mainly controlled by the vertical hydraulic conductivity and dispersivity of the lower Dakota aquifer and Cedar Hills Sandstone. Meanwhile, the amount of recharge from the overlying Upper Cretaceous aquitard is controlled by the vertical hydraulic conductivity of the upper Dakota aquifer. Before the retardation fronts of exchanging cations from the west reach the model domain, the most important reactions occurring in the system are cation exchange reactions caused by the recharge from the overlying Upper Cretaceous confining layer, and concomitant calcite dissolution occurring near the top of the Dakota aquifer. Considering the small recharge rates from above, the impact of the overlying recharge on the Dakota aquifer is remarkable. The occurrence of calcite dissolution would increase the local permeability and could be a reason for the uncemented sandstone found in parts of the Dakota aquifer.

The coupled hydrogeochemical models can interpret the complex flow and chemical reaction problem more relevantly than separate geochemical and mass transport models. For example, the feature of ion chromatography caused by cation exchange cannot be described by either the geochemical or mass transport models. Although only limited functions are available for the existing coupled hydrogeochemical models, far more problems can be solved by this type of model than other kinds of models. Further development of more complicated models, i.e., with consideration of aquifer heterogeneity, could be applied to the Dakota aquifer to further interpret the complexities of the aquifer system.

REFERENCES

Andrews, J. N., J.-C. Fontes, J.-F. Aranyossy, A. Dodo, W. M. Edmunds, A. Joseph, and Y. Travi, 1994, The evolution of alkaline groundwaters in the continental intercalaire aquifer of the Irhazer Plain, Niger: Water Resources Research, Vol. 30, No. 1, pp. 45-61.

Angino, E. E., C. K. Bayne, and J. Halepaska, 1972, Preliminary geological investigations of supplemental radioactive waste repository areas in the state of Kansas: Kansas Geological Survey, 95 pages.

Appelo, C. A. J., 1994a, Cation and proton exchange, pH variations, and carbonate reactions in a freshening aquifer: Water Resources Research, Vol. 30, No. 10, pp. 2793-2806.

Appelo, C. A. J., 1994b, Some calculations on multicomponent transport with cation exchange in aquifers: Ground Water Vol. 32, No. 6, pp. 968-975.

Appelo, C. A. J. and D. Postma, 1994, *Geochemistry, groundwater and pollution*: Balkema Publishers, Brookfield, Vermont, 536 pages.

Appelo, C. A. J., J. H. Hendriks, and M. Van Veldhuizen, 1993, Flushing factors and a sharp front solution for solute transport with multicomponent ion exchange: Journal of Hydrology, Vol. 146, pp. 89-113.

Appelo, C. A. J., A. Willemsen, H. E. Beekman, and J. Griffioen, 1990, Geochemical calculations and observations on salt water intrusions, II. Validation of a geochemical model with column experiments: Journal of Hydrology, Vol. 120, pp. 225-250.

Appelo, C. A. J. and A. Willemsen, 1987, Geochemical calculations and observations on salt water intrusions, I. a combined geochemical/mixing cell model: Journal of Hydrology, Vol. 94, pp. 313-330.

Atkinson, R. J., A. M. Posner, and J. P. Quirk, 1967, Adsorption of potential-determining ions at the ferric oxide-aqueous electrolyte interface: Journal of Physical Chemistry, Vol. 71, pp. 550-558.

Bahr, J. M., 1990, Kinetically influenced terms for solute transport affected by heterogeneous and homogeneous classical reactions: Water Resources Research, Vol. 26, No.1, pp. 21-34.

Bahr, J. M. and J. Rubin, 1987, Direct comparison of kinetic and local equilibrium formulations for solute transport affected by surface reactions: Water Resources Research, Vol. 23, pp. 438-452.

Bayne, C. K. and D. Brinkley, 1972, Geology, hydrology, thickness and quality of salt at three alternative sites for disposal of radioactive waste in Kansas: University of Kansas, Center for Research, Inc., 63 pages.

Bayne, C. K. and K. L. Walters, 1959 Geology and ground-water resources of Cloud county, Kansas: Kansas Geological Survey, Bulletin 139, 144 pages.

Bayne, C. K., P. C. Franks, and W. Ives, Jr., 1971, Geology and ground-water resources of Ellsworth county, central Kansas: Kansas Geological Survey, Bulletin 201, 84 pages.

Bear, J. and A. Verruijt, 1987, *Modeling groundwater flow and pollution*: D. Reidel Publishing Company, Boston, 414 pages.

Benick, B. C., 1924, Base exchange in ground water by silicates as illustrated in Montana: U. S. Geological Survey, Water Supply Paper 520-D, pp. 53-72.

Berry, D. W., 1952, Geology and ground-water resources of Lincoln county, Kansas: Kansas Geological Survey, Bulletin 95, 96 pages.

Bjerg, P. L., H. C. Ammentorp, and T. H. Christensen, 1993, Model simulations of a field experiment of cation exchange-affected multicomponent solute transport in a sandy aquifer: Journal of Contaminant Hydrology, Vol. 12, pp. 291-311.

Bolland, M. D. A., A. M. Posner, and J. P. Quirk, 1976, Surface charge on kaolinites in aqueous suspension: Australia Journal of Soil Research, Vol. 14, pp. 197-216.

Bolt, G. H., 1979, Soil chemistry, B. physical-chemical models: Developments in Soil Science 5B, Elsevier Scientific Publishing Company, 479 pages.

Boyle, D. R., 1992, Effect of base exchange softening on fluoride uptake in groundwaters of the Moncton Sub-Basin, New Brunswick, Canada: *in* Kharaka, Y. K. and A. S. Maest (eds.), Proceedings of the 7th International Symposium on Water-Rock Interaction, Park City, Utah. Vol. 1. Low temperature environments. Balkema Publishs, Rotterdam. pp. 771-774.

Bruggenwert, M. G. M. and A. Kamphorst, 1979, Survey of experimental information on cation exchange in soil systems: *in* Bolt, G. H. (ed.) Soil Chemistry B. Physico-chemical models, Developments in soil science 5B, pp. 141-203. Elsevier Scientific Publishing Company.

Bryant, S. L., R. S. Schechter, and L. W. Lake, 1986, Interactions of precipitation/dissolution waves and ion exchange in flow through permeable media: AIChE Journal, Vol. 32, No. 5, pp. 751-764.

Bryant, S. L., R. S. Schechter, and L. W. Lake, 1987, Mineral sequences in precipitation/dissolution waves: AIChE Journal, Vol. 33, No. 8, pp. 1271-1287.

Burt, R. A., 1993, Ground-water chemical evolution and diagenetic processes in the Upper Floridan Aquifer, southern South Carolina and northeastern Georgia: U. S. Geological Survey, Water-Supply Paper 2392, 76 pages.

Carroll-Webb, S. A. and J. V. Walther, 1988, A surface complex reaction model for the pH-dependence of corundum and kaolinite dissolution rates: Geochimica et Cosmochimica Acta, Vol. 52, pp. 2609-2623.

Ceazan, M. L., E. M. Thurman, and R. L. Smith, 1989, Retardation of ammonium and potassium transport through a contaminated sand and gravel aquifer: the role of cation exchange: Environmental Science and Technology, Vol. 23, No. 11, pp. 1402-1408.

Cederberg, G. A., R. L. Street, and J. O. Leckie, 1985, A groundwater mass transport and equilibrium chemistry model for multicomponent systems: Water Resources Research, Vol. 21, No. 8, pp. 1095-1104.

Champ, D. R., J. Gulens, and R. E. Jackson, 1979, Oxidation-reduction sequences in ground-water flow system: Canadian Journal of Earth Science, Vol. 16, No. 1, pp. 12-23.

Chapelle, F. H., 1983, Groundwater geochemistry and calcite cementation of the Aquia aquifer in southern Maryland: Water Resources Research, Vol. 19, No. 2, pp. 545-558.

Chapelle, F. H. and L. L. Knobel, 1983, Aqueous geochemistry and the exchangeable cation composition of glauconite in the Aquia aquifer, Maryland: Ground Water, Vol. 21, No. 3, pp. 343-352.

Chapelle, F. H. and L. L. Knobel, 1985, Stable carbon isotopes of HCO_3^- in the Aquia aquifer, Maryland: evidence for an aquifer-generated source of CO_2: Ground Water, Vol. 23, No. 5, pp. 592-599.

Charbeneau, R. J., 1981, Groundwater contaminant transport with adsorption and ion exchange chemistry: method of characteristics for the case without dispersion: Water Resources Research, Vol. 17, No. 3, pp. 705-713.

Charbeneau, R. J., 1988, Multicomponent exchange and subsurface solute transport: characteristics, coherence, and the Riemann problem: Water Resources Research, Vol. 24, No. 1, pp. 57-64.

Combes, J. and H. R. Feldman, 1993, Valley fill deposits of the Cretaceous Dakota sequences comprising a major aquifer system in Kansas: *in* Archer et al. (eds.), Incised paleovalleys of the Douglas Group in northeastern Kansas: field guide and related contributions: Kansas Geological Survey, Open-file Report 93-24, pp. 16.1-16.6.

Deist, J. and O. Talibudeen, 1967, Ion exchange in soil from the ion pairs K-Ca, K-Rb and K-Na: Journal of Soil Science, Vol. 18, pp. 125-137.

Delhomme E. K. and F. Giannesini, 1979, Reservoir description techniques improve simulation results in Hassi-Messaoud Field, Alegria: Society of Petroleum Engineers (SPE) Paper No. 8435, presented at the 45th Annual Technical Conference and Exhibition of the SPE in Las Vegas, Nevada, Sep 23-26, 1979.

DeVault, D., 1943, The theory of chromatography: Journal of American Chemical Society, Vol. 65, pp. 532-540.

Domenico, P. A. and F. W. Schwartz, 1990, *Physical and chemical hydrogeology*: John Wiley & Sons, Inc., New York, 824 pages.

Dria, M. A., S. L. Bryant, R. S. Schechter, and L. W. Lake, 1987, Interacting precipitation/dissolution waves: the movement of inorganic contaminants in groundwater: Water Resources Research, Vol. 23, No. 11, pp. 2076-2090.

Fader, S. W., 1968, Ground-water in the Republic River area, Cloud, Jewell, and Republic counties, Kansas: Kansas Geological Survey, Bulletin 188, 27 pages.

Ferris, A. P. and W. P. Jepson, 1975, The exchange capacities of kaolinite and the preparation of homoionic clays: Journal of Colloid Interface Science, Vol. 51, pp. 245-259.

Fishel, V. C. and A. R. Leonard, 1955, Geology and ground-water resources of Jewell county, Kansas: Kansas Geological Survey, Bulletin 115, 152 pages.

Franks, P. C., 1966, *Petrology and stratigraphy of the Kiowa and Dakota formations (basal Cretaceous), north-central Kansas*: Unpublished Ph. D. dissertation, Department of Geology, University of Kansas, 312 pages.

Franks, P. C., 1975, The transgressive-regressive sequence of the Cretaceous Cheyenne, Kiowa, and Dakota Formations of Kansas: The Geological Association of Canada, Special Paper No. 13, pp. 469-521.

Franks, P. C., 1979, Paralic to fluvial record of an early Cretaceous marine transgression - Longford Member, Kiowa Formation, north-central Kansas: Kansas Geological Survey, Bulletin 219, 55 pages.

Freeze, A. R. and J. A. Cherry, 1979, *Groundwater*: Prentice-Hall, Englewood Cliffs, New Jersey, 604 pages.

Friedly, J. C. and J. Rubin, 1992, Solute transport with multiple equilibrium-controlled or kinetically controlled chemical reactions: Water Resources Research, Vol. 28, No. 6, pp. 1935-1953.

Frye, J. C. and J.J Brazil, 1943, Ground water in the oil field areas of Ellis and Russell counties, Kansas: Kansas Geological Survey, Bulletin, No. 50, 104 pages.

Gaines, G. L. and H. C. Thomas, 1953, Adsorption studies on clay minerals. II. A formulation of the thermodynamics of exchange adsorption: Journal of Chemical Physics, Vol. 21, pp. 714-718.

Gao, H. W., H. Y. Sohn, and M. E. Wadworth, 1981, A mathematical model for the in situ leaching of primary copper ore: *in* W. J. Schlitt and J. B. Hiskey (eds.), Interfacing technologies in solution mining, Proceedings of the 2nd SME/SPE International Solution Mining Symposium, Denver.

Gapon, E. N., 1933, Theory of exchange adsorption in soils (in Russian): Journal of General Chemistry USSR, No. 3, pp. 144-152.

Garrels, R. M. and F. T. Mackenzie, 1967, Origin of the chemical compositions of some springs and lakes: *in* Gould, R. F. (ed.) Equilibrium Concepts in Natural Water Systems, pp. 222-242, American Chemical Society, Washington D. C.

Gaston, L. A. and H. M. Selim, 1990, Transport of exchangeable cations in a aggregated clay soil: Soil Science Society of America Journal, Vol. 54, No. 1, pp. 31-38.

Gaston, L. A. and H. M. Selim, 1991, Predicting cation mobility in kaolinitic media based on exchange selectivities of kaolinite: Soil Science Society of America Journal, Vol. 55, pp. 1255-1261.

Gelhar, L. W., C. Welty, and K. R. Rehfeldt, 1992, A critical review of data on field-scale dispersion in aquifers: Water Resources Research, Vol. 28, No. 7, pp. 1955-1974.

Gogel, T., 1981, Discharge of saltwater from Permian rocks to major stream-aquifer systems in central Kansas: Kansas Geological Survey, Chemical Quality Series No. 9, pp. 60 pages.

Gregor, J. E. and H. K. J. Powell, 1988, Protonation reactions of fulvic acids: Journal of Soil Science, Vol. 39, pp. 243-252.

Griffioen, J., 1992, Buffering of pH-changes by an aquifer sediment during miscible displacement of Na-Ca-Mg-Cl-CO_2 solutions: *in* Kharaka, Y. K. and A. S. Maest (eds.), Water-rock interaction, Vol. 1, low temperature environments, Proceedings of the 7th International Symposium on Water-Rock Interaction, pp. 45-49.

Griffioen, J., 1993, Multicomponent cation exchange including alkalinization/acidification following flow through sandy sediment: Water Resources Research, Vol. 29, No. 9, pp. 3005-3019.

Griffioen, J. and C. A. J. Appelo, 1993, Adsorption of calcium and its complexes by two sediments in calcium-hydrogen-chlorine-carbon dioxide systems: Soil Science Society of America Journal, Vol. 57, No. 3, pp. 716-722.

Grove, D. B. and W. W. Wood, 1979, Prediction and field verification of subsurface-water quality change during artificial recharge, Lubbork, Texas: Ground Water, Vol. 17, No. 3, pp. 250-257.

Haldorson, H. H., 1983, *Reservoir characterization procedures for numerical simulation*: Unpublished doctoral dissertation, University of Texas at Austin, 556 pages.

Hamilton, V. J., 1989, *Stratigraphic sequences and hydrostratigraphic units in Lower Cretaceous strata, Kansas*: Unpublished master thesis, Department of Geology and Geological Engineering, Colorado School of Mines, 165 pages.

Harshman, E. N., 1966, Genetic implications of some elements associated with uranium deposits, Shirely Basin, Wyoming: U. S. Geological Survey, Professional Paper 550-C, pp. C167-C173.

Hattin, D. E., 1965, Stratigraphy of the Graneros Shale (Upper Cretaceous) in central Kansas: Kansas Geological Survey, Bulletin 178, 83 pages.

Hattin, D. E., 1975, Stratigraphy and depositional environment of Greenhorn Limestone (Upper Cretaceous) of Kansas: Kansas Geological Survey, Bulletin 209, 128 pages.

Hattin, D. E. and C. T. Siemers, 1987, Guidebook Upper Cretaceous stratigraphy and depositional environments of western Kansas: Kansas Geological Survey, Guidebook Series 3, 55 pages.

Helfferich, F. G., 1989, The theory of precipitation/dissolution waves: AIChE Journal, Vol. 35, No. 1, pp. 75-87.

Helfferich, F. G. and G. Klein, 1970, *Multicomponent chromatography: theory of interference*: M. Dekker, New York, 419 pages.

Helgeson, H. C., 1969, Thermodynamics of hydrothermal systems at elevated temperatures and pressures: American Journal of Science, Vol. 267, pp. 729-804.

Helgeson, H. C., R. M. Garrels, and F. T. Mackenzie, 1969, Evaluation of irreversible reactions in geochemical processes involving minerals and aqueous solutions - II. applications: Geochimica et Cosmochimica Acta, Vol. 33, pp. 455-481.

Helgeson, H. C., D. H. Kirkham, and G. C. Flowers, 1981, Theoretical prediction of the thermodynamic behavior of aqueous electrolytes at high pressures and temperatures: IV. calculation of activity coefficients, osmotic coefficients, and apparent molal and standard and relative partial molal properties to 600 °C and 5 KB: American Journal of Science, Vol. 281, pp. 1249-1516.

Hem, J. D., 1985, Study and interpretation of the chemical characteristics of natural water: U. S. Geological Survey, Water-Supply Paper 2254, 263 pages.

Hesse P. R., 1972, *A textbook of soil chemical analysis*: Chemical Publishing Co., New York. 520 pages.

Hodson, W. G., 1959, Geology and ground-water resources of Mitchell county, Kansas: Kansas Geological Survey, Bulletin, No. 140, 132 pages.

Hodson, W. G., 1965, Geology and ground-water resources of Trego County, Kansas: Kansas Geological Survey, Bulletin, No. 174, 80 pages.

Holdoway, K. A., 1978, Deposition of evaporites and red beds of the Nippewalla Group, Permian, western Kansas: Kansas Geological Survey, Bulletin 215, 43 pages.

Hostetler, C. J., R. L. Erikson, 1989, FASTCHEM^{TM} package, Volume 5: user's guide to the EICM coupled geohydrochemical transport code: Electric Power Research Institute, EPRI EA-5870-CCM, Vol. 5, Palo Alto, CA.

Hostetler, P. B. and R. M. Garrels, 1962, Transportation and precipitation of uranium and vanadium at low temperatures, with special reference to sandstone type uranium deposits: Economic Geology, Vol. 57, No.2, pp. 137-167.

Howard, K. W. F. and J. W. Lloyd, 1983, Major ion characterization of coastal saline ground waters: Ground Water, Vol. 21, No. 4, pp. 429-437.

Hutchinson, C. A., Jr., C. F. Dodge, and T. L. Polasek, 1961, Identification, Classification and Prediction of reservoir nonuniformities affecting production operations: Journal of Petroleum Technology, Vol. XIII, No. 3, pp. 223-230.

Jackson, R. E. and R. J. Patterson, 1982, Interpretation of pH and Eh trends in a fluvial-sand aquifer system: Water Resources Research, Vol. 18, No. 4, pp. 1255-1268.

James, G. W., 1972, Mineralogy and distribution of water-insolvable residues from AEC Test Hole 5: *in* Bayne, C. K. and D. Brinkley (eds.), Geology, hydrology, thickness and quality of salt at three alternative sites for disposal of radioactive waste in Kansas: University of Kansas, Center for Research, Inc., pp. 50-57.

Jennings, A. A., D. J. Kirkner, and T. L. Theis, 1982, Multicomponent equilibrium chemistry in groundwater quality models: Water Resources Research, Vol. 18, No. 4, pp. 1089-1096.

Jensen, H. E. and K. L. Babcock, 1973, Cation exchange equilibria on a Yolo loam: Hilgardia, Vol. 41, pp. 475-488.

Jones, C. L., 1965, Petrography of evaporites from the Wellington Formation near Hutchinson, Kansas: U. S. Geological Survey, Bulletin 1202 -A, 69 pages.

Keller, C. K., 1991, Hydrogeochemistry of a clayey till, 2, source of CO_2: Water Resources Research, Vol. 27, No. 10, pp. 2555-2564.

Keller, C. K., G. van der Kamp, and J. A. Cherry, 1991, Hydrogeochemistry of a clayey till, 1, spatial variability: Water Resources Research, Vol. 27, No. 10, pp. 2543-2554.

Kenoyer, G. J. and C. J. Bowser, 1992a, Groundwater chemical evolution in a sandy silicate aquifer in northern Wisconsin, 1, patterns and rates of change: Water Resources Research, Vol. 28, No. 2, pp. 579-590.

Kenoyer, G. J. and C. J. Bowser, 1992b, Groundwater chemical evolution in a sandy silicate aquifer in northern Wisconsin, 2, reaction modeling: Water Resources Research, Vol. 28, No. 2, pp. 591-600.

Kent, D. B., J. A. Davis, L. C. D. Anderson, B. A. Rea, and T. D. Waite, 1994, Transport of chromium and selenium in the suboxic zone of a shallow aquifer: influence of redox and adsorption reactions: Water Resources Research, Vol. 30, No. 4, pp. 1099-1114.

Kharaka, Y. K., W. D. Gunter, P. K. Aggarwal, E. H. Perkins, and J. D. DeBraal, 1988, SOLMINEQ.88: a computer program for geochemical modeling of water-rock interactions: U. S. Geological Survey, Water-Resources Investigations Report 88-4227, 400 pages.

Kirkner, D. J., H. W. Reeves, and A. A. Jennings, 1984, Finite element analysis of multicomponent contaminant transport including precipitation-dissolution reactions: *in* Laible et al. (eds.), Finite elements in water resources, Proceedings of the 5th International Conference, Burlington, Vermont, pp. 309-318, Springer-Verlag, New York.

Knobel, L. L. and S. W. Phillips, 1988, Aqueous geochemistry of the Magothy aquifer, Maryland: U. S. Geological Survey, Water-Supply Paper No. 2323, 27 pages.

Komarneni, S., 1978, Cesium sorption and desorption behavior of kaolinites: Soil Science Society of America Journal, Vol. 42, pp. 531-532.

Kotrlý, S and L. Šucha, 1985, *Handbook of chemical equlibria in analytical chemistry*: John Wiley & Sons, 414 pages.

Krebs, R., M. Sardin, and D. Schweich, 1987, Mineral dissolution, precipitation, and ion exchange in surfactant flooding: AIChE Journal, Vol. 33, No. 8, pp. 1371-1378.

Langmuir, D., 1971, The geochemistry of some carbonate groundwaters in central Pennsylvania: Geochimica et Cosmochimica Acta, Vol. 35, pp. 1023-1045.

Lee, W, C. Leatherock, and T. Botinelly, 1948, The stratigraphy and structural development of the Salina Basin of Kansas: Kansas Geological Survey, Bulletin 74, 155 pages.

Leonard, A. R. and D. W. Berry, 1961, Geology and ground-water resources of southern Ellis County and parts of Trego and Rush counties, Kansas: Kansas Geological Survey, Bulletin 149, 156 pages.

Levy, G. J., H. V. H. Van der Watt, I. Shainberg, and H. M. Du Plessis, 1988, Potassium-calcium and sodium-calcium exchange on kaolinite and kaolinitic soils: Soil Science Society of America Journal, Vol. 52, pp. 1259-1264.

Levy, R. and I. Shainberg, 1972, Calcium-magnesium exchange in montmorillonite and vermiculite: Clays and Clay Minerals, Vol. 20, No. 1, pp. 37-46.

Lewis, F. M., Voss, C. L., and J. Rubin, 1986, Numerical simulation of advective-dispersive multisolute transport with sorption, ion exchange, and equilibrium chemistry: U S. Geological Survey, Water-Resources Investigations Report 86-4022, 165 pages.

Lim, C. H., M. L. Jackson, R. D. Koons, and P. A. Helmke, 1980, Kaolins: Sources of differences in cation-exchange capacities and cesium retention: Clays and Clay Minerals, Vol. 28, pp. 223-229.

Macfarlane, P. A., J. H. Doveton, H. R. Feldman, J. J. Butler, Jr., J. M. Combes, and D. R. Collins, 1994, Aquifer/aquitard units of the Dakota aquifer system in Kansas: methods of delineation and sedimentary architecture effects on ground-water flow and flow properties: Journal of Sedimentary Research, Vol. B64, No. 4, pp. 464-480.

Macfarlane, P. A., H. Jayatilake, and S. Yoder, 1995a, Potentiometric surface of the Dakota aquifer (map): Kansas Geological Survey.

Macfarlane, P. A., H. Jayatilake, and S. Yoder, 1995b, Bottom configuration of the Dakota aquifer (map): Kansas Geological Survey.

Macfarlane, P. A., H. Jayatilake, and S. Yoder, 1995c, Top configuration of the Dakota aquifer (map): Kansas Geological Survey.

Macfarlane, P. A., M. S. Townsend, D. O. Whittemore, J. H. Doveton, and M. Staton, 1988, Hydrogeology and water chemistry of the Great Plains (Dakota, Kiowa, and Cheyenne) and Cedar Hills aquifers in central Kansas - end of contract report: Kansas Geological Survey, Open-File Report 88-39, 184 pages.

Macfarlane, P. A., A. Wade, J. H. Doveton, and V. J. Hamilton, 1991b, Revised Stratigraphic interpretation and implications for pre-Graneros paleogeography from test-hole drilling in central Kansas: Kansas Geological Survey, Open-file Report 91-1A, 73 pages.

Macfarlane, P. A, D. O. Whittemore, M. A. Townsend, J. J. Butler, Jr., J. H. Doveton, V. J. Hamilton, J. Coleman, T.-M. Chu, A. Wade, and G. L. Macpherson, 1991a, The Dakota Aquifer program - annual report, FY90: Kansas Geological Survey, Open-File Report 91-1, 42 pages.

Macfarlane, P. A, D. O. Whittemore, M. A. Townsend, J. H. Doveton, V. J. Hamilton, W. G. Coyle III, A. Wade, G. L. Macpherson, and R. D. Black, 1990, The Dakota Aquifer program: annual report, FY89: Kansas Geological Survey, Open-File Report 90-27, 301 pages.

Mack, L. E., 1962, Geology and ground-water resources of Ottawa county, Kansas: Kansas Geological Survey, Bulletin 154, 145 pages.

Macpherson, G. L., 1990, Chemical trends along ground-water flow paths, Cretaceous Dakota Formation aquifer, Kansas (abstract): Geological Society of American, Abstract with Programs, Vol. 22, No.7, p. 295.

Mansell, R. S., W. J. Bond, and S. A. Bloom, 1993, Simulating cation transport during water flow in soil: two approaches: Soil Science Society of America Journal, Vol. 57, pp. 3-9.

Mansell, R. S., S. A. Bloom, H. M. Selim, and R. D. Rhue, 1988, Simulated transport of multiple cations in soil using variable selectivity coefficients: Soil Science Society of America Journal, Vol. 52, pp. 1533-1540.

Mayo, A. L., P. J. Nielsen, M. Loucks, and W. H. Brimhall, 1992, The use of solute and isotopic chemistry to identify flow patterns and factors which limit acid mine drainage in the Wasatch Range, Utah: Ground Water, Vol. 30, No. 2, pp. 243-249.

Mazor, E., J. I. Drever, J. Finley, P. W. Huntoon, and D. A. Lundy, 1993, Hydrochemical implications of groundwater mixing: an example from the Southern Laramie Basin, Wyoming: Water Resources Research, Vol. 29, No. 1, pp. 193-205.

McMahon, P. B., D. F. Williams, and J. T. Morris, 1990, Production and carbon isotopic composition of bacterial CO_2 in deep coastal plain sediments of South Carolina: Ground Water Vol. 28, No. 5, pp. 693-702.

Means, J. L., D. A. Crerar, and J. O. Duguid, 1978, Migration of radioactive wastes: Radionuclide mobilization by complexing agents: Science, Vol. 200, pp. 1477-1481.

Mercado, A., 1977, The kinetics of mineral dissolution in carbonate aquifers as a tool in hydrologic investigation, (II) hydrogeochemical models: Journal of Hydrology, Vol. 35, pp. 365-384.

Mercado, A., 1985, The use of hydrogeochemical patterns in carbonate sand and sandstone aquifers to identify intrusion and flushing of saline water: Ground Water, Vol. 23, No. 5, pp. 635-645.

Merriam, D. F., 1957, Preliminary regional structural contour map on top of the Dakota Formation (Cretaceous) in Kansas (1:633600 map): Kansas Geological Survey, Oil and Gas Investigations, No. 15.

Merriam, D. F., W. R. Atkinson, P. C. Franks, N. Plummer, and F. W. Preston, 1959, Description of a Dakota (Cretaceous) core from Cheyenne County, Kansas: State Geological Survey of Kansas, Bulletin 134, Part 1, pp. 1-104.

Miller, C. W. and L. V. Benson, 1983, Simulation of solute transport in a chemically reactive heterogeneous systems: model development and application: Water Resources Research, Vol. 19, No. 2, pp. 381-391.

Nesbitt, H. W. and G. M. Young, 1984, Prediction of some weathering trends of plutonic and volcanic rocks based on thermodynamic and kinetic considerations: Geochimica et Cosmochimica Acta, Vol. 48, pp. 1523-1534.

Norton, G. H., 1939, Permian redbeds of Kansas: American Association of Petroleum Geologists Bulletin, Vol. 23, No. 12, pp. 1751-1819.

Novak, C. F., R. S. Schechter, and L. W. Lake, 1988, Rule-based mineral sequences in geochemical flow processes: AIChE Journal, Vol. 34, No. 10, pp. 1607-1614.

Paces, T., 1973, Steady-state kinetics and equilibrium between ground water and granitic rock: Geochimica et Cosmochimica Acta, Vol. 37, pp. 2641-2663.

Paces, T., 1983, Rate constants of dissolution derived from the measurements of mass balance in hydrological catchments: Geochimica et Cosmochimica Acta, Vol. 47, pp. 1855-1864.

Parks, G. A., 1967, Surface chemistry of oxides in aqueous systems: *in* Stumm, W. (ed.), Equilibrium concepts in aqueous systems, Advanced Chemistry Series No. 67, American Chemistry Society, pp. 121-160.

Perdue, E. M. and C. R. Lytle, 1983, Distribution model for binding of protons and metal ions by humic substances: Environmental Science and Technology, Vol. 17, pp. 654-660.

Plummer, L. N., J. F. Busby, R. W. Lee, and B. B. Hanshaw, 1990, Geochemical modeling of the Madison Aquifer in parts of Montana, Wyoming, and South Dakota: Water Resources Research, Vol. 26, No. 9, pp. 1981-2014.

Plummer, N. V., C. S. Edmonds, and M. P. Bauleke, 1963, Test-hole exploration for light-firing clay in Cloud and Ellsworth counties, Kansas: Kansas Geological Survey, Bulletin 165, part 3, 47 pages.

Plummer, N. V. and Romary, J. F., 1942, Stratigraphy of the pre-Greenhorn Cretaceous beds of Kansas: Kansas Geological Survey, Bulletin 41, pp. 313-348.

Plummer, N. V. and Romary, J. F., 1947, Kansas Clay, Dakota Formation: Kansas Geological Survey, Bulletin 67, 241 pages.

Plummer, N. V., A. Swineford, R. T. Runnels, and J. A. Schleicher, 1954, Chemical, petrographic, and ceramic properties of four clays from the Dakota Formation in Kansas: Kansas Geological Survey, Bulletin 109, Part 10, pp. 153-216.

Pope, G. A., L. W. Lake, and F. G. Helfferich, 1978, Cation exchange in chemical flooding: part 1 - basic theory without dispersion: Society of Petroleum Engineers Journal, Vol. 18, No. 6, pp. 418-434.

Prats, M., 1977, The influence of oriented arrays of thin impermeable shale lenses or of high conductivity natural fractures on apparent permeability anisotropy: Journal of Petroleum Technology Vol. 29, No. 10, pp. 1219-1221.

Pratt, P. F., L. D. Whittig, and B. L. Grover, 1962, Effect of pH on the sodium-calcium exchange equilibria in soils: Soil Science Society of America Proceedings, Vol. 26, pp. 227-230.

Rascoe, B., Jr., 1968, Permian system in western Mid-Continent: The Mountain Geologist, Vol. 5, No. 3, pp. 127-138.

Reardon, E. J., J. T. Dance, and J. L. Lolcama, 1983, Field determination of cation exchange properties for calcareous sand: Ground Water, Vol. 21, No. 4, pp. 421-428.

Reed, M. H., 1982, Calculation of multicomponent chemical equilibria and reaction processes in systems involving minerals, gases, and an aqueous phase: Geochimica et Cosmochimica Acta, Vol. 46, pp. 513-528.

Renick, B. C., 1924, Base exchange in ground water by silicates as illustrated in Montana: U. S. Geological Survey, Water-Supply Paper 520-D, pp. 53-72.

Richardson, J. G., D. G. Harris, R. H. Rossen, and G. Van Hee, 1978, The effect of small discontinuous shales on oil recovery: Journal of Petroleum Technology, Vol. 30, No. 11, pp. 1531-1537.

Rieu, M., J. Touma, and H. R. Gheyi, 1991, Sodium-calcium exchange on Brazilian soils: modeling the variation of selectivity coefficients: Soil Science of America Journal, Vol. 55, pp. 1294-1300.

Riffenburg, H. B., 1925, Chemical, character of ground waters of the northern Great Plains: U. S. Geological Survey, Water Supply Paper 560-B, pp. 31-52.

Roberts, P.V., M. N. Goltz, and D. M. MaCkey, 1986, A natural gradient experiment on solute transport in a sand aquifer, 3. retardation estimates and mass balances for organic solutes: Water Resources Research, Vol. 22, No. 13, pp. 2047-2058.

Roberts, P. V., J. E. Schreiner, and G. D. Hopkins, 1982, Field study of organic water quality changes during ground water recharge in the Palo Alto Baylands: Water research, Vol. 16, pp. 1025-1035.

Robinson, B. P., 1962, Ion-exchange minerals and disposal of radioactive wastes - A survey of literature: U. S. Geological Survey, Water-Supply Paper 1616, 132 pages.

Rogers, R. J., 1987, Geochemical evolution of groundwater in stratified-drift and arkosic bedrock aquifers in north central Connecticut: Water Resources Research, Vol. 23, No. 8, pp. 1531-1545.

Rose, W., 1983, A note on the role played by sediment bedding in causing permeability anisotropy: Journal of Petroleum Technology, Vol. 35, No. 2, pp. 330-332.

Rubin, J., 1983, Transport of reacting solutes in porous media: Relation between mathematical nature of problem formulation and chemical natural of reactions: Water Resources Research, Vol. 19, No. 5, pp. 1231-1252.

Rubin, J., and R. V. James, 1973, Dispersion-affected transport of reacting solutes in saturated porous media: Galerkin method applied to equilibrium-controlled exchange in unidirectional steady water-flow: Water Resources Research, Vol. 9, No. 5, pp. 1332-1357.

Schwartz, F. W. and K. Muehlenbachs, 1979, Isotope and ion geochemistry of groundwaters in the Milk River Aquifer, Alberta: Water Resources Research, Vol. 15, No. 2, pp. 259-268.

Schweich, D., M. Sardin, and M. Jauzein, 1993a, Properties of concentration waves in presence of nonlinear sorption, precipitation/dissolution, and homogeneous reactions, 1. fundamentals: Water Resources Research, Vol. 29, No. 3, pp. 723-733.

Schweich, D., M. Sardin, and M. Jauzein, 1993b, Properties of concentration waves in presence of nonlinear sorption, precipitation/dissolution, and homogeneous reactions, 2. illustrative examples: Water Resources Research, Vol. 29, No. 3, pp. 735-741.

Scott, R. W., 1970, Stratigraphy and sedimentary environments of Lower Cretaceous rocks, southern Western Interior: The American Association of Petroleum Geologists Bulletin, Vol. 54, No. 7, pp. 1225-1244.

Selim, H. M., R. Schulin, and H. Fluhler, 1987, Transport and ion exchange of calcium and magnesium in an aggregated soil: Soil Science Society of America Journal, Vol. 51, No. 4, pp. 876-884.

Smith, R. L., B. L. Howes, and J. H. Duff, 1991, Denitrification in nitrate-contaminated groundwater: Occurrence in steep vertical geochemical gradients: Geochimica et Cosmochimica Acta, Vol. 55, No. 7, pp. 1815-1825.

Sparks, D. L., 1986, *Soil physical chemistry*: CRC Press, Inc., Boca Raton, Florida, 308 pages.

Sposito, G., 1981, *The thermodynamics of soil solutions*: Oxford University Press, New Jersey.

Sposito, G., 1989, *The chemistry of soils*: Oxford University Press, Fair Lawn, New Jersey. 277 pages.

Sposito, G., K. M. Holtzclaw, L. Charlet, C. Jouany, and A. L. Page, 1983a, Sodium-calcium and sodium-magnesium exchange in Wyoming bentonite in perchlorate and chloride background ionic media: Soil Science Society of America Journal, Vol. 47, No. 1, pp. 51-56.

Sposito, G., K. M. Holtzclaw, C. Jouany, and L. Charlet, 1983b, Cation selectivity in sodium-calcium, sodium-magnesium, and calcium-magnesium exchange on Wyoming bentonite at 298 K: Soil Science Society of America Journal, Vol. 47, pp. 917-921.

Suarez, D. L. and M. F. Zahow, 1989, Calcium-magnesium exchange selectivity of Wyoming montmorillonite in chloride, sulfate and perchlorate solutions: Soil Science Society of America Journal, Vol. 53, No. 1, pp. 52-57.

Swineford, A., 1947, Cemented sandstones of the Dakota and Kiowa formations in Kansas: Kansas Geological Survey, Bulletin 70, Part 4, pp. 53-104.

Swineford, A., 1955, Petrography of Upper Permian rocks in south-central Kansas: Kansas Geological Survey, Bulletin 111, 179 pages.

Swineford, A. and H. Williams, 1945, The Cheyenne Sandstone and adjacent formations of a part of Russell County, Kansas: Kansas Geological Survey, Bulletin 60, Part 4, pp. 101 - 168.

Thorstenson, D. C., D. W. Fisher, and M. G. Croft, 1979, The geochemistry of the Fox Hills-Basal Hell Creek aquifer in southwestern North Dakota and northwestern South Dakota: Water Resources Research, Vol. 15, No. 6, pp. 1479-1498.

Thurman, E. M., L. B. Barber, and D. LeBlanc, 1986, Movement and fate of detergents in groundwater: a field study: Journal of Contaminant Hydrology, 1 (1986), pp. 143-161.

Totam, T. A., R. S. Schechter, and L. W. Lake, 1981, Factors influencing the in situ acid leaching of uranium ores: *in* W. J. Schlitt and J. B. Hiskey (eds.), Interfacing technologies in solution mining, Proceedings of the 2nd SME/SPE International Solution Mining Symposium, Denver.

Valocchi, A., J., P. V. Roberts, G. A. Parks, and R. L. Street, 1981, Simulation of the transport of ion-exchanging solute using laboratory-determined chemical parameter values: Ground Water, Vol. 19, No. 6, 600-607.

Valocchi, A. J., R. L. Street, and P. V. Roberts, 1981, Transport of ion-exchanging solutes in groundwater: chromatographic theory and field simulation: Water Resources Research, Vol. 17, No. 5, pp. 1517-1527.

Van Ommen, H. C., 1985, The 'mixing cell' concept applied to transport of non-reactive and reactive components in soils and groundwater: Journal of Hydrology, No. 78, pp. 201-213.

Vanselow, A. P., 1932, Equilibria of the base-exchange reactions of bentonites, permutites, soil colloids and zeolites, Soil Science, Vol. 33, pp. 95-113.

Wade, A., 1992, *Ground-water flow systems and the water-resources potential of the Dakota aquifer in a two-county area in north-central Kansas*: Unpublished master thesis, Department of Geology, University of Kansas. 158 pages.

Walsh, M. P., S. L. Bryant, R. S. Schechter, and L. W. Lake, 1984, Precipitation and dissolution of solids attending flow through porous media: AIChE Journal, Vol. 30, No. 2, pp. 317-328.

Walters, K. L. and C. K. Bayne, 1959, Geology and ground-water resources of Clay county, Kansas: Kansas Geological Survey, Bulletin 136, 106 pages.

Weber, K. J., 1982, Influence of common sedimentary structures on fluid flow in reservoir models: Journal of Petroleum Technology, Vol. 34, No. 3, pp. 665-672.

White, G. N. and L. W. Zelazny, 1986, Chapter 2, Charge properties of soil colloids: *in* Sparks, D. L. (ed.), Soil Physical Chemistry, pp. 39-81, CRC Press, Boca Raton, Florida.

Whittemore, D. O., R. Boeken, X. Jian, and R. Eskrootchi, 1995, TDS contours for the upper Dakota aquifer (map): Kansas Geological Survey.

Whittemore, D. O., A. P. Macfarlane, J. H. Doveton, J. J. Butler, Jr., T.-M. Chu, R. Bassler, M. Smith, J. Mitchell, and A. Wade, 1993, The Dakota aquifer program - annual report, FY92: Kansas Geological Survey, Open-File Report 93-1. 170 pages.

Wood, W. W. and M. J. Petraitis, 1984, Origin and distribution of carbon dioxide in the unsaturated zone of the southern High Plains of Texas: Water Resources Research, Vol. 20, No. 9, pp. 1193-1208.

Xue, Y., J. Wu, P. Liu, J. Wang, Q. Jiang, and H. Shi, 1993, Sea-water intrusion in the coastal area of Laizhou Bay, China: 1. distribution of sea-water intrusion and its hydrochemical characteristics: Ground Water, Vol. 31, No. 4, 532-537.

Yeh, G. T., 1992(a), EQMOD: a chemical EQuilibrium MODel of complexation, adsorption, ion-exchange, precipitation/dissolution, oxidation-reduction, and acid-base reactions: Department of Civil Engineering, The Pennsylvania State University.

Yeh, G. T., 1992(b), HYDROFLOW: a finite element model of HYDROlogic FLOW through saturated-unsaturated porous media: Department of Civil Engineering, The Pennsylvania State University.

Yeh, G. T., 1992(c), HYDROGEOCHEM: a coupled model of HYDROlogic transport and GEOCHEMical reaction in saturated-unsaturated media: Department of Civil Engineering, The Pennsylvania State University.

Yeh, G. T. and V. S. Tripathi, 1989, A critical evaluation of recent developments in hydrogeochemical transport models of reactive multichemical components: Water Resources Research, Vol. 25, No. 1, pp. 93-108.

Yeh, G. T. and V. S. Tripathi, 1990, HYDROGEOCHEM: a coupled model of HYDROlogic transport and GEOCHEMical equilibria in reactive multicomponent systems: Oak Ridge National Laboratory, ORNL-6371, 314 pages.

Yeh, G. T. and V. S. Tripathi, 1991, A model for simulating transport of reactive multispecies components: model development and demonstration: Water Resources Research, Vol. 27, No. 12, pp. 3075-3094.

Zack, A. L., 1980, Geochemistry of fluoride in the Black Creek aquifer system of Horry and Georgetown Counties, South Carolina - and its physiological implications: U. S. Geological Survey Water-Supply Paper 2067, 40 pages.

Zack, A. and I. Roberts, 1988, The geochemical evolution of aqueous sodium in the Black Creek Aquifer, Horry and Georgetown counties, South Carolina: U. S. Geological Survey, Water-Supply Paper 2324, 15 pages.

Zeller, D. E., 1968, The stratigraphic succession in Kansas: Kansas Geological Survey, Bulletin 189, 81 pages.

APPENDIX A

LIST OF CONCENTRATIONS OF MAJOR DISSOLVED CONSTITUENTS FOR GROUND-WATER ANALYSES

Explanation

Location : The legal location used in the dissertation conforms to the procedure of the USGS.

USGS geological code :

111RCNT : Recent stage

112ILNN : Illinoisan stage

112PLDK : Pleistocene-Dakota

112PLSC : Pleistocene

112RCIS : Recent-Illinoisan stages

112TRRC : Terrace deposits

211GRNR : Greenhorn Limestone

210DKOT : Dakota Formation

217KIOW : Kiowa Formation

217CYNN : Cheyenne Sandstone

217CYCD : Cheyenne Sandstone-Cedar Hills Sandstone

318CDHL : Cedar Hills Sandstone

318CDKI : Cedar Hills Sandstone-Kiowa Formation

Depth : Either well depth or sampling depth

Remark : Blank indicates record with field pH measurement.

1 : pH is obtained from geochemical simulation by forcing the water to be calcite saturated.

Table A.1. Concentrations of major dissolved constituents for ground waters sampled from alluvial aquifers.

Location	Geology USGS code	Depth feet	pH	Remark	Ca meq/L	Mg meq/L	Na meq/L	HCO_3 meq/L	SO_4 meq/L	Cl meq/L	SiO_2 mg/L	TDS mg/L
01S 03W 02CCB	112PLSC	151	6.93		4.49	0.76	0.718	4.97	0.292	0.339	37.4	343
04S 03W 01AD	112PLSC	42.9	6.86	1	9.28	1.65	4.09	6.64	0.687	3.78	--	913
04S 04W 32CC	111RCNT	34.7	7.11	1	4.84	1.07	1.52	6.08	0.687	0.508	--	391
05S 02W 30BCC	111RCNT	96	7.62	1	1.90	0.909	15.9	5.80	2.46	10.4	31	1110
05S 02W 30BCC	112RCIS	96	6.92	1	11.4	11.6	194	11.5	35.2	170	32	13000
05S 03W 18BBB	112ILNN	110	7.16	1	4.59	0.99	2.09	5.64	0.708	1.24	24	427
05S 03W 19CB	111RCNT	85	7.65	1	2.35	0.99	1.65	3.28	1.19	0.480	22	294
05S 03W 22BC	112RCIS	78	7.27	1	5.34	4.87	71.6	6.80	9.74	60.6	--	4590
05S 03W 28BB	111RCNT	51	7.39	1	2.89	1.07	2.35	4.79	0.833	0.649	--	383
05S 03W 31BB	111RCNT	69	7.03	1	5.34	1.73	4.52	7.52	1.71	2.26	35	659
05S 03W 32AA	111RCNT	122	7.21	1	4.04	1.16	5.05	5.67	1.44	3.10	31	596
05S 03W 32AA	112RCIS	122	7.04	1	5.49	1.40	3.39	6.24	1.89	2.03	--	589
05S 03W 32AA	111RCNT	122	6.9	1	5.89	1.90	4.87	8.52	1.73	2.26	8.6	728
05S 07W 19CD	112RCIS	31.8	6.77	1	30.1	4.38	7.48	4.61	33.7	3.55	--	2716
05S 07W 32DC	112PLSC	32.3	6.53	1	32.8	10.7	19.2	8.11	36.5	17.6	--	3880
07S 06W 20BDD	112TRRC	41	6.9	1	8.58	1.49	8.96	7.03	4.00	7.98	24	1110
07S 06W 27CDD	112TRRC	42	6.55	1	20.1	3.14	5.74	7.80	5.64	8.18	34	1860
07S 06W 32DDD	112TRRC	40	6.87	1	7.29	2.31	10.5	9.00	4.52	5.30	28	1200
07S 06W 36AAB	112TRRC	45	6.89	1	8.33	0.752	2.26	6.60	3.29	1.35	22	658
07S 07W 12BAC	112TRRC	38.5	6.73	1	12.0	1.57	3.87	7.85	6.29	3.02	18	1030
07S 07W 15CBC	112TRRC	37.5	6.75	1	10.5	8.26	74.4	14.1	22.7	56.4	38	5580
07S 07W 21BBB	112TRRC	40	6.6	1	18.5	7.02	48.3	10.4	15.3	48.0	26	4350
07S 07W 29AB	112TRRC	32	6.8	1	9.73	0.826	5.00	7.67	4.52	2.06	32	952
08S 05W 07CB	112TRRC	52	6.99	1	5.14	1.32	3.44	7.60	1.15	1.1	28	550
08S 05W 14AD	112TRRC	47	6.92	1	7.29	1.90	11.3	7.39	2.50	10.1	24	1190
08S 05W 14AD	112TRRC	51	6.74	1	10.9	2.89	11.0	8.00	3.00	11.9	19	1560
08S 05W 17DCA	112TRRC	22	6.73	1	10.8	1.57	1.87	8.46	3.83	1.13	18	828
08S 05W 25CC	112TRRC	50	7.19	1	3.74	1.49	5.18	7.21	0.791	2.34	22	574
12S 10W 24DDC	112PLDK	70.7	7.3		5.09	3.30	18.7	6.00	4.64	16.2	16	1600

Table A.2. Concentrations of major dissolved constituents for ground waters sampled from the Greenhorn Limestone.

Location	Geology USGS code	Depth feet	pH	Remark	Ca meq/L	Mg meq/L	Na meq/L	HCO_3 meq/L	SO_4 meq/L	Cl meq/L	SiO_2 mg/L	TDS mg/L
01S 01W 27BB	211GRNR	11.8	6.56	1	24.1	3.97	8.48	7.75	22.1	5.92	--	2270
01S 01W 33CD	211GRNR	39.1	7.07	1	5.49	0.909	2.18	5.65	1.10	1.33	--	470
02S 01W 10BB	211GRNR	7.4	7.03	1	5.99	0.991	1.48	5.88	1.17	0.705	--	466
03S 04W 09DD	211GRNR	69.2	7.06	1	5.79	1.24	2.83	6.08	2.06	1.52	--	544
03S 05W 13DD	211GRNR	56	7.09	1	6.49	1.65	6.52	6.03	6.16	2.20	--	870
04S 05W 07CB	211GRNR	41.6	6.86	1	10.4	1.32	3.44	6.54	4.75	2.71	--	900
06S 06W 17DDD	211GRNR	39	6.92	1	10.1	1.65	8.13	5.85	5.95	6.26	24	1230
06S 08W 24CDC	211GRNR	28	6.71	1	16.1	4.87	10.3	6.75	7.60	9.17	14	2000
06S 09W 20DCD	211GRNR	55	6.92	1	7.24	0.696	0.87	6.47	1.10	0.79	22	497
06S 10W 16DDC	211GRNR	35.5	7.13	1	5.14	0.785	1.39	5.08	0.583	1.35	42	433
07S 08W 27AAA	211GRNR	35	6.68	1	19.2	2.64	4.65	6.92	17.2	2.03	23	1670
07S 10W 08BBB	211GRNR	62.5	7.02	1	9.88	1.49	5.00	4.88	7.72	3.53	16	1002
07S 10W 25BCB	211GRNR	27.4	6.72	1	21.6	3.72	7.96	5.75	18.8	7.02	45	2135
08S 07W 02BAD	211GRNR	41	6.84	1	15.2	2.07	9.57	5.52	10.9	8.77	24	1676
09S 09W 26AAA	211GRNR	24.5	6.86	1	9.88	1.65	1.91	6.08	3.52	2.54	19	803

Table A.3. Concentrations of major dissolved constituents (with field pH measurement) for ground waters sampled from the unconfined portion of the Dakota aquifer.

Location	Geology USGS code	Depth feet	pH	Ca meq/L	Mg meq/L	Na meq/L	HCO_3 meq/L	SO_4 meq/L	Cl meq/L	SiO_2 mg/L	TDS mg/L
01S 02E 16BDD	210DKOT	--	7.1	2.54	0.743	0.740	3.28	0.625	0.197	22	240
01S 02E 35DDD	210DKOT	--	7.7	1.90	0.421	4.35	4.59	0.854	1.35	17	390
02S 01E 03AAD	210DKOT	--	7.1	2.25	0.471	0.827	2.29	0.333	0.451	23	200
02S 03E 32ABB	210DKOT	120	6.83	1.87	0.562	1.24	2.64	0.416	0.214	29.9	232
03S 01E 07BC	210DKOT	--	7.7	1.50	1.07	9.57	7.21	4.58	0.310	8.4	730
03S 02E 16CCC	210DKOT	--	7.6	3.09	0.512	1.26	3.61	0.437	0.621	23	270
03S 02E 36DDCC	210DKOT	181	6.7	3.38	0.892	1.19	3.72	0.645	0.327	17.7	320
04S 01E 08CCC	210DKOT	--	7.5	9.48	1.487	2.17	5.74	2.71	1.83	16	650
04S 02E 08DCC	210DKOT	125	7.2	3.54	1.07	2.17	4.40	0.604	1.07	21	390
04S 02E 27ADA	210DKOT	--	7.1	1.90	0.587	1.44	2.46	0.396	0.536	15	210
05S 01E 21BB	210DKOT	--	7.4	5.99	1.32	1.61	6.39	0.354	0.903	30	450
05S 01E 21BB	210DKOT	--	7.5	3.09	0.826	1.00	4.10	0.333	0.451	28	280
05S 02E 12CBA	210DKOT	151	6.74	1.22	0.347	0.818	1.26	0.292	0.274	16.2	165
10S 01E 17DCC	210DKOT	110	6.73	0.749	0.248	0.305	0.803	0.479	0.0762	16.4	97
02S 01W 18BCCB	210DKOT	100	6.8	7.14	2.59	5.61	8.06	4.85	2.13	14.2	932
04S 01W 16ACC	210DKOT	100	7.02	5.84	0.900	1.25	6.16	0.979	0.310	25.9	449
04S 03W 35AD	210DKOT	50	7	7.49	0.818	2.37	8.83	1.71	0.384	32.4	613
05S 01W 07BBAB	210DKOT	128	6.7	1.90	0.512	1.03	2.75	0.327	0.367	29.3	222
05S 01W 26ABD	210DKOT	158	7.14	4.17	0.826	1.47	5.26	0.687	0.877	26	378
05S 02W 12ABBD	210DKOT	138	7	3.27	0.925	11.3	6.39	2.67	6.37	13.6	907
05S 03W 06CCCD	210DKOT	85	7.1	5.54	1.04	3.14	7.98	0.829	0.677	31	567
05S 03W 15DCDD	210DKOT	60	6.8	4.99	0.818	1.12	4.97	0.972	0.640	38.7	436
05S 04W 29DAAB	210DKOT	60	6.95	3.96	0.710	2.51	5.79	0.727	0.970	27.6	423
05S 05W 33BBBB	210DKOT	80	7	4.99	0.752	2.11	6.54	0.966	0.674	25.1	453
06S 01W 10CCB	210DKOT	63	6.7	4.34	1.32	3.65	5.99	1.33	2.45	31	560
06S 01W 26BACC	210DKOT	136.5	6.7	1.64	0.454	1.27	2.46	0.402	0.587	20.2	210
06S 01W 26BBBA	210DKOT	100	6.85	2.78	0.710	2.03	3.10	0.562	1.1	20.2	330
06S 03W 11ADAA	210DKOT	110	6.95	4.87	0.884	1.63	5.13	1.33	1.16	34	450

Table A.3. (Continue...)

Location	Geology USGS code	Depth feet	pH	Ca meq/L	Mg meq/L	Na meq/L	HCO_3 meq/L	SO_4 meq/L	Cl meq/L	SiO_2 mg/L	TDS mg/L
06S 03W 28CDAC	210DKOT	145	6.9	8.28	0.892	2.13	7.06	3.29	1.05	28.6	669
06S 05W 15CACB	210DKOT	179	7.45	1.49	0.801	6.74	7.06	1.81	0.536	10.8	529
07S 02W 15BAA	210DKOT	--	7	5.49	1.07	1.00	5.9	1.35	0.197	19	420
07S 02W 15BAA	210DKOT	151	7.1	5.99	0.578	1.00	6.23	0.916	0.339	21	420
07S 02W 35DAAA	210DKOT	180	6.6	3.76	0.76	0.822	4.13	1.31	0.113	19.2	317
07S 03W 21BAD	210DKOT	342	6.7	5.99	0.909	1.17	4.92	1.52	0.621	30	440
07S 07W 10DBAB	210DKOT	54	6.95	9.23	1.17	5.92	6.95	5.23	4.43	22	997
08S 04W 35ABBC	210DKOT	180	6.9	3.67	0.876	1.17	4.87	0.583	0.229	29.5	347
08S 04W 35BADB	210DKOT	205	6.8	3.94	0.958	1.20	5.13	0.854	0.344	19.5	348
08S 04W 35BADB	210DKOT	230	6.8	3.83	0.785	0.944	4.77	0.683	0.265	27.5	328
08S 05W 01CCCD	210DKOT	90	7.05	3.91	1.487	11.2	6.59	2.01	8.29	13.7	963
08S 05W 30DAAC	210DKOT	137	6.95	1.72	0.884	10.7	7.98	2.03	3.50	10.9	773
09S 03W 17DAA	210DKOT	167	6.3	6.49	1.90	2.22	3.80	5.21	1.69	18	680
09S 07W 16CDDD	210DKOT	65	6.95	8.83	1.01	3.41	6.56	3.79	2.59	31.1	786
10S 04W 19CBCB	210DKOT	87	6.85	4.71	1.25	4.39	5.02	1.11	2.49	17.2	611
10S 07W 12ACA	210DKOT	151	7.32	5.34	1.59	8.33	9.05	3.66	3.51	43.1	934
10S 08W 02AAAC	210DKOT	86	6.7	5.34	0.512	1.24	5.02	1.31	0.88	19.6	416
10S 09W 35CBDB	210DKOT	100	6.85	7.24	0.909	2.07	5.57	3.21	1.70	20.7	612
11S 01W 22CCC	217KIOW	20.2	6.3	9.98	4.05	6.09	5.41	5.00	5.08	39	1300
11S 03W 06BCA	210DKOT	215	7	3.24	0.991	1.70	3.98	1.06	0.536	23	352
11S 03W 06CAA	210DKOT	--	7.4	2.79	0.735	1.39	3.77	0.687	0.564	19	290
11S 04W 01DBD	210DKOT	152	6.8	2.40	0.644	1.44	3.11	0.812	0.649	19	270
11S 07W 32ACC	210DKOT	78	7.1	11.5	2.07	1.39	6.39	8.12	0.762	22	940
11S 12W 07DDB	210DKOT	37	7.3	8.98	2.40	10.9	6.95	6.66	7.90	35	1300
12S 03W 01DB	210DKOT	--	7.4	3.59	0.496	1.04	4.59	0.271	0.282	22	290
12S 03W 01DB	210DKOT	--	7.3	3.14	0.587	0.87	3.77	0.396	0.282	22	255
12S 03W 01DB	210DKOT	--	7.3	3.64	1.07	0.696	4.75	0.271	0.310	15	286
12S 03W 01DB	210DKOT	--	7.8	2.79	0.413	0.957	3.44	0.375	0.282	20	240
12S 03W 07BDD	210DKOT	--	7.5	5.49	0.752	1.74	4.92	1.73	1.04	30	460

Table A.3. (Continue...)

Location	Geology USGS code	Depth feet	pH	Ca meq/L	Mg meq/L	Na meq/L	HCO_3 meq/L	SO_4 meq/L	Cl meq/L	SiO_2 mg/L	TDS mg/L
12S 03W 25DAAC	210DKOT	--	6.6	5.28	3.93	7.40	8.99	5.48	5.64	--	1280
12S 04W 26CAAC	210DKOT	--	6.7	3.48	2.38	4.31	7.63	2.39	2.48	--	826
12S 05W 01AA	210DKOT	--	7.8	5.49	2.64	2.87	6.39	2.71	2.43	42	658
12S 05W 01AA	210DKOT	--	7.5	5.99	1.07	1.48	6.72	0.73	0.846	40	474
12S 05W 29BBDB	210DKOT	--	6.9	4.63	2.11	2.10	6.31	2.37	2.54	--	730
12S 06W 32AAA	210DKOT	30.5	7	9.98	4.05	1.70	3.20	1.52	4.65	19	650
12S 07W 06AAB	210DKOT	80	6.9	8.48	1.24	3.04	5.24	5.41	1.30	16	738
12S 07W 06ABD	210DKOT	80	7.1	11.5	1.57	4.18	6.39	7.91	1.92	23	1008
12S 07W 09ADD	210DKOT	38	7.2	2.45	0.636	1.26	2.61	1.04	0.762	46	290
12S 07W 12AAB	210DKOT	130	7.1	6.39	2.56	9.92	5.41	8.52	4.57	11	1100
12S 08W 13DDD	210DKOT	70	6.8	4.59	1.49	1.35	3.84	1.48	1.27	22	454
12S 09W 08AAC	210DKOT	30	6.7	12.0	1.98	6.52	6.06	10.6	3.67	22	1300
12S 09W 11DDC	210DKOT	16	7.3	6.79	2.07	2.65	4.92	4.00	2.12	14	660
12S 12W 31BDC	210DKOT	144	7.45	4.04	0.743	2.96	1.57	2.12	3.78	--	450
12S 13W 36BCCD	210DKOT	134	7	7.49	1.01	4.65	5.93	5.31	2.32	25.2	821
13S 03W 01BDCC	210DKOT	--	6.7	0.79	0.38	0.200	0.800	0.333	0.282	--	132
13S 04W 11DADA	217KIOW	--	6.9	5.36	1.32	3.32	6.67	2.21	1.1	--	817
13S 04W 17DDDD	217KIOW	--	5.7	3.41	1.27	1.74	1.60	3.94	0.790	--	464
13S 05W 23CCCB	217KIOW	--	6.9	3.91	1.78	2.35	4.80	2.25	1.35	--	593
13S 06W 15DAAA	210DKOT	--	7.2	6.27	3.19	3.21	5.99	5.29	1.92	--	905
13S 06W 35BCCD	210DKOT	--	7.1	1.45	0.46	0.731	2.40	0.333	0.423	--	245
13S 07W 33DCC	210DKOT	52.3	7.2	12.0	1.98	1.39	6.39	8.33	0.649	22	940
13S 08W 34CABA	210DKOT	300	6.8	6.49	1.90	4.87	6.72	6.60	0.640	11.1	829
14S 11W 07CAB	210DKOT	100	7.52	8.53	0.810	2.64	6.03	3.06	2.20	22.4	674
14S 11W 07CAB	210DKOT	100	7	9.48	0.727	3.83	7.21	4.16	3.10	26	880
15S 12W 02BAA	210DKOT	245	7.7	9.98	2.48	2.48	4.59	9.37	1.33	7	950

Table A.4. Concentrations of major dissolved constituents for grond waters sampled from the unconfined portion of the Dakota aquifer.

Location	Geology USGS code	Depth feet	pH	Remark	Ca meq/L	Mg meq/L	Na meq/L	HCO_3 meq/L	SO_4 meq/L	Cl meq/L	SiO_2 mg/L	TDS mg/L
05S 03E 14CDC	210DKOT	--	7.67	1	2.30	0.743	2.17	3.03	0.770	0.846	--	263
06S 02E 03ADC	210DKOT	59	7.27	1	4.99	1.40	3.39	4.26	1.12	3.41	14	588
07S 01E 06BB	210DKOT	75	7.19	1	4.44	2.23	2.31	5.52	2.79	0.564	9.5	502
07S 01E 15BCB	210DKOT	65	7.12	1	7.24	1.90	4.61	4.40	1.12	4.82	8.2	861
07S 01E 19BCC	210DKOT	50	8.49	1	0.998	0.38	1.52	1.12	0.645	1.044	7.4	180
08S 02E 30DDD	210DKOT	--	7.13	1	7.53	7.27	4.22	4.80	3.04	6.88	9.4	1144
03S 03W 30AA	210DKOT	97.2	7.05	1	5.79	1.07	5.74	6.79	3.16	1.41	--	779
03S 03W 35DD	210DKOT	23.6	6.97	1	6.94	0.909	1.61	6.19	1.15	0.762	--	541
04S 01W 13BB	210DKOT	38	7.06	1	18.9	2.56	8.31	3.00	12.8	7.28	--	1975
04S 01W 36BD	210DKOT	38.4	7.96	1	2.64	0.909	1.00	1.48	1.42	0.959	--	277
04S 02W 09DC	210DKOT	52.3	7	1	6.44	1.24	7.26	7.19	3.46	3.36	--	866
04S 02W 20BB	210DKOT	70	7.56	1	3.39	1.40	2.04	2.80	0.666	0.846	--	439
04S 03W 14DD	210DKOT	64.2	7.26	1	6.44	1.73	7.22	4.00	4.29	6.57	--	907
04S 03W 15BC	210DKOT	25.8	6.9	1	8.78	1.49	3.00	6.39	1.64	1.49	--	813
04S 04W 36DA	210DKOT	74.7	7	1	5.79	0.810	1.48	6.59	1.06	0.282	--	425
05S 01W 26AD	210DKOT	158	7.3	1	3.64	0.909	1.61	4.92	0.645	0.536	23	343
05S 05W 04AAB1	210DKOT	79	7.2	1	3.59	0.661	8.31	5.91	0.729	5.78	12	708
06S 01W 10CC	210DKOT	87	7.43	1	3.29	0.793	1.26	4.20	0.812	0.367	11	296
06S 01W 24AA	210DKOT	75	7.42	1	11.2	3.97	2.18	1.64	0.396	5.98	14	1191
06S 02W 09DAD	210DKOT	80	7.31	1	4.09	1.07	2.31	4.60	0.937	1.81	14	416
06S 02W 24CC	210DKOT	--	7.96	1	1.45	0.595	3.18	2.60	0.854	1.75	12	328
06S 02W 33DC	210DKOT	69	7.61	1	2.40	1.07	1.70	3.40	0.521	1.13	15	285
06S 02W 33DC	210DKOT	139	7.51	1	2.35	0.909	5.39	4.99	1.12	2.40	11	485
06S 02W 33DC	210DKOT	234	7.45	1	2.64	1.07	4.57	4.99	1.08	2.12	14	465
06S 03W 06DD	210DKOT	305	8.01	1	0.389	0.231	16.1	11.1	1.94	1.97	--	896
06S 04W 05DA	210DKOT	58	6.89	1	8.78	1.07	2.09	6.59	0.999	2.76	22	706
06S 04W 12CD	210DKOT	90	7.35	1	3.49	0.76	1.35	4.20	0.666	0.705	7.4	329
06S 04W 34CC	210DKOT	169	7.12	1	4.79	0.735	1.00	5.59	0.645	0.339	24	363
06S 04W 34CC	210DKOT	379	7.1	1	4.79	0.735	1.31	5.79	0.666	0.367	24	379

Table A.4. (Continued...)

Location	Geology USGS code	Depth feet	pH	Remark	Ca meq/L	Mg meq/L	Na meq/L	HCO_3 meq/L	SO_4 meq/L	Cl meq/L	SiO_2 mg/L	TDS mg/L
07S 01W 29ABA	210DKOT	67	8.02	1	2.15	0.909	1.09	1.56	0.541	1.02	9	259
07S 02W 18AB	210DKOT	--	7.1	1	5.19	1.98	1.78	6.59	1.79	0.480	2	476
07S 03W 35CB	210DKOT	75	7.32	1	14.9	1.24	2.00	2.00	14.4	1.015	23	1240
07S 05W 33AAAC	210DKOT	154	6.97	1	5.89	0.768	1.43	6.44	1.40	0.316	26.3	474
07S 06W 24CDD	210DKOT	40	6.86	1	12.8	4.30	3.91	6.19	13.9	0.846	12	1302
08S 01W 13AD	210DKOT	200	7.89	1	1.70	0.463	1.04	2.60	0.333	0.226	9.2	179
08S 02W 16DC	210DKOT	181	7.56	1	2.94	0.727	0.827	3.40	0.750	0.226	21	256
08S 02W 36AA	210DKOT	69	7.92	1	1.60	0.76	1.22	2.60	0.645	0.339	31	226
08S 03W 26CC	210DKOT	31	7.41	1	4.89	1.49	4.31	3.40	1.12	1.13	23	741
08S 04W 08DDC	210DKOT	70	7.25	1	4.24	1.07	1.57	5.19	0.937	0.677	21	382
08S 04W 08DDC	210DKOT	50	8.77	1	0.120	0.132	7.09	6.19	0.583	0.536	23	428
08S 04W 23CBD	210DKOT	128	7.18	1	4.39	0.991	1.83	5.79	0.916	0.451	16	394
08S 06W 20CDC	210DKOT	165	8.39	1	0.200	0.264	10.5	8.79	1.29	0.903	7	619
09S 01W 12DDB	210DKOT	108	7.16	1	6.74	2.64	3.18	5.00	7.20	0.339	7.5	759
09S 01W 21BCC	210DKOT	56	7.82	1	3.64	1.32	2.09	1.52	0.708	2.62	8.5	469
09S 01W 26BCB	210DKOT	91.5	7.5	1	3.69	1.90	2.44	3.60	3.66	0.677	9	479
09S 01W 33BCB	210DKOT	29.3	7.47	1	3.79	0.991	4.87	3.60	2.08	3.55	12	571
09S 02W 09DCD	210DKOT	99.6	7.74	1	1.80	0.826	1.52	3.40	0.604	0.226	25	255
09S 02W 19AAD	210DKOT	64.3	7.64	1	2.30	0.743	1.09	3.20	0.666	0.197	21	254
09S 02W 35CBC	210DKOT	87	7.62	1	2.84	1.07	1.52	3.00	1.21	0.959	12	317
09S 03W 10CCD	210DKOT	87.1	7.57	1	2.89	1.16	0.957	3.20	1.27	0.423	14	304
09S 03W 27DAD	210DKOT	65.6	7.47	1	3.29	0.793	1.39	3.60	1.02	0.762	25	330
09S 03W 33CBB	210DKOT	127	7.37	1	3.64	1.24	1.00	4.20	1.35	0.282	18	339
09S 04W 12ABA	210DKOT	42	7.72	1	2.20	1.49	1.04	3.00	1.23	0.395	16	314
09S 04W 26AAD	210DKOT	55.4	7.85	1	1.80	0.603	1.65	2.60	0.583	0.564	21	253
09S 05W 02BCC	210DKOT	77	7.08	1	4.94	1.82	3.83	7.20	2.58	0.762	12	601
09S 05W 05BAA	210DKOT	77	6.85	1	12.0	1.82	4.57	6.59	10.0	1.41	16	1131
09S 05W 15CDC	210DKOT	99.4	7.02	1	5.59	2.23	2.78	7.19	2.89	0.254	13	593
09S 06W 29AAA	210DKOT	190	7.4	1	2.59	0.991	4.87	6.00	1.73	0.592	13	482

Table A.4. (Continued...)

Location	Geology USGS code	Depth feet	pH	Remark	Ca meq/L	Mg meq/L	Na meq/L	HCO_3 meq/L	SO_4 meq/L	Cl meq/L	SiO_2 mg/L	TDS mg/L
09S 07W 22DDD	210DKOT	26.5	6.71	1	14.8	1.57	8.70	6.79	4.54	7.62	19	1602
10S 01W 05CCD	210DKOT	78.3	7.7	1	2.05	1.32	1.96	3.40	0.500	1.16	9	328
10S 01W 16DDD	210DKOT	98	7.24	1	4.19	1.57	1.52	5.19	0.833	1.21	18	402
10S 01W 24BAA	210DKOT	66.4	7.46	1	2.84	0.991	1.57	4.20	0.625	0.339	19	304
10S 01W 28DCC	210DKOT	42.2	7.05	1	14.5	7.104	15.1	4.00	14.6	9.25	16	2431
10S 01W 36CBB	210DKOT	42.4	7.79	1	1.70	0.702	1.31	3.00	0.121	0.339	13	210
10S 02W 05ABA	210DKOT	101	7.84	1	1.55	0.653	1.48	3.00	0.198	0.480	23	217
10S 02W 21AAB	210DKOT	82.3	7.81	1	1.85	0.471	1.87	2.80	0.687	0.621	14	248
10S 02W 33CAB	210DKOT	19.7	7.48	1	3.54	1.40	1.70	3.40	1.17	1.30	12	392
10S 03W 06CCC	210DKOT	69	7.77	1	2.94	0.743	2.61	2.20	1.73	1.89	25	403
10S 03W 25BCA	210DKOT	58.8	7.97	1	1.30	0.702	1.00	2.60	0.171	0.310	7.5	182
10S 04W 05AAD	210DKOT	35.4	7.46	1	3.09	0.512	0.957	3.60	0.333	0.367	25	262
10S 05W 01AAB	210DKOT	73	7.22	1	4.44	1.65	2.78	5.39	2.08	0.931	11	515
10S 05W 09DCD	210DKOT	162	7.18	1	4.29	1.82	3.65	6.19	2.31	1.13	10	562
10S 05W 11BAB	210DKOT	57.4	7.07	1	5.94	4.05	4.31	6.39	3.10	3.86	13	812
10S 05W 12AAD	210DKOT	92	7.23	1	4.44	1.32	2.00	5.19	1.96	0.564	13	442
10S 05W 18ABA	210DKOT	96	7.07	1	5.34	2.31	1.52	6.59	1.83	0.733	22	565
10S 05W 19CDA	210DKOT	34.6	6.96	1	7.19	1.57	2.57	6.39	2.04	1.81	25	667
10S 05W 27BBB	210DKOT	49.2	7.45	1	2.69	0.752	2.39	4.60	0.479	0.649	17	331
10S 06W 16DAD	210DKOT	34	6.93	1	7.14	1.49	3.65	6.59	1.37	1.33	7	756
10S 10W 14DAA	210DKOT	206	7.1	1	4.84	0.909	1.65	5.59	1.52	0.226	9.2	409
11S 01W 18AAA	210DKOT	40.2	7.12	1	9.08	4.13	4.83	4.80	12.7	0.508	25	1150
11S 02W 07ADD	210DKOT	75.7	8.59	1	0.649	0.314	0.609	1.16	0.137	0.141	13	98
11S 02W 08DBB	210DKOT	48.2	8.57	1	0.649	0.273	0.609	1.16	0.162	0.141	9	100
11S 02W 10CBC	210DKOT	94.3	7.49	1	3.29	1.16	3.26	3.60	1.333	1.75	14	470
11S 02W 20BDC	210DKOT	15.7	7.8	1	1.55	0.694	2.09	3.20	0.562	0.451	19	249
11S 02W 27ADA	210DKOT	55.8	7.23	1	5.44	2.81	3.83	4.99	5.89	1.1	7.5	720
11S 02W 32ABB	210DKOT	70.7	8.06	1	1.45	0.397	1.00	1.80	0.271	0.395	17	187
11S 02W 36CCC	210DKOT	19.2	8.47	1	0.798	0.322	0.740	1.20	0.198	0.155	16	123

Table A.4. (Continued...)

Location	Geology USGS code	Depth feet	pH	Remark	Ca meq/L	Mg meq/L	Na meq/L	HCO_3 meq/L	SO_4 meq/L	Cl meq/L	SiO_2 mg/L	TDS mg/L
11S 03W 02CDC	210DKOT	58.1	8.23	1	1.30	0.628	1.22	1.40	0.292	0.903	6.5	240
11S 03W 15DDC	210DKOT	47.2	7.41	1	2.94	1.32	2.52	4.80	1.06	0.621	12	384
11S 03W 31ABA	210DKOT	41	7.52	1	2.64	1.24	2.65	4.20	1.06	0.959	16	375
11S 04W 15DAA	210DKOT	47	7.76	1	1.95	1.40	0.957	3.00	0.604	0.310	27	266
11S 04W 20AAD	210DKOT	75	7.82	1	3.59	1.65	2.13	1.80	4.77	0.733	16	487
11S 04W 29AAA	210DKOT	91	7.84	1	2.69	0.991	1.00	1.90	2.19	0.564	12	288
11S 05W 06CCD	210DKOT	49.7	6.97	1	15.8	7.02	4.39	3.60	4.64	6.52	13	1858
11S 05W 08ADC	210DKOT	100	8.26	1	1.45	0.397	0.566	1.18	0.895	0.282	18	157
11S 05W 22ADA	210DKOT	95.6	7.96	1	1.70	0.785	0.653	2.00	0.583	0.367	25	197
11S 05W 32BAA	210DKOT	19.6	7.12	1	5.89	1.73	4.22	5.79	3.46	1.78	15	704
11S 05W 34AAD	210DKOT	172	7.22	1	5.69	1.24	3.83	4.60	3.69	2.20	17	643
11S 08W 36AA	210DKOT	200	7.08	1	6.24	3.97	2.87	5.59	5.52	1.27	10	766
11S 10W 26CBD	210DKOT	194	7.33	1	2.35	0.826	6.96	7.19	1.54	1.24	5	562
12S 02W 04BBA	210DKOT	13.7	7.69	1	2.35	0.628	1.48	2.80	0.604	0.480	22	278
12S 02W 10BCC	210DKOT	38	7.08	1	6.84	1.90	4.26	5.19	2.27	2.31	24	824
12S 02W 11ABB	210DKOT	16.6	7.12	1	8.63	3.30	8.05	4.60	5.93	4.63	19	1306
12S 02W 32CCC	210DKOT	75.7	7.65	1	4.19	2.64	2.83	2.40	6.29	0.733	23	631
12S 03W 01DBA	210DKOT	47	7.38	1	3.19	0.826	1.17	4.24	0.437	0.367	22	292
12S 03W 05BCA	210DKOT	53.2	7.91	1	2.45	1.24	1.13	1.68	0.833	1.24	25	316
12S 03W 09DDD	210DKOT	61.8	7	1	3.79	1.32	9.09	11.2	1.75	1.18	17	806
12S 03W 10DAD	210DKOT	69.3	7.83	1	7.73	4.87	12.8	1.10	10.4	13.8	6.5	1603
12S 03W 24BAD	210DKOT	30	7.68	1	2.05	0.793	1.87	3.40	0.833	0.451	13	276
12S 04W 01BBC	210DKOT	100	7.96	1	2.94	0.545	1.57	1.36	2.79	0.677	17	368
12S 04W 09ABD	210DKOT	92.8	7.66	1	8.73	4.79	6.61	1.28	7.47	6.35	13	1340
12S 04W 11CDD	210DKOT	106	6.8	1	12.9	11.0	6.92	7.59	12.9	7.64	13	1845
12S 04W 19DAA	210DKOT	24.5	7.07	1	7.19	3.22	2.52	5.39	5.39	1.58	19	775
12S 04W 21BBC	210DKOT	38	6.95	1	9.08	1.57	2.26	5.19	1.10	2.43	16	825
12S 05W 11DCD	210DKOT	59	7.24	1	4.14	0.826	1.96	4.99	0.666	0.733	22	406
12S 05W 19ADA	210DKOT	41.5	7.04	1	6.94	3.80	5.79	6.39	6.58	3.33	13	975

Table A.4. (Continued...)

Location	Geology USGS code	Depth feet	pH	Remark	Ca meq/L	Mg meq/L	Na meq/L	HCO_3 meq/L	SO_4 meq/L	Cl meq/L	SiO_2 mg/L	TDS mg/L
12S 05W 28ABA	210DKOT	42	7.74	1	1.85	1.07	1.17	3.20	0.583	0.395	22	238
12S 05W 30CBC	210DKOT	85	7.18	1	6.84	2.15	3.22	4.20	3.44	3.27	25	748
12S 05W 33CCA	210DKOT	64	7.15	1	5.34	2.23	1.65	5.39	2.62	1.13	16	525
13S 10W 15ADA	210DKOT	97	7.19	1	5.39	1.24	1.22	4.46	2.67	0.677	13	457
13S 10W 25DCC	210DKOT	130	7.04	1	5.74	2.15	2.48	6.19	3.21	0.903	4	586

Table A.5. Concentrations of major dissolved constituents (with field pH measurement) for ground waters sampled from the confined Dakota aquifer east of the Cedar Hills subcrop.

Location	Geology USGS code	Depth feet	pH	Ca meq/L	Mg meq/L	Na meq/L	HCO_3 meq/L	SO_4 meq/L	Cl meq/L	SiO_2 mg/L	TDS mg/L
01S 01E 07AA	210DKOT	280	8.1	0.998	0.479	12.0	7.08	2.39	3.98	11	800
03S 04W 13DCDD	210DKOT	142	7.25	3.65	0.768	52.3	7.87	8.12	39.7	8.1	3340
06S 07W 14BADD	210DKOT	80	7.1	4.48	2.94	16.5	7.51	2.67	14.3	20	1400
07S 05W 02BBAB	210DKOT	252	7.2	5.19	1.48	17.5	11.2	11.8	2.20	11	1530
08S 07W 12DDCC	210DKOT	178	7	2.00	1.16	6.52	7.19	1.70	1.21	16.5	571
11S 11W 13DCBB	210DKOT	212	7.7	0.384	0.19	12.5	9.00	2.81	1.33	9.6	764
11S 12W 07DDB	210DKOT	151	7.1	9.48	2.63	15.7	7.65	6.48	12.8	30	1690
11S 12W 07DDC	210DKOT	--	7.2	7.98	2.31	12.6	6.72	5.41	9.31	29	1300
12S 06W 15AABB	210DKOT	115	6.95	9.13	5.30	34.3	9.70	11.5	28.6	9.7	2935
12S 13W 03BBD	210DKOT	255	7	0.599	1.57	56.5	12.4	11.3	33.3	--	3440
12S 18W 29BCBA	210 DKOT	395	8.2	2.05	0.757	8.56	3.74	3.23	3.59	--	757
12S 18W 29BCBA	210 DKOT	415	8.1	3.29	1.37	6.01	3.06	3.98	3.12	--	709
12S 18W 29BCBA	210 DKOT	435	8.1	2.89	1.55	6.37	2.50	5.13	3.12	--	732
12S 18W 29BCBA	210 DKOT	455	7.9	4.37	1.25	4.36	4.32	1.98	3.02	--	668
12S 18W 29BCBA	210 DKOT	475	7.9	4.72	1.58	3.61	4.52	1.46	3.03	--	650
12S 18W 30AA	217CYNN	835	7.45	3.19	58.9	448	17.5	85.6	412	20	30410
13S 11W 03AABA	210DKOT	250	6.35	19.5	4.37	1.33	1.62	24.8	0.333	15.5	1790
14S 11W 10ADD	210DKOT	250	6.95	8.28	1.73	15.1	6.33	6.87	10.9	--	1490
14S 11W 10DCA	210DKOT	215	6.75	8.98	3.47	8.18	6.60	8.87	4.48	--	1204
14S 13W 12DAD	210DKOT	285	6.85	3.69	1.57	17.4	4.90	3.71	14.1	--	1325
14S 18W 03BCC	210DKOT	335	8.1	3.14	1.30	30.2	4.98	5.79	23.4	--	2185
14S 18W 03BCC	210DKOT	355	8.1	1.65	4.51	68.8	6.29	10.8	50.6	--	4365
14S 18W 03BCC	210DKOT	375	8	5.16	2.71	33.0	4.88	5.83	28.9	--	2500
14S 18W 03BCC	210DKOT	395	7.9	7.21	2.04	23.9	4.10	6.44	21.0	--	2025
14S 18W 03BCC	210DKOT	415	7.7	10.1	2.65	25.0	4.02	6.52	26.7	--	2315
14S 18W 03BCC	210DKOT	435	8	6.69	5.87	84.0	6.00	13.5	68.1	--	5565
14S 19W 36DAD	210DKOT	410	7.75	0.55	0.909	46.5	5.85	6.37	34.1	--	2794
15S 12W 14ADD	210DKOT	194	7.55	2.35	1.57	30.3	9.55	10.35	13.6	--	2119

Table A.5. (Continued...)

Location	Geology USGS code	Depth feet	pH	Ca meq/L	Mg meq/L	Na meq/L	HCO_3 meq/L	SO_4 meq/L	Cl meq/L	SiO_2 mg/L	TDS mg/L
15S 14W 26BAAA	210DKOT	221	7.2	10.7	3.63	45.2	8.28	7.79	41.7	--	3716
15S 15W 27BCD	210DKOT	--	7.4	2.00	1.73	46.5	6.21	5.91	35.5	--	2877
15S 16W 14BAB	210DKOT	160	6.7	27.0	3.14	22.4	5.56	23.7	19.6	--	3251
15S 17W 23AB	210DKOT	237	7.45	1.75	2.15	57.9	6.06	8.10	46.5	--	3630
15S 18W 23BABB	210DKOT	238	7.35	1.60	1.98	66.6	6.21	9.20	50.8	--	4034
15S 18W 33ABB	210DKOT	130	7.65	0.549	0.710	30.2	4.85	5.08	20.9	--	1855
15S 18W 33BAA	210DKOT	154	7.8	0.898	0.785	33.1	5.9	5.21	24.0	8	2100
15S 20W 35CAA	210DKOT	365	8.15	0.225	0.223	15.2	5.24	3.73	6.06	--	917

Table A.6. Concentrations of major dissolved constituents for ground waters sampled from the confined Dakota aquifer east of the Cedar Hills subcrop.

Location	Geology USGS code	Depth feet	pH	Remark	Ca meq/L	Mg meq/L	Na meq/L	HCO_3 meq/L	SO_4 meq/L	Cl meq/L	SiO_2 mg/L	TDS mg/L
01S 01W 15CC	210DKOT	253	7.72	1	1.10	0.661	15.5	7.28	3.91	6.04	--	1006
01S 01W 28AA	210DKOT	244	7.5	1	1.70	0.727	9.70	7.19	3.52	1.30	--	706
02S 03W 27CC	210DKOT	157.5	7.54	1	2.59	3.88	127	8.59	11.3	113	--	7875
03S 01W 08C	210DKOT	217	7.41	1	2.10	1.07	7.66	7.00	2.98	0.733	--	618
03S 03W 13AA	210DKOT	121	7.46	1	1.55	1.07	34.9	13.2	4.77	19.3	--	2195
04S 04W 14BB	210DKOT	125.8	7.47	1	1.95	1.40	51.5	10.4	3.58	40.6	--	3180
04S 05W 23BC	210DKOT	127.8	7.67	1	0.958	1.24	66.4	15.1	5.37	46.7	--	3980
05S 05W 04AAB2	210DKOT	410	6.86	1	5.24	17.7	561	21.0	41.3	502	--	36000
05S 06W 34CDD	210DKOT	100	6.81	1	20.9	3.55	10.9	4.80	16.2	10.6	--	2245
06S 04W 36CB	210DKOT	308	8.08	1	0.379	0.413	29.6	12.0	3.14	13.8	--	1715
06S 05W 06CB	210DKOT	190	7.76	1	0.998	1.07	14.8	8.19	1.54	6.97	7.4	955
06S 05W 26AB	210DKOT	--	6.88	1	8.53	3.47	23.0	10.8	11.8	10.4	12	2135
06S 07W 13CDD	210DKOT	140	7.68	1	0.848	1.32	49.6	15.8	5.37	30.5	7.5	3000
06S 07W 14DCC	210DKOT	93	7.12	1	4.04	1.07	9.22	7.79	0.895	5.61	22	807
07S 04W 22BB	210DKOT	182.6	7.06	1	8.58	1.98	5.39	5.19	5.37	5.25	5.8	931
07S 05W 13BAD	210DKOT	240	8.35	1	0.245	0.314	11.4	8.99	2.33	0.480	7.8	682
07S 06W 10CBB	210DKOT	130	8.16	1	0.354	0.19	15.3	9.39	3.21	3.22	10	924
07S 07W 11CBB	210DKOT	145	6.93	1	6.34	1.90	24.4	10.8	6.66	15.2	10	1915
08S 06W 09BCC	210DKOT	50	6.82	1	12.8	1.40	4.44	5.79	5.23	6.60	23	1115
08S 06W 30AAA	210DKOT	165	6.81	1	6.74	3.39	10.5	11.8	5.73	2.96	7	1160
09S 06W 10BCB	210DKOT	180	7.12	1	5.49	1.24	9.40	7.19	7.66	1.18	15	987
09S 08W 34BCC	210DKOT	185	7.7	1	1.10	1.40	36.3	10.4	5.43	22.8	8.5	2273
10S 08W 17CCC	210DKOT	186	7.31	1	2.50	3.47	46.1	11.8	9.68	30.5	21	3083
11S 07W 01BCC	210DKOT	195	7.62	1	1.20	1.24	14.7	9.19	6.93	0.846	12	1040
11S 08W 09BAA	210DKOT	260	8.28	1	0.200	0.264	19.6	12.0	3.46	4.51	12	1160
11S 10W 17BBB	210DKOT	190	8.36	1	0.200	0.314	19.1	10.4	4.41	4.65	10	1160
12S 16W 14BC	210DKOT	404	7.01	1	7.63	14.0	132	10.5	31.6	112	--	9170
12S 17W 31CC	210DKOT	534	7.56	1	1.90	2.97	60.7	6.98	9.06	49.4	--	3870

Table A.6. (Continued...)

Location	Geology USGS code	Depth feet	pH	Remark	Ca meq/L	Mg meq/L	Na meq/L	HCO_3 meq/L	SO_4 meq/L	Cl meq/L	SiO_2 mg/L	TDS mg/L
12S 17W 31CC	210DKOT	611.5	7.44	1	2.20	3.06	55.2	7.54	7.62	45.1	--	3550
12S 17W 31CC	210DKOT	716	6.19	1	21.7	61.6	427	32.0	54.0	423	--	29670
13S 13W 31CB	210DKOT	242.5	7.37	1	2.00	3.55	100	13.9	12.8	79.0	--	6650
13S 13W 31CB	210DKOT	361.5	7.21	1	3.09	5.86	141	14.9	17.5	118	--	9308
13S 13W 31CB	210DKOT	395	6.55	1	19.0	32.9	465	17.5	59.2	440	--	30980
13S 14W 19D	210DKOT	--	6.35	1	30.9	52.0	478	21.8	72.9	480	--	33410
13S 14W 19D	210DKOT	380	6.31	1	28.9	64.4	609	24.1	87.4	564	--	40350
13S 14W 30BC	210DKOT	183.7	7.68	1	1.95	3.47	88.2	8.13	11.5	73.6	--	5535
13S 14W 32CB	210DKOT	229	7.54	1	2.10	3.97	92.9	8.39	11.1	79.3	--	5832
13S 14W 32CB	210DKOT	303	7.44	1	2.54	4.13	97.9	8.95	11.6	83.8	--	6157
13S 14W 32CB	210DKOT	416	7.1	1	6.44	10.9	180	9.83	21.2	166	--	11900
13S 14W 33AB	210DKOT	377	7.04	1	14.2	18.4	251	5.75	28.1	250	--	16650
13S 15W 33CB	210DKOT	210	7.17	1	5.89	5.12	81.2	6.97	12.7	72.5	--	5650
13S 15W 33CB	210DKOT	352.5	6.86	1	8.78	17.6	219	13.8	29.9	202	--	14860
13S 15W 33CB	217CYNN	495	6.22	1	26.8	66.3	716	30.8	98.1	680	--	48480
14S 11W 30BAAB	210DKOT	51	7.32	1	4.04	1.69	21.9	5.92	4.44	17.5	--	1630
14S 11W 30BAAB	210DKOT	115	7.26	1	4.63	1.97	28.8	6.28	4.94	24.7	--	2085
14S 11W 30BAAB	210DKOT	136	7.23	1	5.24	2.90	49.2	6.87	5.83	45.6	--	3390
14S 12W 06CA	210DKOT	--	7.27	1	4.99	3.06	43.5	6.06	3.96	28.2	--	2554
14S 12W 23DDAD	210DKOT	162	7.14	1	5.29	1.44	14.8	6.44	3.79	11.6	--	1265
14S 12W 34DAA	210DKOT	78.8	7.55	1	2.15	1.65	26.1	6.65	4.33	18.8	--	1755
14S 13W 06BB	210DKOT	500	7.23	1	3.29	4.96	113	12.5	13.5	95.9	--	7155
14S 14W 10BA	210DKOT	302.5	6.8	1	10.5	22.1	365	16.3	51.6	330	--	24060
14S 14W 10BA	217CYNN	431	6.66	1	17.0	40.7	506	15.7	74.1	474	--	33800
14S 14W 10DC	210DKOT	272.5	6.97	1	8.73	20.6	305	12.1	31.6	291	--	20000
14S 14W 10DC	210DKOT	362.5	6.86	1	11.3	19.2	312	12.0	29.5	301	--	20460
14S 14W 10DC	217CYNN	456.5	6.4	1	30.5	80.3	838	18.7	111	818	--	56340
14S 14W 14CD	210DKOT	275	6.7	1	13.4	16.8	263	13.1	22.9	257	--	17510
14S 14W 14CD	210DKOT	335	6.31	1	29.2	51.6	616	21.0	78.0	598	--	41610

Table A.6. (Continued...)

Location	Geology USGS code	Depth feet	pH	Remark	Ca meq/L	Mg meq/L	Na meq/L	HCO_3 meq/L	SO_4 meq/L	Cl meq/L	SiO_2 mg/L	TDS mg/L
14S 14W 14CD	217CYNN	428	6.25	1	31.9	61.8	708	22.9	87.3	691	--	47750
14S 14W 15DD	210DKOT	500	7.36	1	2.84	4.05	104	10.2	10.4	93.1	--	6610
14S 14W 21CD	210DKOT	242.5	6.76	1	9.58	7.93	95.1	12.0	8.93	91.7	--	6883
14S 14W 21CD	210DKOT	275.5	6.96	1	9.58	18.6	278	11.2	35.1	259	--	18370
14S 14W 21CD	210DKOT	335	6.31	1	35.6	45.5	502	17.4	69.6	496	--	34820
14S 14W 21CD	217CYNN	457.5	6.46	1	32.3	72.5	873	15.2	105	857	--	57960
14S 14W 23BD	210DKOT	550	7.4	1	1.70	2.56	69.6	13.6	9.79	50.8	--	4352
14S 14W 25BB	210DKOT	117.5	6.95	1	8.33	3.22	22.1	6.11	4.04	23.4	--	2112
14S 14W 25BB	210DKOT	257.5	6.27	1	29.0	54.8	687	25.7	89.3	656	--	46140
14S 14W 25BB	217CYNN	375	6.4	1	38.3	75.8	937	15.0	105	931	--	62170
14S 14W 27DA	210DKOT	165	7.66	1	1.05	1.16	48.0	9.31	3.81	37.1	--	3205
14S 14W 27DA	210DKOT	220	7	1	7.09	9.33	121	9.51	16.9	111	--	8387
14S 14W 27DA	210DKOT	352.5	6.46	1	33.5	75.2	924	13.7	108	911	--	61170
14S 15W 14DD	210DKOT	458.5	6.34	1	38.2	40.3	466	14.6	58.0	472	--	31980
15S 12W 31DDD	210DKOT	244	7.58	1	2.10	2.40	50.6	7.51	7.18	40.1	--	3250
15S 14W 07ABD	210DKOT	174	7.88	1	1.098	1.73	62.6	7.52	6.37	51.2	--	3850
15S 14W 31CC	210DKOT	540	7.88	1	0.898	0.768	17.8	5.41	2.29	11.8	--	1133
15S 14W 31CC	210DKOT	540	7.84	1	0.998	0.826	20.0	5.41	2.29	14.1	--	1265
15S 14W 31CC	210DKOT	540	7.58	1	1.55	1.32	30.4	7.21	2.91	23.1	--	1925
15S 14W 31CC	210DKOT	540	7.6	1	2.59	2.15	43.1	4.75	6.66	36.7	--	2834
15S 14W 31CC	210DKOT	540	7.52	1	2.05	2.48	56.5	7.70	5.41	48.0	--	3565
15S 14W 31CC	210DKOT	389	6.66	1	22.5	37.2	383	11.0	57.0	375	--	26090
15S 16W 09AA	210DKOT	133	7.93	1	2.79	4.13	78.3	3.11	10.8	70.5	--	5025
15S 16W 18BBB	210DKOT	188	7.35	1	4.59	2.07	37.4	5.9	8.54	28.2	--	2587
15S 17W 05BAA	210DKOT	150	7.7	1	2.15	2.15	65.2	6.23	9.58	50.8	--	4025
15S 17W 14DDD	210DKOT	171	7.31	1	4.34	2.89	47.8	7.54	11.7	36.7	--	3316
15S 18W 09BBB	210DKOT	270	6.81	1	28.0	7.35	14.8	4.59	37.5	8.46	38	3270

Table A.7. Concentrations of major dissolved constituents for ground waters sampled from the confined Dakota aquifer west of the Cedar Hills subcrop.

Location	Geology USGS code	Depth feet	pH	Remark	Ca meq/L	Mg meq/L	Na meq/L	HCO_3 meq/L	SO_4 meq/L	Cl meq/L	SiO_2 mg/L	TDS mg/L
11S 24W 26ABB	210 DKOT	950	8.4		0.135	0.0987	27.1	10.5	5.44	10.8	12.5	1620
12S 21W 24CDC	210DKOT	665	7.87	1	0.798	0.826	7.83	5.08	2.08	1.72	8	557
13S 18W 17CBC	210DKOT	495	8.03	1	1.87	1.30	9.53	1.86	5.52	5.16	--	786
13S 18W 17CBC	210DKOT	515	8.04	1	0.948	0.806	22.2	3.92	5.04	14.7	--	1430
13S 18W 17CBC	210DKOT	535	7.78	1	1.55	1.15	16.5	3.44	5.48	10.7	--	1180
13S 18W 17CBC	210DKOT	555	7.94	1	0.873	0.666	27.1	5.66	5.88	17.6	--	1735
13S 18W 17CBC	210DKOT	575	7.95	1	1.023	0.773	22.4	4.56	5.98	14.5	--	1490
13S 18W 19BBBB	210DKOT	455	7.78	1	0.998	0.650	22.9	7.23	5.71	11.4	--	1460
13S 18W 19BBBB	210DKOT	490	7.83	1	1.098	0.568	19.3	5.50	5.29	10.4	--	1270
13S 18W 19BBBB	210DKOT	515	8		2.20	1.62	6.27	1.90	5.81	2.95	--	659
13S 18W 20BABB	210DKOT	415	8		3.59	1.69	7.00	3.12	5.75	3.16	--	745
13S 18W 20BABB	210DKOT	435	8.3		0.923	0.592	19.7	5.52	4.67	11.3	--	1280
13S 18W 20BABB	210DKOT	455	8.2		0.773	0.576	21.6	5.90	4.67	12.7	--	1380
13S 18W 20BABB	210DKOT	495	8.1		0.474	0.337	22.1	6.10	4.54	12.9	--	1390
13S 18W 20BABB	210DKOT	535	8.3		0.599	0.378	22.1	5.86	4.65	13.3	--	1405
14S 18W 18DBBC	210DKOT	459	8.38	1	0.334	0.280	26.6	5.57	4.98	16.4	--	1920
14S 18W 18DCDD	210DKOT	471	8.25	1	0.459	0.658	35.3	5.92	5.98	24.7	--	2180
14S 18W 20BBDD	210DKOT	410	8.37	1	0.349	0.461	30.2	5.79	5.33	19.9	--	1853
14S 19W 13ADCD	210DKOT	497	8.43	1	0.304	0.263	26.4	5.49	5	16.3	--	1608
14S 19W 13CBAC	210DKOT	512	8.4	1	0.314	0.247	26.3	5.52	4.94	16.0	--	1593
14S 19W 14DCCD	210DKOT	514	8.43	1	0.299	0.271	26.5	5.52	4.96	16.3	--	1610
14S 19W 29DDC	210DKOT	350	7.88	1	0.848	0.826	37.0	8.85	5.62	28.2	20	2446
14S 21W 04DAD	210DKOT	525	6.75		21.4	4.71	15.6	6.87	18.4	14.1	--	2464
14S 21W 05ABA	210DKOT	521	6.9		0.220	0.149	19.1	5.46	4.41	8.55	--	1132
14S 22W 20AAA	210DKOT	700	6.95		8.73	8.18	7.00	5.08	13.5	3.72	--	1409
14S 22W 21BCB	210DKOT	500	8.45		0.210	0.182	19.4	7.93	4.00	5.70	--	1122
14S 22W 35AAA	210DKOT	470	8.3	1	0.304	0.223	22.4	6.95	4.12	10.1	--	1298
14S 24W 19CCA	210DKOT	680	8.52	1	0.210	0.140	15.7	5.52	4.00	5.67	--	934

Table A.7. (Continued...)

Location	Geology USGS code	Depth feet	pH	Remark	Ca meq/L	Mg meq/L	Na meq/L	HCO_3 meq/L	SO_4 meq/L	Cl meq/L	SiO_2 mg/L	TDS mg/L
14S 24W 19DDA	210DKOT	500	7.35		0.225	0.157	16.3	5.42	3.91	6.32	--	963
15S 19W 04ADB	210DKOT	290	7.4	1	3.84	2.07	9.13	4.92	6.45	3.67	23	929
15S 20W 26CAAA	210DKOT	315	8.2		4.22	1.86	14.4	3.00	12.6	6.83	--	1382
15S 20W 26CAAA	210DKOT	335	8		3.77	1.94	14.3	3.40	8.33	7.11	--	1190
15S 20W 26CAAA	210DKOT	375	8.2		2.87	0.930	18.0	5.14	5.17	11.4	--	1300
15S 20W 26CAAA	210DKOT	535	8.4		0.449	0.502	22.9	4.62	4.73	14.9	--	1444
15S 20W 27CDCC	210DKOT	455	7.9		6.54	2.45	7.44	3.94	8.29	3.78	--	992
15S 20W 27CDCC	210DKOT	475	8.1		3.57	1.64	12.5	4.58	6.96	5.02	--	1038
15S 20W 27CDCC	210DKOT	495	8.1		1.90	0.938	14.0	5.52	5.15	6.26	--	1016
15S 20W 27CDCC	210DKOT	515	8.2		0.674	0.428	15.1	5.48	4.08	6.88	--	979
15S 20W 27CDCC	210DKOT	555	8.1		0.524	0.411	14.7	5.14	3.60	7.14	--	945
15S 20W 27CDCC	210DKOT	615	8.1		0.449	0.395	18.1	5.30	3.85	9.79	--	1130
15S 20W 27DDDC	210DKOT	375	8		5.59	2.17	7.53	4.44	5.85	3.72	--	868
15S 20W 27DDDC	210DKOT	395	8.2		3.19	1.60	10.2	3.49	5.79	4.77	--	880
15S 20W 27DDDC	210DKOT	415	8.4		0.898	1.69	12.8	5.33	4.15	5.75	--	906
15S 20W 27DDDC	210DKOT	455	8.4		0.474	0.296	14.9	3.08	3.77	7.22	--	895
15S 20W 27DDDC	210DKOT	495	8.4		0.349	0.263	15.2	2.92	3.77	7.16	--	892
15S 20W 27DDDC	210DKOT	575	8.3		0.549	0.452	21.5	5.75	4.40	14.0	--	1402
15S 20W 28CCCC	210DKOT	455	8		8.782	2.52	3.59	4.02	6.08	2.68	--	807
15S 20W 28CCCC	210DKOT	515	8.3		2.17	1.14	18.7	6.93	5.52	9.36	--	1302
15S 20W 28CCCC	210DKOT	535	8.1		4.77	1.91	11.4	5.18	5.94	6.12	--	1048
15S 20W 28CCCC	210DKOT	555	8.4		1.57	1.10	21.5	5.28	5.19	11.3	--	1358
15S 20W 28CCCC	210DKOT	575	8.4		1.37	0.880	22.8	6.02	5.46	12.0	--	1440
15S 20W 28CCCC	210DKOT	595	8.2		3.34	1.48	15.1	5.68	5.92	7.62	--	1165
15S 20W 28CCCC	210DKOT	615	8.4		1.32	0.724	22.6	7.15	5.19	11.3	--	1430
15S 20W 28CCCC	210DKOT	635	8.4		0.649	0.436	27.0	5.68	4.69	18.1	--	1687
15S 20W 28CCCC	210DKOT	655	8.5		0.474	0.502	33.0	3.78	4.79	21.7	--	1895
15S 20W 35CAA	210DKOT	365	8.15		0.225	0.223	15.2	5.24	3.73	6.06	--	917
15S 20W 35DCCB	210DKOT	375	7.8		0.823	0.494	21.1	6.02	4.63	11.8	--	1340

Table A.7. (Continued...)

Location	Geology USGS code	Depth feet	pH	Remark	Ca meq/L	Mg meq/L	Na meq/L	HCO_3 meq/L	SO_4 meq/L	Cl meq/L	SiO_2 mg/L	TDS mg/L
15S 20W 35DCCB	210DKOT	395	7.1		3.19	5.16	70.5	8.09	11.0	62.0	--	4730
15S 20W 35DCCB	210DKOT	415	7.6		6.14	14.3	139	12.6	23.6	119	--	9240
15S 20W 35DCCB	210DKOT	435	7.6		6.04	13.4	128	10.7	22.6	115	--	8705
15S 20W 35DCCB	210DKOT	455	7.6		5.59	12.3	124	12.2	19.1	107	--	8220
15S 20W 35DCCB	210DKOT	475	7.5		6.29	14.4	150	12.1	23.5	129	--	9840
15S 20W 35DCCB	210DKOT	495	7.6		5.84	13.2	133	11.2	21.3	115	--	8780
15S 20W 35DCCB	210DKOT	515	7.6		4.12	8.04	93.5	7.87	14.3	82.2	--	6180
15S 21W 12CCC	210DKOT	420	6.8		0.429	0.322	31.1	9.57	5.21	14.6	--	1800
15S 21W 25DDD	210DKOT	555	7.55		0.200	0.182	21.3	6.52	4.31	9.90	--	1257
15S 24W 15CCC	210DKOT	618	7.1		1.30	0.909	18.7	6.39	6.33	6.88	--	1215
15S 24W 16DDD	210DKOT	640	7.5		0.339	0.264	17.6	5.49	3.89	7.79	--	1054

Table A.8. Concentrations of major dissolved constituents for ground waters sampled from the Permian Cedar Hills Sandstone.

Location	Geology USGS code	Depth feet	pH	Remark	Ca meq/L	Mg meq/L	Na meq/L	HCO3 meq/L	SO4 meq/L	Cl meq/L	SiO2 mg/L	TDS mg/L
12S 18W 30AA	318CDHL	1185	7.60	1	9.08	66.2	500	27.7	96.0	454	27	34140
13S 14W 32CB	318CDHL	590	6.30	1	30.7	76.2	821	25.1	113	790	--	55400
13S 14W 33AB	318CDHL	626	6.57	1	28.8	104	916	14.7	140	894	--	62210
13S 15W 33CB	318CDHL	615	6.47	1	18.4	40.6	459	22.7	64.0	432	--	31180
13S 15W 35DBAD	318CDHL	733	6.85	1	21.8	123	937	10.0	157	914	--	63750
14S 14W 14CD	318CDHL	697	7.13	1	34.3	148	1029	3.56	178	1030	--	71410
14S 14W 25BB	318CDHL	444	6.56	1	39.4	94.3	976	11.4	128	970	--	65610
14S 14W 30BA	318CDCY	515	6.31	1	32.1	75.7	858	23.4	107	835	--	57470
14S 15W 20DA	217CYCD	500	6.35	1	22.9	39.3	473	24.7	64.3	445	--	31470
15S 14W 31CC	318CDKI	540	6.33	1	31.1	46.8	666	20.4	78.2	645	--	43810

APPENDIX B

EXAMPLES OF MODIFIED FORTRAN SOURCE CODE FOR HYDROGEOCHEM MODEL

Table B.1. List of fortran source code where the Gaines and Thomas convention is used to calculate ion exchange. Statements without line number or with offset line number are those that have been modified or added.

```
      SUBROUTINE RIES(RE,CW,ISCN,VJ,EQKM,AXYZP,LOCZ)                    ries 020
C                                                                       ries 025
C  TO COMPUTE RESIDUES FOR EQUATIONS GOVERNING ION-EXCHANGED SPECIES    ries 030
C  REACTIONS.                                                           ries 035
C                                                                       ries 040
C  Rather than use of molal fraction of adsorbed species to calculate
C  the activity of exchanged (adsorbed) species, this subroutine is
C  modified to calculate activity of ion-exchange species by its eqivalent
C  fraction on surface sites.
C
C**  This subroutine is only good for cation exchange.  If ion exchange
C**  involved anion, the negative value of VJ(i) have to be taken care of.
C
C  Tyan-ming Chu, Nov., 1993 at the Kansas Geological Survey
C
C         CEC: number of eqivalent on surface site for ion exchange per
C              unit volume of solution (NOT eq/(unit weight of dry solid))
C        CWI1: Adsorbed concentration of reference species
C        CWII: Adsorbed concentration of exchanging species
C        CWJ1: Aqueous concentration of reference species
C        CWJI: Aqueous concentration of exchanging species
C       AMTOT: Total equivalent concentration on solid surface per
C              unit volume of solution
C
      IMPLICIT REAL*8(A-H,O-Z)                                          ries 045
C                                                                       ries 050
      COMMON /DIM/ MAXN,MAXM,MAXMZ,MAXMP,MAXPD,MAXEQ                    ries 055
      COMMON /NUM/ NON,NONA,NONS,NOM,NOMX,NOMY,NOMZ,NOMP,NOPD,NOEQ      ries 060
      COMMON /SBT/ CEC,CAP1,CAP2,SREA,TEMP,PRESU,IADS,LNO,LNB,LNI       ries 065
```

```
C                                                                       ries 070
      DIMENSION RE(MAXEQ),CW(MAXM),ISCN(MAXM),VJ(MAXM)                  ries 075
      DIMENSION EQKM(MAXPD),AXYZP(MAXPD,MAXN)                           ries 080
      DIMENSION LOCZ(MAXMZ)                                             ries 085
C                                                                       ries 090
      IF(NOMZ.EQ.0) RETURN                                              ries 095
      NOMXY=NOMX+NOMY                                                   ries 100
      IROW=NON                                                          ries 105
      DO 110 I=1,NOMZ                                                   ries 110
      IROW=IROW+1                                                       ries 115
      RE(IROW)=0.0                                                      ries 120
  110 CONTINUE                                                          ries 125
C                                                                       ries 130
C ------- ONE SITE CONSTRAINT EQUATION                                  ries 135
C                                                                       ries 140
      IROW=NON+LNI                                                      ries 145
      RE(IROW)=CEC                                                      ries 150
      AMTOT=0                                                           ries 155
      DO 520 I=1,NOMZ                                                   ries 160
      II=NON+NOMXY+I                                                    ries 165
      RE(IROW)=RE(IROW)-VJ(II)*CW(II)                                   ries 170
      AMTOT=AMTOT+CW(II)*vj(ii)                                          ries 175
  520 CONTINUE                                                          ries 180
C                                                                       ries 185
C ------- (NOMZ -1) ION-EXCHANGE EQUATIONS                              ries 190
C                                                                       ries 195
      IF(NOMZ.EQ.1) RETURN                                              ries 200
C                                                                       ries 205
C ------- PLEASTE NOTE THAT J1 SHOULD BE ONE OF THE AQUEOUS COMPONENT   ries 210
C ------- SPEICES                                                       ries 215
C                                                                       ries 220
      J1=LOCZ(LNI)                                                      ries 225
      I1=NON+NOMXY+LNI                                                  ries 230
      IROW=NON                                                          ries 235
      DO 590 I=1,NOMZ                                                   ries 240
```

```
      IROW=IROW+1                                                       ries 245
      IF(I.EQ.LNI) GO TO 590                                            ries 250
      IPD=NOMXY+I                                                       ries 255
      II=NON+IPD                                                        ries 260
      IF(ISCN(II).EQ.3) GO TO 580                                       ries 265
      JI=LOCZ(I)                                                        ries 270
      VJJ1=VJ(J1)                                                       ries 275
      VJJI=VJ(JI)                                                       ries 280
c      CWI1=CW(I1)                                                       ries 285
c      CWII=CW(II)                                                       ries 290
      cwi1=cw(i1)*vj(i1)
      cwii=cw(ii)*vj(ii)
      CWJ1=CW(J1)                                                       ries 295
      CWJI=CW(JI)                                                       ries 300
      IF(JI.LE.NON) GO TO 560                                           ries 305
C                                                                       ries 310
C --- CWJI SHOULD BE COMPUTED BASED ON CW(J), J=1,2,..NON IF JI.GT.NON  ries 315
C --- THIS IS SO BECAUSE WE WILL HAVE CONSISTENT NUMERICAL EVALUATION   ries 320
C --- IN JACOBIAN IN JIES                                              ries 325
C                                                                       ries 330
      IF(ISCN(JI).EQ.3) GO TO 550                                       ries 335
      IPD1=JI-NON                                                       ries 340
      PROD=EQKM(IPD1)                                                   ries 345
      DO 540 K=1,NONA                                                   ries 350
      AXYIK=AXYZP(IPD1,K)                                               ries 355
      IF(AXYIK.EQ.0.0) GO TO 540                                        ries 360
      PROD=PROD*CW(K)**AXYIK                                            ries 365
  540 CONTINUE                                                          ries 370
      CWJI=PROD                                                         ries 375
      GO TO 560                                                         ries 380
  550 CWJI=CW(II)                                                       ries 385
C                                                                       ries 390
  560 CONTINUE                                                          ries 395
c      DENOM=(AMTOT**VJJI*CWJ1**VJJI)**(1.0D0/VJJ1)                     ries 400
      DENOM=(cec**VJJI*CWJ1**VJJI)**(1.0D0/VJJ1)                        ries 400
```

```
c       RE(IROW)=CWII*DENOM -                                              ries 405
c      1(EQKM(IPD)*CWI1**VJJI*AMTOT**VJJ1*CWJI**VJJ1)**(1.0D0/VJJ1)       ries 410
       RE(IROW)=CWII*DENOM -
      1(EQKM(IPD)*CWI1**VJJI*cec**VJJ1*CWJI**VJJ1)**(1.0D0/VJJ1)
       GO TO 590                                                        ries 415
C                                                                       ries 420
  580 RE(IROW)=0.0                                                      ries 425
C                                                                       ries 430
  590 CONTINUE                                                          ries 435
C                                                                       ries 440
       RETURN                                                           ries 445
       END                                                              ries 450
```

Table B.2. List of the fortran source code where the B$^{\bullet}$ method is used to calculate the activity coefficient. Statements without line number or with offset line number have been modified or added.

```
      SUBROUTINE ACOEF(GAMA,EQK,AXYZP,ELCONC, CW,VJ, temp,azero)          acoe 020
C                                                                        acoe 025
C***********************************************************************
C
C  TO COMPUTE ACTIVITY COEFFICIENTS OF ALL SPECIES.                      acoe 030
C
C  Note from Tyan-ming Chu, Nov., 1993 at the Kansas Gelogical Survey
C
C  The B-dot method is adapted to this subroutine to calaulate
C  activity coefficients.  The Debye-Hukle parameters Ar and Br are obtained
C  from Helgeson et al., 1981.  The values of deviation function B-dot and
C  ion size parameters are obtained from the SOLMINEQ.88 manual.
C
C  Helgeson, H. C., D. H. Kirkham, and G. C. Flowers, 1981,  Theoritical
C  prediction of the thermodynamic behavior of aqueous electrolytes at high
C  pressure and temperatures: IV. calculation of activity coefficients,
C  osmotic coefficients, and apparent molal and standard and relative partial
C  molal properties to 600 oC and 5 KB:  American Journal of Science, Vol. 281,
C  pp. 1249-1516.
C
C  Kharaka, Y. K., Gunter, W. D., P. K. Aggarwal, E. H. Perkins, and
C  J. D. DeBraal, 1988,  SOLMINEQ.88: a computer program for geochemical
C  modeling of water-rock reactions:  U.S. Geological Survey  Water-Resources
C  Investigations Report 88-4227.
C
C                                                                        acoe 035
      IMPLICIT REAL*8 (A-H,O-Z)                                          acoe 040
C                                                                        acoe 045
      COMMON /DIM/ MAXN,MAXM,MAXMZ,MAXMP,MAXPD,MAXEQ                     acoe 050
```

```
      COMMON /NUM/ NON,NONA,NONS,NOM,NOMX,NOMY,NOMZ,NOMP,NOPD,NOEQ      acoe 055
      COMMON /HEI/ SICOR,ICOR,LNH,LNE                                   acoe 060
C                                                                       acoe 065
      DIMENSION EQK(MAXPD),AXYZP(MAXPD,MAXN)                            acoe 070
      DIMENSION GAMA(MAXM),CW(MAXM),VJ(MAXM),azero(maxm)                acoe 075
C
      Data t0 /273.0/
C                                                                       acoe 080
      NOMXY=NOMX+NOMY                                                   acoe 085
      NOMXYZ=NOMX+NOMY+NOMZ                                             acoe 090
C                                                                       acoe 095
C ######## CALCULATION OF IONIC STRENGTH                               acoe 100
C                                                                       acoe 105
      CTOT=0.0                                                          acoe 110
      SI=0.                                                             acoe 115
      TC=0.0
      if (icor .lt. 2) goto 140
      DO 110 J=1,NONA                                                   acoe 120
      IF (J.EQ.LNE) GO TO 110                                           acoe 125
      CC=CW(J)                                                          acoe 130
      VJJ=VJ(J)                                                         acoe 135
      CTOT=CTOT+VJJ*CC                                                  acoe 140
      SI=SI+CC*VJJ*VJJ                                                  acoe 145
  110 CONTINUE                                                          acoe 150
      IF(NOMX.EQ.0) GO TO 130                                           acoe 155
      DO 120 I=1,NOMX                                                   acoe 160
      II=NON+I                                                          acoe 165
      VJJ=VJ(II)                                                        acoe 170
      if (vjj .eq. 0.0) goto 120
      IJ=0                                                              acoe 175
      DO 115 J=1,NON                                                    acoe 180
      AIJ=DABS(AXYZP(I,J))                                              acoe 185
      IIJ=IDINT(AIJ)                                                    acoe 190
      IJ=IJ+IIJ                                                         acoe 195
  115 CONTINUE                                                          acoe 200
```

```
      DLOGK=DLOG10(EQK(I))                                                  acoe 205
      IF(IJ.EQ.1 .AND. DABS(DLOGK).LE.1.0D-38) THEN                         acoe 210
        CC=0                                                                acoe 215
      ELSE                                                                  acoe 220
        CC=CW(II)                                                           acoe 225
      END IF                                                                acoe 230
      CTOT=CTOT+VJJ*CC                                                      acoe 235
      SI=SI+CC*VJJ*VJJ                                                      acoe 240
  120 CONTINUE                                                              acoe 245
  130 CONTINUE                                                              acoe 250
C      SI=SI+DABS(CTOT)                                                      acoe 255
c      ELCONC=0.5D0*SI                                                       acoe 260
C
C ###### Calculation of Debye-Hukle parameter, Agama and Bgama, and
C ###### B-dot deviation function.  Only good for temperature ranges
C ###### from 0 to 50 degree C.
C
  140 TC=temp-t0
C
c      print '(a8,f6.2)',' temp = ',temp
c      print '(a8,f6.2)',' t0   = ',t0
      if (tc .lt. 0.0) then
         print
         print *,' Temperature below Freezing point?! STOP!'
         stop
      elseif (tc .lt. 10.0) then
         agama=0.4913+tc*0.0063/10.0
         bgama=0.3247+tc*0.0014/10.0
      elseif (tc .lt. 20.0 .and. tc .ge. 10.0) then
         agama=0.4976+(tc-10.0)*0.0074/10.0
         bgama=0.3261+(tc-10.0)*0.0015/10.0
      elseif (tc .lt. 30.0 .and. tc .ge. 20.0) then
         agama=0.5050+(tc-20.0)*0.0085/10.0
         bgama=0.3276+(tc-20.0)*0.0015/10.0
      elseif (tc .lt. 40.0 .and. tc .ge. 30.0) then
```

```
         agama=0.5135+(tc-30.0)*0.0096/10.0
         bgama=0.3291+(tc-30.0)*0.0016/10.0
      elseif (tc .le. 50.0 .and. tc .ge. 50) then
         agama=0.5231+(tc-40.0)*0.0105/10.0
         bgama=0.3307+(tc-40.0)*0.0018/10.0
      endif
C
      bdot=0.038+0.004*tc/50.0
C                                                                    acoe 265
C #######  CALCULATION OF ACTIVITY COEFFICIENTS                       acoe 270
C                                                                    acoe 275
      IF(ICOR .GT. 0) GO TO 200                                      acoe 280
C                                                                    acoe 285
C ******* FOR THE CASE OF ZERO IONIC STRENGTH                        acoe 290
C                                                                    acoe 295
      DO 160 I=1,NOM                                                 acoe 300
      GAMA(I)=1.0D0                                                  acoe 305
  160 CONTINUE                                                       acoe 310
      RETURN                                                         acoe 315
C                                                                    acoe 320
C ******* FOR THE CASE OF NONZERO IONIC STRENGTH                     acoe 325
C                                                                    acoe 330
  200 IF(ICOR .GT. 1) GO TO 205                                      acoe 335
      SI=2.0d0*SICOR                                                 acoe 340
c  205 CIONST=0.5D0*SI                                               acoe 345
  205 elconc=0.5d0*si
      si=dsqrt(elconc)
c      SI=DSQRT(CIONST)                                              acoe 350
C      FI=0.5D0*(SI/(1.0D0+SI)-0.3D0*CIONST)                         acoe 355
C                                                                    acoe 360
C ------- ACTIVITY COEFFICIENTS OF AQUEOUS COMPONENT SPECIES         acoe 365
C                                                                    acoe 370
      DO 210 J=1,NONA                                                acoe 375
      VJJ=VJ(J)                                                      acoe 380
      azeroj=azero(j)
```

```
c      IF(J.EQ.LNE) VJJ=0.0                                          acoe 385
c      G=FI*VJJ*VJJ                                                  acoe 390
       if (j .eq. lne) then
          vjj=0.0
          bdot=0.0
       endif
       fi=(agama*vjj**2*si)/(1+azeroj*bgama*si)
       g=fi-bdot*elconc
       AG=DABS(G)                                                    acoe 395
       IF(AG.GT.10.) G=0.0                                           acoe 400
       GAMA(J)=10.**(-G)                                             acoe 405
  210 CONTINUE                                                       acoe 410
C                                                                    acoe 415
C ------- ACTIVITY COEFFICIENTS OF ADSORBENT COMPONENT SPECIES       acoe 420
C                                                                    acoe 425
       IF(NONS.EQ.0) GO TO 300                                       acoe 430
       DO 220 J=1,NONS                                               acoe 435
       JJ=NONA+J                                                     acoe 440
       GAMA(JJ)=1.0D0                                                acoe 445
  220 CONTINUE                                                       acoe 450
C                                                                    acoe 455
C ------- ACTIVITY COEFFICIENTS OF COMPLEXED SPECIES                 acoe 460
C                                                                    acoe 465
  300 IF(NOMX.EQ.0) GO TO 400                                        acoe 470
       DO 310 I=1,NOMX                                               acoe 475
       II=NON+I                                                      acoe 480
       VJJ=VJ(II)                                                    acoe 485
       azeroj=azero(ii)
       if (vjj .eq. 0.0) bdot=0.0
       fi=(agama*vjj**2*si)/(1+azeroj*bgama*si)
       gcx=fi-bdot*elconc
c      GCX=FI*VJJ*VJJ                                                acoe 490
       AGCX=DABS(GCX)                                                acoe 495
       IF(AGCX.GT.10.) GCX=0.0                                       acoe 500
       GAMA(II)=10.**(-GCX)                                          acoe 505
```

```
  310 CONTINUE                                                          acoe 510
C                                                                       acoe 515
C ------- ACTIVITY COEFFICIENTS OF ADSORBED SPECIES                     acoe 520
C                                                                       acoe 525
  400 IF(NOMY.EQ.0) GO TO 500                                           acoe 530
      DO 410 I=1,NOMY                                                   acoe 535
      II=NON+NOMX+I                                                     acoe 540
      GAMA(II)=1.0D0                                                    acoe 545
  410 CONTINUE                                                          acoe 550
C                                                                       acoe 555
C ------ ACTIVITY COEFFICIENTS OF ION-EXCHANGED SPECIES                 acoe 560
C                                                                       acoe 565
  500 IF(NOMZ.EQ.0) GO TO 600                                           acoe 570
      DO 510 I=1,NOMZ                                                   acoe 575
      II=NON+NOMXY+I                                                    acoe 580
      GAMA(II)=1.0D0                                                    acoe 585
  510 CONTINUE                                                          acoe 590
C                                                                       acoe 595
C ------- ACTIVITY COEFFICIENTS OF PRECIPITATED SPECIES                 acoe 600
C                                                                       acoe 605
  600 IF(NOMP.EQ.0) RETURN                                              acoe 610
      DO 610 I=1,NOMP                                                   acoe 615
      II=NON+NOMXYZ+I                                                   acoe 620
      GAMA(II)=1.0D0                                                    acoe 625
  610 CONTINUE                                                          acoe 630
C                                                                       acoe 635
      RETURN                                                            acoe 640
      END                                                               acoe 645
```

APPENDIX C

HYDROGEOCHEM INPUT FILE FOR MODEL 1D00

```
0140 1D concenptual mod- transport with complex and ion-ex. L=m,T=day,M=g  00000
*** Data set 2: Basic integer parameters (FREE FORMAT)
 402 200 01 000 197 1 9 -1 0 0 1 0 20 27 150 0 1 0
*** Data set 3: Basic real parameters (FREE FORMAT)
2.00D02 0.5D00 1.400D03 3.65D10 1.0 1.0  0.8  1.0 4.0D-3 0.8
*** Data set 4: Printer and disk store control and times for step size resetting
40000000000000000000000000000000000000000000000000000000000000000000000000000
00000000000000000000000000000000000000000000000000000000000000000000000000000
00000000000000000000000000004                 (80I1)
00000000000000000000000000000000000000000000000000000000000000000000000000000
00000000000000000000000000000000000000000000000000000000000000000000000000000
00000000000000000000000000000000              (80I1)
5.0000d2  1.0000D3  1.5000D3  2.0000d3  2.5000d3  3.0000d3  3.5000d3  4.0000d3
4.5000d3  5.0000d3  5.5000d3  6.0000d3  6.5000d3  7.0000d3  7.5000d3  8.0000d3
2.0075d5  2.0125d5  2.0175d5  2.0225d5  2.0275d5
2.0325d5  2.0375d5  2.0425d5  2.0475d5  2.0525d5  2.0575d5  (FREE FORMAT)
*** Data set 5: Chemical printout    (FREE FORMAT)
0
0
 0
 00  00 00
*** Data set 6: Material properties (FREE FORMAT)  9th item = porosity
2.5D01 0.0D-2 0.0D00  2.00D00 2.50D-2 0.0 0.0 0.0  0.20
*** Data set 7: Nodal point coordinate
  1    2  2    0.0  15.0  0.0
  2    2  2    0.0  15.0  0.0
  7   24  2   40.0  10.0  0.0
  8   24  2   40.0  10.0  0.0
 57    9  2  295.0  15.0  0.0
 58    9  2  295.0  15.0  0.0
 77    5  2  450.0  20.0  0.0
 78    5  2  450.0  20.0  0.0
```

```
 89     2   2   580.0   30.0   0.0
 90     2   2   580.0   30.0   0.0
 95   133   2   680.0   40.0   0.0
 96   133   2   680.0   40.0   0.0
363    19   2  6050.0   50.0   0.0
364    19   2  6050.0   50.0   0.0
 0     0   0     0      0     0    end of X-coordinate
 1   200   2   0.0    0.0   0.0
 2   200   2   1.0    0.0   0.0
 0     0   0     0      0     0    end of Y-coordinate
*** Data set 8: Element incidences
 1   1   3   4   2   1   1   200
*** Data set 10: Chemical component information  FORMAT(A10,2I5,2d11.4)
 7
hydrogen           01     0 1.0000d-10 1.0000d-03
calcium            02     1 1.0000d-06 1.0000d-03
magnesium          03     1 1.0000d-06 1.0000d-02
sodium             04     1 5.0000d-05 1.0000d-02
carbonate          05     1 1.0000d-07 1.0000d-03
sulfate            06     0 5.0000d-06 1.0000d-02
chloride          007     0 1.0000d-05 1.0000d-02
*** Data set 11: Card input for initial or pre-initial conditions
    1  401    1  3.0962d-3     0 0
 0    0  0         0 0 0    end of initial conditions for H+
    1  401    1 499.7420d-3    0 0     NI NSEQ NAD RNI RAD 0.0   Material type 1
 0    0  0         0 0 0    end of initial conditions for Ca++
    1  401    1  121.04430d-3 0 0     NI NSEQ NAD RNI RAD 0.0   Material type 1
 0    0  0         0 0 0    end of initial conditions for Mg++
    1  401    1 1312.3075d-3   0 0     NI NSEQ NAD RNI RAD 0.0   Material type 1
 0    0  0         0 0 0    end of initial conditions for Na+
    1  401    1 502.7911d-3    0 0     NI NSEQ NAD RNI RAD 0.0   Material type 1
 0    0  0         0 0 0    end of initial conditions for CO3--
```

```
    1  401    1  9.5849d-2     0 0      NI NSEQ NAD RNI RAD 0.0   Material type 1
 0     0  0          0 0 0     end of initial conditions for SO4--
    1  401    1  1.1087d-0     0 0      NI NSEQ NAD RNI RAD 0.0   Material type 1
 0     0  0          0 0 0     END OF INITIAL CONDITIONS FOR Cl-
*** Data set 12: Integer parameters for source and boundary conditions
 0 0 0  00 00 0  02 01 02 00 00 0 0
*** Data set 15: Dirichlet boundary conditions  (FREE FORMAT)
0.0000d0 7.8162d-3  3.5000d5 7.8162d-3  (FREE FORMAT)
 1  1  1  1  0
 0  0  0  0  0      END OF H+ DIRICHLET BOUNDARY CONDITION
0.0000d0 591.8526d-3  3.5000d5 591.8526d-3    (FREE FORMAT)
 1  1  1  1  0
 0  0 0  0 0      END OF Ca++ DIRICHLET BOUNDARY CONDITION
0.0000d0 34.7326d-3  3.5000d5  34.7326d-3    (FREE FORMAT)
 1  1  1  1  0
 0  0 0  0 0      END OF Mg++ DIRICHLET BOUNDARY CONDITION
0.0000d0 4.2062d-3  3.5000d5 4.2062d-3    (FREE FORMAT)
 1  1  1  1  0
 0  0 0  0 0      END OF Na+ DIRICHL
0.0000d0 506.3801d-3  3.5000d5 506.3801d-3    (FREE FORMAT)
 1  1  1  1  0
 0  0 0  0 0      END OF CO3-- DIRICHLET BOUNDARY CONDITION
0.0000d0 6.6640d-4  3.5000d5 6.6640d-4    (FREE FORMAT)
 1  1  1  1  0
 0  0 0  0 0      END OF SO4-- DIRICHLET BOUNDARY CONDITION
0.0000d0 1.1622d-3  3.5000d5 1.1622d-3    (FREE FORMAT)
 1  1  1  1  0
 0  0 0  0 0      END OF Cl- DIRICHLET BOUNDARY CONDITION
 1  1  1     1  1
 0  0 0     0  0      END OF DIRICHLET NODES
*** Data set 16: Velocity and moisture content
 1   401  1  5.0000d-3  0.0000d00  0.00  0.00
```

```
 0      0  0           0           0      0      0
 1    199  1       0.200         0.0
 0      0  0           0           0
*** Data set 17: Number of components and product species  (FREE FORMAT)
 7   0   6   0   3   1    80   13   0.70   2.00d-3
*** Data set 18: H+, e-, ionic strength and sorption information (UNFORMATED)
 0.00   2   1   0                    SICOR ICOR LNH LNE
 288.15   1.0   0   0   0   3        TEMP PRESU IADS LNO LNB LNI
 -16.0   11.0   3.0   13.0          PEMN PEMX PHMN PHMX
*** Data set 19: Compnent species and their ion-exchanged species FORMAT(A20,I5,f6.2)
FREE H+              0    9.0      SPECN ISCN azero (ion size parameter)
1.00d-7   +1   0                       CW VJ IONX
FREE Ca++            0    6.0      SPECN ISCN azero
2.00d-3   +2   1                       CW VJ IONX
Ca-X2(no charge      0    0.0
5.0800d-02      1.01030
FREE Mg++            0    8.0      SPECN ISCN azero
1.80d-2   +2   1                       CW VJ IONX
Mg-X2(no charge      0    0.0
1.1600d-02      0.7005
FREE Na+             0    4.0      SPECN ISCN azero
5.00d-1   +1   1                       CW VJ IONX
Na-X(no charge)      0    0.0
8.6400d-02      0.00
FREE CO3--           0    4.5      SPECN ISCN azero
1.00d-5   -2   0                       CW VJ IONX
FREE SO4--           0    4.0      SPECN ISCN azero
4.00d-2   -2   0                       CW VJ IONX
FREE Cl-             0    3.0      SPECN ISCN azero
5.00d-1   -1   0                       CW VJ IONX
*** Data set 20: Complexed species and their ion-exchanged species (A20,I5,F6.2)
OH-                  0    3.5
```

```
3.00d-8  -14.37  -1.  0.  0.  0.  0.  0.  0.  0  -1.  0.  0.  0.  0.  0.  0.0
HCO3-              0   4.5
5.00d-3   10.44   1.  0.  0.  0.  1.  0.  0.  0   1.  0.  0.  0.  1.  0.  0.0
H2CO3              0   0.0
1.00d-5   16.87   2.  0.  0.  0.  1.  0.  0.  0   2.  0.  0.  0.  1.  0.  0.0
CaSO4(q)           0   0.0
1.00d-3   2.285   0.  1.  0.  0.  0.  1.  0.  0   0.  1.  0.  0.  0.  1.  0.0
MgSO4(q)           0   0.0
5.00d-4   2.37    0.  0.  1.  0.  0.  1.  0.  0   0.  0.  1.  0.  0.  1.  0.0
NaSO4-(q)          0   5.4
1.00d-3   1.133   0.  0.  0.  1.  0.  1.  0.  0   0.  0.  0.  1.  0.  1.  0.0
*** Data Set 22: precipitated/dissolved species
Ca.95Mg.05CO3(s    0
5.0000d-1  8.4  0.  0.95  0.05  0.  1.  0.  0.  0.  0.95  0.05  0.  1.  0.  0.0
                 END OF JOB
```